OCS Report
MMS 88-0089

Geological and Operational Summary, North Aleutian Shelf COST No. 1 Well, Bering Sea, Alaska

U.S. Department of the Interior
Minerals Management Service
Alaska OCS Region

Front cover, drawing made by Jean E. Thomas from Scanning Electron Photomicrograph:

Clinoptilolite is a common pore-filling mineral in sedimentary rocks that contain abundant volcanic detritus. Authigenic crystal growth often occludes pore spaces and decreases porosity and permeability. Magnification is about 13,000X.

Back cover, Scanning Electron Photomicrographs, from top to bottom:

Authigenic chlorite clay filling pores between detrital grains in the sediments at 11,086 feet in the North Aleutian Shelf COST No. 1 well. Magnification is about 500X.

Coscinodiscus cf. pustulatus, a Neogene diatom. Magnification is about 1,280X.

Elphidium bartletti, a Neogene foraminifera. Magnification is about 60X.

Coscinodiscus marginatus, a Neogene diatom corroded and overgrown by authigenic minerals. Detail magnified about 3,750X.

Authigenic minerals in pores of North Aleutian shelf sediments. The large plates at the left are probably clinoptilolite (a zeolite); the hexagonal rods may be minerals of the apatite group. Magnification is about 6,000X.

OCS Report
MMS 88-0089

Geological and Operational Summary, North Aleutian Shelf COST No. 1 Well, Bering Sea, Alaska

by
Ronald F. Turner
Colleen M. McCarthy
Maurice B. Lynch
Peter J. Hoose
Gary C. Martin
John A. Larson
Tabe O. Flett
Kirk W. Sherwood
Allen J. Adams

edited by
Ronald F. Turner

U. S. Department of the Interior
Minerals Management Service
Alaska OCS Region

Anchorage, Alaska
November 1988

Contents

Page

Figures

Plates

Tables

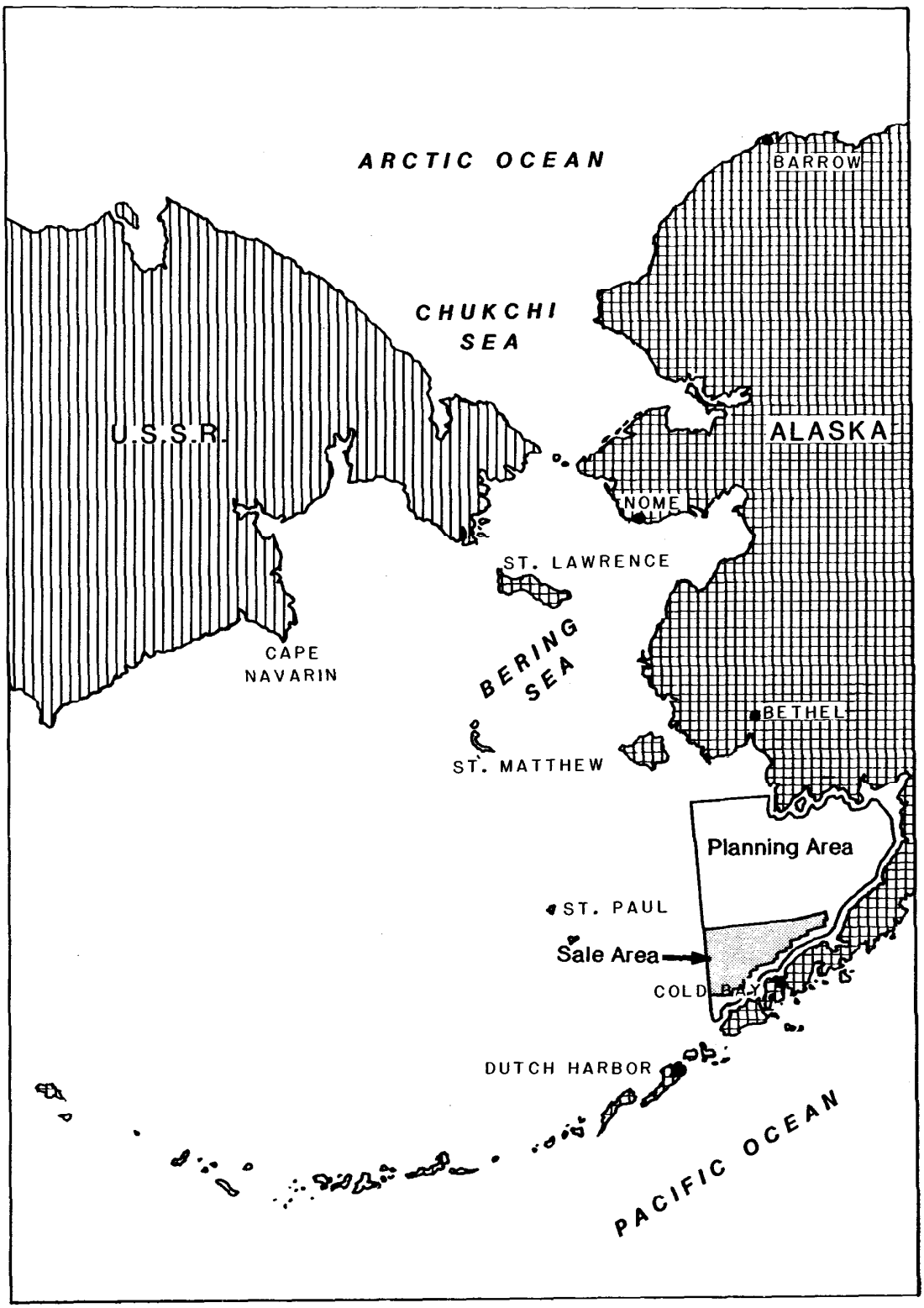

FIGURE 1. **Location of the North Aleutian Basin Planning Area.**

Introduction

by

Ronald F. Turner

Title 30, Code of Federal Regulations (CFR), paragraph 251.14, stipulates that geological data and processed geological information obtained from Deep Stratigraphic Test (DST) wells drilled on the Outer Continental Shelf (OCS) be made available for public inspection 60 calendar days after issuance of the first Federal lease within 50 nautical miles of the well site or 10 years after the completion of the well if no leases are issued. Tracts within this distance of the North Aleutian Shelf Deep Stratigraphic Test well (termed the ARCO North Aleutian Shelf COST No. 1 Well by the operator) were initially offered for lease in Sale 92 by the Minerals Management Service (MMS) in January of 1986. However, legal complications delayed the opening of bids until October 11, 1988. At that time, 23 blocks received 31 bids (fig. 2). Nine companies ultimately participated in the sale. The sum of high bids was $95,439,500.00. The effective date of the first leases issued was November 1, 1988.

Figure 1 shows the location of the North Aleutian Basin Planning Area, and figure 2 shows the Sale 92 area. The well is located in Block 666, approximately 200 miles northeast of Dutch Harbor, Alaska, and was abandoned on January 14, 1983.

Most subsurface depths referred to in this report are measured from the Kelly bushing (KB), which was given as 85 feet (logger's measurement) above sea level. For the most part, measurements are in U.S. Customary Units except where scientific convention dictates metric usage. The interpretations herein are chiefly the work of Minerals Management Service personnel, although substantial contributions were made by various geoscience consulting companies.

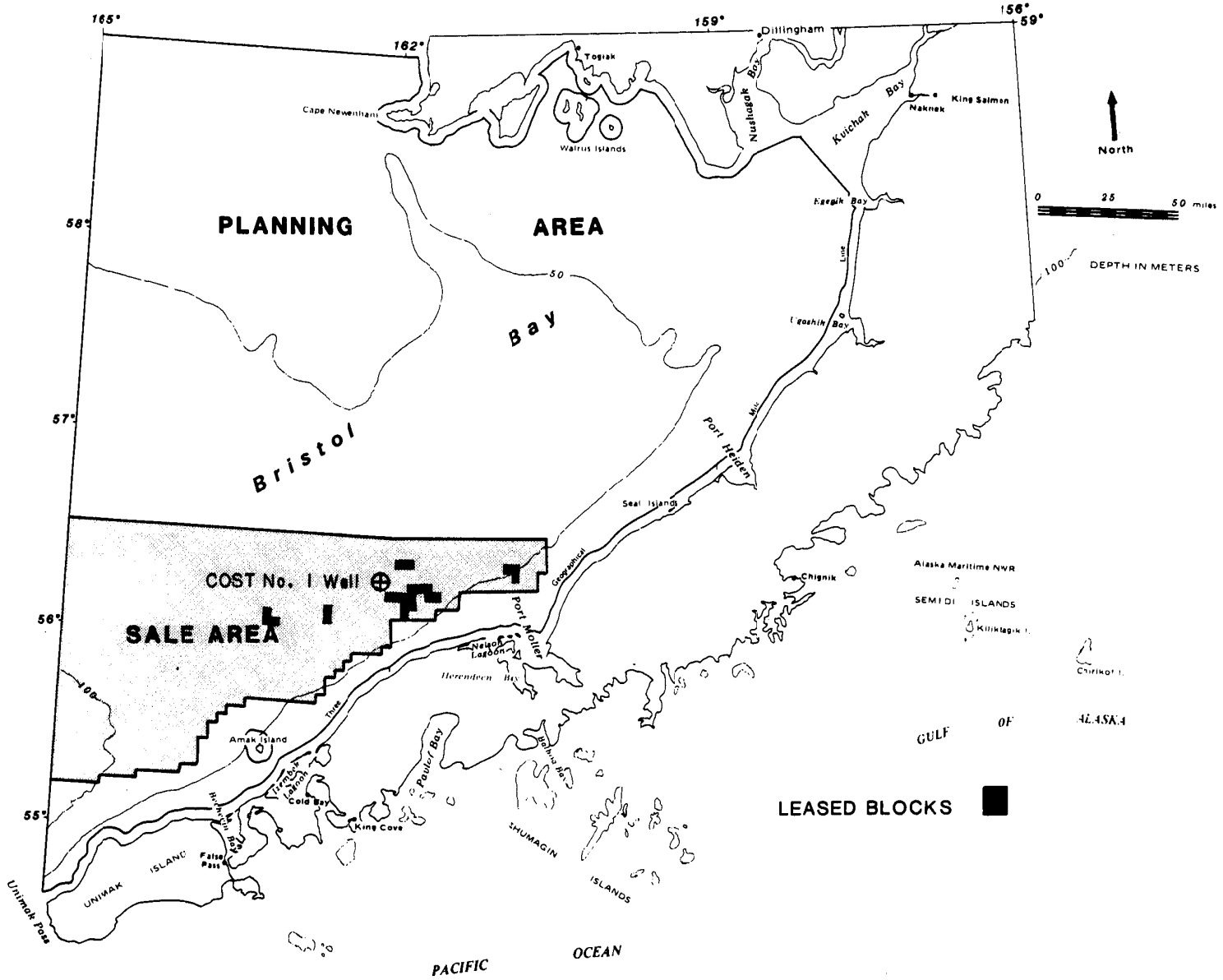

FIGURE 2. **North Aleutian Basin Planning Area and sale area showing blocks leased.**

1. Operational Data

by

Colleen M. McCarthy

The ARCO North Aleutian Shelf COST No. 1 Well was drilled by the SEDCO 708, a self-propelled semisubmersible drilling rig. The SEDCO 708, owned by SEDCO FOREX (formerly SEDCO Maritime, Inc.), was built in 1977 by Kaiser Steel Corp. at Oakland, California, and was given a classification by the American Bureau of Shipping (ABS) of ✠ A1 (E) (M) Column-Stabilized Drilling Unit, ✠ AMS. The rig was designed to withstand 100-foot waves and 100-knot winds, and is rated to drill to 25,000 feet in 1,200 feet of water. The ABS-approved extreme operating temperature is -30 °C.

The SEDCO 708 was inspected before drilling commenced, and operations were monitored by Minerals Management Service personnel to ensure compliance with U.S. Department of the Interior regulations.

Dutch Harbor, Alaska, which is approximately 200 miles southwest of the well site, was used as the shore base for sea transport. Cold Bay, Alaska, was the air support base. Kenai, Alaska, was used as an occasional source of non-routine equipment and materials supply.

Two sea-going supply vessels were used to transport drilling materials, supplies, and fuel to the rig; a large sea-going storage barge was also used to transport materials.

Chartered and commercial air carriers transported personnel, equipment, and supplies between Cold Bay and Anchorage, Alaska. Helicopters certified for instrument flight were used to transport personnel, groceries, and light-weight equipment between Cold Bay and the rig.

ARCO Alaska acted as the operator for the following 17 petroleum companies who shared expenses for the well:

American Petrofina Exploration Company
Amoco Production Company
Chevron U.S.A., Inc.
Cities Service Company
Conoco, Inc.
Elf Aquitaine Oil and Gas
Exxon Company U.S.A.
Getty Oil Company
Gulf Oil Company, U.S.A.

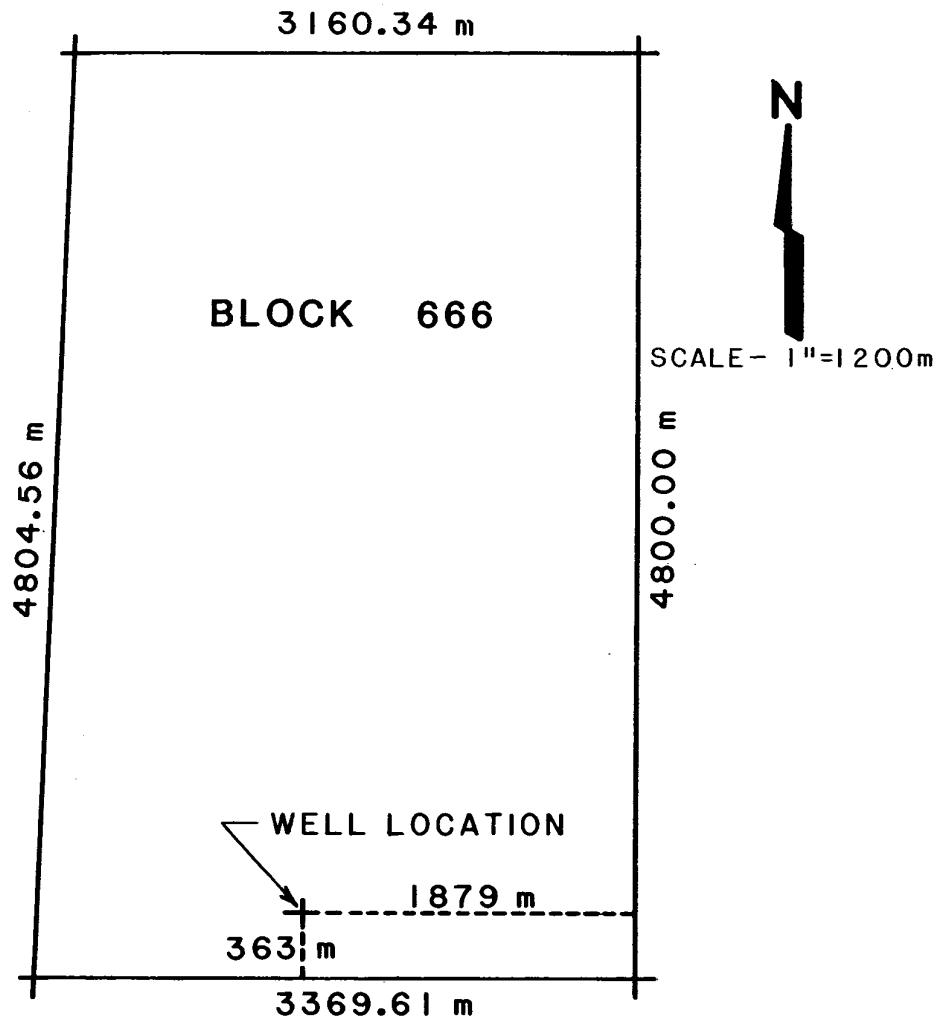

UTM ZONE 4
N 6,240,363
E 315,721

GEODETIC POSITION NAD-27
LATITUDE 56° 16′ 26.99″ N
LONGITUDE 161° 58′ 34.37″ W

FIGURE 3. **Final location plat showing the position of the North Aleutian Shelf COST No. 1 well in OCS protraction diagram Chignik 4-7.**

Marathon Oil Company
Mobil Exploration and Producing Services, Inc.
Murphy Oil
Pennzoil Company
Phillips Petroleum Company
Sohio Alaska Petroleum Company
Texaco, Inc.
Union Oil Company of California

Drilling stipulations outlined in the "Conditions for Approval to Drill" required the operator to provide the Minerals Management Service with all well logs, samples, core slabs, and operational and technical reports at the same time these were provided to industry participants.

The location of the COST No. 1 well was lat 56°16'26.99" N., long 161°58'34.37" W., or UTM coordinates (zone 4) X = 315,721 meters and Y = 6,240,363 meters. The well site was located in Block 666 (fig. 3). The water depth was 285 feet and all measurements were made from the Kelly bushing (KB), which was 74 feet (completion report depth; most authors used the logger's depth of 85 feet, however) above mean sea level (MSL) and 359 feet above the sea floor.

The well was spudded September 8, 1982, and reached a total depth of 17,155 feet on January 6, 1983, after 120 days on location. The well was plugged and abandoned on January 14, 1983, and the rig released by 0730 hours A.S.T., January 15, 1983.

DRILLING PROGRAM

The well was drilled with less than 1° deviation from vertical to a depth of 5,737 feet. The angle increased gradually to 3° at 10,513 feet, and the total depth deviation was 4.5°.

The well was drilled to a depth of 13,350 feet using twenty-six 12 1/4-inch drill bits and deepened to the total depth of 17,155 feet with thirteen 8 1/2-inch bits. Additional bits were used to open the hole before setting the larger casing strings, to drill through cement, for cleanout trips, and for the conventional coring program. Drilling rates ranged from 3 to 250 feet per hour. For the first 5,700 feet of hole, the average rate was 100 feet per hour; from 5,700 to 10,000 feet, 50 feet per hour. Below 10,000 feet, the rate gradually decreased, to 10 feet per hour at total depth. Figure 4 shows the daily drilling progress for the well.

Four strings of casing were cemented in place as shown in figure 5. The 30-inch structural casing was set with 675 sacks of cement at 459 feet. At 1,358 feet, 2,100 sacks of cement were used to set the 20-inch, 133-pounds-per-foot (lb/ft), K-55 conductor casing. At 4,865 feet, 1,871 sacks of cement were used to set the 13 3/8-inch, 72-lb/ft, N-80 casing. At 13,287 feet, 2,710 sacks of cement were used to set the 9 5/8-inch, 47-lb/ft, S-95 casing. Class G cement

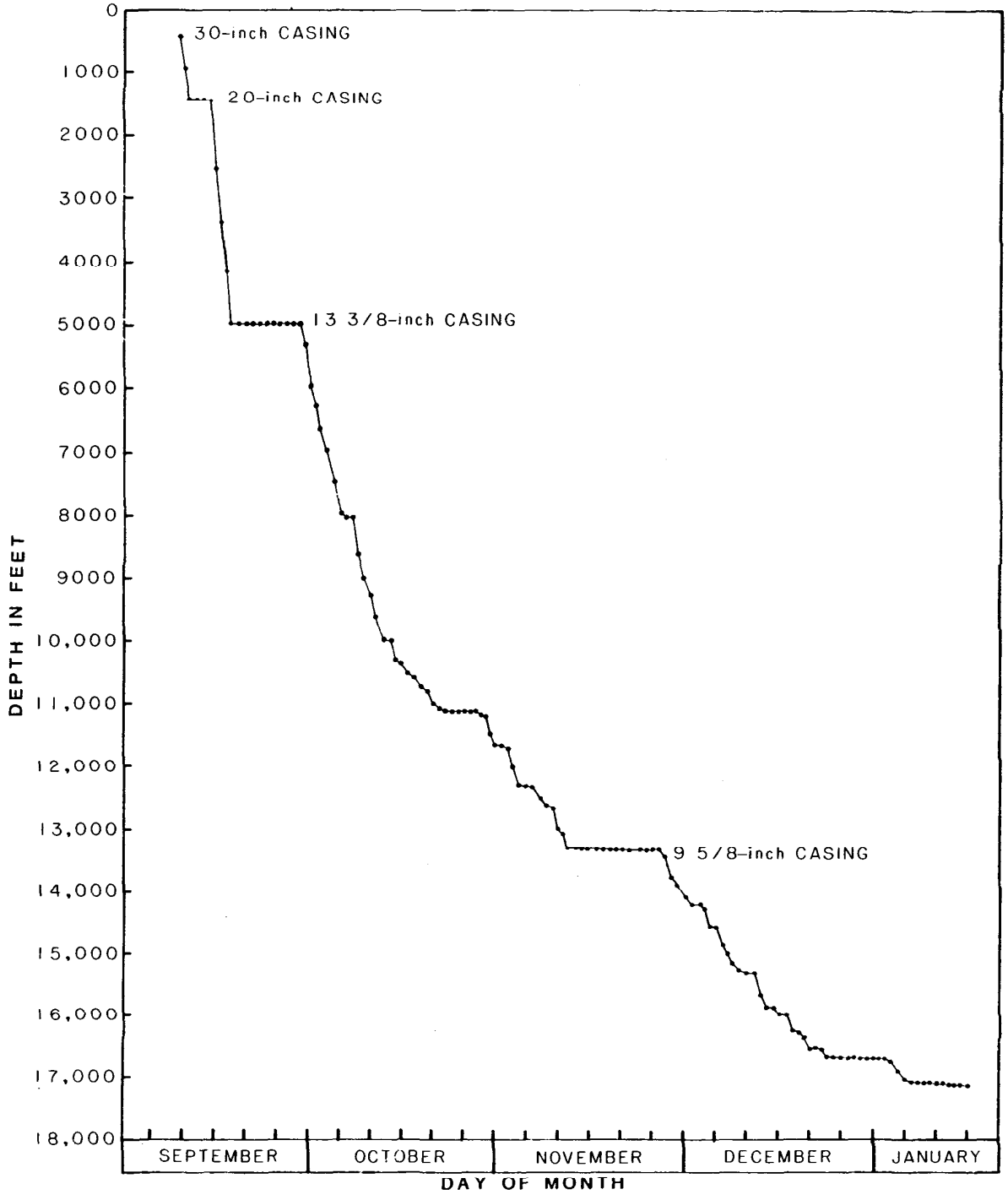

FIGURE 4. **Graph showing daily drilling progress for the North Aleutian Shelf COST No. 1 well, 1982–1983.**

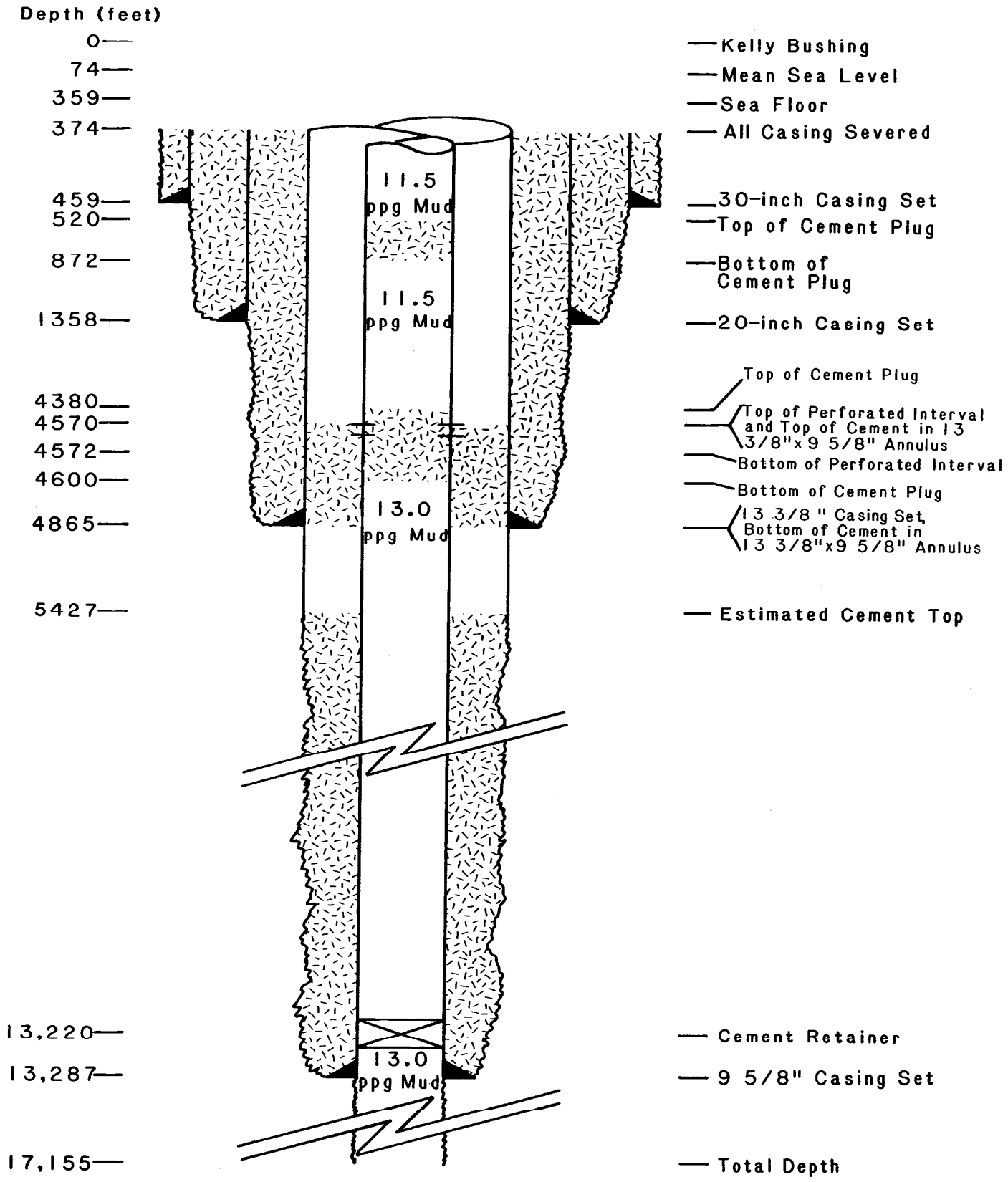

FIGURE 5. **Schematic diagram showing casing and cement programs, North Aleutian Shelf COST No. 1 well.**

was used for all casing strings. The well was uncased from the 9 5/8-inch casing shoe to total depth, leaving 3,868 feet of open hole.

The abandonment program is also shown in figure 5. A sudden and unusually rapid advance of the Bering Sea ice pack necessitated an abbreviated well abandonment program. After an intensive examination of the mechanical condition of the well and the geologic strata exposed below the last casing shoe by MMS and ARCO Alaska, the following abandonment program was approved and executed. A cement retainer was set at 13,220 feet in the 9 5/8-inch casing, and the 9 5/8-inch casing was then perforated between 4,570 and 4,572 feet with 4 shots per foot. A formation breakdown was established after pumping 10 barrels of 11.5-pounds-per-gallon (ppg) mud at 2 1/2 barrels per minute and 700 pounds per square inch (psi) through the perforations. The 9 5/8-inch and 13 3/8-inch annulus was then squeeze cemented, leaving cement between 4,570 and 4,865 feet. Two balanced cement plugs were left in the 9 5/8-inch casing, one above the squeeze between 4,380 and 4,600 feet and the other between 520 and 872 feet. A 27-pound nitromethane charge was then set off in the wellhead, severing all casing at 15 feet below the mud line.

Before abandonment procedures could be initiated, the mud and blowout prevention lines froze, necessitating circulation time for thawing. By the completion of abandonment, both of the workboats, as well as the drilling vessel itself, had experienced some superstructure icing, although abandonment and de-anchoring operations were not impaired.

DRILLING MUD

Changes in selected drilling mud properties are shown in figure 6. Seawater and gel were used to drill to 1,370 feet, where a freshwater gel mud having a mud weight of 8.7 ppg and a funnel viscosity of 39 seconds replaced the seawater. A dispersed mud was used from 11,110 feet to total depth. The initial mud weight of 8.7 ppg increased gradually to 9.7 ppg at 13,600 feet and reached 13.0 ppg at total depth. At 16,230 feet, gas in the mud lowered the mud weight from 9.9 ppg to 9.2 ppg. The mud weight was increased and circulated, but gas continued to be encountered from 16,230 to 16,701 feet. The funnel viscosity of the mud ranged between 40 and 45 seconds for most of the well, increasing to 49 seconds at 15,550 feet, but returning to 44 seconds at total depth. The pH remained below 12, the initial pH, for the duration of the well. A low pH value of 9 was reached at 7,100 feet, increasing to 10.7 at total depth. Chloride concentrations of 2,000 parts per million (ppm) were encountered initially and at total depth; the lowest concentration, 1,150 ppm, was encountered at 7,100 feet. Mud logging services below 1,370 feet were provided by Exploration Logging Company, Inc.

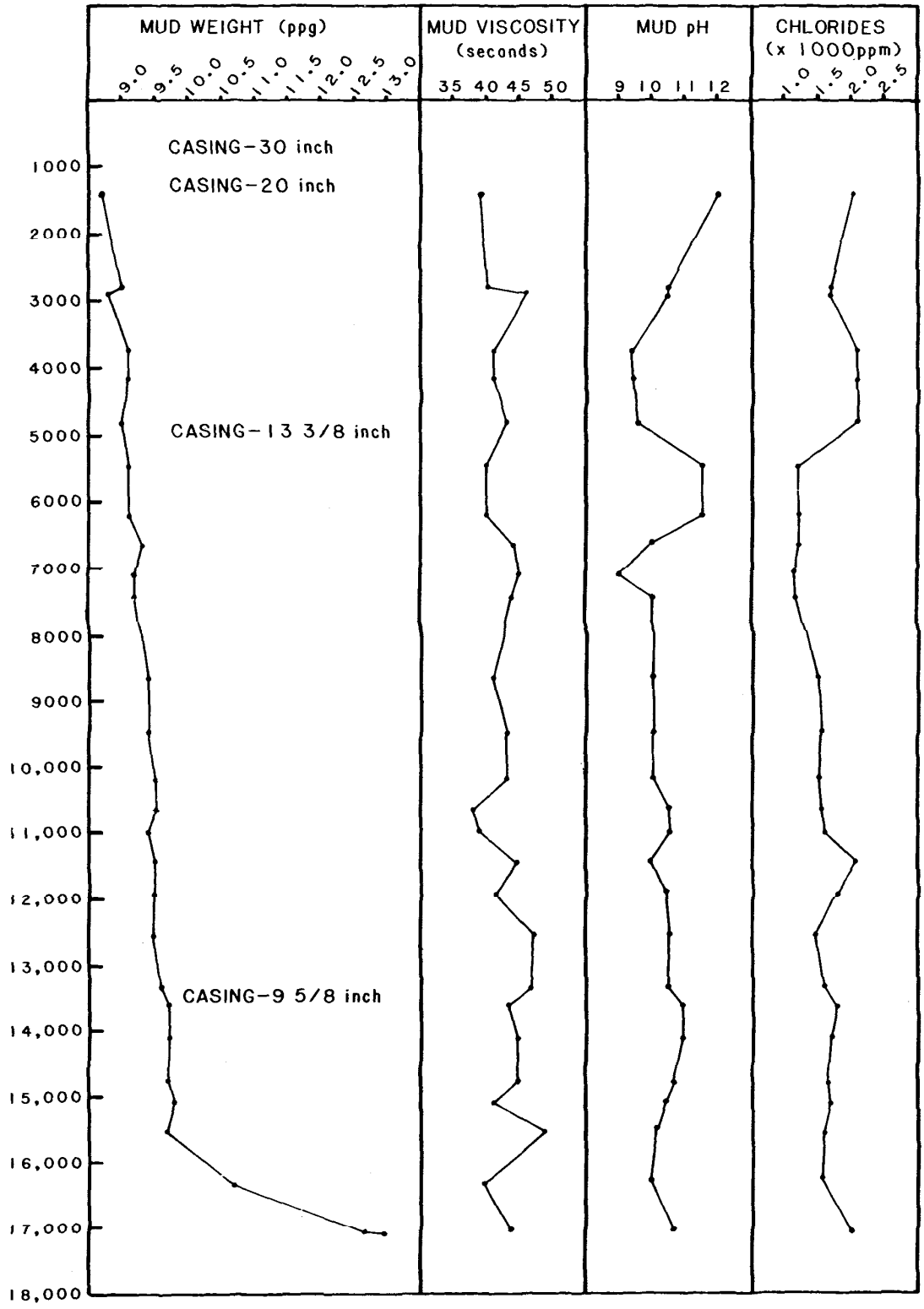

FIGURE 6. **Changes with depth of drilling-fluid properties, North Aleutian Shelf COST No.1 well.**

SAMPLES AND TESTS

Drill cuttings were collected at 30-foot intervals for lithologic description and paleontology and were later analyzed for organic geochemistry. Nineteen conventional cores were obtained and analyzed for porosity, permeability, and grain density. Thin sections made from conventional and sidewall cores were used for petrographic descriptions. The mineral content of selected cores and drill cutting samples was determined by X-ray diffraction. Coring data are given in table 1.

TABLE 1. Conventional cores.

CORE NO.	INTERVAL (feet)	RECOVERED	
		Feet	Percent
1	3,363-3,393	1	3.3
2	4,191-4,222	9.5	31
3	5,227-5,262	18.5	53
4	5,970-6,000	26	87
5	6,665-6,695	6	20
6	8,050-8,055	2	40
7	8,055-8,093	38	100
8	8,628-8,658	30	100
9	9,255-9,265	10	100
10	9,945-9,985	38.6	97
11	10,327-10,341	12	86
12	10,730-10,740	10.3	103
13	11,085-11,110	22	88
14	12,249-12,269	21	105
15	12,630-12,657	26.8	99
16	14,165-14,188	21.5	93
17	15,347-15,369	21.9	100
18	16,006-16,033	25	93
19	16,701-16,722	19.9	95

Two series of percussion sidewall cores were taken. Between 1,904 and 4,858 feet, 23 cores were recovered in 111 attempts. From 4,941 to 13,350 feet, 419 cores were recovered in 630 attempts.

Logging runs were made at depths of 4,903, 13,350, and 16,701 feet (table 2). The interval above 1,200 feet was not logged.

TABLE 2. Types of logs and intervals logged.

LOG	RUN	INTERVAL (feet)
2" and 5" Borehole Compensated Sonic Log (BHC)	Run 1, 2, & 3	1,363-16,686
2" and 5" Compensated Formation Density Log (FDC)	Run 1, 2, & 3	1,363-16,696
2" and 5" Dual Induction Laterolog with Spherically Focused Log (DIL-SFL)	Run 1, 2, & 3	1,363-16,686
2" Dual Induction Laterolog with Spherically Focused Log with Linear Correlation	Run 1, 2, & 3	1,363-16,686
5" High-Resolution Dipmeter Tool (HDT)	Run 1 Run 2 Run 3	1,363-4,884 4,864-13,345 13,282-16,556
2" and 5" Long-Spaced Sonic Log (LSS)	Run 1, 2, & 3	1,200-16,545
2" and 5" Natural Gamma Ray Spectrometry Tool (NGT)	Run 1 Run 3	1,363-4,891 13,280-16,696
5" Proximity Microlog (PML)	Run 1, 2, & 3	1,363-16,560
Repeat Formation Tester (RFT)	Run 1 Run 2 Run 3	2,830-4,878 5,112-13,292 13,287-16,458
2" and 5" Simultaneous Compensated Neutron - Formation Density Log (CNL-FDC)	Run 1, 2, & 3	1,363-16,696
5" Sonic Waveform 8'	Run 1 Run 2 Run 3	1,200-4,888 4,800-13,345 13,085-16,545
5" Sonic Waveform 10'	Run 1	1,200-4,888
5" Sonic Waveform 12'	Run 1	1,200-4,888

WEATHER

Weather, particularly ice conditions, was of special concern during the drilling of the North Aleutian Shelf COST No. 1 well. Because it was anticipated that operations would extend into the ice

season, which normally begins in early January, MMS required ARCO Alaska to initiate an ice surveillance program. The surveillance program (Grittner, 1983) was designed to allow sufficient warning time to secure or abandon the well without encountering ice. The program consisted of six parts: (1) a review of available historical ice-edge data, including satellite imagery; (2) the development of a probabilistic scheduling model; (3) the development of a statistical ice-edge motion model; (4) aerial surveillance of the ice-edge using an aircraft equipped with side-looking air-borne radar (SLAR); (5) development of a system to manage the flow of ice-edge data; and (6) the development of contingency plans for abandoning the well in the event of an ice intrusion.

Rapid ice advancement did occur during abandonment procedures, with the ice moving to within 35 nautical miles northwest of the drilling rig. However, the surveillance and contingency planning allowed the initial target depth of 13,500 feet to be extended to 17,155 feet, and an orderly and safe abandonment of the well to be completed.

In addition to ice surveillance, other weather conditions were monitored from mid-September through mid-January. During this period, maximum wind speeds of 59 knots and maximum wave heights of 28 feet were recorded. A low temperature of 13 ^{o}F was noted on January 7, with the high for the period being 51 ^{o}F on September 13, 1983.

2. Lithology and Core Data

by

Maurice B. Lynch

The following lithologic descriptions are based on the examination of 96 sidewall cores, 196 samples taken from 19 conventional cores, and washed and unwashed rotary drill bit cuttings taken at 30-foot intervals from 1,590 to 17,155 feet (TD). The ARCO mud logger on the rig began collecting cuttings at 1,590 feet. The first sidewall core was taken at 1,904 feet and the first conventional core was started at 3,392 feet. Depths used in this report are measured in feet from the Kelly bushing, which was 85 feet above mean sea level and 359 feet above the sea floor. A detailed reservoir quality study was prepared by AGAT Consultants, Inc. (1983), who analyzed 43 cuttings samples, 96 sidewall cores, and 196 core plugs taken from the 19 conventional cores. AGAT analyzed the cores from the well using a scanning electron microscope with energy-dispersive spectrometry on 180 samples, X-ray diffraction on 335 samples, and petrographic microscopy on 328 thin sections. Measured porosity and permeability values were determined by Core Laboratories, Inc. (1983). Visible porosities were estimated by AGAT geologists. Values for vitrinite reflectance and total organic carbon content were derived by Robertson Research (U.S.)(Dow, 1983). A lithology log prepared by ARCO geologists during drilling was also utilized.

The subsurface sedimentary section penetrated by the well has been divided into 11 zones on the basis of lithology, depositional environment, diagenetic alteration, seismic response, and well log characteristics. A number of illustrations and tables have been included to show the lithology of these zones: Plate 1 is a stratigraphic column and summary chart of geologic data observed in the well. Conventional cores are described in figures 7 through 25. Figure 26 is a summary chart showing percentages of various minerals at different depths in the well derived from X-ray diffraction data from the 19 conventional cores. Figure 27 shows the occurrence of diagenetic alterations in the well. Figures 28 through 45 are ternary plots of percentages of the principle framework constituents (quartz, feldspar, and lithic fragments) determined from each conventional core. Figures 46 through 55 are ternary diagrams showing sandstone classification based on modal percentages of framework grains (quartz, feldspar, and lithic fragments) in each of the 11 lithologic zones. Table 3 lists each sample analyzed, its depth, type, lithology, measured porosity, estimated visible porosity, and measured permeability. Table 4 shows percentages of

various minerals present in the whole-rock fraction of the 19 conventional cores. Table 5 shows percentages of several clays present in the less-than-5-micron fraction of the 19 conventional cores. Table 6 is a summary of petrographic data in the 11 zones. Table 7 is a summary of reservoir characteristics in the 11 zones. All the figures and tables appear at the end of this chapter.

ZONE A (1,000 to 2,510 feet),

QUATERNARY AND PLIOCENE

Zone A consists of unconsolidated mud, sandy ooze, and clay. The drill cuttings contain clear, angular quartz grains (up to coarse sand size), volcanic rock fragments, chert, feldspar, siltstone, sandstone, clays, metamorphic rock fragments, pyrite, magnetite, pumice, glauconite, biotite, garnet, pyroxenes, amphiboles, siderite, muscovite, Foraminifera, and mollusc shell fragments. Clay-sized minerals make up 4 to 11 percent of the whole rock in zone A. This fraction consists of 32 to 44 percent chlorite, 14 to 26 percent illite, 13 to 19 percent kaolinite, and 23 to 29 percent illite-smectite. The zeolite clinoptilolite is present in very small amounts. Three sidewall core samples from this zone were examined at 1,904, 2,338, and 2,510 feet (AGAT, 1983). The samples were classified as diatomaceous feldspathic litharenite in the Folk classification (Folk, 1974).

The sediments of this zone were derived primarily from a volcanic terrane with minor inputs from metamorphic, plutonic, and sedimentary sources. Deposition was in a middle or outer neritic environment, as determined from the marine fossils and glauconite present. Reservoir quality ranges from extremely poor in the matrix-rich samples to good in the matrix-poor samples. Visible intergranular porosity ranges from 3 percent to greater than 30 percent. Although clays constitute 15 percent or less of the samples with high porosity, the clay coats the framework grains, reducing permeabilities somewhat.

ZONE B-1 (2,510 to 4,110 feet),

PLIOCENE AND MIOCENE

Zone B-1 consists of mudstone and poorly sorted, laminated, diatomaceous, volcanic sandstone with angular to subrounded grains. Minerals and organic material observed in the drill cuttings are similar to those seen in zone A. Seven sidewall core samples and one sample from conventional core 1 were studied in this zone. X-ray analysis of these samples indicates the following minerals and average percentages: 52 percent quartz, 23 percent plagioclase feldspar, 7 percent potassium feldspar, 3 percent siderite, 1 percent pyrite, 1 percent calcite, 1 percent ankerite, 1 percent clinopyroxene, and 11 percent clays. The clays consist of 36 percent

chlorite, 18 percent kaolinite, 20 percent illite, and 26 percent mixed-layer illite-smectite.

The sandstone framework grains include quartz, feldspar, and lithic fragments. The quartz fraction (33 to 44 percent) consists predominantly of monocrystalline grains, although polycrystalline grains are also present. The feldspathic constituents, which range from 16 to 28 percent, include plagioclase and potassium feldspar. Potassium feldspars include orthoclase and a limited amount of microcline. The lithic constituents (32 to 48 percent) include, in order of decreasing abundance, fragments of volcanic rock, plutonic rock, altered rock, sedimentary rock, volcanic glass shards, pumice, pyroxenes, amphiboles, chert, muscovite, and quartz-mica schist. About half the plagioclase grains have been altered by vacuolization, sericitization, or partial dissolution. Devitrification of volcanic glass and dissolution of volcanic rock fragments and pyroxenes are rare to common. Siderite occurs as a minor authigenic mineral.

The sediment source area was primarily volcanic, with a minor input from a plutonic terrane. The environment of deposition was inner neritic.

Diagenesis has affected the reservoir quality of this zone very little, although compaction and the precipitation of authigenic pyrite have lowered initial porosity. The rocks of this zone have relatively high porosities because of their fine-grained nature and high clay content. Most of the porosity is microporosity in the clays and abundant diatoms. Because of the very small size of these pores, permeabilities should be very low. The sediment in this zone has very little reservoir potential.

ZONE B-2 (4,110 to 4,870 feet),

MIOCENE

Zone B-2 consists of mudstone and clay-rich, fine- to medium-grained sandstone. The sorting in the sandstone ranges from moderate to very poor. The drill cuttings contain angular quartz grains, light-gray siltstone, calcite, lignite, coal, plagioclase feldspar, muscovite, pyrite, very fine grained sandstone, glauconite, chalcopyrite, chert, volcanic rock fragments, hornblende, garnet, pumice, Foraminifera, and mollusc shell fragments. Four samples from conventional core 2 and six samples from sidewall cores were examined. X-ray diffraction analysis of these samples revealed averages of 56 percent quartz, 15 percent plagioclase feldspar, 8 percent potassium feldspar, 3 percent pyrite, 3 percent siderite, 2 percent clinopyroxene, 1 percent calcite, 1 percent ankerite, 1 percent hornblende, and 10 percent clays. The clays consist of 37 percent chlorite, 19 percent kaolinite, 15 percent illite, and 29 percent mixed-layer illite-smectite.

The sandstone framework components are 47 to 60 percent lithic fragments, 7 to 27 percent quartz, and 19 to 30 percent feldspar. Lithic framework constituents, in order of decreasing abundance, are fragments of volcanic rock, altered rock, metamorphic rock, sedimentary rock, micas, hornblende, chert, plutonic rock, broken diatoms, and pyroxene. The altered rock fragments are probably highly altered volcanic rock.

The most likely provenance is a mixed volcanic, metamorphic, and plutonic terrane, with the volcanic input being dominant. The environment of deposition was inner neritic.

Bioturbation and the introduction of clay-rich matrix were the primary mechanisms of porosity and permeability reduction. In addition, the authigenic development of clinoptilolite, siderite, pyrite, and clay has further reduced pore diameters and volumes. Somewhat offsetting these reservoir degradation events was the partial dissolution of unstable framework grains. The clay-rich detrital matrix had the effect of creating abundant microporosity and, consequently, very poor permeabilities. Reservoir potential in this zone ranges from negligible to high, depending on the location in the zone.

ZONE B-3 (4,870 to 5,675 feet),

OLIGOCENE

Zone B-3 consists of siltstone and fine- to coarse-grained sandstone containing angular to subrounded grains. Examination of drill cuttings revealed the presence of angular, clear quartz grains, gray siltstone, chert, mollusc shell fragments, lignite, glauconite, Foraminifera, coal, pyrite, calcite-cemented sandstone, mica, magnetite, pyrrhotite, feldspar, and volcanic fragments. Four sidewall cores and 10 samples from conventional core 3 were analyzed from this zone. X-ray analysis of the 14 samples indicated the following average mineral percentages: 48 percent quartz, 25 percent plagioclase feldspar, 9 percent potassium feldspar, 4 percent calcite, 3 percent clinopyroxene, 3 percent hornblende, 2 percent siderite, 1 percent ankerite, and 4 percent clays. The clay consists of 35 percent chlorite, 10 percent kaolinite, 22 percent illite, and 33 percent mixed-layer illite-smectite.

The framework constituents include quartz, feldspar, and lithic fragments. Quartz, which occurs primarily as monocrystalline grains, makes up 13 to 40 percent of the framework. Plagioclase feldspar, along with a minor amount of potassium feldspar, makes up 14 to 30 percent of the framework grains. The remaining framework grains are composed of lithic fragments (45 to 61 percent) which include the following in order of decreasing abundance: volcanic rock fragments, chert, claystone (altered rock fragments?), clay clasts (glauconite?), amphiboles, shale fragments, plutonic rock fragments, quartz-mica-schist fragments, micas, slate or phyllite, and argillite fragments.

The variety of framework grains indicates a complex source terrane or multiple sources. The depositional environment was inner neritic. Diagenetic events include slight compaction, minor dissolution and alteration of framework grains, and the development of authigenic cements. The authigenic cements include clinoptilolite, calcite, siderite, ankerite, and opaques. The calcite cement has significantly reduced porosity and permeability. Hydrocarbon reservoir potential ranges from negligible in the siltstone and poorly sorted sandstone to good in the well-sorted sandstone.

ZONE C-1 (5,675 to 6,470 feet),

OLIGOCENE

Zone C-1 consists of siltstone, clayey sandstone, and medium-gray, very poorly to moderately sorted, friable, fine- to coarse-grained sandstone. The drill cuttings contain both clear and cloudy angular quartz grains, volcanic rock fragments, chert, feldspar, glauconite, mica, hornblende, pyrite, coal, siltstone and sandstone fragments, and mollusc shell fragments. Sixteen samples from this zone were analyzed by X-ray diffraction: 14 from conventional core 4 and two from sidewall cores. This analysis revealed the following mineral percentages: 46 percent quartz, 20 percent plagioclase feldspar, 10 percent potassium feldspar, 3 percent pyrite, 3 percent hornblende, 2 percent clinopyroxene, 1 percent siderite, 1 percent calcite, 1 percent ankerite, and 13 percent clays. The clays consist of 31 percent chlorite, 14 percent kaolinite, 13 percent illite, and 42 percent mixed-layer illite-smectite.

The framework grains consist of 21 to 51 percent quartz, 13 to 41 percent feldspar, and 25 to 65 percent lithic fragments. The quartz grains are mostly monocrystalline, though up to 8 percent are polycrystalline. The feldspars include plagioclase (oligoclase to andesine) and orthoclase. A minor amount of the plagioclase grains have been altered to sericite or are vacuolized, and a slightly greater number of plagioclase grains have been partially dissolved. Potassium feldspar grains are usually unaltered. A trace of graphic granite, most commonly associated with pegmatites, was present at 5,983.6 feet, and a trace of antiperthite was seen at 5,981.5 feet. The lithic fragments include, in order of decreasing abundance, volcanic rock fragments, clay clasts, plutonic rock fragments, chert, claystone (altered rock fragments?), amphiboles, micas, fossil fragments, slate-phyllite, shale, quartz-mica schist, argillite, chlorite, carbonaceous fragments, and siltstone.

The source terrane was almost entirely volcanic, with minor metamorphic and plutonic input. The depositional environment was transitional between nonmarine and inner neritic. The relatively coarse-grained nature of core 4 (5,970 to 5,996 feet), the presence of large pebbles, the nature and extent of bioturbation, and the presence of fossil fragments and transported organic debris suggest

that these sediments were probably deposited in a lower shoreface environment. Most of the core exhibits extensive mottling as a result of bioturbation.

Diagenetic events include moderate compaction, alteration of plagioclase and volcanic rock fragments, and the dissolution of plagioclase grains, volcanic rock fragments, and heavy minerals. Minor amounts of authigenic minerals, including clinoptilolite, pyrite, and clays, are locally present. The reservoir potential ranges from extremely poor in the zones with abundant matrix and lower porosities, to fair in the zones with less matrix and authigenic clays.

ZONE C-2 (6,470 to 7,900 feet),

OLIGOCENE

Zone C-2 consists of siltstone and fine- to coarse-grained, poorly to moderately sorted, wavy, laminated sandstone with some shaly laminations. The cuttings contain angular quartz grains, chert, volcanic rock fragments, pyrite, feldspar, coal, mica, and rare Foraminifera and mollusc fragments. Twenty samples were examined in this zone by X-ray diffraction: 3 from conventional core 5 and 17 from sidewall cores. X-ray diffraction analysis indicated the following average mineral percentages: 50 percent quartz, 26 percent plagioclase feldspar, 10 percent potassium feldspar, 2 percent calcite, 2 percent clinopyroxene, 2 percent hornblende, 1 percent ankerite, and 5 percent clays. The clays consist of 9 percent chlorite, 7 percent kaolinite, 7 percent illite, and 77 percent mixed-layer illite-smectite.

Framework grains observed in conventional core 5 include rock fragments of volcanic, plutonic, metamorphic, and sedimentary origin, quartz, feldspars, chert, mica, amphiboles, opaques, and heavy minerals. Quartz, both monocrystalline and polycrystalline, is the most abundant mineral. A large, euhedral, inclusion-free beta-quartz grain in the sample at 6,665.3 feet is indicative of a volcanic source terrane. Plagioclase and potassium feldspar are present in moderate to abundant amounts. Highly altered volcanic rock fragments are abundant and consist of lath-shaped (or partially dissolved) zoned plagioclase phenocrysts in a glassy, altered groundmass. Metamorphic rock fragments consist of relatively coarse quartz-mica-schist and phyllites. Also present in minor amounts are quartz grains containing inclusions of epidote, which are probably of metamorphic origin. Coarsely crystalline plutonic rocks composed of intergrown quartz and plagioclase and potassium feldspar are present in minor amounts. Chert, siltstone, shale, hornblende, opaques, and heavy minerals are present in minor to moderate amounts.

The wide variety of framework grains suggests a complex source terrane or multiple source areas. The well-sorted texture and lack of detrital matrix suggest a relatively high-energy depositional environment, most likely a littoral setting.

Slight to moderate compaction is indicated by ductilely deformed muscovite and phyllite fragments. Detrital matrix is present in minor amounts. Authigenic smectitic clay coats most framework grains, ridges pore throats, and lines intragranular moldic voids. Pore-lining clinoptilolite, pyrite, and siderite are present in very minor amounts. Reservoir quality in most of this zone is good.

ZONE D-1 (7,900 to 9,555 feet),

OLIGOCENE

Zone D-1 consists of claystone; shale; poorly to moderately sorted, very fine to coarse-grained sandstone; and pebble- and cobble-conglomerate. The drill cuttings contain angular quartz, feldspar, chert, pyrite, mica, coal, volcanic rock fragments, chalcopyrite, siltstone, and rare Foraminifera and mollusc shell fragments. Sixty-four samples from this zone were analyzed by X-ray diffraction: 45 from sidewall cores and 19 from conventional cores 6, 7, 8, and 9. The following minerals and average percentages were identified: 41 percent quartz, 25 percent plagioclase feldspar, 9 percent potassium feldspar, 2 percent siderite, 2 percent calcite, 2 percent pyrite, 1 percent ankerite, 1 percent clinopyroxene, and 17 percent clays. The clay fraction consisted of 24 percent chlorite, 18 percent kaolinite, 7 percent illite, and 51 percent mixed-layer illite-smectite.

Framework grains include quartz; feldspars; volcanic, metamorphic, and sedimentary rock fragments; vesicular pumice; and carbonaceous material. In the conglomerates, the coarse-grained sand- to granule-sized rock fragments are subrounded, whereas the larger sandstone clasts are more angular. Volcanic rock fragments are dark gray-green and contain clear, lath-shaped phenocrysts in a fine-grained matrix. Sedimentary fragments include carbonaceous shale and poorly sorted, fine-grained, cross-bedded and ripple laminated sandstone. Carbonaceous fragments are locally abundant. Detrital matrix is a minor component, and most of the fine-grained material appears to be authigenic. Calcite cement is present in minor to moderate amounts throughout the interval. Coaly fragments are concentrated in the coarser laminae and range in length from 1 millimeter to 1 centimeter. A well-rounded fragment of amber was recovered at 8,092.8 feet. The presence of amber is indicative of coniferous vegetation at the time of deposit. There are probably numerous thin bands of conglomerate in this zone; eight have been observed in conventional cores 7, 8 and 9, with the maximum thickness being about 3 feet. The pebbles and granules of the conglomerate beds are rounded to well rounded and are composed almost exclusively of quartz and fine-grained igneous rock fragments of probable volcanic origin. Minor amounts of gravel-sized metamorphic and sedimentary rock fragments are also present. The conglomerate beds are matrix supported, consisting of elongate granules and pebbles up to 5 centimeters long embedded in a very fine to medium-grained sandy matrix. A small amount of clay is also

present in some of the conglomerate. The bed contacts of the conglomerates are abrupt, and they are usually overlain by finely laminated claystone. Rip-up clasts of mudstone are typically incorporated into the basal part of the conglomerate beds. Two highly altered pelecypod shells greater than 5 centimeters in length occur near the base of one of the conglomerate units. The sand-sized grains of both the conglomerate matrix and the sandstone beds of this zone are composed predominantly of quartz and lithic fragments. Some of the conglomerate is tightly cemented with calcite. Authigenic pyrite is locally abundant and is associated with carbonaceous material.

Based on the nature and relative abundances of framework grains, a likely provenance for the rocks of this zone is a composite volcanic, sedimentary, and metamorphic terrane containing limited exposures of plutonic rocks. The range in particle size (from clay to pebbles) indicates that deposition occurred in an environment with extremely variable energy conditions. The lenticular and wavy sandstone and claystone beds, along with the horizontally laminated claystone beds, are interpreted to represent deposition under the normal or prevailing environmental conditions, whereas the conglomerate beds are interpreted to represent sedimentation from short-duration, high-energy events that periodically interrupted the normal mode of deposition. The sandstone is interpreted to have been deposited as migrating small-scale ripples, whereas the clay laminae accumulated from suspension under quieter conditions. The massive conglomerate units are interpreted to have been rapidly deposited by density or turbidity currents. Evidence in support of this conclusion includes the randomly oriented conglomerate clast fabric, the fact that the conglomerates are matrix supported, the lack of abundant clay in the matrix (which is required for a debris flow), the occurrence of inverse grading of gravel-sized particles, the occurrence of scours at the bases of the conglomerate beds, the incorporation of claystone rip-up clasts in the basal part of the conglomerate beds, and the abrupt return to clay deposition above the conglomerate beds.

The sedimentary rocks of this zone were probably deposited in a marine, lower shoreface environment, as suggested by the occurrence of alternating sandstone and claystone, the abundance of carbonaceous material, the dominance of physical sedimentary structures over biogenic sedimentary structures, and the dominance of horizontal feeding burrows over vertical burrows. The occurrence of conglomerate indicates close proximity to a rocky shoreline, a river-mouth delta, or a fan-delta system from which episodic storm-generated, sediment-laden density currents derived their gravel load.

Diagenesis includes compaction and local precipitation of calcite cement, authigenic clay, clinoptilolite, and siderite. Intergranular porosity was locally enhanced by variable dissolution of volcanic rock fragments, plagioclase, hornblende, and mica. Reservoir potential ranges from none in the siltstone and claystone, to excellent in the well-sorted sandstone.

ZONE D-2 (9,555 to 10,380),

OLIGOCENE AND EOCENE

Zone D-2 consists of fine- to coarse-grained sandstone, siltstone, muddy sandstone, sandy mudstone, and mudstone. The drill cuttings contain quartz, feldspar, volcanic rock fragments, biotite, coal, pyrite, chert, gray sandstone, glauconite, gray siltstone, mollusc shell fragments, and very rare, abraded Foraminifera. Forty-five samples from this zone were analyzed by X-ray diffraction: 11 from sidewall cores, 26 from conventional core 10, and 8 from conventional core 11. The following minerals and average percentages were determined: 32 percent quartz, 22 percent plagioclase feldspar, 6 percent potassium feldspar, 8 percent calcite, 4 percent pyrite, 1 percent siderite, 1 percent ankerite, and 26 percent clays. The clays consist of 33 percent chlorite, 25 percent kaolinite, 6 percent illite, and 36 percent mixed-layer illite-smectite.

The framework constituents are primarily quartz, feldspars, and lithic fragments. Quartz, both monocrystalline and polycrystalline, makes up 4 to 31 percent of the framework grains, feldspars make up 5 to 47 percent, and lithic fragments make up 41 to 89 percent. Polycrystalline quartz occurs with both nonsutured internal grain boundaries characteristic of volcanic quartz, and the elongate, highly sutured internal grain boundaries indicative of a metamorphic origin. Volcanic rock fragments are composed of weakly aligned or randomly oriented lath-shaped plagioclase or hornblende phenocrysts in an altered, yellow-stained glassy groundmass. Some hornblende grains have been altered to chlorite and most are corroded. Most of the altered rock fragments contain no recognizable textures, although they are probably of volcanic origin. Rarely, plagioclase, hornblende, and volcanic rock fragments have been partially to totally dissolved to produce minor amounts of intragranular moldic porosity. Metamorphic rock fragments include quartz-mica schist and phyllite. Plutonic rock fragments are composed of intergrown quartz, plagioclase, and potassium feldspar. Detrital matrix is abundant in most samples examined. Slight to moderate compaction is indicated by the total lack of intergranular porosity and slightly deformed micaceous grains. Authigenic minerals include smectitic clay, pyrite, siderite, clinoptilolite, and calcite. Fossil bivalve fragments occur in many of the samples examined; most exhibit a fibrous structure and a few have been recrystallized to sparry calcite.

The compositional variety of the framework grains indicates a complex or multiple source terrane. The abundance of volcanic and metamorphic rock fragments indicates these constituents were derived from a nearby source. The poorly sorted texture suggests a relatively low-energy, inner or middle neritic depositional environment, although the poor sorting is due in large part to bioturbation.

Post-depositional changes include compaction, the dissolution of plagioclase, quartz overgrowths, and the precipitation of authigenic clays and carbonates. Compaction has caused ductile deformation of chlorite clasts and resulted in an abundant pseudomatrix in about half of the samples. Partial to total dissolution of plagioclase grains has occurred to a minor extent in some samples. Some dissolution voids are filled by clay. The authigenic clay (abundant at 10,355 and 10,447 feet, common at 10,390 and 10,417 feet, and rare at 10,269 and 10,316 feet) consists of kaolinite, green chlorite, and a brown clay that is probably a mixed-layer illite-smectite. Calcite is common to abundant in some samples, where it occurs as large crystals which surround and replace framework grains. Calcite is probably a relatively late diagenetic mineral in all of these samples. Quartz overgrowths are present on many quartz grains and are separated from the host grain by a layer of authigenic chlorite, thus reflecting a later diagenetic event than the chlorite. Siderite is abundant (42 percent of the sample at 10,302 feet) and forms microcrystalline rhombs. It does not appear to replace framework grains and it may have been precipitated during deposition.

Reservoir potential in this zone ranges from fair to none, with most of the zone being very poor because of authigenic mineral precipitation, compaction, the presence of a detrital matrix, and poor sorting. Microporosity is present, but because the pores are not interconnected, the permeability is generally very poor.

ZONE E (10,380 to 15,620 feet),

EOCENE

Zone E consists of very fine to coarse-grained sandstone, pebble- and granule-conglomerate, siltstone, claystone, mudstone, shale, muddy sandstone, sandy mudstone, calcareous sandstone, and ironstone. The drill cuttings consist of quartz, volcanic rock fragments, feldspar, coal, pyrite, light-gray sandstone, chert, biotite, tan and gray siltstone flakes, magnetite, welded tuff, and vein calcite. Eighty-nine samples from this zone were analyzed by X-ray diffraction: 28 from sidewall cores; 5 from conventional core 12; 14 from core 13; 9 from core 14; 7 from core 15; 13 from core 16; and 13 from core 17. The following minerals and average percentages were identified in these samples: 33 percent quartz, 26 percent plagioclase feldspar, 4 percent potassium feldspar, 8 percent calcite, 3 percent siderite, 2 percent pyrite, 1 percent ankerite, 1 percent clinopyroxene, and 22 percent clays. The clays identified were 45 percent chlorite, 15 percent kaolinite, 4 percent illite, 28 percent mixed-layer illite-smectite, and 8 percent mixed-layer chlorite-smectite.

The framework grains are mainly quartz, feldspar, lithic fragments, and undifferentiated silt-sized grains. Quartz occurs both as monocrystalline and polycrystalline grains, indicating volcanic and nonvolcanic origin. Most of the feldspar is plagioclase that exhibits albite twinning and concentric zoning, which are both

characteristic of a volcanic origin. Alteration of the feldspars to calcite and clays is common. The framework grains of the sandy mudstone and sandstone contain the following lithic constituents in order of decreasing abundance: volcanic rock fragments, clay clasts, carbonaceous fragments, shale fragments, plutonic fragments, amphiboles, and micas. The soft, dark-brown clay clasts sometimes contain feldspar grains that are probably remnant volcanic phenocrysts. Reddish-brown carbonaceous material exhibiting woody-plant cell structure is present in some samples. Etched hornblende was observed in trace amounts. Biotite is the predominant mica, although a trace of muscovite is also present. The biotite is sometimes splayed with siderite between some of the cleavage planes. Trace amounts of epidote are present. The volcanic rock fragments, commonly altered to or replaced by chlorite, generally are microcrystalline or porphyritic, with plagioclase microlites or phenocrysts in a microcrystalline groundmass. They commonly exhibit a trachytic texture, with the microlites aligned in a subparallel manner due to flow. The plutonic rock fragments consist of quartz and plagioclase. The intergranular material in the sandstones includes minor clay matrix (which may be authigenic or detrital), authigenic chlorite, authigenic quartz, calcite, and opaques. The chlorite occurs in grain rims, as a fibrous pore-liner, and as radiating sphericles.

The abundance of volcanic lithologies in these samples indicates a source region dominated by basaltic and andesitic rocks. Minor contributions from an associated dioritic plutonic complex are also indicated, as are minor metamorphic and sedimentary inputs. The depositional environment was nonmarine and varied from high to low energy. The presence of conglomerates, cross-bedding, graded beds, and laminated shales and siltstones containing abundant carbonaceous material suggests fluvial channel deposition and related vertical accretion. The claystones were probably deposited in a swamp or coastal lagoon, and the sandstones were deposited during floods as crevasse-splays.

Anatase was one of the first authigenic minerals precipitated, followed by microcrystalline quartz and calcite. Authigenic chlorite was probably precipitated in several stages. Many of the volcanic rock fragments are nearly replaced by clay. Extreme compaction, including rotation of grains and ductile deformation of altered volcanic rock fragments, took place after many of the pore-filling cements were precipitated. The pore-filling elements behaved as rigid framework grains, whereas many of the altered rock fragments have been deformed to the extent that they are molded around the pore-fillers.

Visually estimated porosity and permeability are negligible in most of the samples. Porosity is low because of compaction, the fine grain size of the mudstone, poor sorting, the abundance of detrital matrix, and the presence of pore-filling cements in the sandstone. Primary porosity was low in the sandstone, and secondary porosity produced by the dissolution of feldspars and volcanic rock fragments was effectively destroyed by later authigenic calcite, analcime,

adularia, and chert. Permeability is correspondingly low. Reservoir potential in this zone is poor to nonexistent.

ZONE F (15,620 to 16,652 feet),

EOCENE

Zone F consists of mudstone, siltstone, fine- to coarse-grained sandstone, and both framework-supported and matrix-supported pebble- to cobble-conglomerate. The drill cuttings contain siltstone flakes, volcanic rock fragments, quartz, coal, mica, feldspar, pyrite, chert, sandstone fragments, vein calcite, medium and dark gray finely-micaceous siltstone, and rare calcite prisms. Fourteen samples from core 18 were analyzed by X-ray diffraction and the following minerals and average percentages were obtained: 21 percent quartz, 29 percent calcite, 14 percent plagioclase feldspar, 2 percent pyrite, 2 percent siderite, 1 percent potassium feldspar, and 30 percent clays. The clays consisted of 52 percent chlorite, 27 percent kaolinite, and 21 percent mixed-layer illite-smectite.

Framework grains, in order of abundance, include altered rock fragments, volcanic rock fragments, carbonaceous material, quartz, and feldspar. The volcanic rock fragments are composed of lath-shaped plagioclase and hornblende phenocrysts in a highly-altered cherty groundmass. The chert probably replaces glassy volcanic material. Clays and carbonaceous fragments are commonly ductilely deformed around more rigid grains which, in conjunction with the strong parallel alignment of some samples, indicates moderate to strong compaction. Quartz occurs as both monocrystalline and polycrystalline grains. Plagioclase was the predominant feldspar observed, along with trace amounts of potassium feldspar. All identifiable grains show signs of dissolution or replacement. Most of the altered framework grains are probably of volcanic origin. Matrix is abundant in all samples, although much of it is probably authigenic pseudomatrix.

The source terrane was almost entirely volcanic with minor input from a metamorphic source. The large grain size observed in some of the samples suggests rapid deposition in a relatively high-energy environment with no subsequent winnowing. The sedimentary structures observed in core 19 are characteristic of fluvial channel and overbank flood plain deposits.

In addition to considerable compaction, the diagenetic changes include dissolution, alteration, and the precipitation of authigenic chert, chlorite, smectitic clay, pyrite, and siderite. Abundant authigenic chert is present within the matrix and probably is an alteration product of volcanic material. Calcite has extensively replaced many framework grains and in some cases has almost completely replaced the original rock. In many places, calcite partially replaces detrital quartz and plagioclase as well as plagioclase and hornblende phenocrysts in volcanic rock fragments. Calcite also commonly occurs as a fracture-filling cement.

Authigenic smectitic clay is an abundant alteration product of the feldspars and rock fragments. Authigenic pyrite and siderite are present in minor amounts in the siltstone. Visually-estimated porosity and permeability are negligible. Porosity and permeability, already low due to poor initial sorting, have been further reduced by precipitation of calcite cement and clays, the alteration of labile framework grains to chert and clay, and strong compaction. Samples studied from this zone exhibit no hydrocarbon reservoir potential.

ZONE G (16,652 to 17,155 feet),

EOCENE

Zone G consists of mudstone, siltstone, sandstone, and conglomerate. *Sorting is generally poor throughout the interval.* The drill cuttings contain gray micaceous siltstone fragments, sandstone fragments, mollusc shell fragments, volcanic rock fragments, feldspar, chert, brown glassy sandstone fragments, vein calcite, and rare coal and pyrite. Fourteen samples from conventional core 19 were analyzed by petrographic microscope, scanning election microscope, and X-ray diffraction. The following minerals and percentages were observed: quartz 26, calcite 11, plagioclase feldspar 3, pyrite 3, potassium feldspar 2, siderite 2, and clays 52. The clays consist of 47 percent mixed-layer illite-smectite, 38 percent chlorite, and 15 percent kaolinite. Clay is abundant in most of the core samples but was removed from drill cuttings during processing for microfossils.

The framework grains consist of quartz, feldspar, volcanic rock fragments, schistose metamorphic rock fragments, and shale clasts. The majority of the framework grains are classified as altered rock fragments. Most of these altered grains are probably of volcanic origin. Authigenic chert matrix, authigenic clay, and detrital matrix are abundant. Organic material is locally abundant in the siltstones. The shale clasts may have been derived from within the formation. Authigenic minerals include chert, chlorite, smectitic clay, calcite, pyrite, and siderite. Authigenic chert, clay, and calcite compose the bulk of most of the samples studied from core 19. Authigenic chert is most abundant within the matrix or as an alteration of volcanic rock fragments. Chlorite and mixed-layer illite-smectite clays are very abundant as most rock fragments have been completely altered to these clays. Calcite selectively replaces plagioclase phenocrysts in volcanic rock fragments, whereas the groundmass has been altered to chlorite. Pyrite and siderite occur in minor amounts in most samples and increase in abundance in the organic-rich siltstone.

The source terrane was mainly volcanic with a minor metamorphic input. Fining-upward sequences, ripple and wavy discontinuous lamination, cross bedding, calcite cement, leaf fossils and organic fragments, and scoured basal contacts are common in core 19. Each fining-upward sequence is interpreted to represent a single episode of initial scour, followed by rapid deposition of coarse sediment and

slower deposition of progressively finer material from suspension. These sedimentary structures and sequences are indicative of fluvial channel and overbank deposits.

Visually estimated porosity and permeability are negligible. Primary intergranular porosity is low due to the poorly-sorted texture. Porosity and permeability have been reduced further by precipitation of calcite cement, strong compaction, and the alteration of framework grains to chlorite, smectitic clay, and chert. Core 19, and probably all of zone G, exhibits no hydrocarbon reservoir potential.

A structural dip of approximately 20 degrees was determined from the laminated mudstone in core 19, indicating a possible angular unconformity between cores 18 and 19.

EXPLANATION

Figures 7 through 25

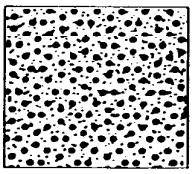
CONGLOMERATE

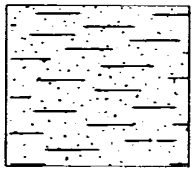
MUDDY SANDSTONE

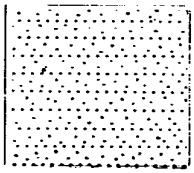
SANDSTONE

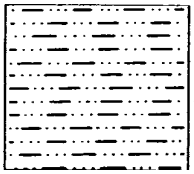
SILTSTONE

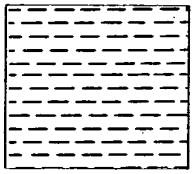
CLAYSTONE

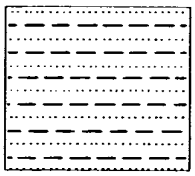
MUDSTONE


FORAMINIFERA


MOLLUSC SHELL


BIOTURBATION

Color codes from the Rock Color Chart, published by the Geological Society of America, reprinted 1970.

Porosity and permeability data from Core Laboratories, Inc.

Random vitrinite reflectance and total organic carbon data from Robertson Research (U.S.), Inc.

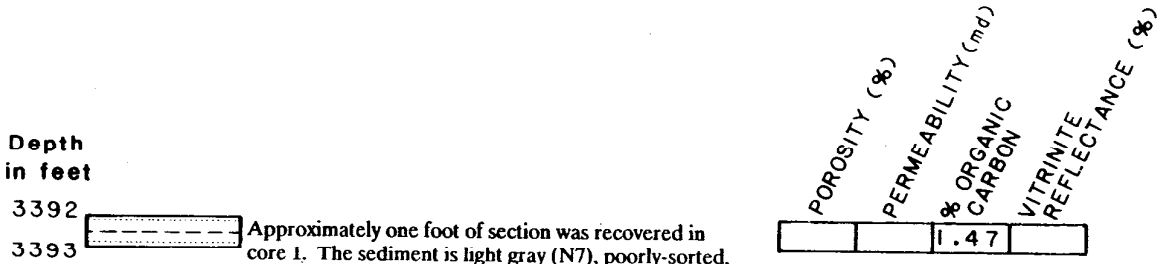

Approximately one foot of section was recovered in core 1. The sediment is light gray (N7), poorly-sorted, laminated, diatomaceous mudstone with thin (0.1 inch), discontinuous lenses of silt and fine- and very fine-grained sand. The sand and silt lenses are well-sorted; the mudstone poorly-sorted. The only primary sedimentary structures visible are horizontally aligned muscovite flakes and silt and sand lenses. The sandstone is a litharenite following the classification of Folk (1970). The framework constituents are angular clasts of quartz, feldspars, and lithic fragments. Minerals present are quartz (38 percent), plagioclase feldspar (15 percent), potassium feldspar (1 percent), siderite (16 percent), pyrite (2 percent), hematite (1 percent), mica (1 percent), and less than 1 percent each of ankerite and calcite. Twenty-six percent of the core consists of clay (36 percent illite and 26 percent mixed- layer illite and smectite). The siderite, pyrite, hematite, ankerite, and calcite are probably authigenic in origin, whereas the clay is probably both detrital and authigenic. Most of the lithic fragments are of volcanic origin, the most common being pumiceous glass fragments with rare plagioclase feldspar microlites in a glassy matrix. Green hornblende is present in trace amounts. Organic fragments and broken diatoms are relatively common. The source area was predominately volcanic, but with some metamorphic input, as suggested by the presence of white mica. The environment of deposition was probably inner neritic. Porosity and permeability data were not obtained from this short core. The porosity in this interval is probably high; the permeability is likely to be low because most of the porosity is represented by micropores within the clay matrix and diatom fragments. The sediment is poorly consolidated. The rock does not appear to possess good reservoir characteristics.

FIGURE 7. **Description of conventional core 1, North Aleutian Shelf COST No.1 well.**

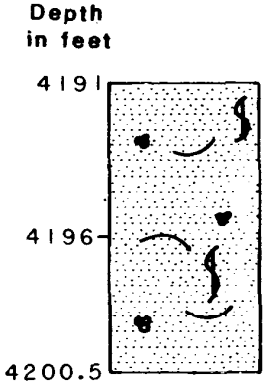

Core 2 is a clay-rich, fine- and medium-grained, medium-light gray sandstone. Color of the core is medium-dark gray (N4) and medium-gray (N5). Angular and rounded chert, black aphanitic volcanic granules, and pebbles up to 0.75 inches in diameter are distributed throughout the core. Primary sedimentary structures have been destroyed by extensive bioturbation. Diatom fragments, organic material, mollusc fragments, and Foraminifera are present. The rock is moderately- to well-sorted and is classified as a feldspathic litharenite. Framework grains are generally subrounded and consist mainly of lithic fragments (47 to 50 percent), quartz (7 to 27 percent), and feldspars (19 to 30 percent). The lithic fragments are volcanic, metamorphic, sedimentary, and plutonic in origin, with volcanic fragments the most abundant. On the basis of whole rock analysis, the minerals present in the cored interval are quartz (44 to 59 percent), plagioclase feldspar (12 to 17 percent), potassium feldspar (5 to 15 percent), pyrite (5 to 8 percent), siderite (1 to 4 percent), and about 1 percent each of hornblende, ankerite, calcite, and clinopyroxene. Minor amounts of epidote and garnet are also present. Clays constitute 10 to 15 percent of the rock (30 percent chlorite, 22 percent kaolinite, and 30 percent mixed-layer illite and smectite). The source terrane was probably mixed volcanic, metamorphic, sedimentary, and igneous, with volcanic being dominant. The bioturbation of the sediments and the presence of well-preserved pelecypod shells indicate a relatively low energy, neritic depositional environment. The clay was probably deposited from suspension and the pebbles were probably transported by storm currents. Compaction has reduced the porosity somewhat. The abundant clay-rich matrix and the lack of large intergranular pores suggest that this rock has low (10 to 350 md) permeability and generally poor reservoir potential.

POROSITY (%)	PERMEABILITY (md)	% ORGANIC CARBON	VITRINITE REFLECTANCE (%)
36.8	262.0		
		0.30	
40.4	11.0		
35.6	16.0		
		0.52	0.26
31.1	20.0	0.32	

FIGURE 8. **Description of conventional core 2, North Aleutian Shelf COST No.1 well.**

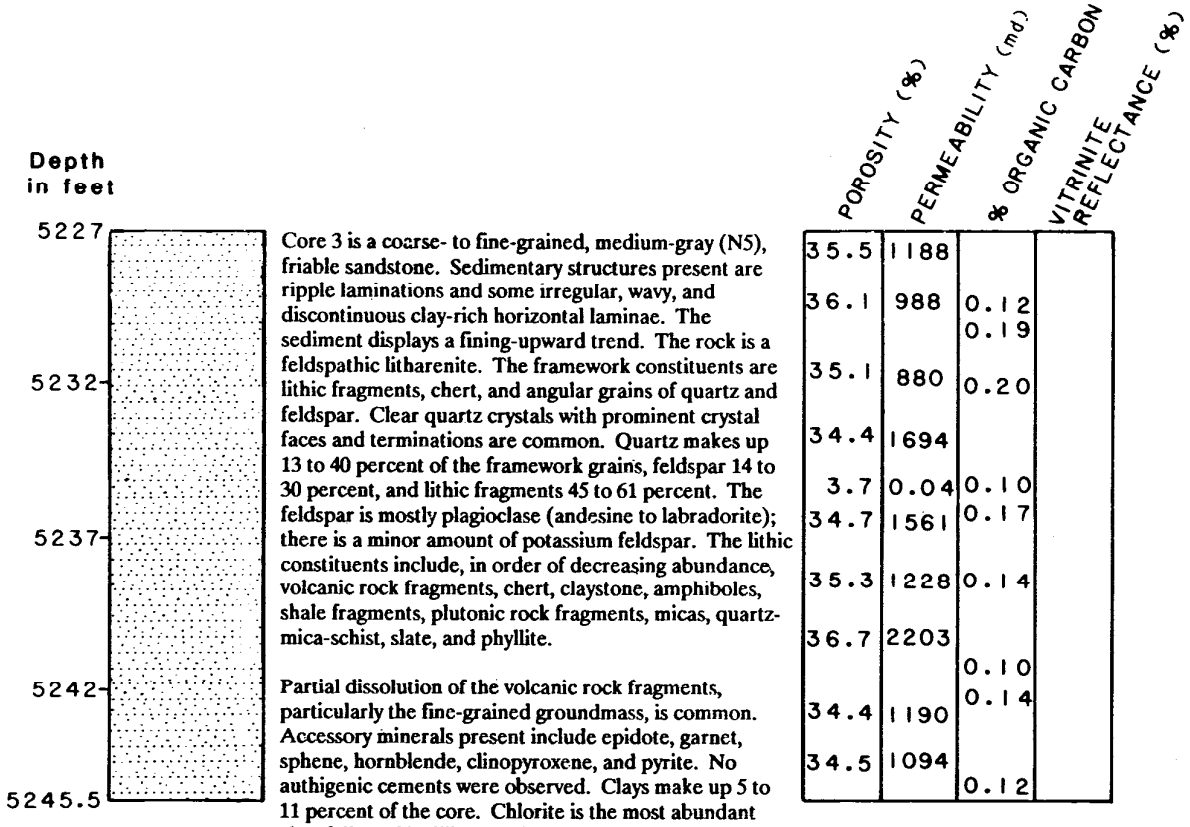

Core 3 is a coarse- to fine-grained, medium-gray (N5), friable sandstone. Sedimentary structures present are ripple laminations and some irregular, wavy, and discontinuous clay-rich horizontal laminae. The sediment displays a fining-upward trend. The rock is a feldspathic litharenite. The framework constituents are lithic fragments, chert, and angular grains of quartz and feldspar. Clear quartz crystals with prominent crystal faces and terminations are common. Quartz makes up 13 to 40 percent of the framework grains, feldspar 14 to 30 percent, and lithic fragments 45 to 61 percent. The feldspar is mostly plagioclase (andesine to labradorite); there is a minor amount of potassium feldspar. The lithic constituents include, in order of decreasing abundance, volcanic rock fragments, chert, claystone, amphiboles, shale fragments, plutonic rock fragments, micas, quartz-mica-schist, slate, and phyllite.

Partial dissolution of the volcanic rock fragments, particularly the fine-grained groundmass, is common. Accessory minerals present include epidote, garnet, sphene, hornblende, clinopyroxene, and pyrite. No authigenic cements were observed. Clays make up 5 to 11 percent of the core. Chlorite is the most abundant clay, followed by illite, kaolinite, and mixed-layer clays. The source area was predominantly volcanic, with minor input from plutonic and metamorphic provenances. Bits of coalified terrestrial plant material are present, some displaying cellular structures. The depositional environment is difficult to estimate because of the unconsolidated and fragmented condition of the core. Changes after deposition include slight compaction and minor dissolution and alteration of plagioclase and volcanic rock fragments. Porosities and permeabilities are high in this interval, which appears to have excellent reservoir qualities.

FIGURE 9. **Description of conventional core 3, North Aleutian Shelf COST No.1 well.**

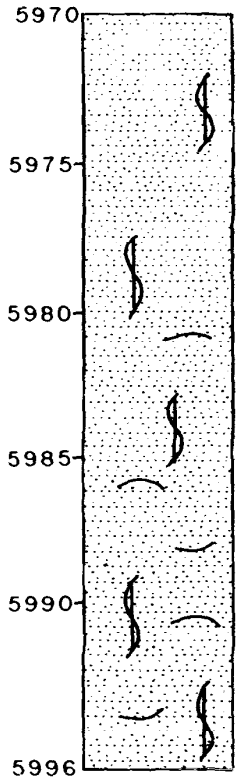

Core 4 consists of fine- and medium-grained, moderately- to very poorly-sorted, medium-gray (N5) sandstone and muddy sandstone. Extensive bioturbation has destroyed any primary sedimentary structures. Rounded chert and volcanic pebbles up to 2 inches in size are present in the lower third of the core. Pelecypod, gastropod, and echinoid fragments are present, including a complete pelecypod valve 1.5 inches long. The sandstones are lithic arkose, feldspathic litharenite, and litharenite. Framework constituents include lithic fragments, quartz, feldspar, and chert. The lithic fragments are mainly of volcanic origin, with smaller amounts of plutonic and metamorphic rock fragments present. The quartz grains are mostly monocrystalline, clear, and angular; some are nearly, perfect doubly-terminated hexagonal prisms of medium-sand size. The feldspars are primarily plagioclase, with some potassium feldspar present. Other minerals present are pyrite, siderite, calcite, ankerite, amphiboles, micas, epidote, garnet, and sphene. Organic fragments are distributed throughout the core. Minor amounts of authigenic minerals include clinoptilolite, pyrite, and clays. Clays make up 5 to 27 percent of the core and include chlorite, kaolinite, illite, and mixed-layer illite-smectite. The provenance was mostly volcanic with some minor input from plutonic and metamorphic terranes. The relatively coarse-grained nature of the sediments in this core, the presence of large pebbles and marine fossil fragments, and the presence of transported terrestrial organic material suggest that these sediments were deposited in an inner neritic environment. Diagenetic features include moderate compaction and the alteration of plagioclase, volcanic clasts, and heavy minerals. Visible porosity is fair in the upper part of the core and poor in the lower part. Permeabilities are generally low, especially in the lower part of the core, because of abundant matrix and authigenic clay. Reservoir potential is poor in the lower part of the core and fair in the upper part.

POROSITY (%)	PERMEABILITY (md)	% ORGANIC CARBON	VITRINITE REFLECTANCE (%)
31.3	129.0	0.31	
		0.24	
31.4	61.0		
		0.39	0.35
31.3	53.0		
32.4	181.0	0.25	
29.8	66.0		
		0.26	
29.8	67.0		
29.7	93.0	0.13	
30.2	61.0		
29.5	30.0	0.32	
30.1	84.0		
		0.38	
28.2	72.0		
27.0	17.0	0.43	
26.3	11.0		
27.0	18.0	0.34	

FIGURE 10. **Description of conventional core 4, North Aleutian Shelf COST No.1 well.**

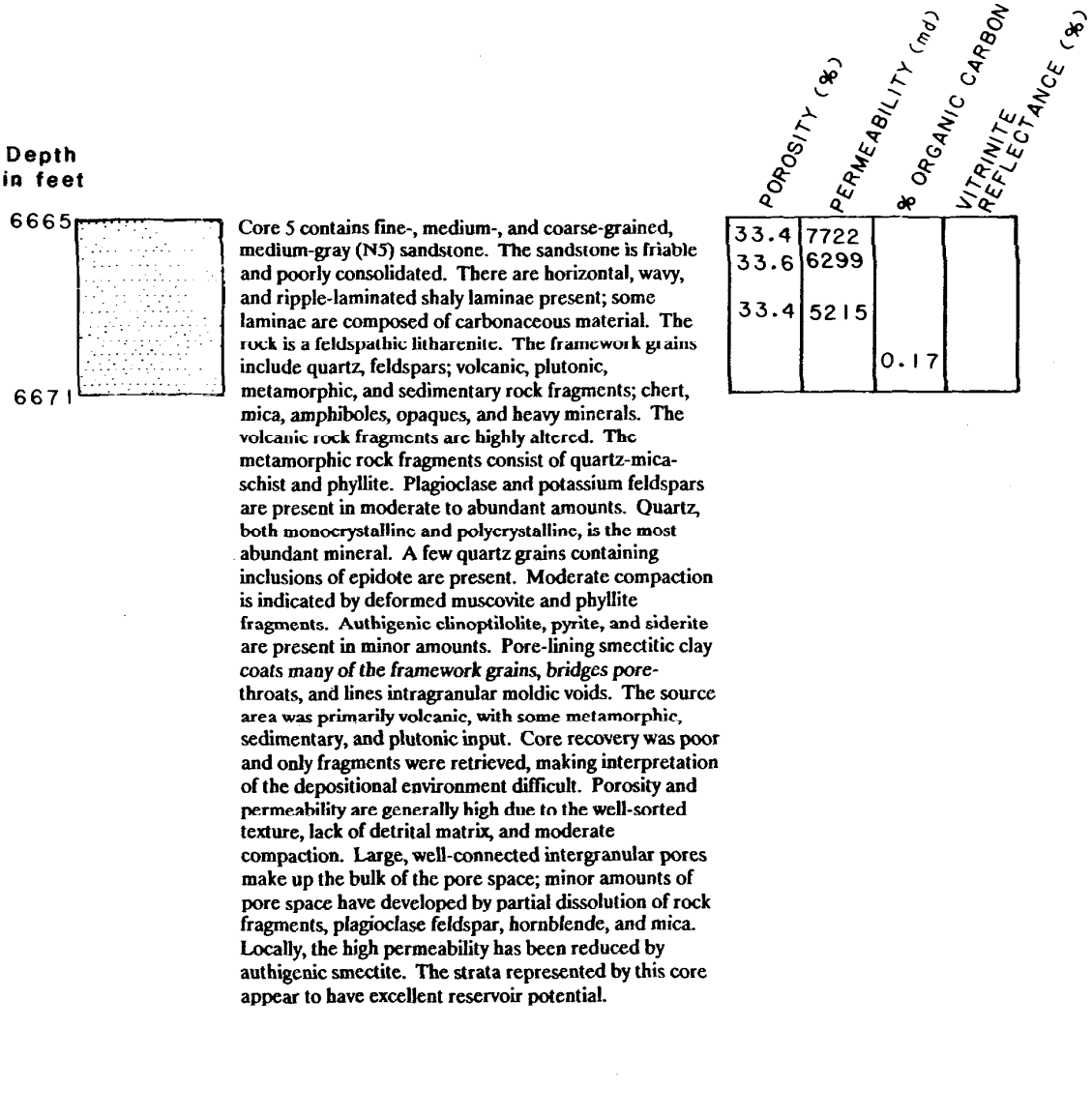

Core 5 contains fine-, medium-, and coarse-grained, medium-gray (N5) sandstone. The sandstone is friable and poorly consolidated. There are horizontal, wavy, and ripple-laminated shaly laminae present; some laminae are composed of carbonaceous material. The rock is a feldspathic litharenite. The framework grains include quartz, feldspars; volcanic, plutonic, metamorphic, and sedimentary rock fragments; chert, mica, amphiboles, opaques, and heavy minerals. The volcanic rock fragments are highly altered. The metamorphic rock fragments consist of quartz-mica-schist and phyllite. Plagioclase and potassium feldspars are present in moderate to abundant amounts. Quartz, both monocrystalline and polycrystalline, is the most abundant mineral. A few quartz grains containing inclusions of epidote are present. Moderate compaction is indicated by deformed muscovite and phyllite fragments. Authigenic clinoptilolite, pyrite, and siderite are present in minor amounts. Pore-lining smectitic clay coats many of the framework grains, bridges pore-throats, and lines intragranular moldic voids. The source area was primarily volcanic, with some metamorphic, sedimentary, and plutonic input. Core recovery was poor and only fragments were retrieved, making interpretation of the depositional environment difficult. Porosity and permeability are generally high due to the well-sorted texture, lack of detrital matrix, and moderate compaction. Large, well-connected intergranular pores make up the bulk of the pore space; minor amounts of pore space have developed by partial dissolution of rock fragments, plagioclase feldspar, hornblende, and mica. Locally, the high permeability has been reduced by authigenic smectite. The strata represented by this core appear to have excellent reservoir potential.

FIGURE 11. **Description of conventional core 5, North Aleutian Shelf COST No.1 well.**

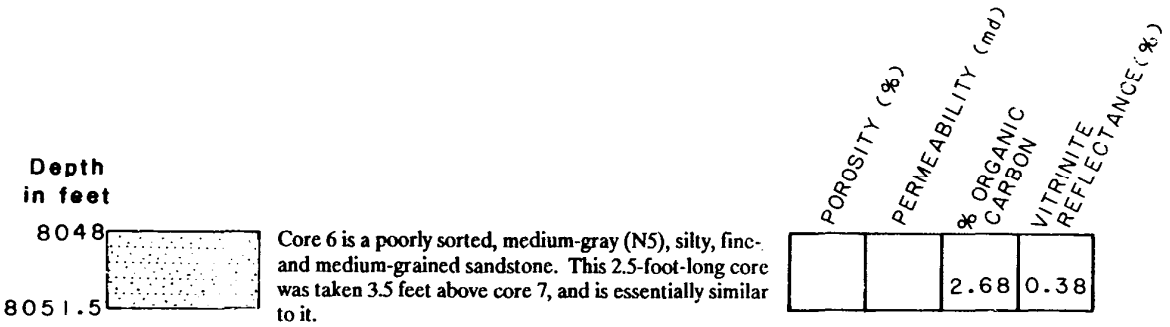

FIGURE 12. Description of conventional core 6 , North Aleutian Shelf COST No.1 well.

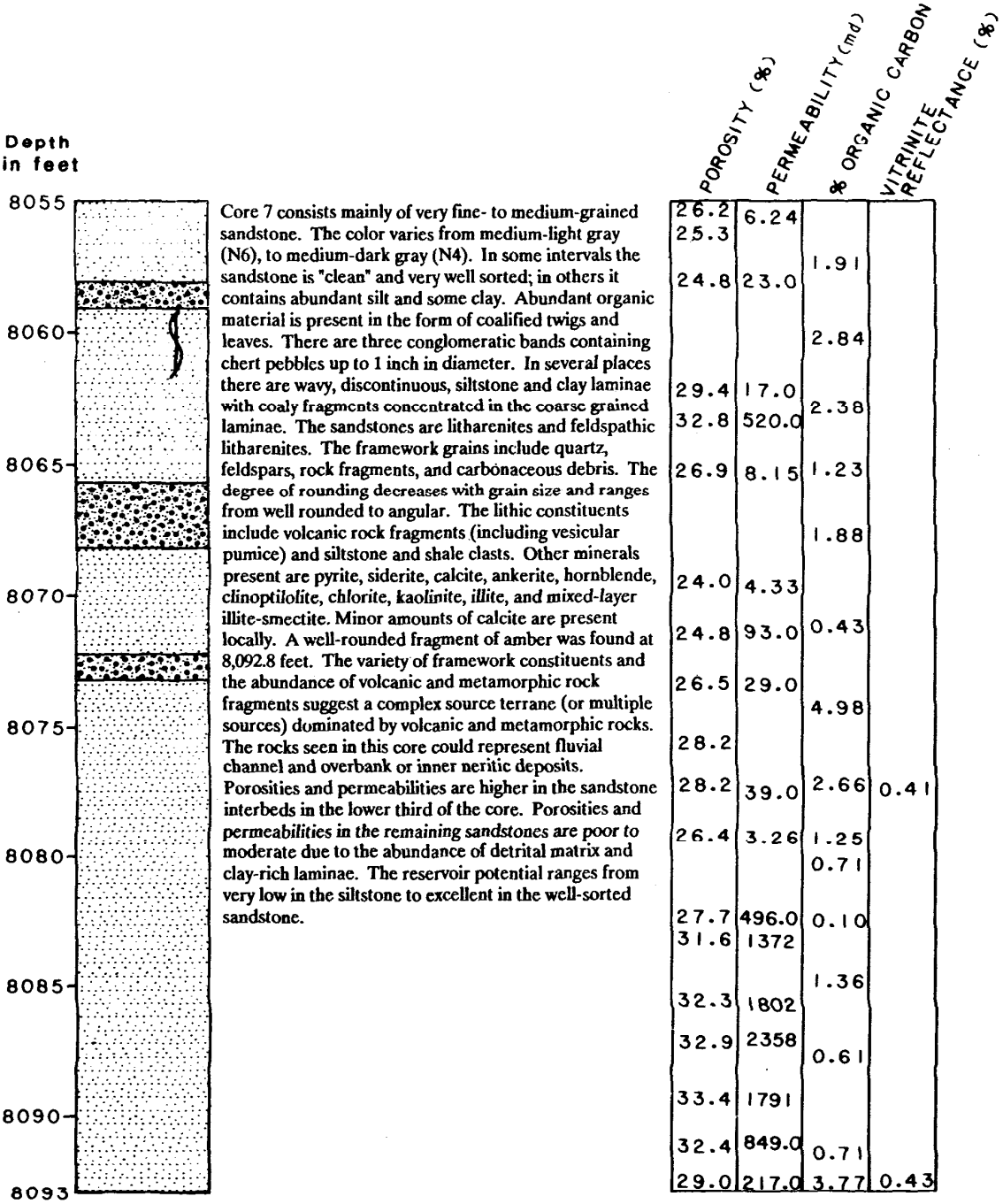

Core 7 consists mainly of very fine- to medium-grained sandstone. The color varies from medium-light gray (N6), to medium-dark gray (N4). In some intervals the sandstone is "clean" and very well sorted; in others it contains abundant silt and some clay. Abundant organic material is present in the form of coalified twigs and leaves. There are three conglomeratic bands containing chert pebbles up to 1 inch in diameter. In several places there are wavy, discontinuous, siltstone and clay laminae with coaly fragments concentrated in the coarse grained laminae. The sandstones are litharenites and feldspathic litharenites. The framework grains include quartz, feldspars, rock fragments, and carbonaceous debris. The degree of rounding decreases with grain size and ranges from well rounded to angular. The lithic constituents include volcanic rock fragments (including vesicular pumice) and siltstone and shale clasts. Other minerals present are pyrite, siderite, calcite, ankerite, hornblende, clinoptilolite, chlorite, kaolinite, illite, and mixed-layer illite-smectite. Minor amounts of calcite are present locally. A well-rounded fragment of amber was found at 8,092.8 feet. The variety of framework constituents and the abundance of volcanic and metamorphic rock fragments suggest a complex source terrane (or multiple sources) dominated by volcanic and metamorphic rocks. The rocks seen in this core could represent fluvial channel and overbank or inner neritic deposits. Porosities and permeabilities are higher in the sandstone interbeds in the lower third of the core. Porosities and permeabilities in the remaining sandstones are poor to moderate due to the abundance of detrital matrix and clay-rich laminae. The reservoir potential ranges from very low in the siltstone to excellent in the well-sorted sandstone.

FIGURE 13. **Description of conventional core 7, North Aleutian Shelf COST No.1 well.**

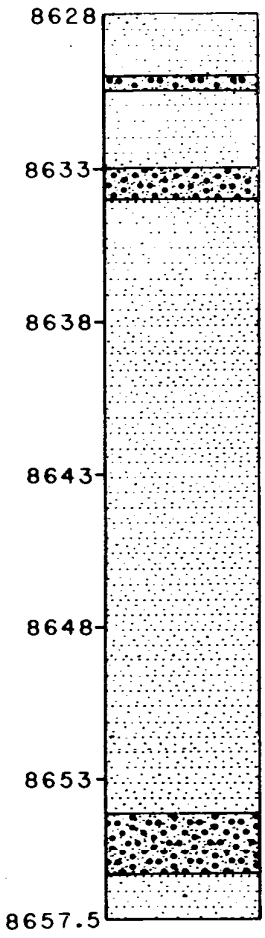

Core 8 consists of moderately- and well-sorted, silty, medium and coarse grained sandstone. The color is medium gray (N5) and medium-light gray (N6). There are three bands of conglomerate that contain siliceous granules and pebbles up to 2 inches in length. Other sedimentary features include fining-upward graded-bed sequences, wavy and low-angle inclined laminae, cross-bedding, ripple laminations, and flame structures. The sandstones are litharenites and feldspathic litharenites. The framework grains are mainly quartz, feldspar, chert, and lithic fragments (volcanic, plutonic, and metamorphic). Lithic fragments make up 39 to 71 percent of the framework grains, quartz 9 to 27 percent, and feldspar 18 to 34 percent. Minerals identified by whole- rock analysis include quartz, feldspar, pyrite, siderite, ankerite, calcite, clinopyroxene, hornblende, zeolites, micas, and very small amounts of other accessory minerals. Authigenic minerals present include zeolites, siderite, and calcite. The clays include chlorite, kaolinite, illite, and mixed-layer illite-smectite. A predominantly volcanic source is suggested by the abundance and variety of volcanic rock fragments, and the presence of hornblende, clinopyroxene, and euhedral and subhedral zoned plagioclase. The plutonic component is represented by coarsely crystalline aggregrates of quartz and feldspar. Lithic constituents from a metamorphic source include pelitic schist, quartzite, polycrystalline quartz, biotite, muscovite, and accessory minerals such as epidote, piedmontite, and kyanite. The presence of argillaceous carbonate rock fragments and chert suggests limited input from sedimentary sources. The sediments seen in the core may have been deposited in a fluvial channel environment, as indicated by an overall fining-upward cycle, basal lag conglomerate, cross- bedding, and the presence of carbonaceous material. Porosity and permeability have been reduced by compaction and locally at 8635.8 feet by pore-filling calcite cement. Authigenic clay, clinoptilolite, and siderite precipitation have reduced pore diameters. Intergranular porosity has been locally enhanced by variable dissolution of volcanic fragments and mica. Overall this core displays good reservoir potential with permeabilities between 100 and 1000 md.

POROSITY (%)	PERMEABILITY (md)	% ORGANIC CARBON	VITRINITE REFLECTANCE (%)
29.8	109.0		
31.3	340.0		
30.7	1040	0.60	
12.5	0.98	0.74	
28.0	67.0	6.34	0.42
30.8	349.0		
30.7	929.0	3.57	
31.8	473.0		
30.8	284.0	3.19	
29.8	336.0		
31.1	123.0	0.09	
31.3	1010		
29.8	132.0		
31.5	460.0	2.28	
24.3		0.76	
30.1	274.0		
		0.16	
31.7	3193		

FIGURE 14. **Description of conventional core 8, North Aleutian Shelf COST No.1 well.**

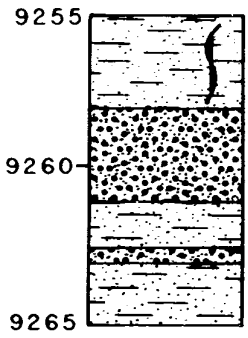

Core 9 consists of interbedded sandstone, claystone, and sandy pebble conglomerate. The color is medium gray (N5) and medium-light gray (N6). The contacts between the interbedded claystone and sandstone are sharp. Horizontal and vertical burrows that have been filled with coarse sand and granules are present in the claystone units. Horizontal burrows, which are more numerous than the vertical and inclined burrows, are as much as 1 inch in diameter. Most of the sand occurs in beds up to 3 inches thick and is medium to very fine grained. Fragments of carbonaceous material are scattered through the sandstone layers and occur as horizontal parting planes in the claystone layers. The matrix-supported conglomerate beds contain granules and pebbles up to 3 inches in a very fine- to medium-grained sandy matrix with minor clay. These rocks are classified as litharenites and feldspathic litharenites. The framework pebbles and granules in the conglomerates are rounded and composed mainly of quartz and volcanic clasts. Minor amounts of metamorphic and sedimentary rock fragments are also present. The sand-sized grains in the core are predominately composed of angular quartz and lithic fragments. Minerals present include quartz, feldspars, pyrite, siderite, calcite, ankerite, hornblende, hematite, and zeolites. Authigenic pyrite is abundant and is associated with the carbonaceous material. Clays present include chlorite, kaolinite, illite, and mixed-layer illite-smectite. Calcite cement, abundant in the upper conglomerate, is rare in other parts of the core. On the basis of the composition and relative abundances of framework grains, a likely provenance for these rocks is a composite volcanic, metamorphic, and sedimentary terrane with limited exposures of plutonic rocks. The range in particle size (from clay to pebble) indicates a depositional environment characterized by variable energy conditions. These rocks were probably deposited in an inner neritic environment near a rocky shoreline, a river mouth delta, or a fan delta system. There are some intervals with good porosity and permeability, but overall, this core does not represent good reservoir rock.

POROSITY (%)	PERMEABILITY (md)	% ORGANIC CARBON	VITRINITE REFLECTANCE (%)
19.6	13.0		
25.2	1615.0		
18.8	189.0	2.16	0.41
5.8	0.11		
12.7	1.91		
21.2	867.0		
		0.50	
22.1	436.0	1.93	0.40
		1.28	

FIGURE 15. **Description of conventional core 9, North Aleutian Shelf COST No.1 well.**

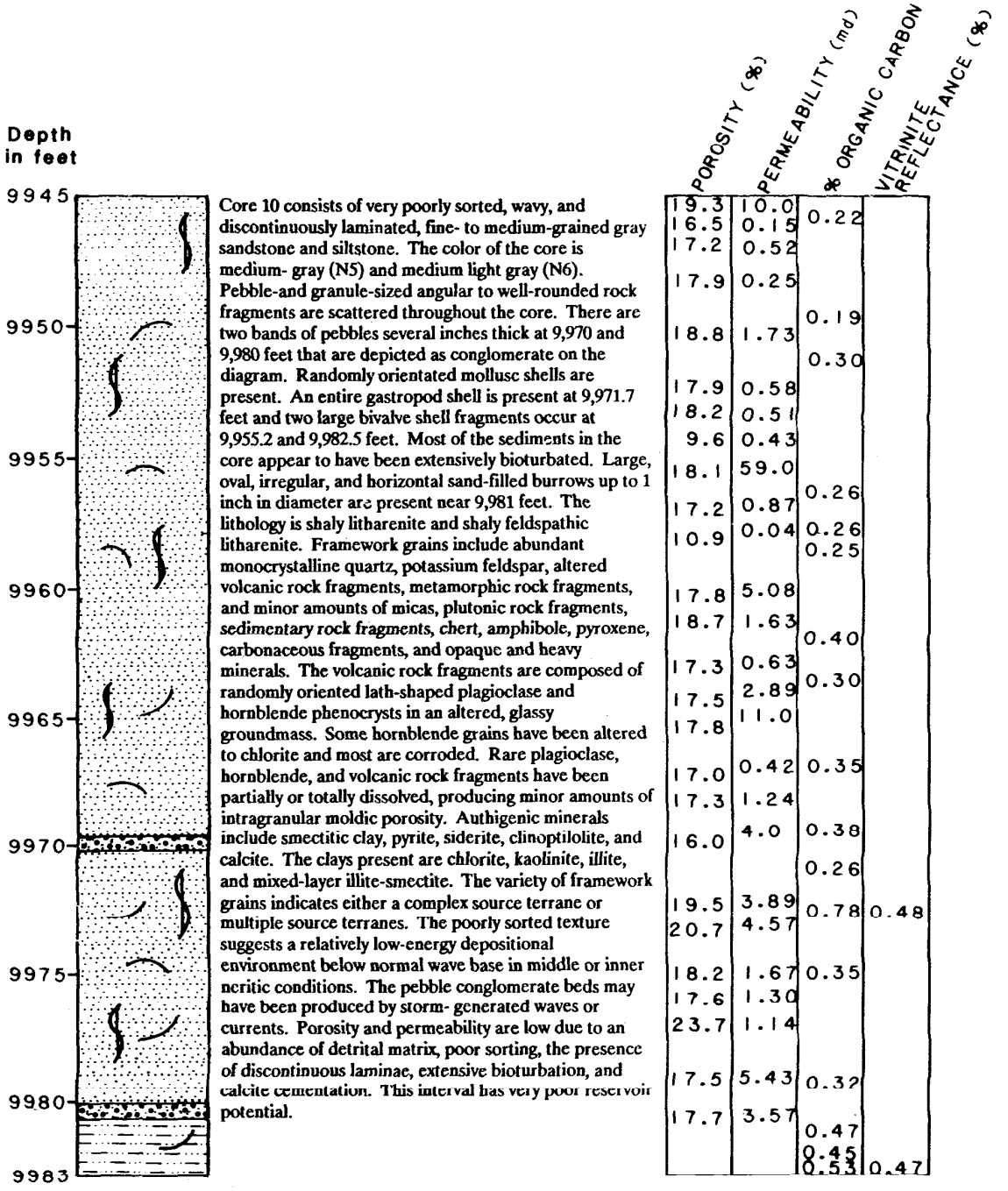

Core 10 consists of very poorly sorted, wavy, and discontinuously laminated, fine- to medium-grained gray sandstone and siltstone. The color of the core is medium- gray (N5) and medium light gray (N6). Pebble-and granule-sized angular to well-rounded rock fragments are scattered throughout the core. There are two bands of pebbles several inches thick at 9,970 and 9,980 feet that are depicted as conglomerate on the diagram. Randomly orientated mollusc shells are present. An entire gastropod shell is present at 9,971.7 feet and two large bivalve shell fragments occur at 9,955.2 and 9,982.5 feet. Most of the sediments in the core appear to have been extensively bioturbated. Large, oval, irregular, and horizontal sand-filled burrows up to 1 inch in diameter are present near 9,981 feet. The lithology is shaly litharenite and shaly feldspathic litharenite. Framework grains include abundant monocrystalline quartz, potassium feldspar, altered volcanic rock fragments, metamorphic rock fragments, and minor amounts of micas, plutonic rock fragments, sedimentary rock fragments, chert, amphibole, pyroxene, carbonaceous fragments, and opaque and heavy minerals. The volcanic rock fragments are composed of randomly oriented lath-shaped plagioclase and hornblende phenocrysts in an altered, glassy groundmass. Some hornblende grains have been altered to chlorite and most are corroded. Rare plagioclase, hornblende, and volcanic rock fragments have been partially or totally dissolved, producing minor amounts of intragranular moldic porosity. Authigenic minerals include smectitic clay, pyrite, siderite, clinoptilolite, and calcite. The clays present are chlorite, kaolinite, illite, and mixed-layer illite-smectite. The variety of framework grains indicates either a complex source terrane or multiple source terranes. The poorly sorted texture suggests a relatively low-energy depositional environment below normal wave base in middle or inner neritic conditions. The pebble conglomerate beds may have been produced by storm- generated waves or currents. Porosity and permeability are low due to an abundance of detrital matrix, poor sorting, the presence of discontinuous laminae, extensive bioturbation, and calcite cementation. This interval has very poor reservoir potential.

FIGURE 16. Description of conventional core 10, North Aleutian Shelf COST No.1 well.

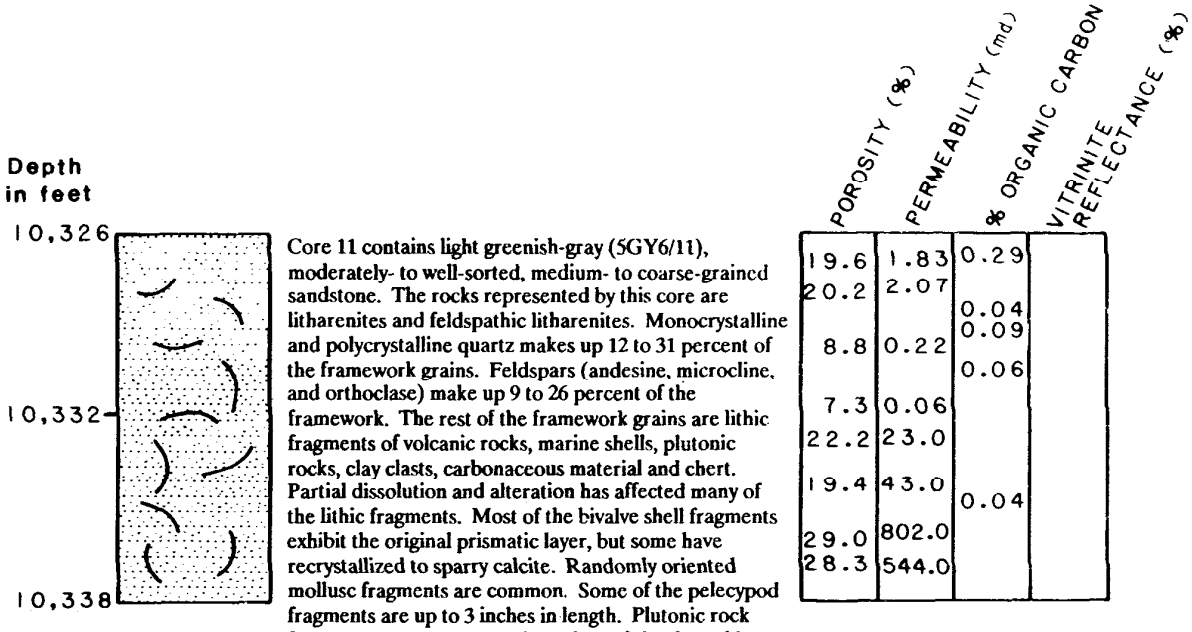

Core 11 contains light greenish-gray (5GY6/11), moderately- to well-sorted, medium- to coarse-grained sandstone. The rocks represented by this core are litharenites and feldspathic litharenites. Monocrystalline and polycrystalline quartz makes up 12 to 31 percent of the framework grains. Feldspars (andesine, microcline, and orthoclase) make up 9 to 26 percent of the framework. The rest of the framework grains are lithic fragments of volcanic rocks, marine shells, plutonic rocks, clay clasts, carbonaceous material and chert. Partial dissolution and alteration has affected many of the lithic fragments. Most of the bivalve shell fragments exhibit the original prismatic layer, but some have recrystallized to sparry calcite. Randomly oriented mollusc fragments are common. Some of the pelecypod fragments are up to 3 inches in length. Plutonic rock fragments are common and consist mainly of roughly equant grains of plagioclase and potassium feldspar. Clay clasts and glauconite are common. Chlorite constitutes up to 32 percent of the framework grains and is probably an alteration product of the volcanic rock fragments. Micas are a minor constituent and include biotite and muscovite flakes that have been splayed and ductilely deformed. Carbonaceous fragments are scattered throughout the core and occur in horizontal seams. Chert is present in trace amounts in all the samples. Diagenetic changes include compaction, dissolution of framework grains, and the precipitation of authigenic cements that include calcite, kaolinite, chlorite, siderite, potassium feldspar, albite, quartz, pyrite, anatase, and chert. The abundance of volcanic rock fragments indicates a predominately volcanic source terrane. The intervals of well-sorted coarse sand and the presence of large, thick shell fragments indicate a relatively high- energy depositional environment, perhaps inner neritic. Dissolution has created some secondary porosity, some of which has since been filled with authigenic minerals. The reservoir potential in this interval ranges from good to practically none.

FIGURE 17. **Description of conventional core 11, North Aleutian Shelf COST No.1 well.**

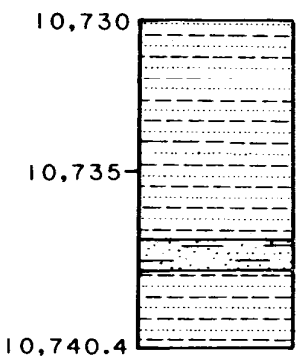

Core 12 is mudstone with a 1-foot-thick layer of medium-grained muddy sandstone at 10,737 feet. The sediment colors are medium-light gray (N6), medium gray (N5), and medium-dark gray (N4). Where there are coal fragments, the color is black (N1). The only apparent sedimentary features are parallel, horizontal laminae in the lower part of the core. No bioturbation or marine bioclastic material was observed. The rocks are feldspathic litharenites. Framework constituents in the sandstone layer consist of quartz, feldspar, and lithic fragments. Quartz makes up 11 to 13 percent of the framework grains and the feldspars 18 to 29 percent. Plagioclase is the predominant feldspar. Lithic framework grains, in order of decreasing abundance, are volcanic rock fragments, clay clasts, carbonaceous fragments, shale fragments, and plutonic rock fragments. Carbonaceous particles that range in size from 0.05 to 0.5 inches and retain cellular structure indicative of woody plants are distributed throughout the core. Plutonic rock fragments are a minor constituent and consist of equant grains of feldspar and quartz. Hornblende occurs in trace amounts and is strongly etched. Biotite is more common than muscovite. Microcrystalline and granular siderite is abundant in the lower part of the core. The source area was mainly volcanic with minor contributions from metamorphic and plutonic terranes. The depositional environment appears to have been characterized by low energy and may have been lacustrine, paludal, or a flood plain. Diagenesis includes compaction; the precipitation of abundant siderite and pore-filling chlorite and clinoptilolite or heulandite; and the growth of authigenic potassium feldspar and chert in the matrix. Most of the porosity and permeability have been diagenetically destroyed with the exception of a limited amount of fracture porosity in the mudstone and within framework grains. The sandstone layer is tightly cemented with calcite. This core does not represent good reservoir rock.

POROSITY (%)	PERMEABILITY (md)	% ORGANIC CARBON	VITRINITE REFLECTANCE (%)
		0.34	
22.4	0.19		
		0.67	
		0.48	
24.1	130.0		
13.4	0.95		
19.9	1.73	0.27	
		4.92	
28.0	74.0		

FIGURE 18. **Description of conventional core 12 . North Aleutian Shelf COST No.1 well.**

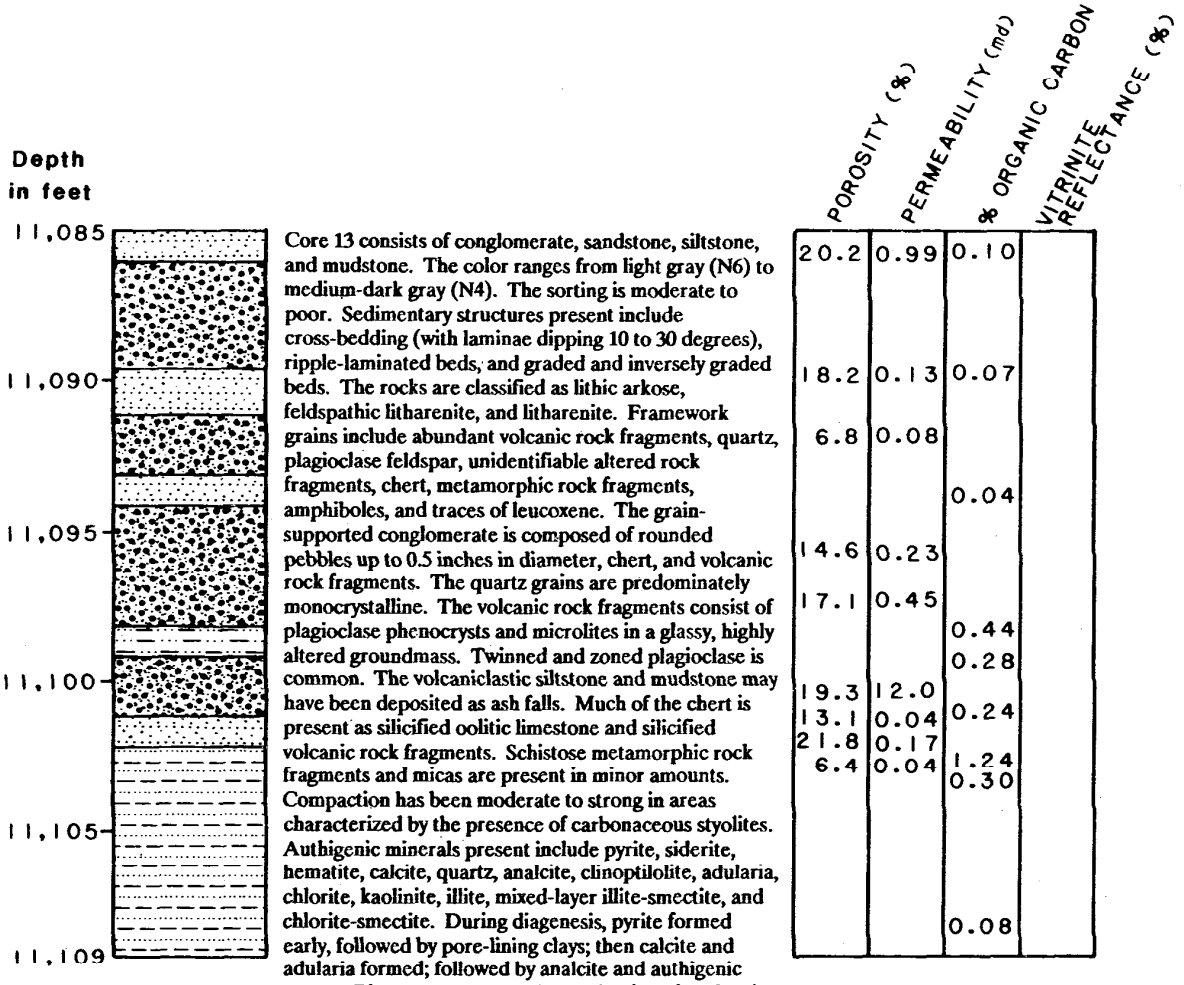

Core 13 consists of conglomerate, sandstone, siltstone, and mudstone. The color ranges from light gray (N6) to medium-dark gray (N4). The sorting is moderate to poor. Sedimentary structures present include cross-bedding (with laminae dipping 10 to 30 degrees), ripple-laminated beds, and graded and inversely graded beds. The rocks are classified as lithic arkose, feldspathic litharenite, and litharenite. Framework grains include abundant volcanic rock fragments, quartz, plagioclase feldspar, unidentifiable altered rock fragments, chert, metamorphic rock fragments, amphiboles, and traces of leucoxene. The grain-supported conglomerate is composed of rounded pebbles up to 0.5 inches in diameter, chert, and volcanic rock fragments. The quartz grains are predominately monocrystalline. The volcanic rock fragments consist of plagioclase phenocrysts and microlites in a glassy, highly altered groundmass. Twinned and zoned plagioclase is common. The volcaniclastic siltstone and mudstone may have been deposited as ash falls. Much of the chert is present as silicified oolitic limestone and silicified volcanic rock fragments. Schistose metamorphic rock fragments and micas are present in minor amounts. Compaction has been moderate to strong in areas characterized by the presence of carbonaceous styolites. Authigenic minerals present include pyrite, siderite, hematite, calcite, quartz, analcite, clinoptilolite, adularia, chlorite, kaolinite, illite, mixed-layer illite-smectite, and chlorite-smectite. During diagenesis, pyrite formed early, followed by pore-lining clays; then calcite and adularia formed; followed by analcite and authigenic quartz. The source terrane was predominantly volcanic. The depositional environment was probably a braided stream complex and flood plain. The reservoir potential represented by this core ranges from negligible to fair locally, and is related to the amount of authigenic mineral growth in the pore spaces of the sandstone and conglomerates. The nonreservoir rocks are the fine-grained volcanic siltstone and mudstone.

FIGURE 19. **Description of conventional core 13, North Aleutian Shelf COST No.1 well.**

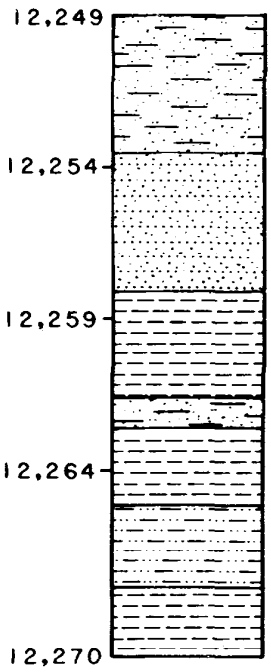

Core 14 contains sandstone, muddy sandstone, siltstone, and claystone. The contacts are gradational. The color ranges from black (where there are coal layers nearly 0.5 inch thick) to medium-light gray (N6). The grain size ranges from clay to medium sand. Carbonized leaf and twig debris is distributed throughout, often in thin, horizontal laminae. Visible sedimentary structures include fining-upward sequences, cross-bedding, and wavy, discontinuous bedding. The lithologies present are lithic arkose, feldspathic litharenite, and litharenite. The framework grains consist of quartz, feldspar, and rock fragments. Anhedral to subhedral quartz composes up to 35 percent of the framework grains. Feldspars make up 15 to 68 percent of the framework grains. The relative abundance of plagioclase and potassium feldspars is variable due to the local replacement of plagioclase by adularia. The andesine present commonly displays oscillatory zoning and often has been replaced by adularia, kaolinite, mixed-layer clay, and calcite. Lithic fragments constitute 23 to 80 percent of the framework clasts and are mainly volcanic fragments with lesser amounts of mica, sedimentary rock, and chert. Biotite and muscovite display ductile deformation. The rare sedimentary rock fragments present are mostly mudstone and calcarenite. Accessory heavy minerals present include epidote, iron-titanium oxides, and apatite. Clay matrix constitutes up to 68 percent of the core in some places. Authigenic kaolinite, chlorite, illite, and mixed- layer clays fill the pores. Other authigenic minerals present are calcite, siderite, pyrite, quartz, and clinoptilolite. Amber is present in trace amounts. The source area for these deposits was predominately volcanic with minor input from plutonic, metamorphic, and sedimentary terranes. The sandstones, siltstones, and claystones were probably deposited in a nonmarine flood basin associated with a fluvial system. The claystones are overbank backswamp deposits and the sandstones are probably crevasse-splay flood deposits. The post- depositional reduction in porosity and permeability is attributable to the widespread development of pore-lining and pore-filling authigenic clay, and the local precipitation of pore-filling calcite cement. The section represented by this core has very poor reservoir potential.

POROSITY (%)	PERMEABILITY (md)	% ORGANIC CARBON	VITRINITE REFLECTANCE (%)
2.31	0.26	0.14	
11.8	0.15		
		5.23	0.52
6.2	5.02		
		0.03	
		0.04	
9.6	0.04		
17.4	1.74		
		0.97	
		35.89	0.57
		0.61	
		1.11	
10.5	2.56		
		0.80	
		28.77	0.55
		0.24	

FIGURE 20. **Description of conventional core 14, North Aleutian Shelf COST No.1 well.**

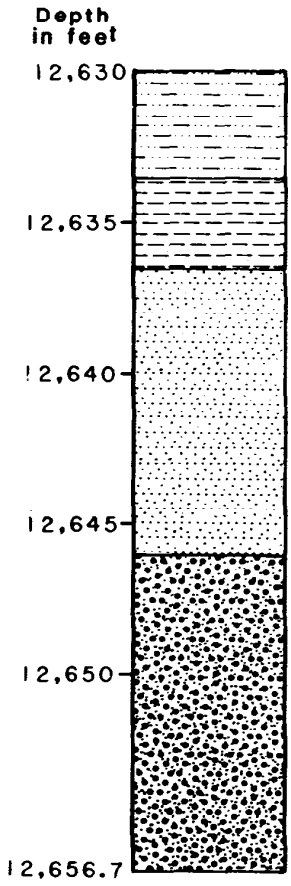

Core 15 consists of several different but related lithologies. The top 3.5 feet is volcanic siltstone, the next 3 feet is claystone, followed by 9.5 feet of sandstone and 10.7 feet of volcanic pebble conglomerate. The colors are various shades of gray. The particle-size range is from clay to pebble. Most of the sediments are poorly sorted, but some of the sandstone and siltstone is well sorted. The visible sedimentary structures include wavy and lenticular laminations, small, localized cross-beds, and some fining-upward sequences. The framework constituents are mainly quartz, plagioclase feldspar, and volcanic lithic fragments. Potassium feldspar is exceedingly rare. There are a few metamorphic and sedimentary rock fragments. Both monocrystalline and polycrystalline quartz grains are present and make up about 4 percent of the framework. The plagioclase feldspar, which makes up 21 to 39 percent of the framework grains, displays considerable zoning and patchy optical extinction. Some plagioclase appears to have been replaced by calcite. The volcanic rock fragments are microcrystalline or porphyritic and are commonly altered to or replaced by chlorite. Intergranular material in the sandstones includes detrital and authigenic clay matrix, authigenic chlorite, authigenic quartz, calcite, and pyrite. The chlorite occurs as rims about 0.05 inch thick on the grains, as fibrous pore-lining material, and as radial spherules. Diagenesis includes compaction, precipitation of quartz coatings, calcite cementation, dissolution of lithic fragments, zeolite precipitation, and pore filling with chlorite. The source area was mainly volcanic. The upper half of the core contains abundant disseminated coal and thin lignite seams. On the basis of the fining-upward sequences, basal conglomerate section, cross-bedding and graded beds, and the organically rich laminated shales and siltstones at the top of the interval, this core probably represents a fluvial channel (and related vertical accretion) deposit. Porosity and permeability are low due to poor sorting, abundant phyllosilicate matrix, pore-filling authigenic minerals, and compaction. This core does not represent good reservoir rock.

POROSITY (%)	PERMEABILITY (md)	% ORGANIC CARBON	VITRINITE REFLECTANCE (%)
		3.65	
		0.66	
		1.74	0.64
		5.87	0.60
		5.14	
		1.20	
19.1	2.27		
		0.09	
12.4	0.02		
19.0	0.02		
15.6	0.01		
16.9	0.04		
10.0	0.02		

FIGURE 21. **Description of conventional core 15, North Aleutian Shelf COST No. 1 well.**

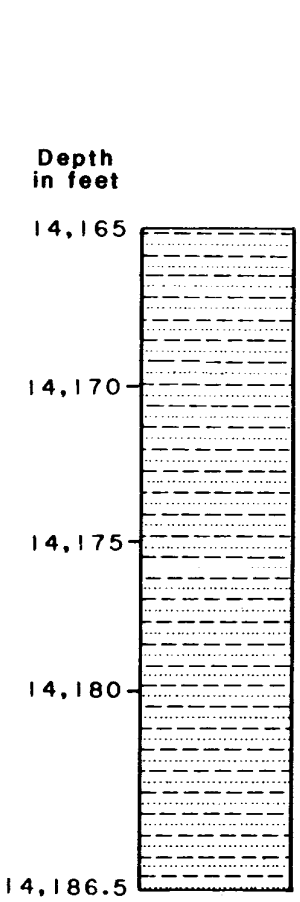

Core 16 consists of claystone, mudstone, siltstone, and sandstone. The color ranges from grayish black (N2) to very light gray (N8). The sedimentary structures visible include abundant parallel laminations, small-scale ripples, scours, and root structures. The lithology is a feldspathic litharenite. The samples examined include calcareous, moderately- to well-sorted, laminated mudstone; poorly sorted, calcareous, zeolitic, feldspathic litharenite; and lithic arkose with angular to subrounded grains. These rocks contain abundant authigenic chert matrix and moderate to abundant patchy calcite and analcime cements. Carbonaceous fragments, rootlets, and organic stringers are common. The sand- and silt-sized grains consist of quartz, feldspar, and volcanic rock fragments. The mudstone is interlaminated with sandy mudstone and sandstone. The framework grains include moderate amounts of monocyrstalline quartz, rare polycrystalline quartz, moderate amounts of twinned and zoned plagioclase, rare potassium feldspar, abundant highly altered volcanic rock fragments, and rare hornblende and carbonaceous fragments. Volcanic rock fragments are composed of twinned and zoned plagioclase phenocrysts in an altered and glassy groundmass. Slight to moderate compaction is indicated by ductilely deformed micas, and compacted clays and carbonaceous fragments. Authigenic minerals present include pyrite, siderite, calcite, analcime, adularia, and chert. The clays present are chlorite, kaolinite, illite, and mixed-layer illite- smectite. The source area was almost entirely volcanic with only minor input from a metamorphic terrane. These clay-rich rocks were probably deposited in a quiet environment characterized by periodic influxes of sand. Deposition occurred in the form of wavy laminations, probably due to the presence of abundant plant material and soft, readily deformed sediments. The most likely depositional environments were a nonmarine fluvial, paludal and lacustrine flood basin. Porosity and permeability are negligible due to the poorly sorted texture and the abundance of detrital matrix. Calcite cement and authigenic mineral deposition have further reduced the pore space. These rocks do not display any reservoir potential.

POROSITY (%)	PERMEABILITY (md)	% ORGANIC CARBON	VITRINITE REFLECTANCE (%)
10.3	0.02		
		13.91	
		17.84	
5.0	0.04		
2.0	0.03		
10.3	0.09	18.69	0.64
		17.18	
1.9	0.04		
		10.19	
14.9	0.11		
14.1	0.10	3.98	

FIGURE 22. **Description of conventional core 16, North Aleutian Shelf COST No.1 well.**

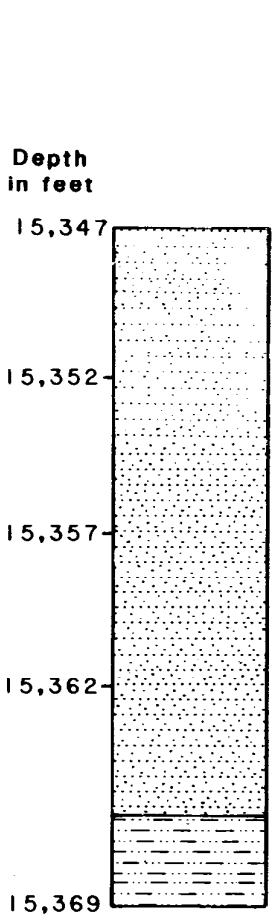

Core 17 consists of 19 feet of medium-light gray (N6) poorly to moderately sorted, medium- to coarse-grained sandstone underlain by 3 feet of medium-dark gray (N4) shaly siltstone. The basal 3 feet contains thin, discontinuous laminae of light gray, fine- and medium-grained sandstone. Carbonaceous fragments up to 0.2 inches in diameter are present. The upper 19 feet of the core is texturally and mineralogically homogeneous. Rip-up clasts of shale with deformed internal laminae occur at several locations. The clasts are up to 0.5 inch in diameter, nearly horizontal and have scoured upper contacts. The fine-grained horizons represent periods of essentially nondeposition between periods of sandstone deposition. Organic material is present throughout much of the sandstone as thin carbonaceous fragments up to 0.5 inch in diameter. These rocks are classified as feldspathic litharenites and litharenites. Framework constituents in the sandstone include quartz, feldspar, and lithic fragments. Monocrystalline and polycrystalline quartz grains make up 1 to 5 percent of the framework grains, feldspars 17 to 41 percent, and lithic fragments 42 to 82 percent. The feldspars are almost exclusively plagioclase. The plagioclase grains exhibit both albite twinning and concentric zoning. Alteration of the plagioclase to calcite and clays is common. The lithic constituents consist primarily of volcanic fragments containing feldspar microlites and a microcrystalline groundmass altered to dark-brown clay matrix, chlorite, and calcite. Some volcanic rock fragments have been totally altered. Intergranular material in the sandstone consists of clay matrix, and authigenic chlorite, quartz, calcite, anatase, and opaques. The primary source area was volcanic. A few rock fragments contain biotite and muscovite, which indicates a minor input from a metamorphic or plutonic source area. The depositional environment was probably nonmarine, fluvial and lacustrine. The porosity and permeability of these rocks have been greatly reduced by compaction. This core displays no reservoir potential.

POROSITY (%)	PERMEABILITY (md)	% ORGANIC CARBON	VITRINITE REFLECTANCE (%)
9.1	0.02	0.42	
9.1	0.02		
		0.91	
6.5	0.02		
7.0	0.02	0.51	
10.0	0.02		
		2.59	
10.8	0.05		
10.8	0.05		
11.3	0.05	1.06	
		0.67	
		0.62	
		0.78	
		0.82	0.77

FIGURE 23. **Description of conventional core 17, North Aleutian Shelf COST No.1 well.**

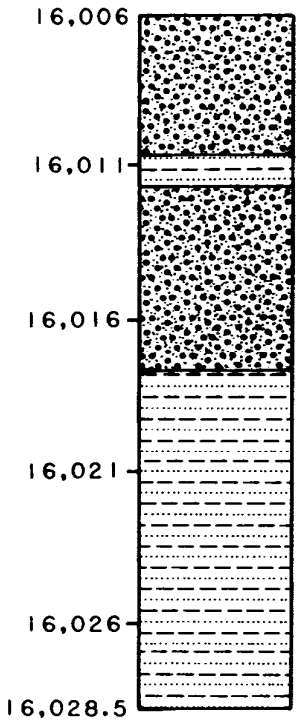

Core 18 contains a mixture of conglomerate, sandstone, siltstone, mudstone, and claystone. The color ranges from light to dark gray. The top 4.5 feet are pebble- to cobble- conglomerate with silt- to sand-sized matrix. The next foot down is siltstone with stringers of medium-sized quartz and feldspar grains. The next 6 feet are conglomerate similar to the top 4.5 feet of the core. The lower 11 feet consists of silty sandstone, silty mudstone, and claystone in stacked, fining-upward sequences. Sedimentary structures include horizontal and low-angle, parallel laminations, ripple laminations, wavy and discontinuous laminations, and cross-bedding. A typical fining-upward sequence consists of low-angle, parallel- laminated sandy siltstone, with sandstone laminae grading upward into laminated silty mudstone, containing abundant coaly plant fragments and leaf impressions. There is a pebbly layer at 16,020 feet. The framework grains present, in order of decreasing abundance, include altered rock fragments, volcanic rock fragments, carbonaceous rock fragments, quartz, and feldspar. The volcanic rock fragments are composed of lath-shaped plagioclase feldspar and hornblende phenocrysts in a highly altered cherty groundmass. Authigenic minerals present include chert, calcite, smectitic clay, pyrite, and siderite. Pyrite and siderite are present in minor amounts in the siltstone. Clays present include chlorite, kaolinite, illite, and mixed- layer illite-smectite. Most of the large clasts are of volcanic origin, which indicates a predominately volcanic source terrane. The large grain size and poorly sorted texture of some intervals suggest rapid deposition in a relatively high-energy environment without subsequent winnowing. The conglomeratic sections may represent debris flows. The finer grained lithologies appear to be floodplain deposits. Visually estimated porosities and permeabilities are negligible. Compacted clays and carbonaceous fragments have been ductilely deformed around more rigid grains, which, in conjunction with the strong parallel alignment in some areas, indicates moderate to strong compaction. Porosity and permeability have been further reduced by calcite cement and the precipitation of chert and authigenic clays. The strata represented by this core have no reservoir potential.

POROSITY (%)	PERMEABILITY (md)	% ORGANIC CARBON	VITRINITE REFLECTANCE (%)
13.2		1.35	
15.5	3.88		
		1.76	0.94
9.6			
		1.48	
12.5	2.23		
8.1	0.02		
15.3	4.25	1.22	
		0.98	
1.3	0.02		
		0.88	
		2.05	
11.7		1.45	
		1.58	

FIGURE 24. Description of conventional core 18 , North Aleutian Shelf COST No.1 well.

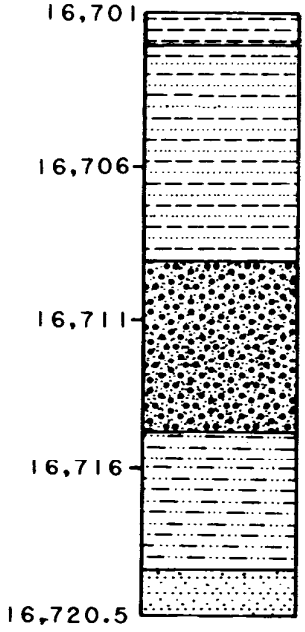

Core 19 contains conglomerate, sandstone, siltstone, claystone, and mudstone. The core can be conveniently divided into three zones. From 16,701 to 16,709 feet, there is a sequence of stacked, fining-upward layers 0.5 to 2.5 feet thick. The beds grade from ripple-laminated sandstone to wavy- and horizontally-laminated mudstone. Organic fragments and leaf impressions are locally abundant in the siltstone and mudstone. Calcite cement is common in the sandier laminae. This zone is interpreted as a levee deposit. The stacked, fining-upward sequences were probably produced by rapid deposition of sediment from waning flood currents. The middle zone (from 16,709 to 16,714.5 feet) consists of clast-supported granule- and cobble-conglomerate with a matrix of fine- grained sandstone and siltstone. Wavy, discontinuous lamination is present in the finer sandstone and siltstone. Calcite cement is common throughout the middle zone. This zone is interpreted as a fluvial channel lag deposit. The lower zone (from 16,714.5 to 16,720.5 feet) consists of a fining- upward sequence that grades from coarse- grained sandstone into sandy siltstone and mudstone with several thin (3- to 4-inch) graded sandstone laminae. Wavy, discontinuous laminae and sandstone lenses are common, as are calcite cement and organic fragments. The lower zone is interpreted as an abandoned fluvial channel deposit. The entire core interval (16,701 to 16,720.5 feet) is highly fractured and faulted, with offsets up to 1 inch commonly filled with calcite. These rocks are all classified as litharenites. The framework grains consist of altered volcanic rock fragments, quartz, feldspar, slightly deformed shale clasts, and very minor amounts of schistose metamorphic rock fragments. Authigenic minerals present include chert, chlorite, smectitic clay, calcite, pyrite, and siderite. The source terrane was almost entirely volcanic with very minor amounts of metamorphic and sedimentary input. The porosity and permeability are low due to poor sorting, strong compaction, the abundance of detrital matrix, and the presence of calcite cement. The reservoir potential of the rocks represented by this core is negligible.

POROSITY (%)	PERMEABILITY (md)	% ORGANIC CARBON	VITRINITE REFLECTANCE (%)
		2.17	
12.4	0.70		
13.0	1.70	2.22	0.99
7.4	0.24		
		2.03	
7.9	0.16		
		2.76	
12.2	2.01		
7.3	0.04		
		1.17	1.01
		1.93	
11.0			
		1.21	
11.3	1.57		
13.6	0.56	2.34	0.98
8.3	0.07		

FIGURE 25. **Description of conventional core 19, North Aleutian Shelf COST No. 1 well.**

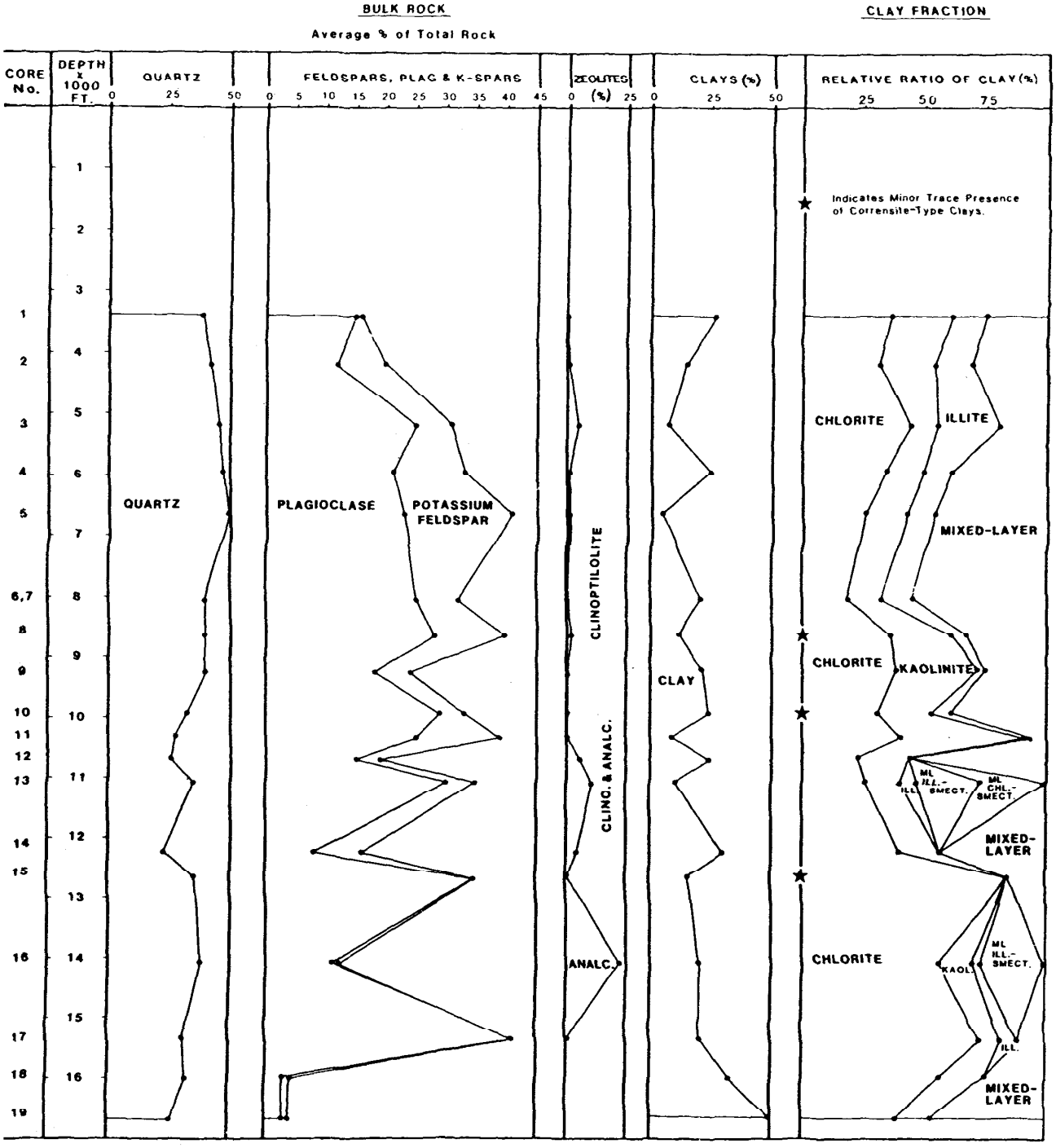

FIGURE 26. **Summary chart of X-ray diffraction data (from AGAT Consultants, Inc.).**

FIGURE 27. **Occurrence of diagenetic alterations (from AGAT Consultants, Inc.).**

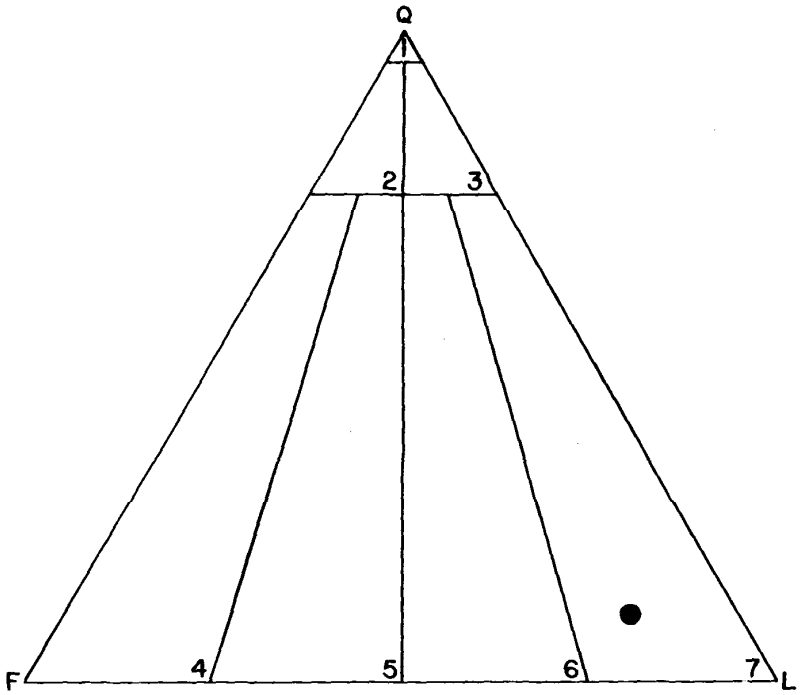

FIGURE 28. **Ternary plot of percentages of principle framework constituents (quartz, feldspar, and lithic fragments) from the North Aleutian Shelf COST No. 1 well, core 1.**

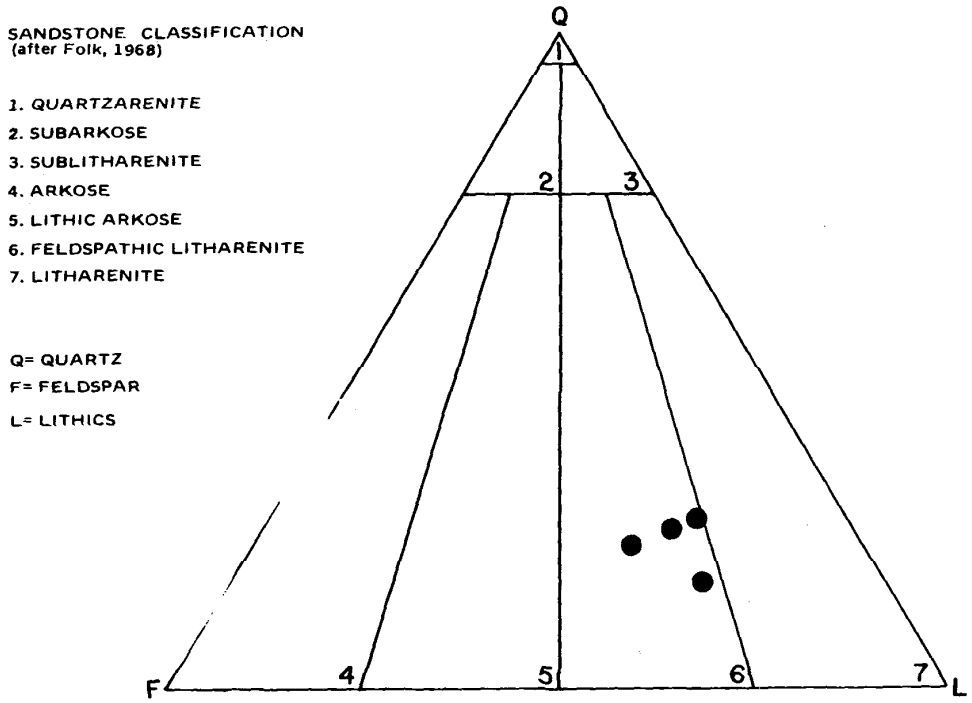

FIGURE 29. **Ternary plot of percentages of principle framework constituents (quartz, feldspar, and lithic fragments) from the North Aleutian Shelf COST No. 1 well, core 2.**

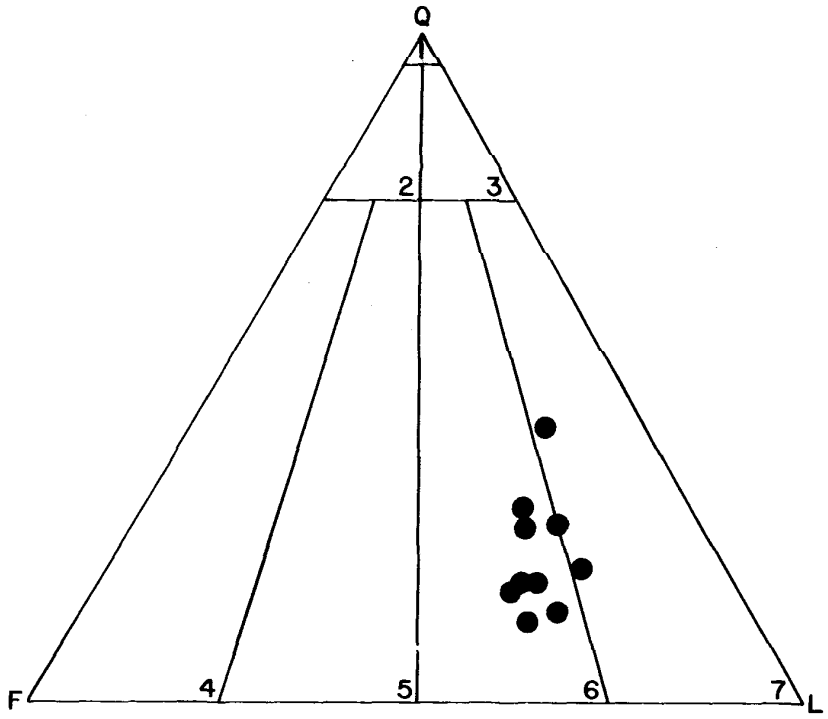

FIGURE 30. **Ternary plot of percentages of principle framework constituents (quartz, feldspar, and lithic fragments) of the sandstones, from the North Aleutian Shelf COST No. 1 well, core 3.**

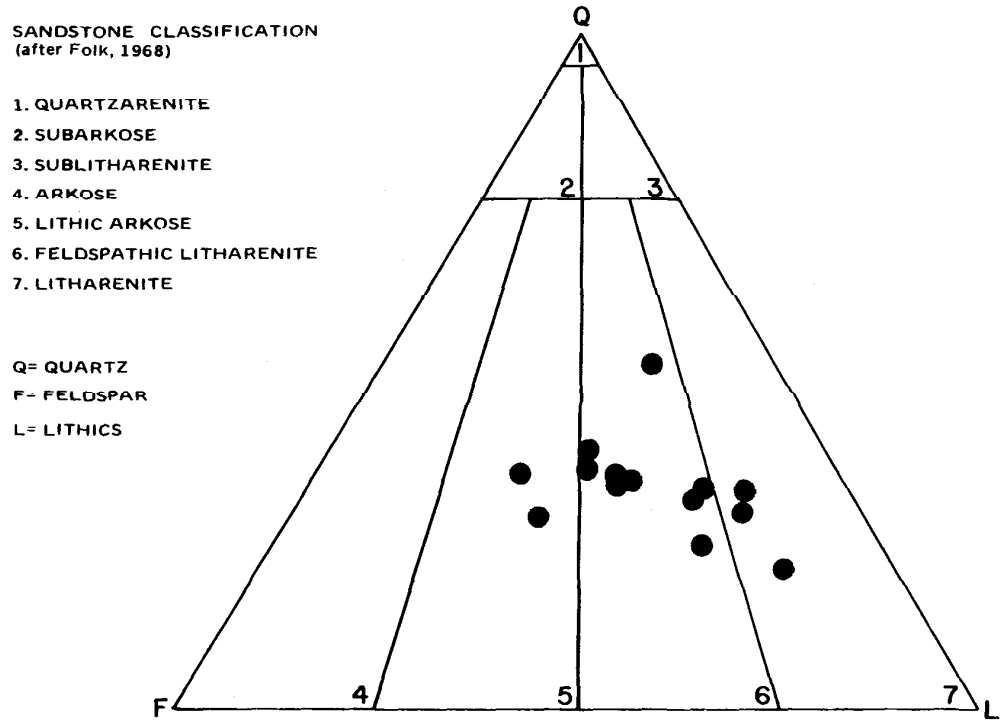

FIGURE 31. **Ternary plot of percentages of principle framework constituents (quartz, feldspar, and lithic fragments) from the North Aleutian Shelf COST No. 1 well, core 4.**

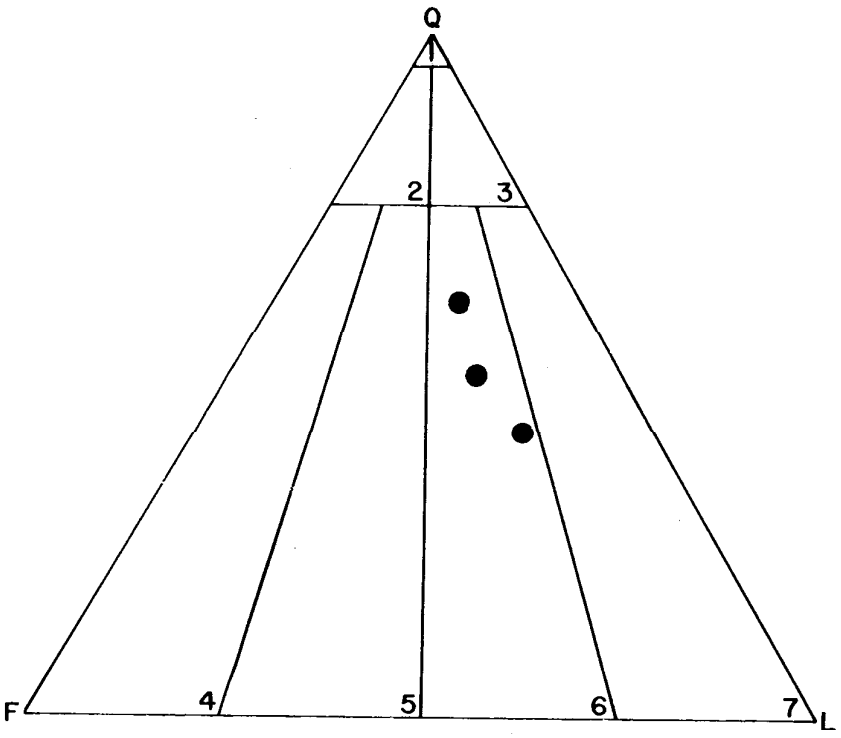

FIGURE 32. **Ternary plot of percentages of principle framework constituents (quartz, feldspar, and lithic fragments) from the North Aleutian Shelf COST No. 1 well, core 5.**

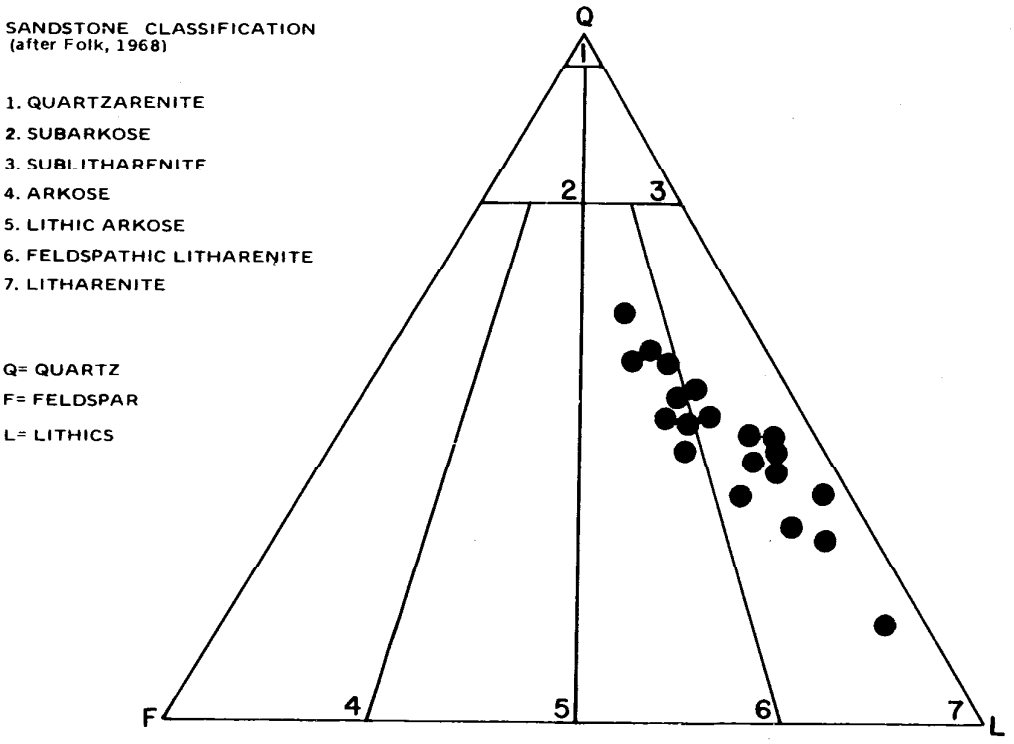

FIGURE 33. **Ternary plot of percentages of principle framework constituents (quartz, feldspar, and lithic fragments) from the North Aleutian Shelf COST No. 1 well, cores 6 and 7.**

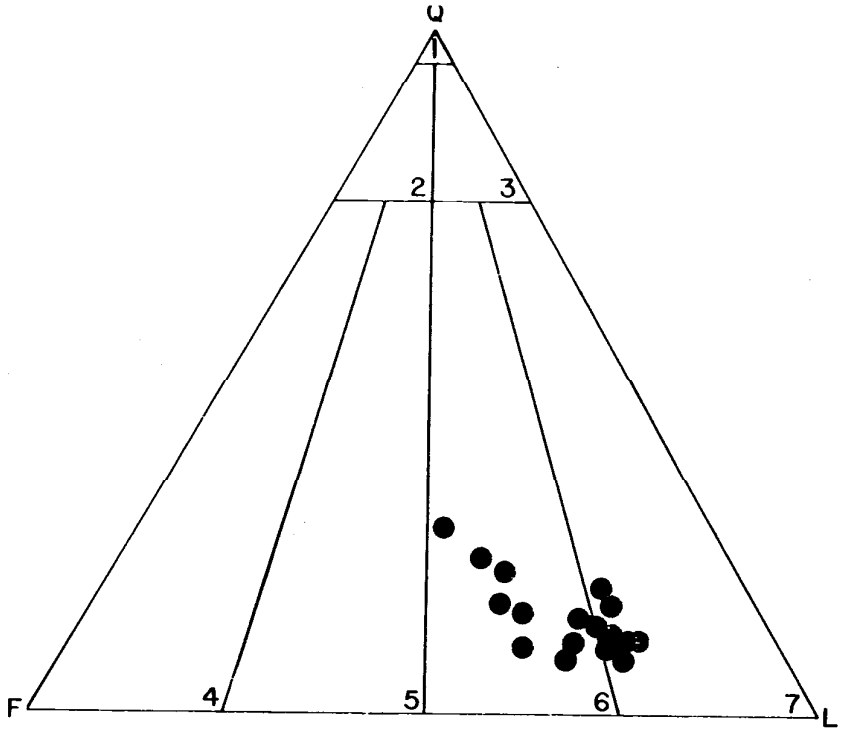

FIGURE 34. **Ternary plot of percentages of principle framework constituents (quartz, feldspar, and lithic fragments) from the North Aleutian Shelf COST No. 1 well, core 8.**

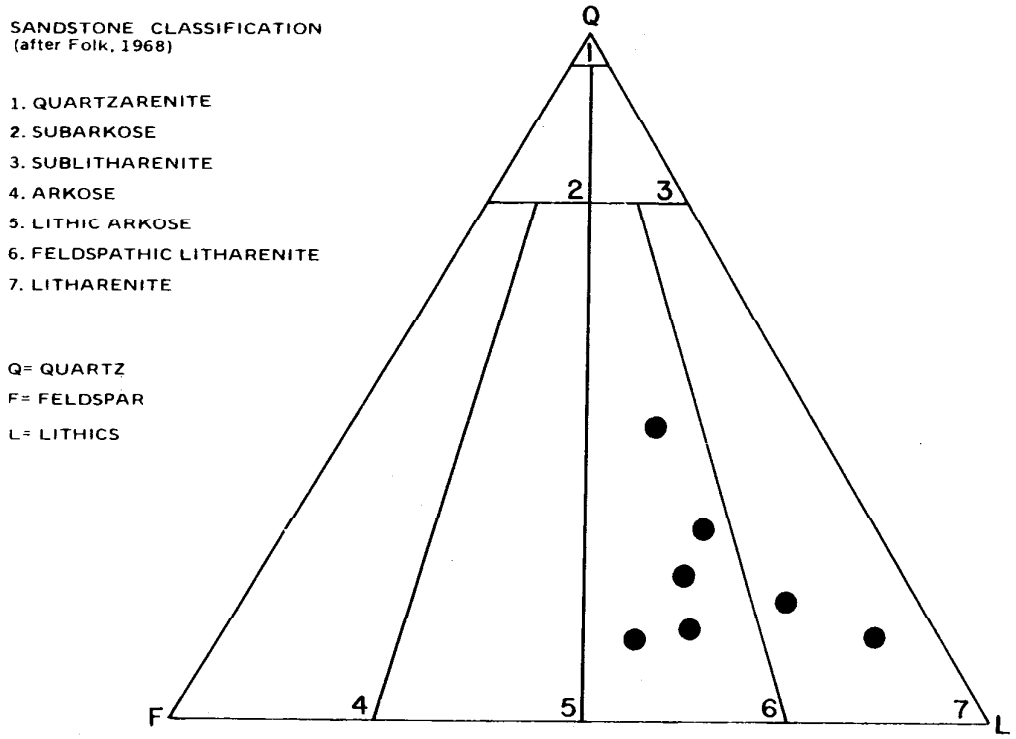

FIGURE 35. **Ternary plot of percentages of principle framework constituents (quartz, feldspar, and lithic fragments) from the North Aleutian Shelf COST No. 1 well, core 9. Included are mudstone, sandstones, and conglomerates.**

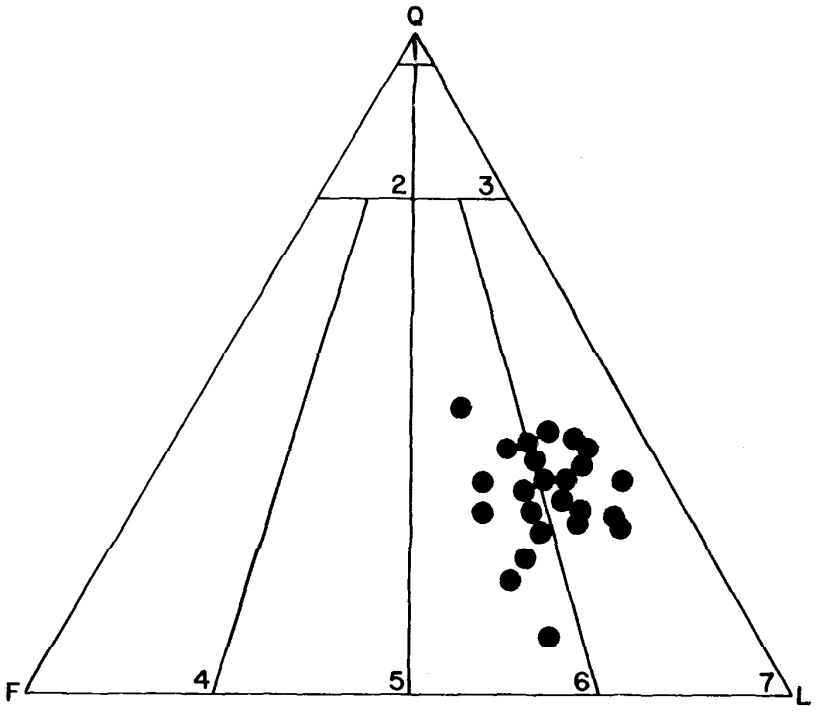

FIGURE 36. **Ternary plot of percentages of principle framework constituents (quartz, feldspar, and lithic fragments) from the North Aleutian Shelf COST No. 1 well, core 10.**

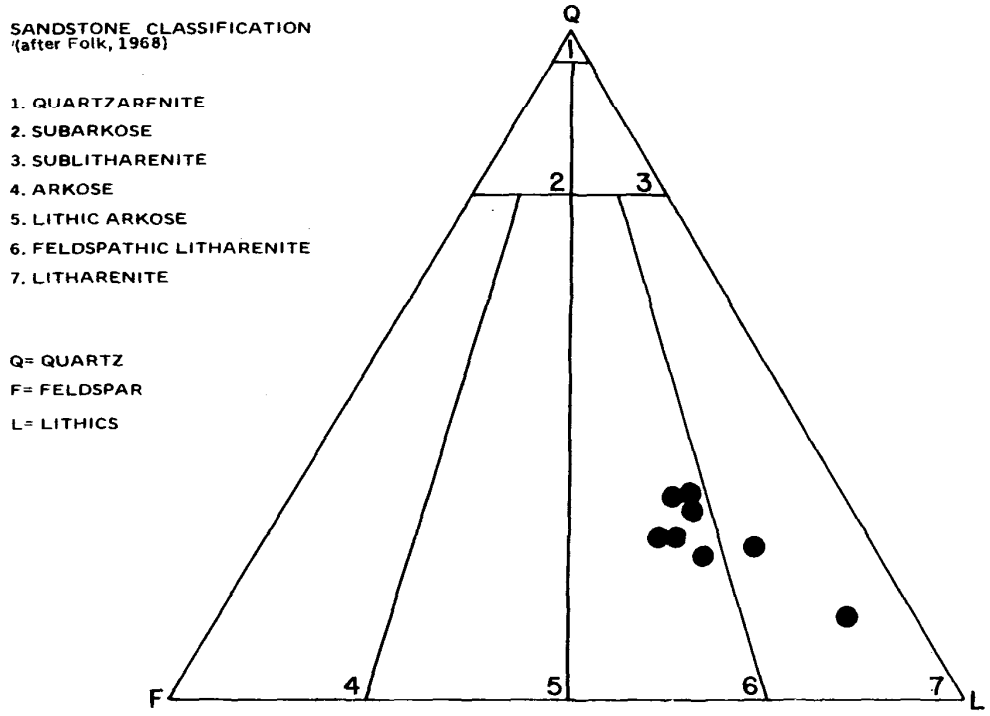

FIGURE 37. **Ternary plot of percentages of principle framework constituents (quartz, feldspar, and lithic fragments) from the North Aleutian Shelf COST No. 1 well, core 11.**

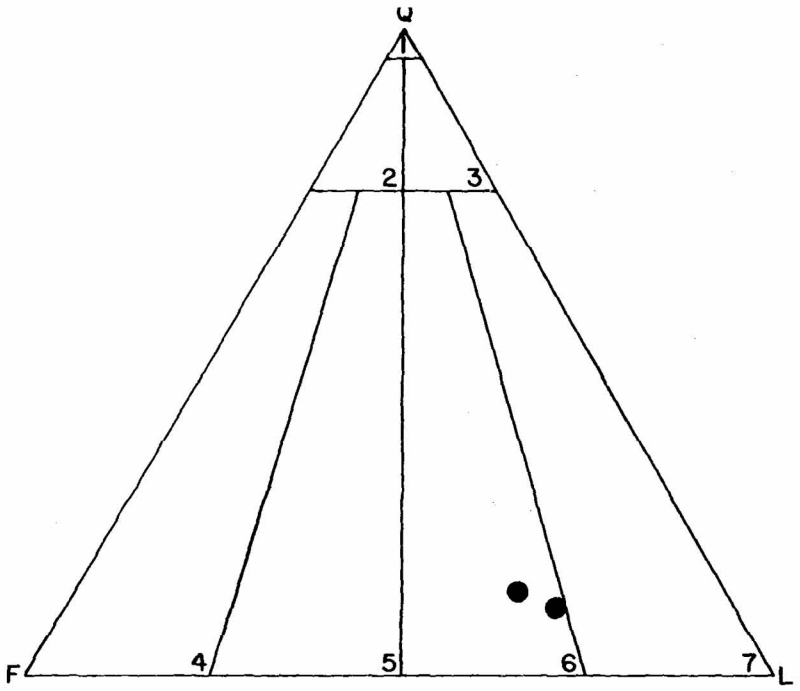

FIGURE 38. **Ternary plot of percentages of *principle framework* constituents (quartz, feldspar, and lithic fragments) of sandy mudstone and calcareous sandstone from the North Aleutian Shelf COST No.1 well, core 12.**

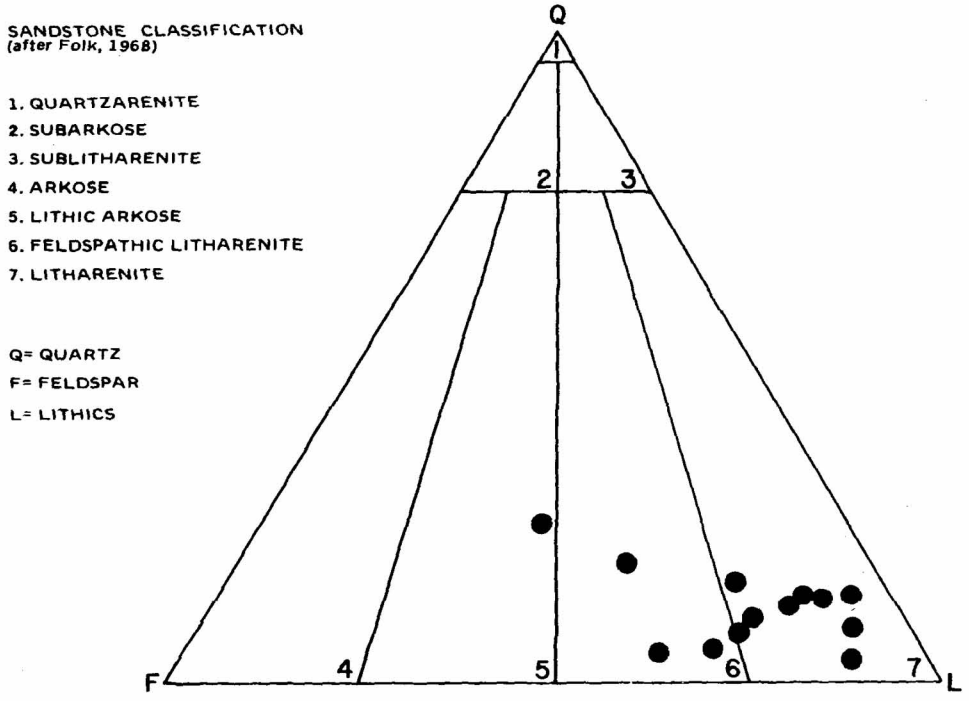

FIGURE 39. **Ternary plot of percentages of principle framework constituents (quartz, feldspar, and lithic fragments) from the North Aleutian Shelf COST No. 1 well, core 13.**

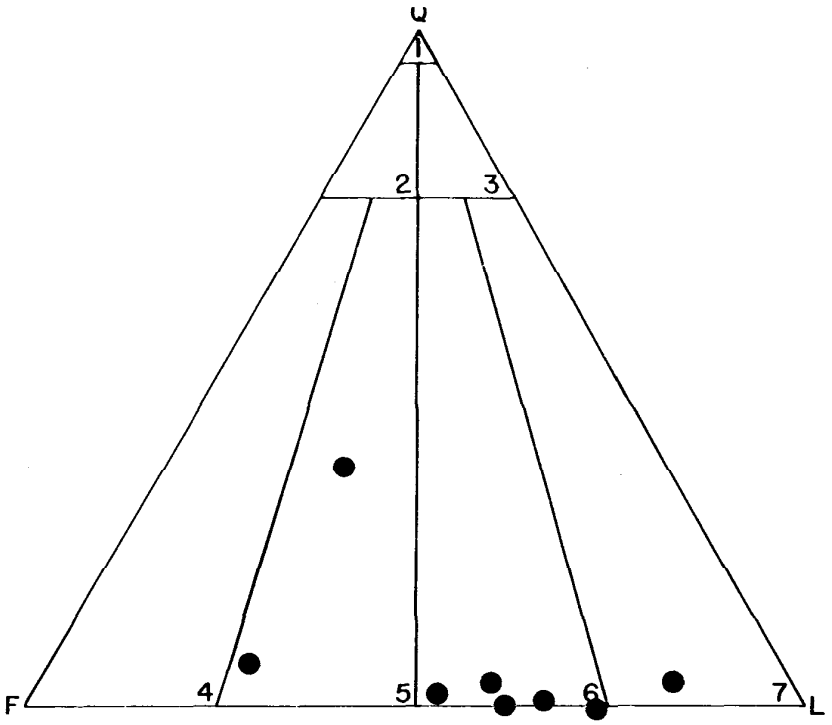

FIGURE 40. **Ternary plot of percentages of principle framework constituents (quartz, feldspar, and lithic fragments) from the North Aleutian Shelf COST No. 1 well, core 14.**

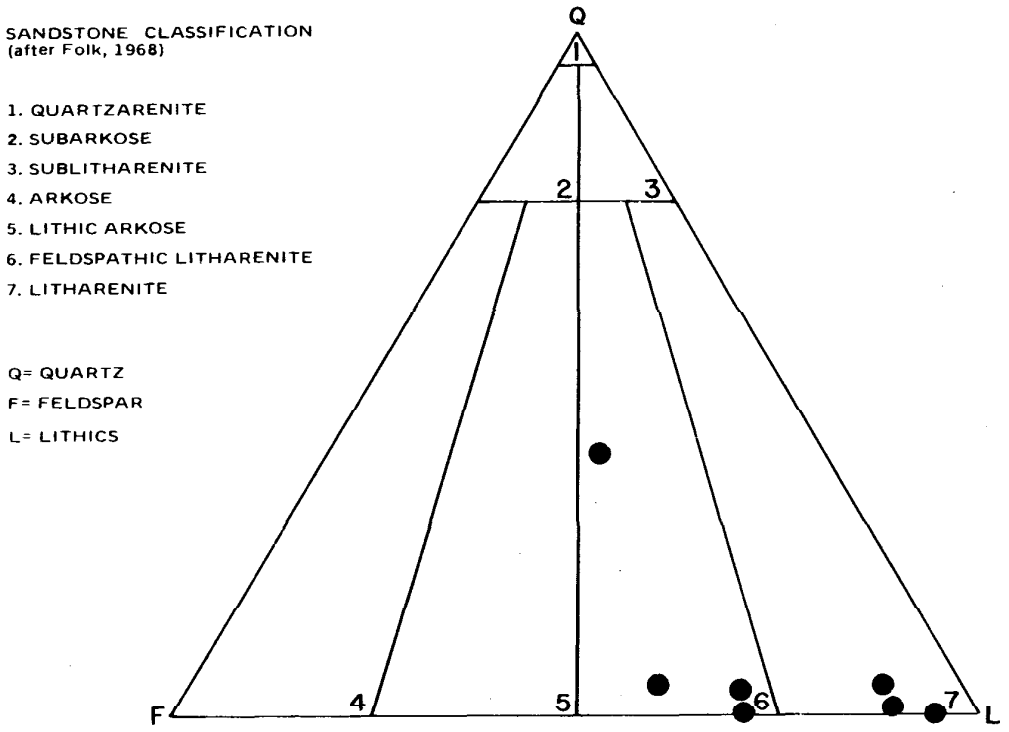

FIGURE 41. **Ternary plot of percentages of principle framework constituents (quartz, feldspar, and lithic fragments) from the North Aleutian Shelf COST No. 1 well, core 15.**

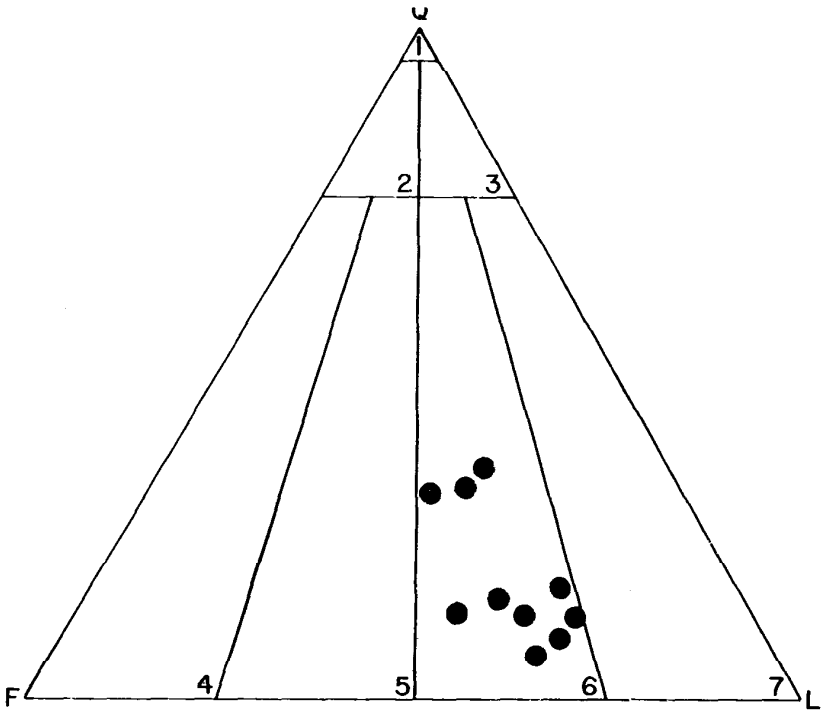

FIGURE 42. **Ternary plot of percentages of principle framework constituents (quartz, feldspar, and lithic fragments) from the North Aleutian Shelf COST No. 1 well, core 16.**

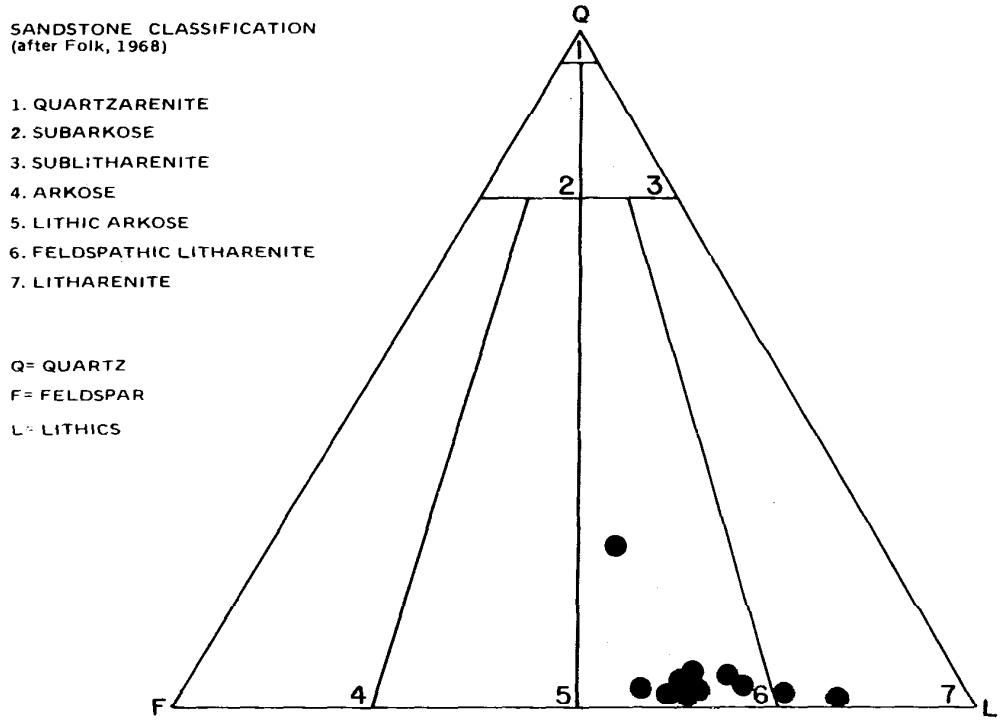

FIGURE 43. **Ternary plot of percentages of principle framework constituents (quartz, feldspar, and lithic fragments) of sandstone and mudstone from the North Aleutian Shelf COST No. 1 well, core 17.**

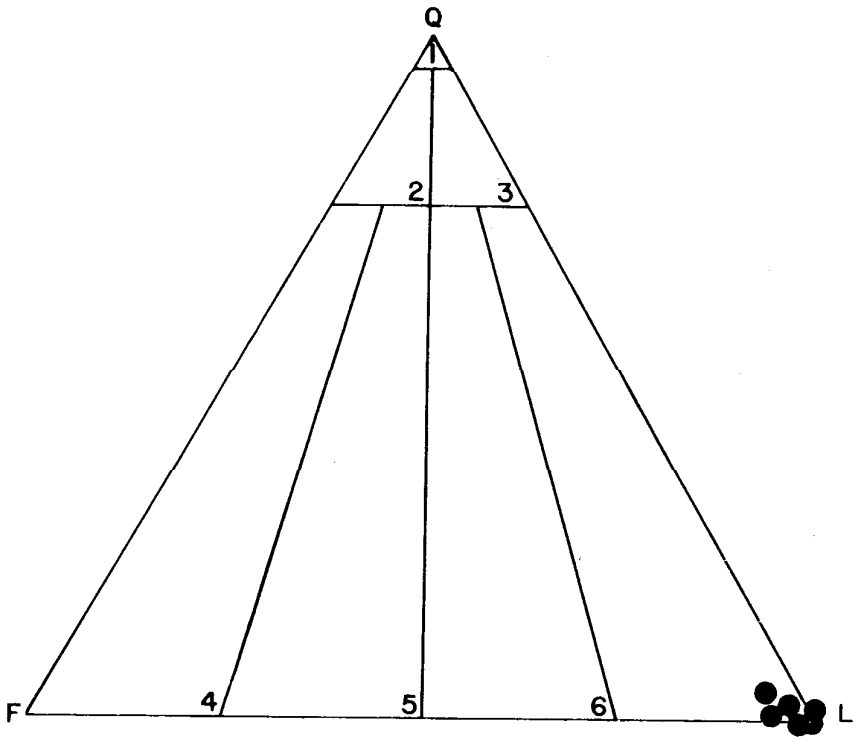

FIGURE 44. **Ternary plot of percentages of principle framework constituents (quartz, feldspar, and lithic fragments) from the North Aleutian Shelf COST No. 1 well, core 18.**

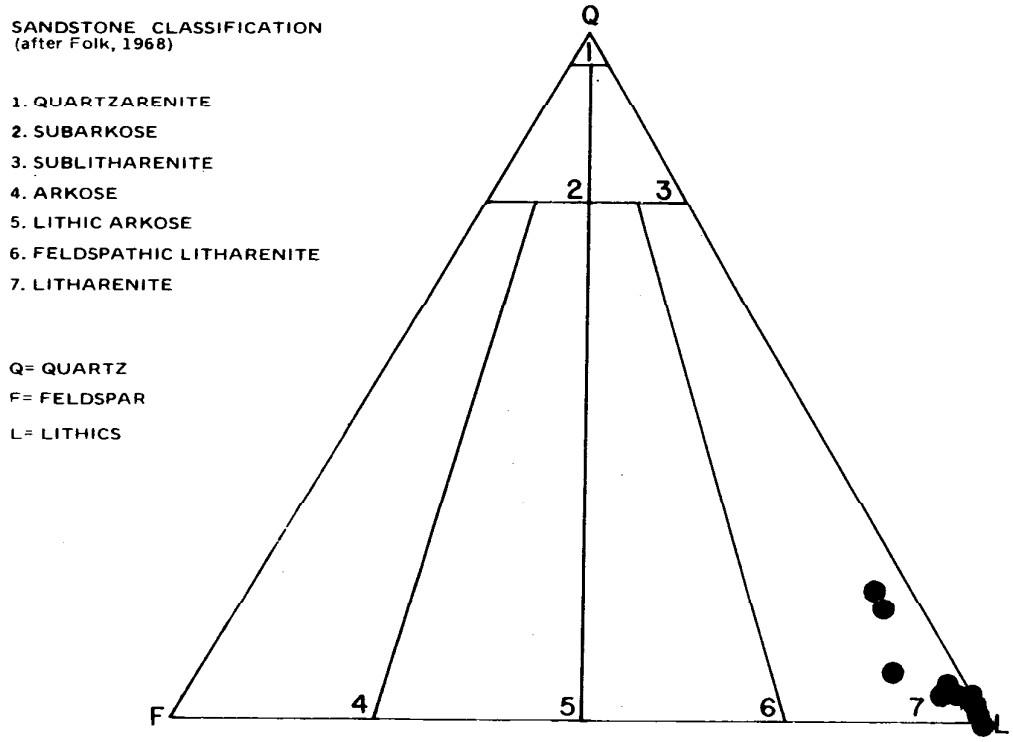

FIGURE 45. **Ternary plot of percentages of principle framework constituents (quartz, feldspar, and lithic fragments) from the North Aleutian Shelf COST No. 1 well, core 19.**

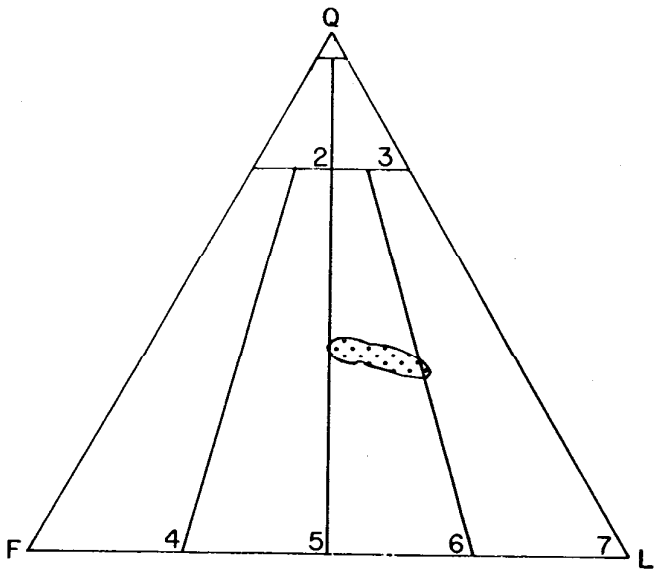

FIGURE 46. **Ternary quartz/feldspar/lithics (QFL) plot for lithologic zone A (1000–2510 feet) in the North Aleutian Shelf COST well. (Modified from AGAT Consultants Inc.)**

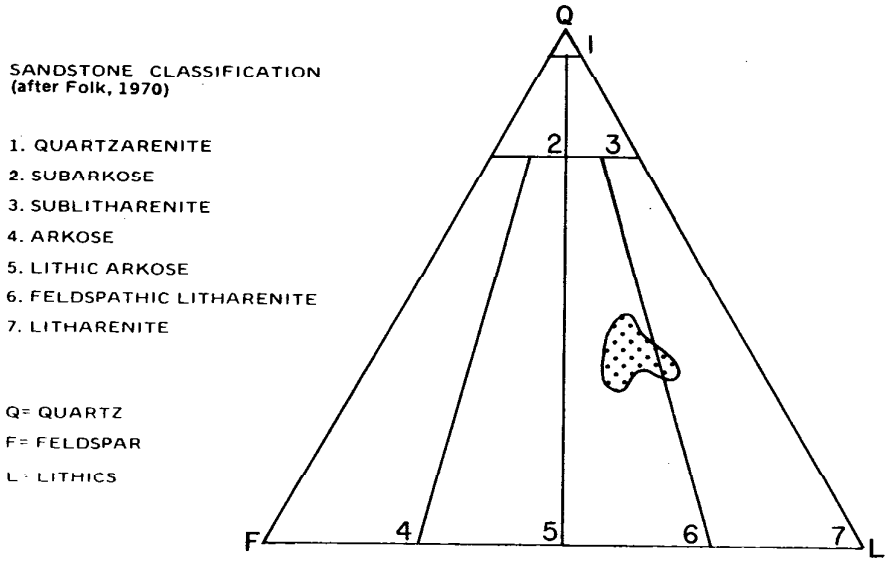

FIGURE 47. **Ternary quartz/feldspar/lithics (QFL) plot for lithologic zone B1 (2510–4110 feet) in the North Aleutian Shelf COST well. (Modified from AGAT Consultants Inc.)**

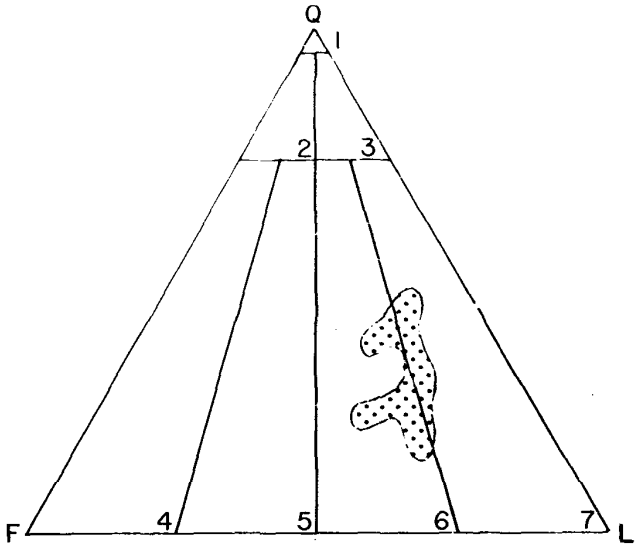

FIGURE 48. **Ternary quartz/feldspar/lithics (QFL) plot for lithologic zone B2 (4110–4870 feet) in the North Aleutian Shelf COST well. (Modified from AGAT Consultants Inc.)**

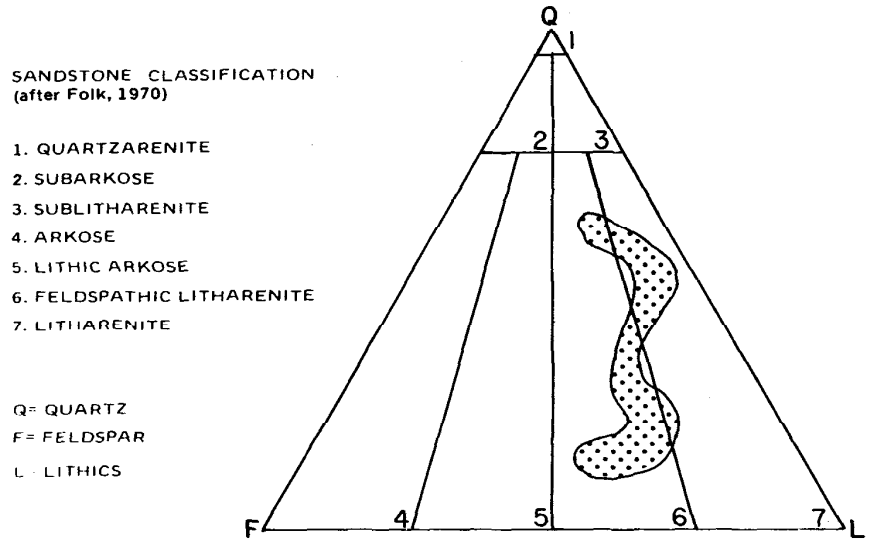

FIGURE 49. **Ternary quartz/feldspar/lithics (QFL) plot for lithologic zone B3 (4870–5675 feet) in the North Aleutian Shelf COST well. (Modified from AGAT Consultants Inc.)**

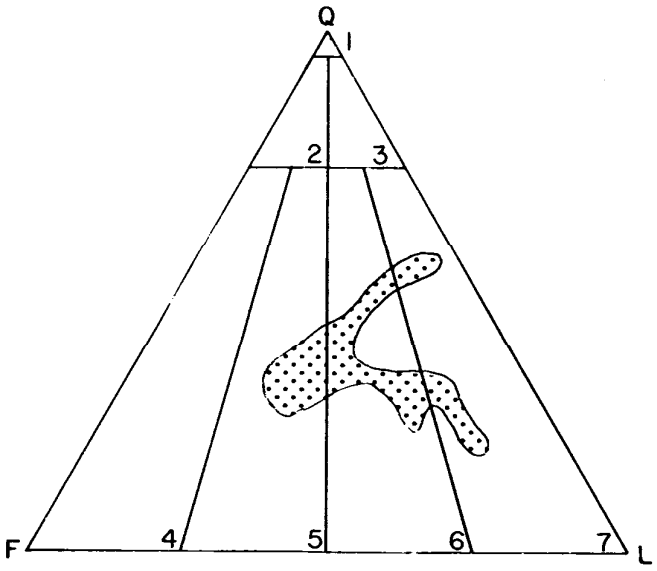

FIGURE 50. Ternary quartz/feldspar/lithics (QFL) plot for lithologic zone C1 (5675-6470 feet) in the North Aleutian Shelf COST well. (Modified from AGAT Consultants Inc.)

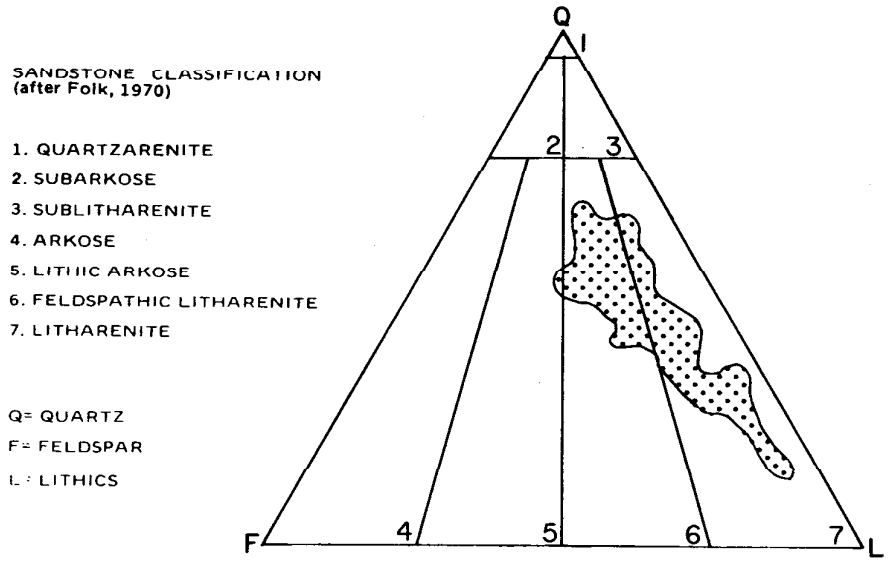

FIGURE 51. Ternary quartz/feldspar/lithics (QFL) plot for lithologic zone C2 (6470-7900 feet) in the North Aleutian Shelf COST well. (Modified from AGAT Consultants Inc.)

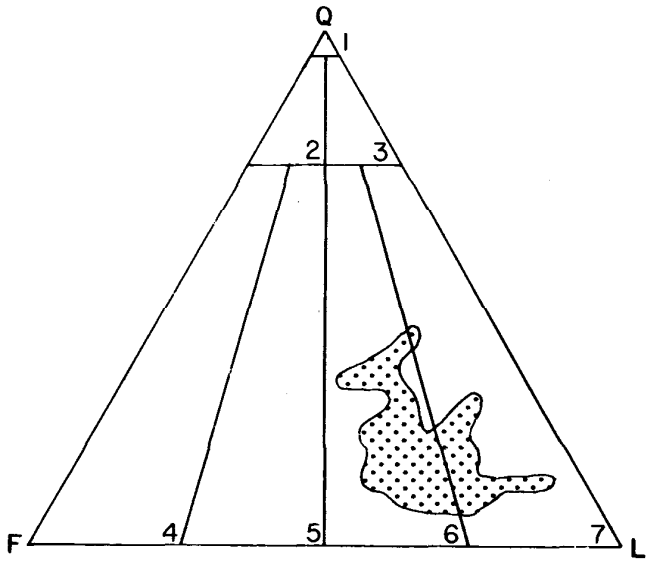

FIGURE 52. Ternary quartz/feldspar/lithics (QFL) plot for lithologic zone D1 (7900–9555 feet) in the North Aleutian Shelf COST well. (Modified from AGAT Consultants Inc.)

SANDSTONE CLASSIFICATION
(after Folk, 1970)

1. QUARTZARENITE
2. SUBARKOSE
3. SUBLITHARENITE
4. ARKOSE
5. LITHIC ARKOSE
6. FELDSPATHIC LITHARENITE
7. LITHARENITE

Q= QUARTZ
F= FELDSPAR
L = LITHICS

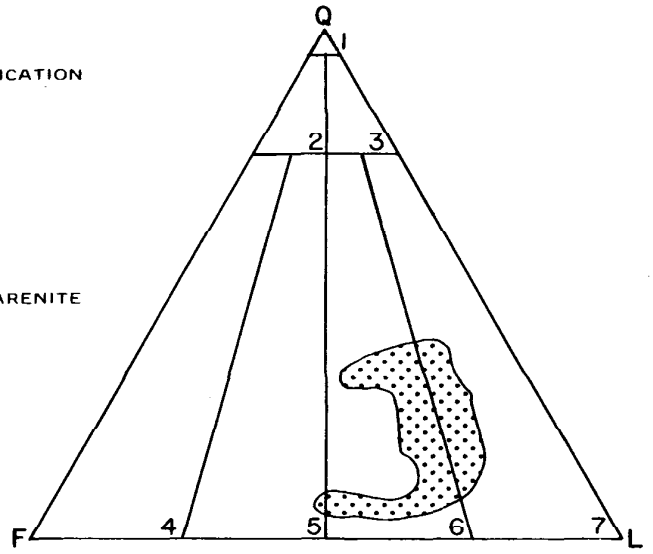

FIGURE 53. Ternary quartz/feldspar/lithics (QFL) plot for lithologic zone D2 (9555–10,380 feet) in the North Aleutian Shelf COST well. (Modified from AGAT Consultants Inc.)

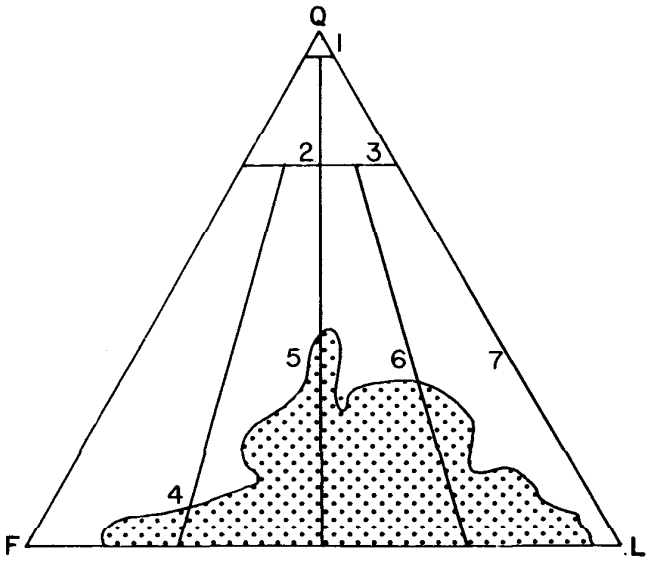

FIGURE 54. **Ternary quartz/feldspar/lithics (QFL) plot for lithologic zone E (10,380–15,620 feet) in the North Aleutian Shelf COST well. (Modified from AGAT Consultants Inc.)**

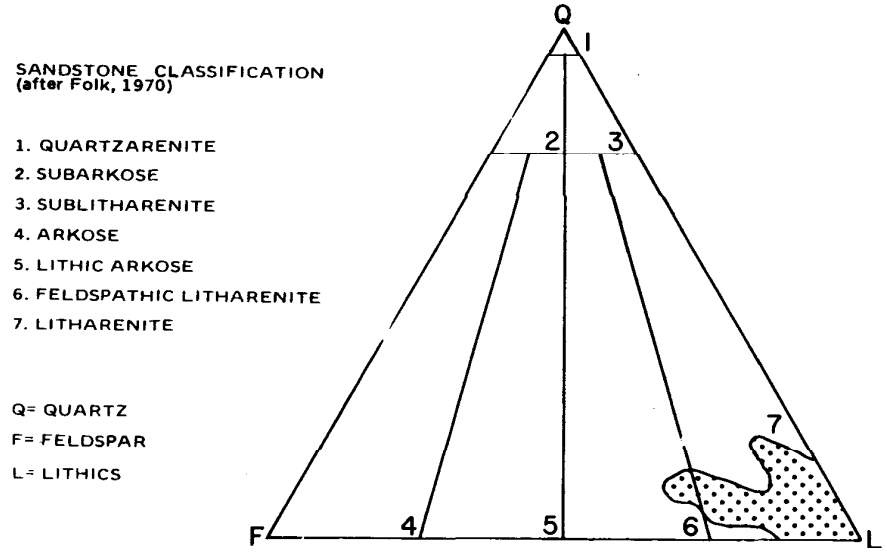

FIGURE 55. **Ternary quartz/feldspar/lithics (QFL) plot for lithologic zones F and G (15,620–17,155 feet TD) in the North Aleutian Shelf COST well. (Modified from AGAT Consultants Inc.)**

TABLE 3. Lithology, measured porosity, estimated visible porosity, and measured permeability of samples from sidewall and conventional cores. Lithology and estimated visible porosities were determined from thin sections by geologists at AGAT Consultants in Denver. Measured porosity and permeability were derived by Core Laboratories in Anchorage. SWC --- sidewall core. Conv --- Conventional centerline core.

Sample Depth (Feet)	Sample Type	Lithology	Measured Porosity (Percent)	Estimated Visible Porosity (Percent)	Measured Permeability (Millidarcies)
1,904	SWC	Sandy diatom ooze	-	-	-
2,214	SWC	-	33.3	-	-
2,338	SWC	Diatomaceous feldspathic litharenite	-	-	-
2,427	SWC	litharenite	34.4	-	408
2,510	SWC	Diatomaceous feldspathic litharenite	-	-	-
2,610	SWC	-	35.3	-	-
2,750	SWC	Muddy feldspathic litharenite	-	-	-
2,836	SWC	-	35.3	-	2,844
2,952	SWC	Feldspathic litharenite	-	-	-
3,060	SWC	-	35.4	-	154
3,338	SWC	Feldspathic litharenite	-	-	-
3,392.4	Conv	Diatom ooze	-	-	-
3,430	SWC	-	35.5	-	-
3,463	SWC	Feldspathic litharenite	-	-	-
3,696	SWC	-	36.0	-	1,218
3,752	SWC	Litharenite	-	-	-
3,918	SWC	-	40.0	-	-
3,990	SWC	Mudstone	-	-	-

Table 3 (cont.)

Sample Depth (Feet)	Sample Type	Lithology	Measured Porosity (Percent)	Estimated Visible Porosity (Percent)	Measured Permeability (Millidarcies)
4,136	SWC	Litharenite	-	-	-
4,190	SWC	Litharenite	-	-	-
4,191.6	Conv	Feldspathic litharenite	36.8	8.4	262
4,195.8	Conv	Feldspathic litharenite	40.4	4.4	11
4,197.4	Conv	Feldspathic litharenite	35.6	4.0	16
4,200.3	Conv	Feldspathic litharenite	31.1	2.4	20
4,399	SWC	Litharenite	-	-	-
4,520	SWC	Litharenite	-	-	-
4,710	SWC	Feldspathic litharenite	-	-	-
4,858	SWC	Litharenite	-	-	-
4,941	SWC	Litharenite	-	-	-
5,150	SWC	Litharenite	-	-	-
5,227.3	Conv	Feldspathic litharenite	35.5	20.8	1,188
5,229.6	Conv	Feldspathic litharenite	36.1	29.6	988
5,231.6	Conv	Clayey feldspathic litharenite	35.1	15.6	880
5,233.5	Conv	Litharenite	34.4	22.0	1,694
5,235.4	Conv	Calcareous litharenite	3.7	0	0.04
5,236.4	Conv	Feldspathic litharenite	34.7	30.8	1,561

Table 3 (cont.)

Sample Depth (Feet)	Sample Type	Lithology	Measured Porosity (Percent)	Estimated Visible Porosity (Percent)	Measured Permeability (Millidarcies)
5,238.5	Conv	Feldspathic litharenite	35.3	26.4	1,228
5,240.3	Conv	Feldspathic litharenite	36.7	24.8	2,203
5,242.7	Conv	Feldspathic litharenite	34.4	27.6	1,190
5,244.3	Conv	Feldspathic litharenite	34.5	26.0	1,094
5,353	SWC	Litharenite	-	-	-
5,588	SWC	Feldspathic litharenite	-	-	-
5,720	SWC	Siltstone/ litharenite	-	-	-
5,805	SWC	Litharenite	25.2	0.8	139
5,970.3	Conv	Clayey feldspathic litharenite	31.3	14.4	129
5,973.4	Conv	Muddy feldspathic litharenite	31.4	8.8	61
5,975.5	Conv	Clayey lithic arkose	31.3	7.2	53
5,977.5	Conv	Clayey lithic arkose	32.4	9.2	181
5,979.5	Conv	Clayey feldspathic litharenite	29.8	13.2	66
5,981.5	Conv	Clayey feldspathic litharenite	29.8	14.2	67
5,983.6	Conv	Clayey feldspathic litharenite	29.7	12.0	93
5,985.4	Conv	Clayey feldspathic litharenite	30.2	13.2	61

Table 3 (cont.)

Sample Depth (Feet)	Sample Type	Lithology	Measured Porosity (Percent)	Estimated Visible Porosity (Percent)	Measured Permeability (Millidarcies)
5,986.7	Conv	Clayey feldspathic litharenite	29.5	8.8	30
5,988.7	Conv	Muddy feldspathic litharenite	30.1	11.2	84
5,990.7	Conv	Clayey litharenite	28.2	12.0	72
5,991.8	Conv	Muddy litharenite	27.0	2.4	17
5,993.2	Conv	Muddy feldspathic litharenite	26.3	2.4	11
5,995.3	Conv	Muddy litharenite	27.0	2.8	18
6,665.3	Conv	Feldspathic litharenite	33.4	17.6	7,722
6,666.6	Conv	Feldspathic litharenite	33.6	-	6,299
6,668.4	Conv	Feldspathic litharenite	33.4	13.6	5,215
6,671	SWC	Feldspathic litharenite	21.5	1.6	-
6,694	SWC	Micaceous siltstone/ litharenite	-	-	-
6,768	SWC	Feldspathic litharenite	23.9	2.8	72
6,869	SWC	Feldspathic litharenite	-	-	-
6,942	SWC	Feldspathic litharenite	-	-	-
7,245	SWC	Litharenite	-	-	-
7,330	SWC	Feldspathic litharenite	21.5	-	-
7,340	SWC	Feldspathic litharenite	-	-	-

Table 3 (cont.)

Sample Depth (Feet)	Sample Type	Lithology	Measured Porosity (Percent)	Estimated Visible Porosity (Percent)	Measured Permeability (Millidarcies)
7,368	SWC	Calcareous feldspathic litharenite	-	-	-
7,442	SWC	Feldspathic litharenite	-	-	-
7,483	SWC	Litharenite	-	-	-
7,512	SWC	Litharenite	25.9	2.4	441
7,552	SWC	Litharenite	32.3	1.2	162
7,635	SWC	Litharenite	-	-	-
7,691	SWC	Litharenite	34.2	4.0	106
7,737	SWC	Feldspathic litharenite	30.4	3.6	19
7,778	SWC	Feldspathic litharenite	-	-	-
7,959	SWC	Feldspathic litharenite	-	-	-
8,051	Conv	Calcareous litharenite	26.2	2.0	-
8,055.7	Conv	Silty litharenite	26.2	1.2	6.24
8,056.5	Conv	Micaceous siltstone	25.3	0.4	-
8,058.3	Conv	Carbonaceous litharenite	24.8	12.0	23
8,062.3	Conv	Litharenite	29.4	9.6	17
8,063.6	Conv	Feldspathic litharenite	32.8	22.4	520
8,065.4	Conv	Siltstone	26.9	0	8.15
8,069.7	Conv	Micaceous siltstone	24.0	5.6	4.33
8,071.6	Conv	Silty litharenite	24.8	2.4	-

Table 3 (cont.)

Sample Depth (Feet)	Sample Type	Lithology	Measured Porosity (Percent)	Estimated Visible Porosity (Percent)	Measured Permeability (Millidarcies)
8,073.5	Conv	Feldspathic litharenite	26.5	6.0	29
8,075.6	Conv	Carbonaceous siltstone	28.2	0.8	-
8,077.5	Conv	Micaceous silty litharenite	28.2	2.4	-
8,079.3	Conv	Siltstone	26.4	1.2	3.26
8,081.3	Conv	Litharenite	27.7	14.0	496
8,083.2	Conv	Feldspathic litharenite	31.6	20.8	1,372
8,085.8	Conv	Feldspathic litharenite	32.3	23.2	-
8,087.3	Conv	Feldspathic litharenite	32.9	24.4	2,358
8,089.4	Conv	Feldspathic litharenite	33.4	23.2	1,791
8,091.2	Conv	Feldspathic litharenite	32.4	19.2	849
8,092.9	Conv	Silty litharenite	29.0	4.4	217
8,150	SWC	Feldspathic litharenite	-	-	-
8,224	SWC	Volcanic rock fragment	-	-	-
8,298	SWC	Silty litharenite	-	-	-
8,361	SWC	Litharenite	-	-	-
8,446	SWC	Clay-rich feldspathic litharenite	25.1	4.8	34
8,628.2	Conv	Feldspathic litharenite	29.8	11.2	109
8,629.3	Conv	Feldspathic litharenite	-	-	-

Table 3 (cont.)

Sample Depth (Feet)	Sample Type	Lithology	Measured Porosity (Percent)	Estimated Visible Porosity (Percent)	Measured Permeability (Millidarcies)
8,631.5	Conv	Litharenite	31.3	6.0	340
8,633.8	Conv	Feldspathic litharenite	30.7	13.2	1,040
8,635.8	Conv	Litharenite	12.5	0.4	0.98
8,637.4	Conv	Litharenite	28.0	4.8	67
8,639.8	Conv	Feldspathic litharenite	30.8	12.8	349
8,641.5	Conv	Feldspathic litharenite	30.7	13.6	929
8,643.4	Conv	Litharenite	31.8	13.2	473
8,645.8	Conv	Feldspathic litharenite	30.8	11.6	284
8,647.2	Conv	Litharenite	29.8	2.8	336
8,649.3	Conv	Feldspathic litharenite	31.1	16.0	123
8,651.5	Conv	Feldspathic litharenite	31.3	16.4	1,010
8,651.9	Conv	Feldspathic litharenite	29.8	15.6	132
8,653.2	Conv	Feldspathic litharenite	31.5	12.4	460
8,654.4	Conv	Siltstone	-	-	-
8,655.3	Conv	Feldspathic litharenite	30.1	4.4	-
8,656.8	Conv	Litharenite	31.7	16.8	3,193
8,730	SWC	Litharenite	-	-	-
8,758	SWC	Litharenite	27.6	2.0	92
8,764	SWC	Litharenite	30.1	1.6	180

Table 3 (cont.)

Sample Depth (Feet)	Sample Type	Lithology	Measured Porosity (Percent)	Estimated Visible Porosity (Percent)	Measured Permeability (Millidarcies)
8,834	SWC	Feldspathic litharenite	-	-	-
8,863	SWC	Feldspathic litharenite	27.8	17.0	197
8,897	SWC	Clay-rich feldspathic litharenite	-	-	-
8,993	SWC	Feldspathic litharenite	28.2	12.0	188
9,038	SWC	Feldspathic litharenite	30.5	13.2	234
9,133	SWC	Feldspathic litharenite	-	-	-
9,255.9	Conv	Mudstone	5.8	0	0.11
9,256.2	Conv	Feldspathic litharenite	25.2	8.4	1,615
9,257.2	Conv	Quartzose mudstone	-	-	-
9,258.9	Conv	Polymictic pebble conglomerate	-	-	-
9,259.9	Conv	Litharenite	12.7	0.8	1.91
9,261.3	Conv	Feldspathic litharenite	21.2	2.0	867
9,263.9	Conv	Feldspathic litharenite	-	-	-
9,293	SWC	Feldspathic litharenite	-	-	-
9,389	SWC	Feldspathic litharenite	-	-	-
9,505	SWC	Feldspathic litharenite	-	-	-
9,646	SWC	Clay-rich lithic arkose	-	-	-

Table 3 (cont.)

Sample Depth (Feet)	Sample Type	Lithology	Measured Porosity (Percent)	Estimated Visible Porosity (Percent)	Measured Permeability (Millidarcies)
9,738	SWC	Muddy litharenite	-	-	-
9,887	SWC	Sandy mudstone	-	-	-
9,945.2	Conv	Shaley feldspathic litharenite	19.3	0	10
9,946.2	Conv	Shaley litharenite	16.5	0	0.15
9,947.6	Conv	Shaley litharenite	17.2	0.4	0.52
9,948.5	Conv	Shaley feldspathic litharenite	17.9	0.4	0.25
9,950	SWC	Shaley feldspathic litharenite	19.3	0	37
9,950.5	Conv	Shaley feldspathic litharenite	18.8	0	1.73
9,952.5	Conv	Shaley feldspathic litharenite	17.9	0	0.58
9,953.4	Conv	Shaley feldspathic litharenite	18.2	0	0.51
9,954.6	Conv	Shaley feldspathic litharenite	9.6	0	0.43
9,955.8	Conv	Shaley feldspathic litharenite	18.1	0.8	-
9,957.2	Conv	Shaley feldspathic litharenite	17.2	0	0.87
9,958.4	Conv	Calcareous feldspathic litharenite	10.9	0	0.04
9,960.6	Conv	Shaley feldspathic litharenite	17.8	0	5.08
9,961.5	Conv	Shaley feldspathic litharenite	18.7	0	1.63
9,963.2	Conv	Shaley litharenite	17.3	0	0.63
9,964.4	Conv	Shaley litharenite	17.5	0	2.89

Table 3 (cont.)

Sample Depth (Feet)	Sample Type	Lithology	Measured Porosity (Percent)	Estimated Visible Porosity (Percent)	Measured Permeability (Millidarcies)
9,965.6	Conv	Shaley litharenite	17.8	0	11
9,967.5	Conv	Shaley litharenite	17.0	0	0.42
9,968.5	Conv	Shaley litharenite	17.3	0	1.24
9,969.9	Conv	Pebble conglomerate	16.0	1.2	4.0
9,972.5	Conv	Shaley litharenite	19.5	0	3.89
9,973.5	Conv	Shaley litharenite	20.7	0	4.57
9,975.2	Conv	Shaley litharenite	18.2	0	1.67
9,976.3	Conv	Shaley litharenite	17.6	0.4	1.30
9,977.3	Conv	Shaley litharenite	23.7	0	1.14
9,979.2	Conv	Shaley litharenite	17.5	0	5.43
9,980.6	Conv	Shaley litharenite	17.7	0	3.57
10,010	SWC	Mudstone	-	-	-
10,226	SWC	Sandy mudstone	-	-	-
10,252	SWC	Muddy feldspathic litharenite	23.4	0	-
10,269	SWC	Muddy litharenite	-	-	-
10,302	SWC	Sideritic feldspathic litharenite	20.4	0	17
10,316	SWC	Muddy feldspathic litharenite	26.6	1.0	12
10,326.8	Conv	Muddy feldspathic litharenite	19.6	2.0	1.83
10,328.2	Conv	Muddy feldspathic litharenite	20.2	3.2	2.07
10,329.7	Conv	Calcareous feldspathic litharenite	8.8	1.2	0.22
10,331.6	Conv	Calcareous litharenite	7.3	0	0.06

Table 3 (cont.)

Sample Depth (Feet)	Sample Type	Lithology	Measured Porosity (Percent)	Estimated Visible Porosity (Percent)	Measured Permeability (Millidarcies)
10,332.8	Conv	Muddy feldspathic litharenite	22.2	5.6	23
10,334.2	Conv	Muddy litharenite	19.4	1.2	43
10.336.2	Conv	Muddy feldspathic litharenite	29.0	-	802
10,336.8	Conv	Muddy feldspathic litharenite	28.3	3.6	544
10,355	SWC	Muddy litharenite	22.2	0.5	38
10,390	SWC	Calcareous lithic arkose	23.6	0	-
10,417	SWC	Volcanic arenite	20.1	0	-
10,447	SWC	Volcanic arenite	-	-	-
10,569	SWC	Muddy subarkose	-	-	-
10,622	SWC	Sideritic mudstone	-	-	-
10,732.6	Conv	Sandy mudstone	-	-	-
10,737.2	Conv	Calcareous litharenite	24.1	0.8	130
10,737.7	Conv	Sideritic mudstone	-	-	-
10,738.2	Conv	Muddy ironstone	-	-	-
10,739.7	Conv	Muddy ironstone	-	-	-
10,768	SWC	Volcanic arenite	-	-	-
10,943	Conv	Feldspathic litharenite	-	-	-
11,085.7	Conv	Volcanic granule conglomerate	20.2	3.6	0.99
11,087.6	Conv	Volcanic granule conglomerate	18.2	5.3	0.13
11,089.7	Conv	Lithic arkose	19.4	3.6	5.63

Table 3 (cont.)

Sample Depth (Feet)	Sample Type	Lithology	Measured Porosity (Percent)	Estimated Visible Porosity (Percent)	Measured Permeability (Millidarcies)
11,091.7	Conv	Calcareous volcanic litharenite	-	-	-
11,093.9	Conv	Feldspathic litharenite	-	-	-
11,095.9	Conv	Feldspathic litharenite	14.6	2.8	0.23
11,097.3	Conv	Calcareous volcanic granule conglomerate	17.1	0.4	0.45
11,098.3	Conv	Volcanic zeolitic litharenite	-	-	-
11,100.2	Conv	Feldspathic litharenite	19.3	14.4	12
11,100.6	Conv	Volcanic zeolitic litharenite	13.1	4.4	0.04
11,101.7	Conv	Volcanic litharenite	21.8	8.0	0.17
11,102.9	Conv	Volcanic zeolitic litharenite	6.4	0.4	0.04
11,105.1	Conv	Volcanic zeolitic siltstone	-	-	-
11,107.1	Conv	Volcanic zeolitic litharenite	-	-	-
11,109	SWC	Volcanic rock fragment	-	-	-
11,223	SWC	Organic material	-	-	-
11,271	SWC	Feldspathic litharenite	-	-	-
11,304	SWC	Feldspathic litharenite	-	-	-
11,390	SWC	Feldspathic litharenite	-	-	-
11,541	SWC	Feldspathic litharenite	24.1	0	-

Table 3 (cont.)

Sample Depth (Feet)	Sample Type	Lithology	Measured Porosity (Percent)	Estimated Visible Porosity (Percent)	Measured Permeability (Millidarcies)
11,773	SWC	Calcareous lithic arkose	-	-	-
11,878	SWC	Lithic arkose	22.3	0	25
11,936	SWC	Organic material	-	-	-
12,083	SWC	Volcanic rock fragment	-	-	-
12,192	SWC	Litharenite	-	-	-
12,221	SWC	Lithic arkose	-	-	-
12,249	Conv	Carbonaceous mudstone	-	-	-
12,249.5	Conv	Lithic arkose	-	-	-
12,251.8	Conv	Lithic arkose mudstone	-	-	-
12,253.9	Conv	Feldspathic litharenite	-	-	-
12,256.4	Conv	Feldspathic litharenite	-	-	-
12,257.5	Conv	Feldspathic litharenite	17.4	4.4	1.74
12,261.9	Conv	Feldspathic litharenite	-	-	-
12,266.1	Conv	Litharenite	-	-	-
12,266.4	Conv	Feldspathic litharenite	10.5	1.6	2.56
12,342	SWC	Litharenite	-	-	-
12,540	SWC	Litharenite	-	-	-
12,638.8	Conv	Sandy claystone	-	-	-
12,641.3	Conv	Calcareous feldspathic litharenite	12.4	1.2	0.02
12,644.7	Conv	Volcanic arenite	19.0	1.6	0.02

Table 3 (cont.)

Sample Depth (Feet)	Sample Type	Lithology	Measured Porosity (Percent)	Estimated Visible Porosity (Percent)	Measured Permeability (Millidarcies)
12,647.4	Conv	Feldspathic litharenite	15.6	1.6	0.01
12,649.7	Conv	Volcanic arenite	16.9	0.8	0.04
12,653.5	Conv	Volcanic arenite	-	-	-
12,654.9	Conv	Calcareous feldspathic litharenite	-	-	-
12,659	SWC	Litharenite	26.8	2.8	-
12,757	SWC	Mudstone	-	-	-
12,891	SWC	Lithic arkose	-	-	-
12,989	SWC	Volcanic rock fragment	-	-	-
13,124	SWC	Feldspathic litharenite	-	-	-
13,254	SWC	Arkose	24.8	4.4	-
13,291	SWC	Litharenite	-	-	-
14,165.6	SWC	Mudstone	-	-	-
14,169.2	Conv	Calcareous mudstone	-	-	-
14,171.3	Conv	Zeolitic calcareous lithic arkose	5.0	0.4	0.04
14,171.4	Conv	Zeolitic sandy siltstone	-	-	-
14,174.9	Conv	Zeolitic calcareous feldspathic litharenite	-	-	-
14,176.2	Conv	Zeolitic calcareous lithic arkose	-	-	-
14,177.6	Conv	Calcareous mudstone	-	-	-
14,177.8	Conv	Calcareous mudstone	-	-	-
14,178.9	Conv	Calcareous feldspathic lithic arkose	10.3	0	0.09

Table 3 (cont.)

Sample Depth (Feet)	Sample Type	Lithology	Measured Porosity (Percent)	Estimated Visible Porosity (Percent)	Measured Permeability (Millidarcies)
14,179	Conv	Micaceous feldspathic lithic arkose	-	-	-
14,182.2	Conv	Zeolitic feldspathic litharenite	-	-	-
14,182.7	Conv	Zeolitic feldspathic litharenite	1.9	0.8	0.04
14,184.8	Conv	Feldspathic litharenite	14.9	0.8	0.11
14,185.9	Conv	Micaceous feldspathic litharenite	-	-	-
15,347.3	Conv	Volcanic arenite	9.1	0	0.02
15,348.1	Conv	Feldspathic litharenite	-	-	-
15,350.2	Conv	Feldspathic litharenite	6.5	0	0.02
15,352.4	Conv	Calcareous feldspathic litharenite	7.0	0	0.02
15,354.2	Conv	Muddy feldspathic litharenite	10.0	0	0.02
15,356.2	Conv	Feldspathic litharenite	10.8	0	0.05
15,358.2	Conv	Volcanic arenite	10.8	0	0.05
15,359.9	Conv	Feldspathic litharenite	11.3	0	0.05
15,361.8	Conv	Calcareous feldspathic litharenite	6.9	0	0.02
15,363.2	Conv	Muddy feldspathic litharenite	10.9	0	0.02
15,364.5	Conv	Muddy feldspathic litharenite	9.3	0	0.02

Table 3 (cont.)

Sample Depth (Feet)	Sample Type	Lithology	Measured Porosity (Percent)	Estimated Visible Porosity (Percent)	Measured Permeability (Millidarcies)
15,365.8	Conv	Muddy feldspathic litharenite	0.8	0	0.05
15,366.2	Conv	Sandy mudstone	12.5	0	2.23
16,006.5	Conv	Siltstone	-	-	-
16,008	Conv	Calcareous litharenite	-	-	-
16,011.1	Conv	Calcareous litharenite	-	-	-
16,013.2	Conv	Calcareous litharenite	-	-	-
16,014.8	Conv	Calcareous litharenite	8.1	0	0.02
16,017.6	Conv	Calcareous sandy litharenite	-	-	-
16,018.3	Conv	Calcareous litharenite	15.3	0	4.25
16,022.2	Conv	Calcareous litharenite	1.3	0	0.02
16,027.2	Conv	Siltstone	-	-	-
16,701.6	Conv	Mudstone	-	-	-
16,702.8	Conv	Calcareous litharenite	12.4	0	0.70
16,703.4	Conv	Litharenite	13.0	0	1.70
16,704.3	Conv	Calcareous litharenite	-	-	-
16,704.8	Conv	Calcareous litharenite	7.4	0	0.24
16,706.8	Conv	Litharenite	7.9	0	0.16
16,708.4	Conv	Siltstone/litharenite	-	-	-
16,710.6	Conv	Calcareous conglomerate	7.3	0	0.04
16,711.9	Conv	Calcareous mudstone	-	-	-
16,713.8	Conv	Conglomerate	-	-	-
16,716.8	Conv	Calcareous siltstone/ litharenite	-	-	-

Table 3 (cont.)

Sample Depth (Feet)	Sample Type	Lithology	Measured Porosity (Percent)	Estimated Visible Porosity (Percent)	Measured Permeability (Millidarcies)
16,719.9	Conv	Calcareous litharenite	11.3	0	1.57
16,720.4	Conv	Calcareous litharenite	13.6	0	0.56
16,720.6	Conv	Calcareous litharenite	8.3	0	0.57

TABLE 4. X-ray diffraction data from conventional cores--ranges for North Aleutian Shelf COST No. 1 well for the whole-rock fraction (from AGAT Consultants, Inc., 1983).

Core Number	Depth in feet	Whole-Rock Fraction Percent*											
		**Qtz	Plag	K-spar	Sid	Pyr	Cal	Hbl	Clino	Anlc	Hem	Ank	Clay
1	3,392.4	/38	/15	/1	/16	/2	/1	/10	/0	/0	/1	/1	/26
2	4,191.6 to 4,200.3	44/59	12/17	4/15	0/4	4/8	0/1	1/3	0/2	0/0	0/0	1/1	10/15
3	5,227.3 to 5,244.3	29/55	10/48	0/15	0/2	0/2	0/42	0/6	2/6	0/0	0/0	0/3	4/11
4	5,970.3 to 5,995.3	34/56	15/27	5/15	0/3	1/9	0/1	1/15	0/3	0/0	0/0	1/2	5/27
5	6,665.3 to 6,668.4	40/66	16/36	10/33	0/1	0/1	0/1	1/1	0/2	0/0	0/0	0/1	3/5
6/7	8,051.0 to 8,092.9	29/64	12/52	0/14	0/8	0/9	0/2	0/1	0/2	0/0	0/0	0/3	0/40
8	8,628.2 to 8,656.8	23/56	11/51	0/30	0/11	0/4	0/22	0/1	0/8	0/0	0/0	0/2	1/43
9	9,255.9 to 9,263.9	35/46	13/33	3/10	0/1	0/9	0/27	0/1	0/0	0/0	0/1	1/2	8/34
10	9,945.2 to 9,980.6	21/41	12/52	0/11	0/2	0/18	0/47	0/1	0/4	0/0	0/1	0/2	12/37
11	10,326.8 to 10,336.8	8/48	6/46	8/19	0/4	0/2	0/64	0/0	0/0	0/0	0/0	0/4	0/13
12	10,732.6 to 10,739.7	14/38	8/29	3/6	0/46	0/2	0/11	0/1	0/12	0/0	0/0	0/3	19/32
13	11,085.7 to 11,107.1	13/58	5/67	0/23	0/5	0/6	0/41	0/1	0/23	0/38	0/1	0/3	0/38
14	12,249.0 to 12,266.4	3/57	0/22	0/20	0/3	0/38	0/67	0/1	0/2	0/0	0/3	0/1	5/63
15	12,638.8 to 12,654.9	16/51	21/52	0/0	0/3	0/0	2/41	0/0	0/0	0/0	0/0	0/1	0/48
16	14,165.6 to 14,185.7	6/60	2/29	0/4	0/3	0/3	0/31	0/0	0/0	0/52	0/0	0/0	0/55
17	15,354.2 to 15,366.2	22/43	19/54	0/0	0/0	0/0	2/29	0/0	0/0	0/0	0/0	0/0	9/49
18	16,006.5 to 16,027.2	18/45	0/9	0/1	1/4	2/9	3/73	0/0	0/0	0/0	0/0	0/1	0/63
19	16,701.6 to 16,720.6	8/63	1/6	0/3	0/5	1/6	0/40	0/0	0/0	0/0	0/0	0/1	27/72

---

* These numbers represent high and low values for the several samples examined from each core, except for core 1 where only one sample was studied.

**Abbreviations: Qtz, quartz; Plag, plagioclase feldspar; K-spar, potassium feldspar; Sid, siderite; Pry, pyrite; Cal, calcite; Ebl, hornblende; Clino, clinoptilolite; Anlc, analcite; Hem, hematite; Ank, ankerite.

TABLE 5. X-ray diffraction data from conventional cores--ranges for North Aleutian Shelf COST No. 1 well for the fraction finer than 5 microns (from AGAT Consultants, Inc., 1983).

Core Number	Depth in feet	Percent*				
		**Chl	Kaol	Ill	Ml	Chl-Smect
1	3,392.4	/36	/25	/13	/26	0/0
2	4,191.6 to 4,200.3	31/39	20/23	11/20	29/32	0/0
3	5,227.3 to 5,244.3	34/65	0/17	11/47	0/27	0/0
4	5,970.3 to 5,995.3	7/61	0/24	7/22	29/82	0/0
5	6,665.3 to 6,668.4	1/34	12/16	9/16	37/54	0/0
6/7	8,051.0 to 8,092.9	11/26	8/21	5/23	45/69	0/0
8	8,628.2 to 8,656.8	20/65	18/36	1/5	8/51	0/0
9	9,255.9 to 9,263.9	30/48	27/39	2/6	17/36	0/0
10	9,945.2 to 9,980.6	20/52	0/43	4/12	26/54	0/1
11	10,326.8 to 10,336.8	27/48	37/65	0/1	4/16	0/0
12	10,732.6 to 10,739.7	15/44	11/33	0/0	31/69	0/0.
13	11,085.7 to 11,107.1	0/43	0/30	0/15	3/93	5/41
14	12,249.0 to 12,266.4	0/100	0/32	0/3	0/100	0/1
15	12,638.8 to 12,654.9	26/98	0/0	0/0	2/74	0/1
16	14,165.6 to 14,185.7	0/100	0/34	0/41	0/100	0/0
17	15,354.2 to 15,366.2	23/83	0/25	3/25	1/44	0/0
18	16,006.5 to 16,027.2	29/89	10/28	0/1	0/51	0/0
19	16,701.6 to 16,720.6	10/73	7/31	0/2	8/82	0/0

---

* These numbers represent high and low values for the several samples examined from each core, except for core 1 where only one sample was studied.

**Abbreviations: Chl, chlorite; Kaol, kaolinite; Ill, illite; Ml, mixed-layer clays (commonly illite and smectite); Chl-Smect, mixed-layer chlorite and smectite.

TABLE 6. Summary of petrographic data. Modified from AGAT Consultants.

Zone	Zone Depth (feet)	Number of Samples	Major Lithologies	Average Q/F/L Framework	Sandstone Sorting & Grain Size	Relative Amounts of Lithics
A	1,000-2,510	3	Mud, clay, sandy diatom ooze	37/23/40	P-M, VF-F	V >> S > M
B-1	2,510-4,110	7	Laminated diatomaceous ooze, sandy mudstone	39/19/42	P-W, VF-F	V >> S > M
B-2	4,110-4,870	10	Clay-rich fine- to medium-grain sandstone	34/17/49	VP-W, VF-M	V > S = M
B-3	4,870-5,675	14	Siltstone, fine- to coarse-grain sandstone	29/21/50	P-M, VF-M	V > S > M
C-1	5,675-6,470	16	Fine- to coarse-grain sandstone, and siltstone	35/23/42	VP-P, F-M	V > S = M
C-2	6,470-7,900	20	Fine- to coarse-grain sandstone, siltstone	49/14/35	P-W, VF-VC	V > M > S
D-1	7,900-9,555	64	Very fine- to coarse-grain sandstone, conglomerate, shale, claystone	20/22/58	P-M, VF-M	V >> S > M
D-2	9,555-10,380	45	Fine- to coarse-grain sandstone, siltstone, mudstone, sandy mudstone	26/21/53	VP-P, VF-M	V >> M > S
E	10,380-15,620	89	Fine- to coarse-grain sandstone, conglomerate, siltstone, shale, mudstone	10/29/61	VP-W, VF-VC	V
F	15,620-16,652	10	Fine- to coarse-grain sandstone, mudstone, siltstone, conglomerate	6/6/88	P-M, VF-M	V
G	16,652-17,155	13	Fine- to coarse-grain sandstone, mudstone, siltstone, conglomerate	9/5/86	P-M, VF-M	V

Abbreviations: **Q** - quartz, **F** - feldspar, **L** - lithic fragments, **V** - volcanic, **M** - metamorphic, **S** - sedimentary; Sorting, **P** - poor, **M** - moderate, **W** - well, **VP** - very poor; Grain size, **VF** - very fine, **F** - fine, **M** - medium, **VC** - very coarse

TABLE 7. Summary of reservoir characteristics. Modified from AGAT.

Zone	Zone Depth (feet)	Number of Samples	Estimated Visible Porosity (%)	Average Measured Porosity (%)	Average Measured Permeability (millidarcies)	Reservoir Potential
A	1,000-2,510	3	3 - 10	33.9	408.0	Extremely poor to good
B-1	2,510-4,110	7	28 - 33	37.3	1,358.0	Nonreservoir to poor
B-2	4,110-4,870	10	2 - 20	36.0	77.0	Extremely poor to good
B-3	4,870-5,675	14	0 - 30	32.0	1,203.0	Extremely poor to good
C-1	5,675-6,470	16	1 - 14	29.3	72.0	Extremely poor to fair
C-2	6,470-7,900	20	1 - 24	28.8	2,648.0	Poor to good
D-1	7,900-9,555	64	1 - 17	27.2	490.0	Nonreservoir to good
D-2	9,555-10,380	45	0 - 2	17.5	3.9	Nonreservoir to fair
E	10,380-15,620	89	0 - 8	15.0	27.1	Nonreservoir to poor
F	15,620-16,652	10	0	9.9	1.0	Nonreservoir
G	16,652-17,155	13	0	10.15	0.69	Nonreservoir

3. Velocity Analysis in Relation to Seismic Reflection Correlation and Depth Conversion

by

Peter J. Hoose

Seismic velocity in strata penetrated by the COST No. 1 well was evaluated for the purpose of depth conversion. Data used in this interpretation included the long-spaced sonic log, 11 velocity spectra displays from two seismic profiles that intersect near the well, and two unreversed sonobuoy refraction profiles shot by the U.S. Geological Survey near the well (Cooper and others, 1982). The results of a borehole velocity survey submitted by ARCO under the terms of the permit were also used in this evaluation. Unless otherwise specified, depths were measured from sea level.

A borehole velocity survey, shot as a vertical seismic profile (VSP), was conducted for the purpose of calibrating the borehole-compensated sonic log. Seismograph Service Corporation, which conducted the survey and calibrated the log, reported that during the survey, shots were made every 50 feet, but in order to avoid producing unrealistic interval velocities due to the small depth intervals, the sonic log was calibrated in 200-foot increments. The calibration procedure involved comparing measured travel-time intervals from the borehole velocity survey with the corresponding integrated travel-time intervals from the raw sonic data. A deviation plot (fig. 56), which shows differences between the borehole velocity survey and the sonic data, was constructed from this comparison. The deviation plot was then used to adjust the raw sonic data in such a way that when reintegrated, the sonic data agreed with the borehole velocity survey. Adjustments consisted of either linear or differential lateral shifts of the raw sonic data on the log. Differential adjustments were applied whenever the borehole velocity survey travel time minus the sonic-log travel time integrated over a discrete interval was positive, thus indicating that the sonic velocities for that interval were too low. Anomalously low sonic velocities result from borehole effects such as washout, formation alteration, and fracturing. Borehole effects do not affect checkshot velocities. Differential adjustments are expressed as a percentage of the raw sonic log data. Linear adjustments were applied whenever the difference between the velocity survey and sonic log data indicated that the error was negative,

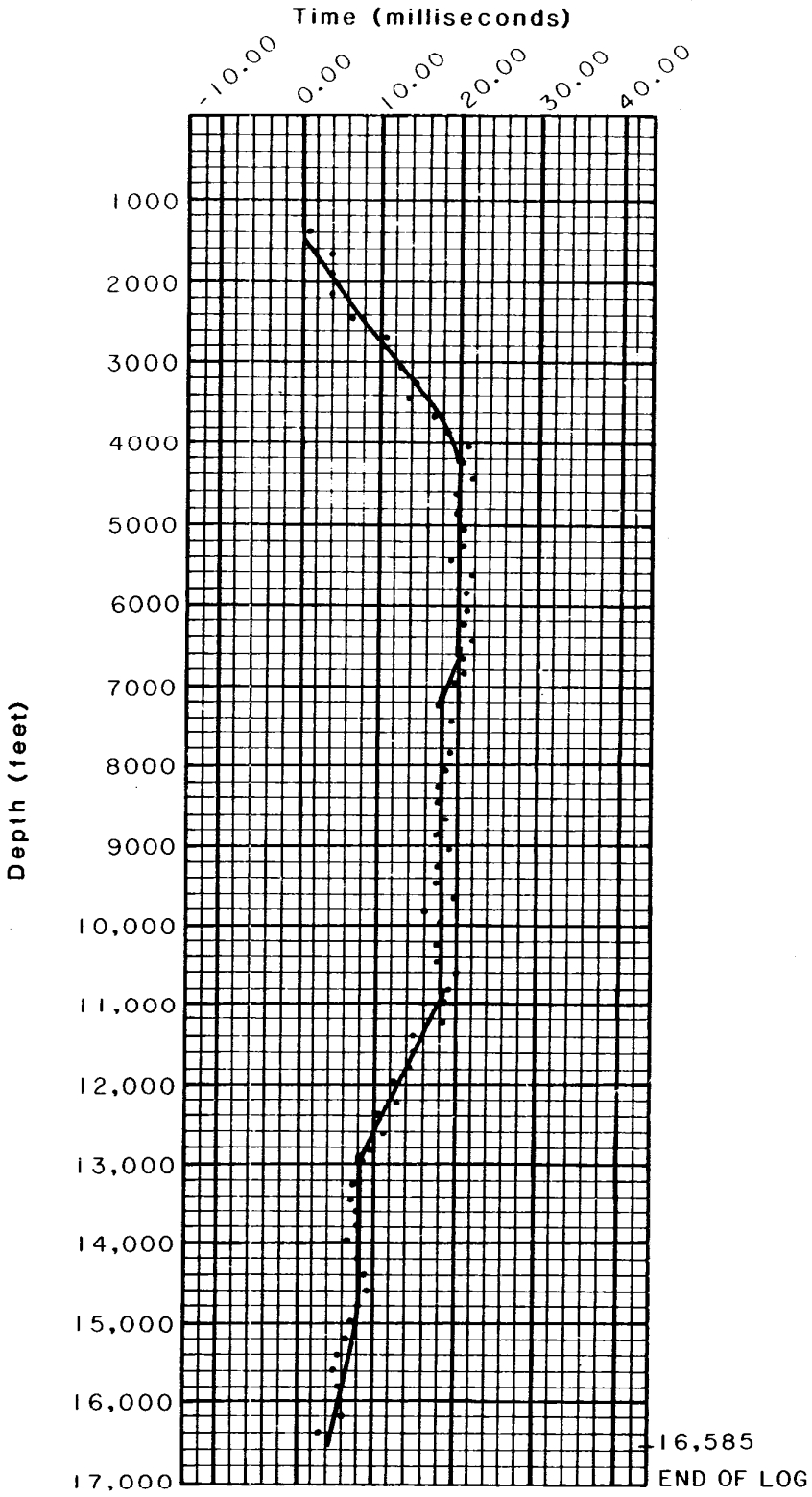

FIGURE 56. **Sonic–log deviation plot showing differences between travel-time data from the velocity survey and the corresponding integrated time intervals from the raw sonic log. Dots represent the arithmetic difference at each velocity calculation depth. Depths are below sea level.**

hence instrumental in origin. Calibration parameters and their corresponding depth ranges are listed below.

Depth Range (feet)	Adjustment
top of log - 2,328	96.2% differential
2,328 - 3,750	94.7% differential
3,750 - 4,344	97.6% differential
4,344 - 6,778	no adjustment
6,778 - 7,334	3.6 microseconds per foot
7,334 - 10,990	no adjustment
10,990 - 13,186	4.6 microseconds per foot
13,186 - 14,718	no adjustment
14,718 - end of log	2.0 microseconds per foot

Interval velocities (fig. 57), a time-depth curve (fig. 59), and root-mean-square (RMS) velocities (fig. 60) were calculated from the sonic log by computer at MMS. A comparison of sonic travel times between the uncalibrated, long-spaced sonic log and the calibrated, borehole-compensated sonic log made at 400-foot intervals revealed that the average difference between the two logs was 3.9 microseconds per foot and the standard deviation of this differential was 3.7 microseconds per foot. Since this differential was relatively small, the uncalibrated, 5-inch, long-spaced sonic log was used rather than the calibrated log because it was felt that errors introduced by digitizing the calibrated log, which was displayed at 1 inch per 100 feet, would offset the advantage of the calibration procedure.

A synthetic seismogram was generated by MMS personnel from the digitized long-spaced sonic log. The 5-inch log was used in order to minimize errors from digitizing, and accuracy is estimated to be better than 1 microsecond per foot in transit time and 0.5 foot in depth. Reflection coefficients were determined from the travel-time data while assuming constant density. Reflection coefficients were then convolved with a standard 8 to 55 Hz Ricker wavelet in a computer program that generates a synthetic seismogram without multiples. The computer program assumes horizontal strata and planar incident waves that propagate perpendicular to reflecting surfaces. The synthetic seismogram is displayed in both normal and reverse polarity and is shown with a segment of a nearby seismic profile in figure 57.

In figure 57, reflections on the synthetic seismogram fail to correlate precisely with reflections on the seismic profile. This discrepancy may be attributed, in part, to two causes: (1) the COST well was not sited exactly on the seismic profile but, rather,

slightly downdip of it; (2) whereas the seismic profile was processed using a minimum-phase wavelet, the synthetic seismogram was generated using a zero-phase wavelet. This difference in wavelet phase would result in a slight time differential between the seismic profile and the synthetic seismogram.

In addition to the analysis performed by MMS using the sonic log, a curve derived from the borehole velocity survey that depicts interval velocities calculated at 200-foot intervals is shown in figure 58. Refraction velocities calculated by MMS personnel from USGS sonobuoys shot near the well site (Cooper and others, 1982) are also shown in figure 58. Interval velocities calculated from the sonobuoy data agree fairly well with borehole-derived velocities. The relatively high velocity at a depth of 9,400 feet calculated from sonobuoy 202 may be attributed to the location of the profile, which was north of and almost normal to the basin axis and thus resulted in shooting updip across its northern flank.

At the COST No. 1 well, interval velocities generally increase with depth down to approximately 10,000 feet (figs. 57, 58). Below this depth, interval velocities are slower than would be predicted on the basis of both the depth range and the velocity gradient from the start of the data at 1,363 feet down to 10,000 feet. Because borehole effects have a negligible effect on velocities determined from the vertical seismic profile technique, these unexpectedly low velocities are considered to reflect some lithologic parameter. An evaluation of conductivity, density, and sonic travel time in shale layers penetrated by the COST well (see Abnormal Formation Pressure chapter) revealed that abnormally high formation pressures exist in the well below approximately 11,200 feet below KB. High interstitial fluid pressure tends to lower sonic velocities measured in fractured or porous rock because it reduces both the bulk and shear moduli. Although overpressuring is evident below approximately 11,200 feet, VSP-derived interval velocities (fig. 58) begin to fall off just below 10,000 feet. This apparent discrepancy is partially reconciled by the presence of coal beds below 10,400 feet below KB, which also tend to reduce interval velocities.

Figure 59 shows a comparison between time-depth (T-D) curves derived from the sonic log and from nearby common-depth-point (CDP) seismic reflection data. The sonic log T-D curve was generated by integrating interval transit times, whereas the seismic T-D curve was generated by integrating interval thicknesses calculated from the Dix equation (Dix, 1955) using stacking velocities. These curves show very good agreement between the depth conversion functions determined from the two methods.

Maximum coherency stacking velocities were picked from 11 velocity spectra displays along two CDP seismic reflection lines that intersect approximately 900 feet east of the well. Velocities were picked at major velocity changes, and linear interpolations were made between them to depths corresponding to major reflectors. These values were then averaged over 100-millisecond intervals and a curve was fitted to them.

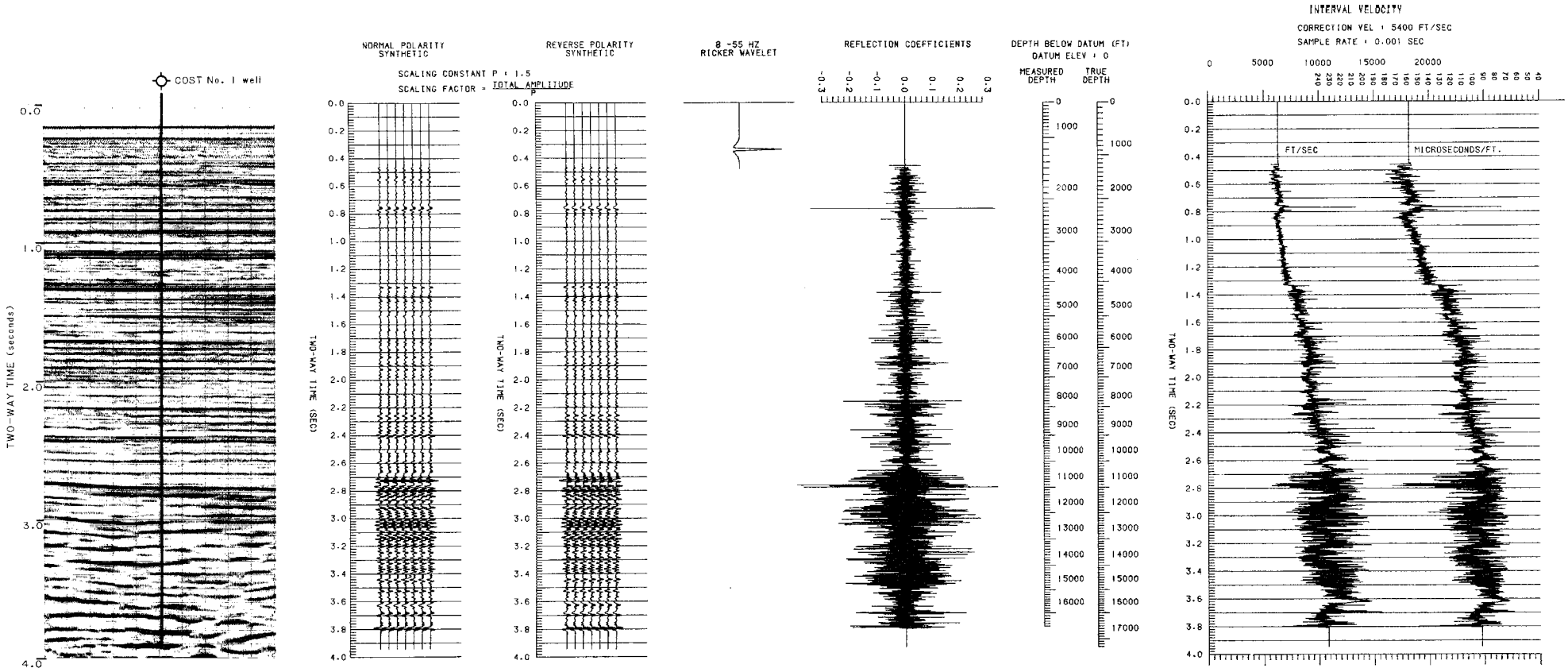

FIGURE 57. Synthetic seismogram of the North Aleutian Shelf COST No. 1 well and part of a nearby seismic reflection profile.

This page was intentionally left blank.

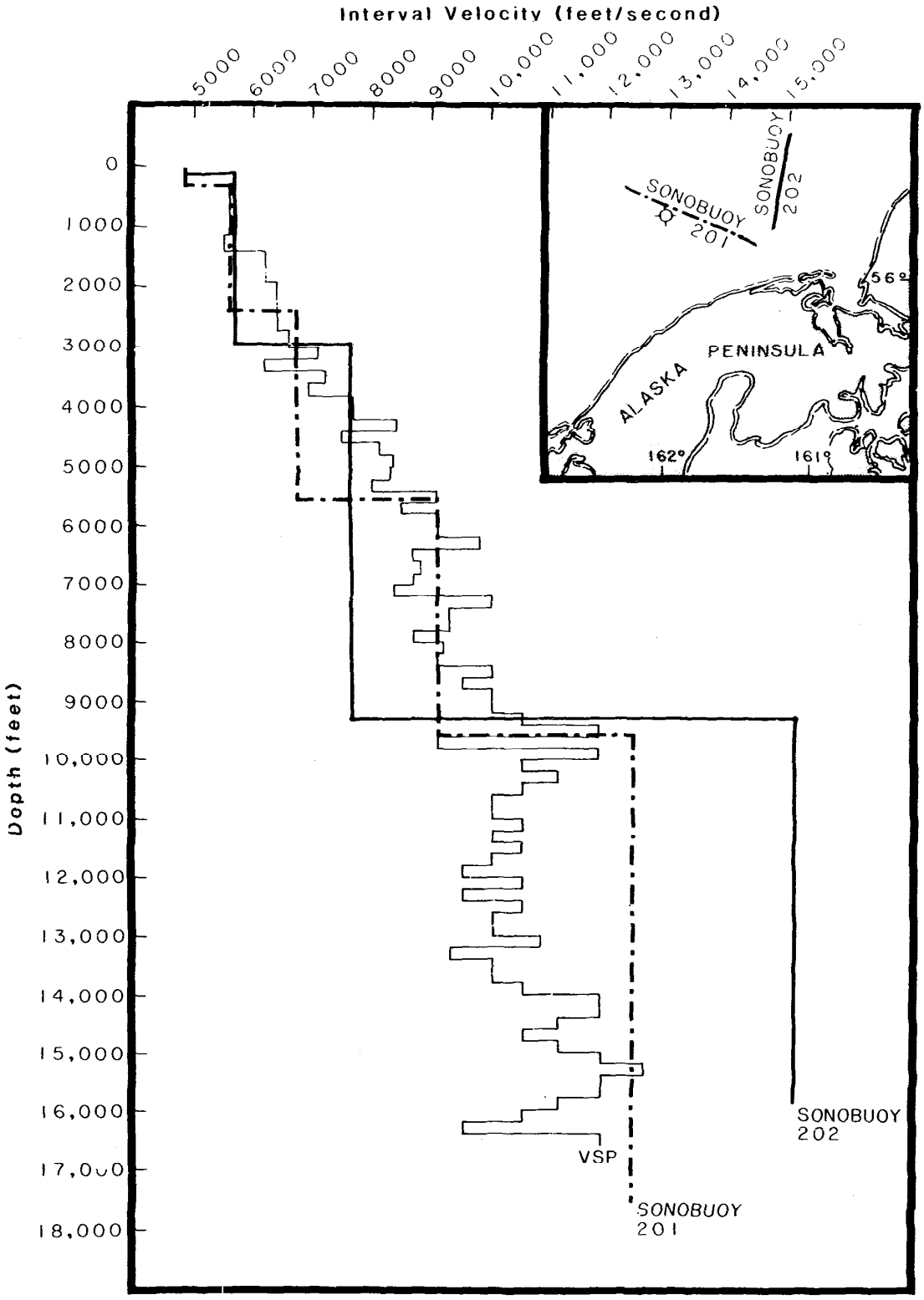

FIGURE 58. **Comparison between VSP-derived and sonobuoy-derived interval velocities. VSP-derived interval velocities were submitted by ARCO. Depths are below sea level.**

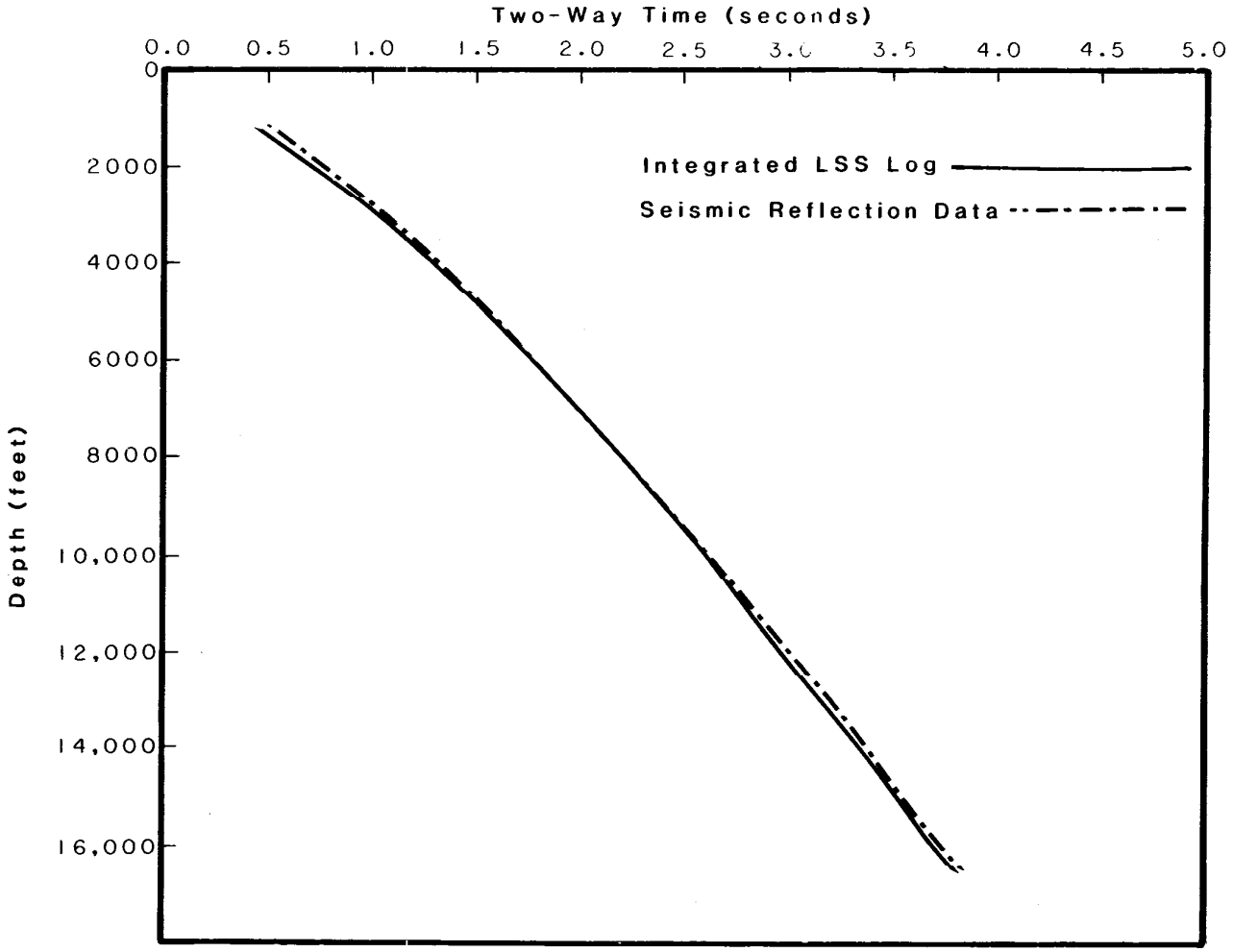

FIGURE 59. **Comparison between time-depth curves generated from an integrated long-spaced sonic (LSS) log and from seismic reflection data in the vicinity of the COST No.1 well. Depths are below sea level.**

No stacking velocity picks were made below 2.8 seconds two-way reflection time because of low coherence due to the presence of complexly dipping reflectors. Below this depth, the stacking velocity curve was extrapolated. This curve is shown in figure 60 along with a computer-generated RMS velocity curve derived from the sonic log. This figure shows fairly good agreement between the two curves.

Anstey (1977) indicates that some of the differences frequently observed between stacking and RMS velocities may be accounted for by the broad spread of the CDP ray paths relative to the vertical alignment of the sonic data. This geometric difference can amplify the effects of absorption, short-path multiples, and scattering, thus resulting in greater loss of high frequencies and producing a stacking velocity that is correspondingly lower than the RMS velocity. Banik (1983, 1984) cites five other possible causes of discrepancies observed between stacking and well log RMS velocities: (1) velocity anisotropy of subsurface layers, (2) the presence of dipping beds, (3) processing errors, (4) short cable lengths, and (5) the fundamental assumption that stacking velocities are equivalent to RMS velocities. The following analysis addresses the first two possible causes cited by Banik (the last three causes are beyond the scope of this study).

Banik (1983) derived a formula to quantitatively express velocity anisotropy. His formula calculates an anisotropy parameter (A) from vertically aligned interval velocities measured from the sonic log (Vv) and from horizontally aligned interval velocities calculated from stacking velocities (Vh)(Levin, 1978). Figure 61 shows how the anisotropy parameter, defined by the equation

$$A = 100(Vh - Vv)/Vv$$

and calculated at 200-millisecond intervals, varies with two-way travel time in strata underlying North Aleutian Basin. For comparison, figure 61 also shows the stacking velocity and RMS velocity curves. In two depth intervals, which correspond to lithologic zone C-2 and to the lower part of lithologic zone B-1, A is nearly zero and stacking velocities are approximately 3 percent less than RMS velocities. In almost all other depth intervals, A is negative (vertically aligned interval velocities are faster than horizontally aligned interval velocities) and stacking velocities are less than RMS velocities. In his regional study of velocity anisotropy in strata underlying the North Sea, Banik (1983, 1984) determined that anisotropy in that basin is due to the presence of shale. Uhrig and Van Melle (1955) noted that some limestone and chalk formations also behave anisotropically. Kaarsberg (1959) reported a pronounced anisotropy in shale samples studied in the laboratory. In all of these cases, however, the seismic velocity in the plane of bedding was greater than the velocity normal to bedding, and the anisotropy parameter was accordingly positive. Thus velocity anisotropy is not a satisfactory explanation for the differences observed between stacking and RMS velocities in the North Aleutian Basin.

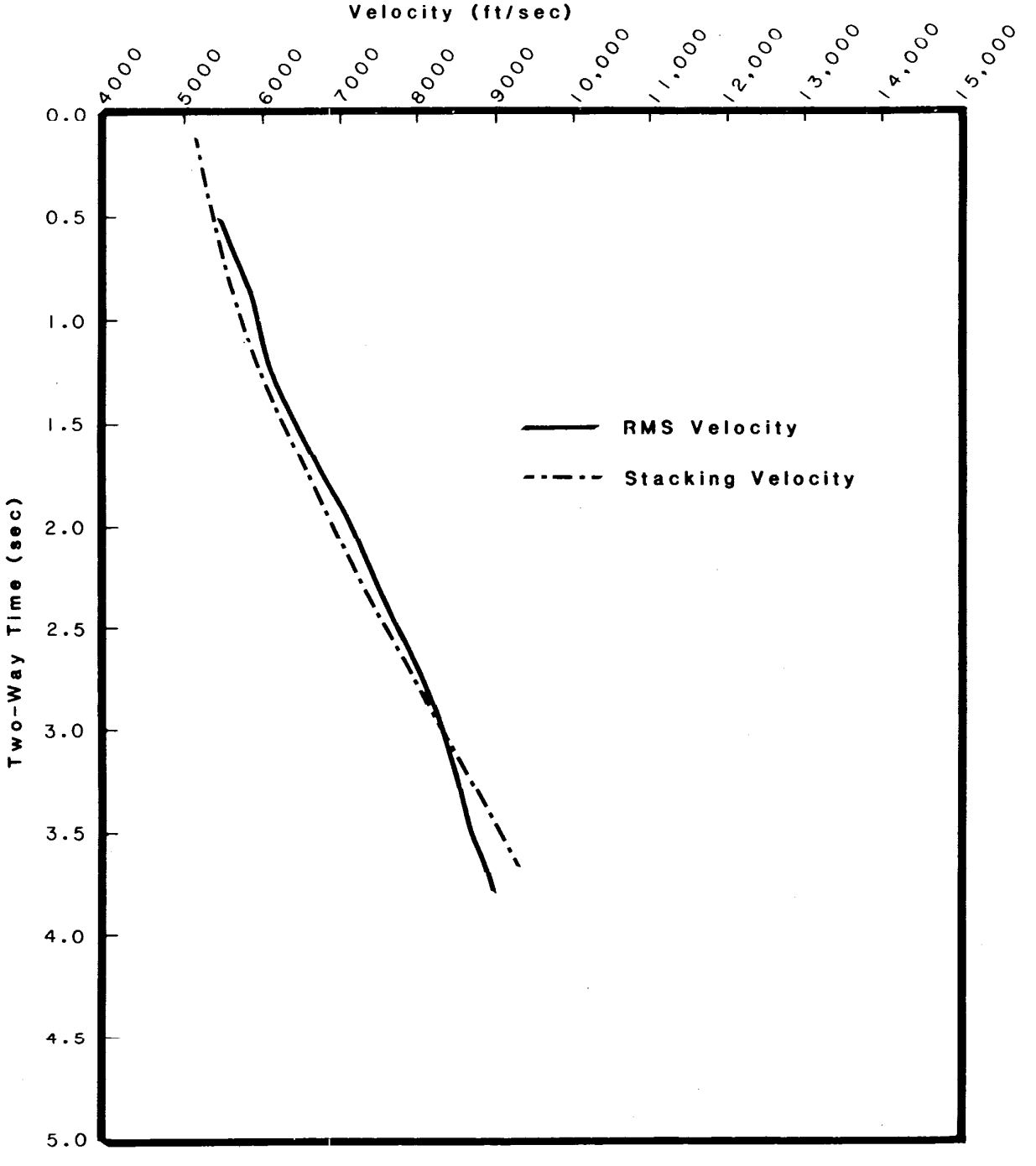

FIGURE 60. Comparison between RMS velocities derived from the long-spaced sonic log and stacking velocities determined from CDP seismic profiles in the vicinity of the COST No.1 well.

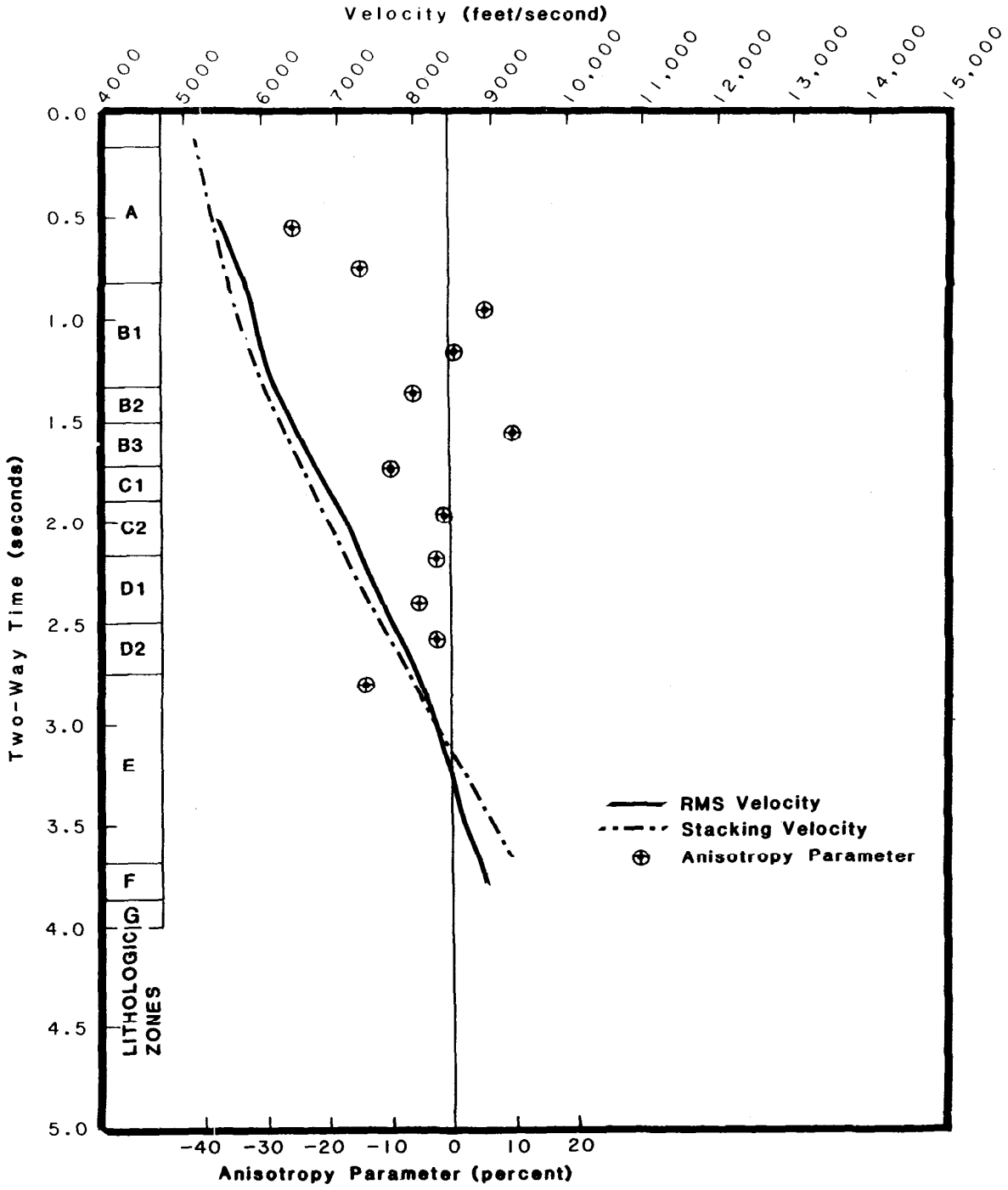

FIGURE 61. Anisotropy parameter (A), lithologic zones, RMS velocities calculated from the integrated long-spaced sonic log, and an averaged stacking velocity curve derived from CDP seismic reflection data in the vicinity of the COST No.1 well.

To evaluate whether dip may be responsible for the velocity discrepancy, this author traced four marker reflections along the seismic profiles from which the stacking velocity picks were made. At the well site, these reflections ranged in depth from 0.80 to 2.74 seconds two-way reflection time. Reflection times to the four reflectors along the 8.4 miles of profiles stay within 3, 2, 3, and 12 milliseconds, respectively, of the reflection times recorded closest to the well site, and the greatest local apparent dip measured from the profiles was 6.7^{o}. A dip of this magnitude will produce a differential of less than 1 percent between the stacking and RMS velocities. These relatively low values indicate that dip is not responsible for the observed velocity discrepancy.

In summary, RMS velocities determined from the sonic log are slightly higher than stacking velocities determined from nearby seismic reflection data but are otherwise in fairly good agreement. Time-depth curves calculated from both data sets are nearly identical. Interval velocities calculated from the COST No. 1 well sonic log agree fairly well with interval velocities measured from the vertical seismic profile, and interval velocities determined from sonobuoy data are also comparable. Interval velocities generally increase with depth down to approximately 10,000 feet below sea level; below this depth, they fall off markedly. This drop, evident on both the sonic log and on check shot data, is attributed to the presence of coal beds and overpressuring.

4. Geologic Setting and Tectonic Framework

by

Peter J. Hoose

The Atlantic Richfield Company (ARCO) North Aleutian Shelf COST No. 1 Well was drilled in the North Aleutian Basin (fig. 2) near the southern margin of the Bering Sea shelf. Both the North Aleutian Basin, formerly called the Bristol Bay Basin, and the eastern half of Amak Basin are included within the boundaries of the North Aleutian Basin Outer Continental Shelf Planning Area. The planning area lies north of the Aleutian magmatic arc, which is the intrusive and extrusive manifestation of the convergence between the Pacific and North American lithospheric plates. The well penetrated 17,155 feet of Cenozoic strata which unconformably overlie economic basement composed of Mesozoic and possibly older clastic, volcaniclastic, and volcanic rock.

The Bering Sea shelf is one of the most expansive continental shelves in the world. Defined by the 500-foot isobath near the shelf break, the shelf comprises 470,000 square miles, approximately half the area of the entire Bering Sea. It is the world's widest shelf; at its widest section, it extends 400 miles from shoreline to shelf break. The shelf is extremely flat, with an average gradient of only 0.24 meter per kilometer (1.25 feet per mile)(Sharma, 1979). The most dramatic physical features of the otherwise flat and featureless shelf are large submarine canyons that incise the shelf edge.

The structure, stratigraphy, and tectonic evolution of the Bering Sea shelf and the adjacent Alaska Peninsula and Aleutian arc have been discussed by Hoare (1961), Burk (1965), Scholl and others (1968), Plafker (1969), Patton (1973), Reed and Lanphere (1973), Nelson and others (1974), Brockway and others (1975), Scholl and others (1975), Cooper and others (1976), Marlow and others (1976, 1977), Cooper and others (1977), Mancini and others (1978), Lyle and others (1979), McLean (1979a, 1979b), Stone and Packer (1979), Marlow and Cooper (1980, 1983), Gardner and Vallier (1981), Wallace and Engebretson (1984), and Wilson (1985).

The southern Bering Sea continental shelf is underlain by Cenozoic strata that overlie a structurally complex assemblage of lithologically diverse rocks that are Mesozoic and older in age. Five regional structural features underlie the shelf. These features, which are elongate and trend parallel to the continental margin, are the St. George, Amak, and North Aleutian Basins, and the

Black Hills and Pribilof ridges. Unlike St. George Basin, which is a graben, the North Aleutian Basin is a structural depression that lacks major bounding faults. An angular unconformity separates the Mesozoic and older rocks that form the core of the Pribilof and the Black Hills ridges from the relatively undeformed overlying Cenozoic strata. Marlow and Cooper (1980) traced this unconformity off the crests of the ridges and into the subjacent basins where it becomes a disconformity. They proposed that the North Aleutian Basin began to subside in the late Mesozoic on the basis of an inferred Cretaceous age for this unconformity. However, on the basis of seismic and paleontologic data discussed elsewhere in this report, this unconformity is assigned a probable late Oligocene age.

Marlow and others (1977) invoked oblique convergence and subduction of the Kula plate along the Beringian margin during the Mesozoic to account for some of the principal aspects of geology and structural trends in this region. More recently, Marlow and Cooper (1983) interpreted the offshore extension of the Black Hills structural high to be part of the allochthonous Peninsular terrane of southern Alaska. Paleomagnetic data from this and other terranes that make up the western North American cordillera indicate that they originated in more southerly latitudes and were subsequently transported northward and accreted onto the craton (Jones and others, 1970, 1972; Jones and Silberling, 1979; Monger and others, 1972; Coney and others, 1980; Beck, 1980; Wallace, 1983; Marlow and Cooper, 1983).

5. Seismic Stratigraphy

by

Peter J. Hoose

The strata in the North Aleutian Basin are here divided into five seismic sequences designated I through V (fig. 62). Each seismic sequence represents a relatively conformable unit of genetically related strata bounded by unconformities or their correlative conformities. Depositional facies were inferred from seismic facies on the basis of the scheme developed by Mitchum and others (1977), Sangree and Widmier (1977), and Brown and Fisher (1982). Collectively, these sequences represent and reflect much of the geologic history and evolution of the basin.

Evidence of at least five Tertiary unconformities is present on seismic profiles collected in the North Aleutian Basin. At the COST No. 1 well, these unconformities are manifested by Tertiary horizons A through D and by an unmapped Oligocene unconformity of limited regional extent. Two of these unconformities, horizons B and C, are particularly significant because of their nearly basin-wide extent. The origins of these two unconformities are probably linked to the subduction of the Kula-Pacific spreading center (DeLong and others, 1978, 1980) during late Oligocene or early Miocene time, and to a substantial drop in global sea level during middle Oligocene time (Vail and others, 1977)

The stratigraphic interpretation of the North Aleutian Basin presented herein was based primarily on 120-channel, common-depth-point (CDP) seismic reflection data shot by private industry (fig. 63). Also used in the interpretation was a synthetic seismogram generated from the COST No. 1 well sonic log by MMS personnel (fig. 57). Unless otherwise specified, depths are measured from sea level rather than from the Kelly bushing (KB), which is 85 feet higher.

In the following discussion, the term "amplitude" is frequently used. Since the seismic profiles were processed with time-varying gain (TVG), the term "amplitude" should not be considered a quantitative assessment of the amount of energy returned from a particular reflecting surface, but rather a subjective comparison of the relative differences in acoustic impedance across reflectors.

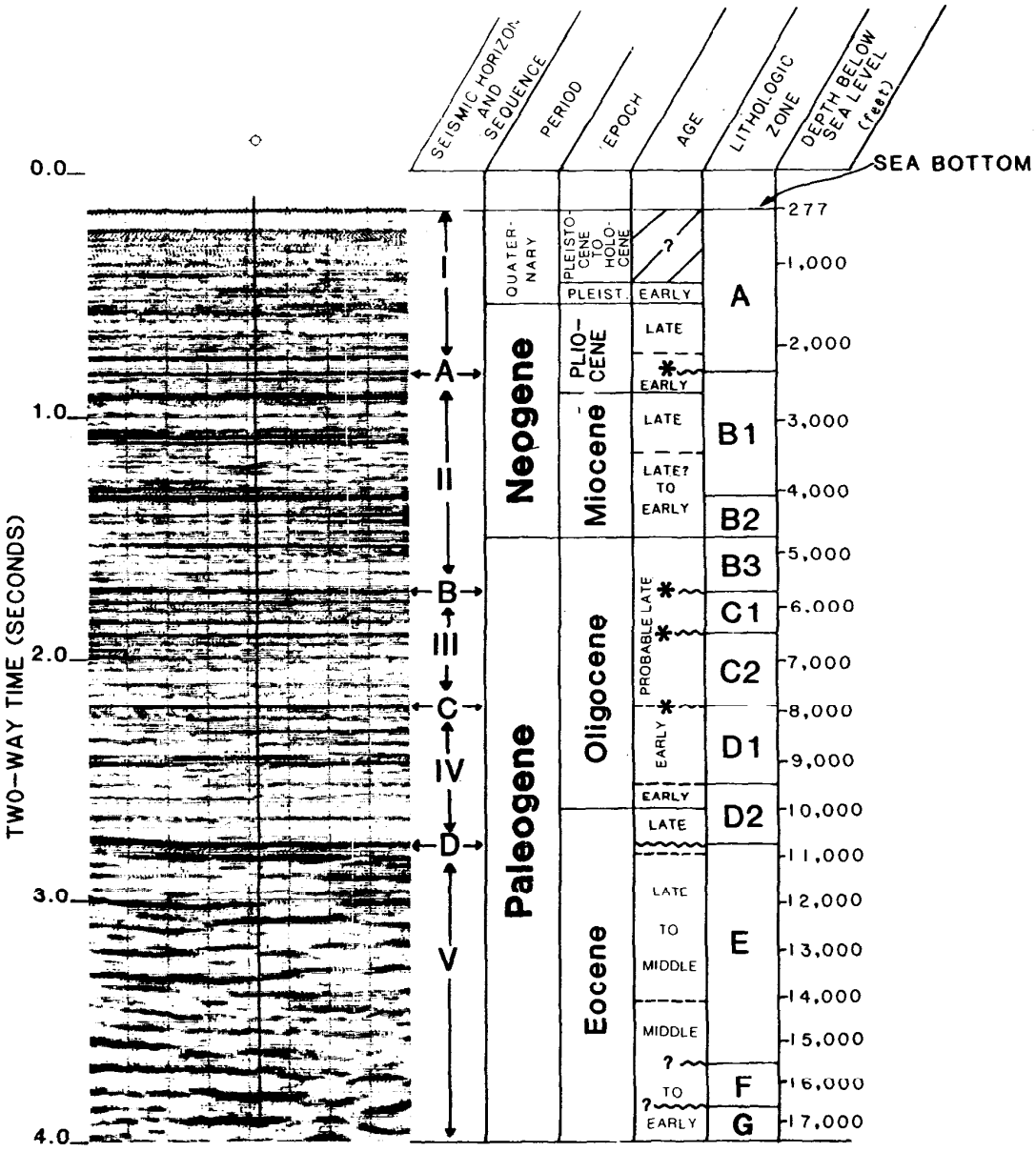

FIGURE 62. Seismic sequences, seismic horizons, and a time-stratigraphic column interpreted from COST No. 1 well data. Also shown is a portion of a seismic profile near the well. Horizon D is shown deeper than on other figures because the well was drilled slightly north and up-dip of the seismic profile.Horizons that correlate with basin-flank unconformities are indicated by asterisks.

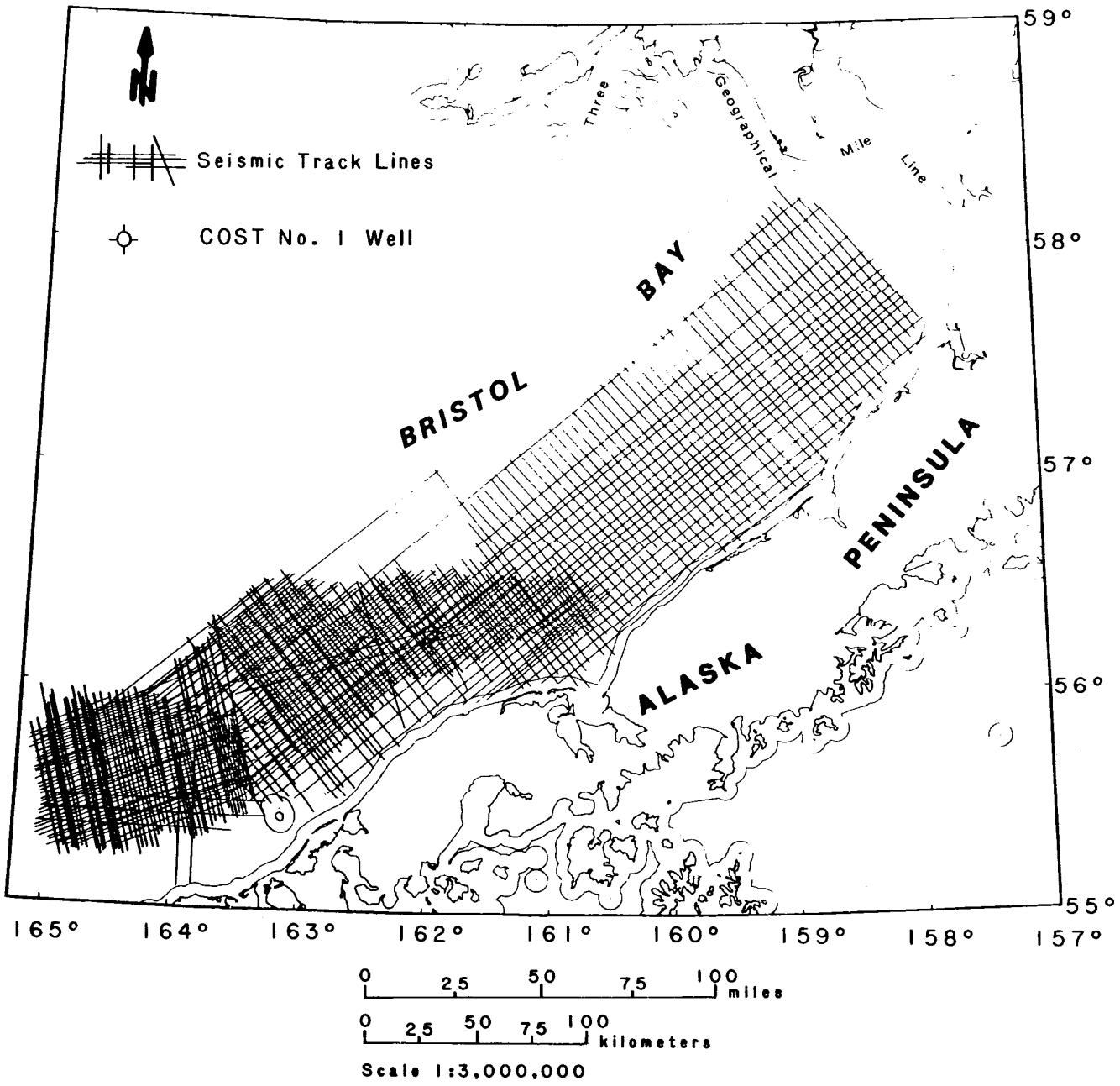

FIGURE 63. CDP seismic reflection data coverage in the North Aleutian Basin Planning Area.

SEISMIC SEQUENCE I

At the COST No. 1 well, seismic sequence I (sea floor to 2,425 feet) is made up of unconsolidated sediment of Pleistocene and Pliocene age. The sequence consists of two similar yet distinct seismic facies. The base of sequence I, horizon A, is represented by a moderately continuous reflection with variable amplitude.

The upper seismic facies of seismic sequence I consists of parallel reflections of moderate to high amplitude and moderate to high continuity. Amplitude and continuity remain relatively uniform throughout this facies. This combination of seismic characteristics suggests a shelf depositional environment (Sangree and Widmier, 1977) that was probably reworked by bottom currents and long-period waves in much the same way as is the present Bering Sea shelf. Such reworking by currents and waves and the resultant redistribution of sea-floor sediment could account for why some reflections are less continuous than others.

In contrast with the uniformity of the upper facies of seismic sequence I, the lower seismic facies is represented by a complex interval of concordant, predominantly parallel reflections of variable amplitude and moderate continuity that are punctuated by packages of prograding clinoforms (fig. 64). The prograding clinoforms commonly display a shingled configuration. Occasionally, they have a toplapped upper surface which may indicate a period of shallow marine conditions. The apparent dip of the clinoforms indicates that the sediment isochrons which they represent prograded from the Alaska Peninsula roughly towards the northwest.

Reflection amplitude and continuity within the lower seismic facies vary with the orientation of the seismic profile. On dip lines (fig. 64), the reflection amplitude is moderate and the continuity is broken by interference between horizontal reflections and clinoforms. On strike lines (fig. 65), a few widely spaced and highly continuous reflections are separated by reflections of variable amplitude and continuity. These seismic characteristics generally denote a prograding delta system (Brown and Fisher, 1982). Those intervals on strike lines that are characterized by variable amplitude and continuity represent cross sections through the prograding sedimentary units, whereas the few widely spaced and highly continuous reflections represent either thin delta platform facies or the facies boundaries between depositional units. The transition from the lower to the upper seismic facies occurs at a depth of 1,145 feet at the COST No. 1 well and represents the change from a deltaic depositional environment to a more laterally uniform shelf environment.

Typical of the lower seismic facies is that the packages of prograding clinoforms occur at more than one depth and location on the same seismic profile. On some profiles, superior clinoformal packages occur landward of inferior packages, indicating that the basin experienced multiple sediment advances rather than a single progradational event. This depositional pattern can be produced by a

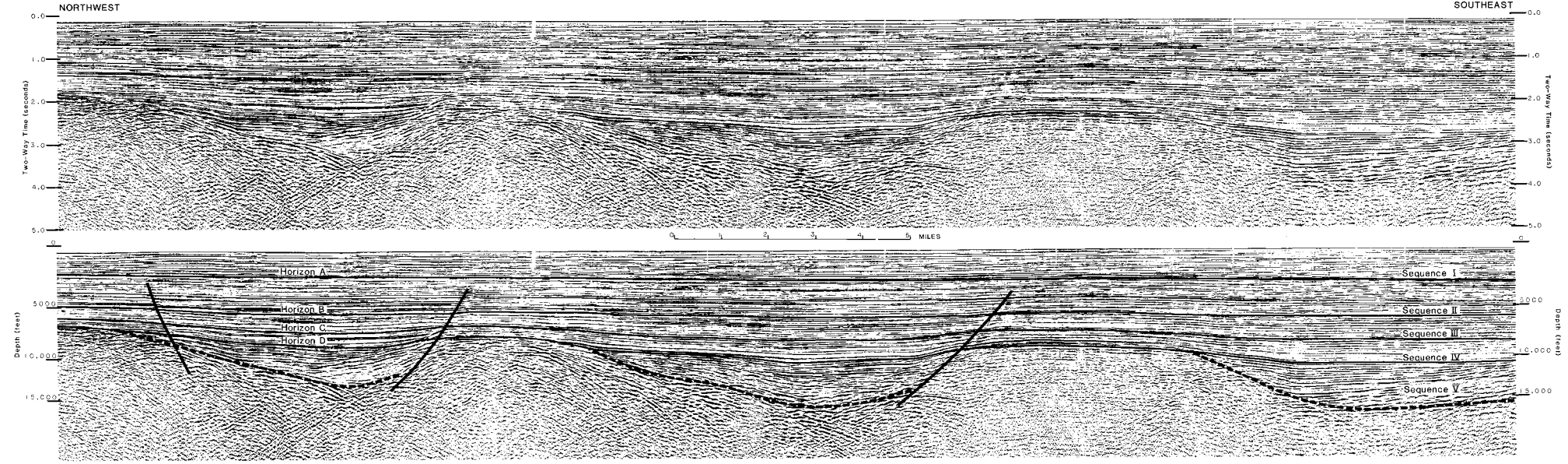

FIGURE 64. Seismic reflection profile (northwest-southeast) and MMS interpretation. Depth conversion based on the COST No. 1 well velocity analysis.

This page was intentionally left blank.

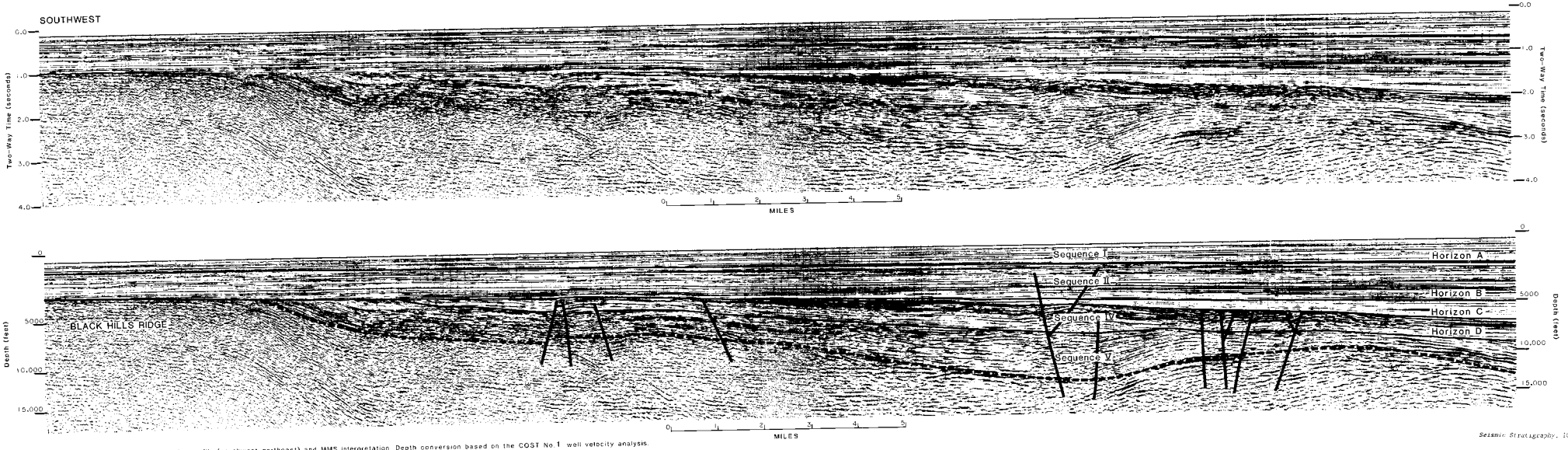

FIGURE 65. Seismic reflection profile (southwest-northeast) and MMS interpretation. Depth conversion based on the COST No. 1 well velocity analysis. Seismic sequence fill is not labeled.

This page was intentionally left blank.

waxing and waning sediment supply being deposited in a basin that is experiencing a rise in relative sea level. The time period during which the lower seismic facies was deposited correlates with an early Pliocene third-order cycle of global sea level rise recognized by Vail and others (1977). Accordingly, the multiple progradational events observed on the seismic records might have been produced by pulsations in the sedimentation rate which alternately exceeded and then fell short of the combined effects of basin subsidence and sea level rise. Data from the COST No. 1 well reveal that most of the detritus comprising this seismic facies is volcaniclastic, as is the correlative Milky River Formation on the Alaska Peninsula. An intensification of volcanic activity in the North Pacific at this time was recognized by Scholl and Creager (1973) on the basis of lithologic data collected during Deep Sea Drilling Project (DSDP) leg 19. Conceivably, the multiple progradational events evident on seismic profiles collected in the North Aleutian Basin could reflect pulses in volcanic activity along the arc.

Volcanic activity at this time is also apparent in other data from the COST well. Between the depths of 2,210 and 2,220 feet (below KB) on the COST No. 1 well sonic log, the interval velocity jumps abruptly to 13,500 feet per second. This velocity, which is anomalously high for lithified or semi-lithified clastic sediment at this depth, corresponds to a 3-foot layer that shows up on the gamma ray log as being considerably more radioactive than the sediment above or below it. The combination of high sonic velocity and anomalously higher radioactivity suggests that this layer is composed of either welded tuff or highly altered volcanic ash. Similar volcanic deposits were sampled in holes drilled along the Aleutian arc during DSDP leg 19 (Creager and others, 1973). In particular, cores from the nearest DSDP site, site 183, drilled in the Aleutian Abyssal Plain approximately 200 miles south of the COST No. 1 well, sampled several ash layers, including one that was 36 centimeters thick (approximately 14 inches). This ash layer occurs at the same stratigraphic depth, just above the base of the upper Pliocene, as the radioactive interval delineated by well logs in the North Aleutian Shelf COST No. 1 well. The occurrence of volcanic ash at nearly identical stratigraphic horizons in both the COST well and at DSDP site 183 attests to both the large volume of volcanic detritus produced at this time and the effectiveness of wind-borne transport.

In the North Aleutian Basin, the amplitude of horizon A (the base of seismic sequence I) is variable. At the COST well, horizon A is concordant with the underlying reflections at the top of seismic sequence II. At other locations in the basin, horizon A is an angular unconformity. On seismic profiles near the COST No. 1 well and elsewhere in the basin, prograding clinoforms at the bottom of the lower seismic facies downlap on to horizon A (fig. 64). Lithologic data from the COST No. 1 well indicate that the reflection corresponding to horizon A is generated by a contrast in acoustic impedance between a thick shale layer and an underlying sandstone. The positive polarity and variable amplitude of horizon A are consistent with the depositional mode and accompanying contrasts in acoustic impedance that would be expected from a series of

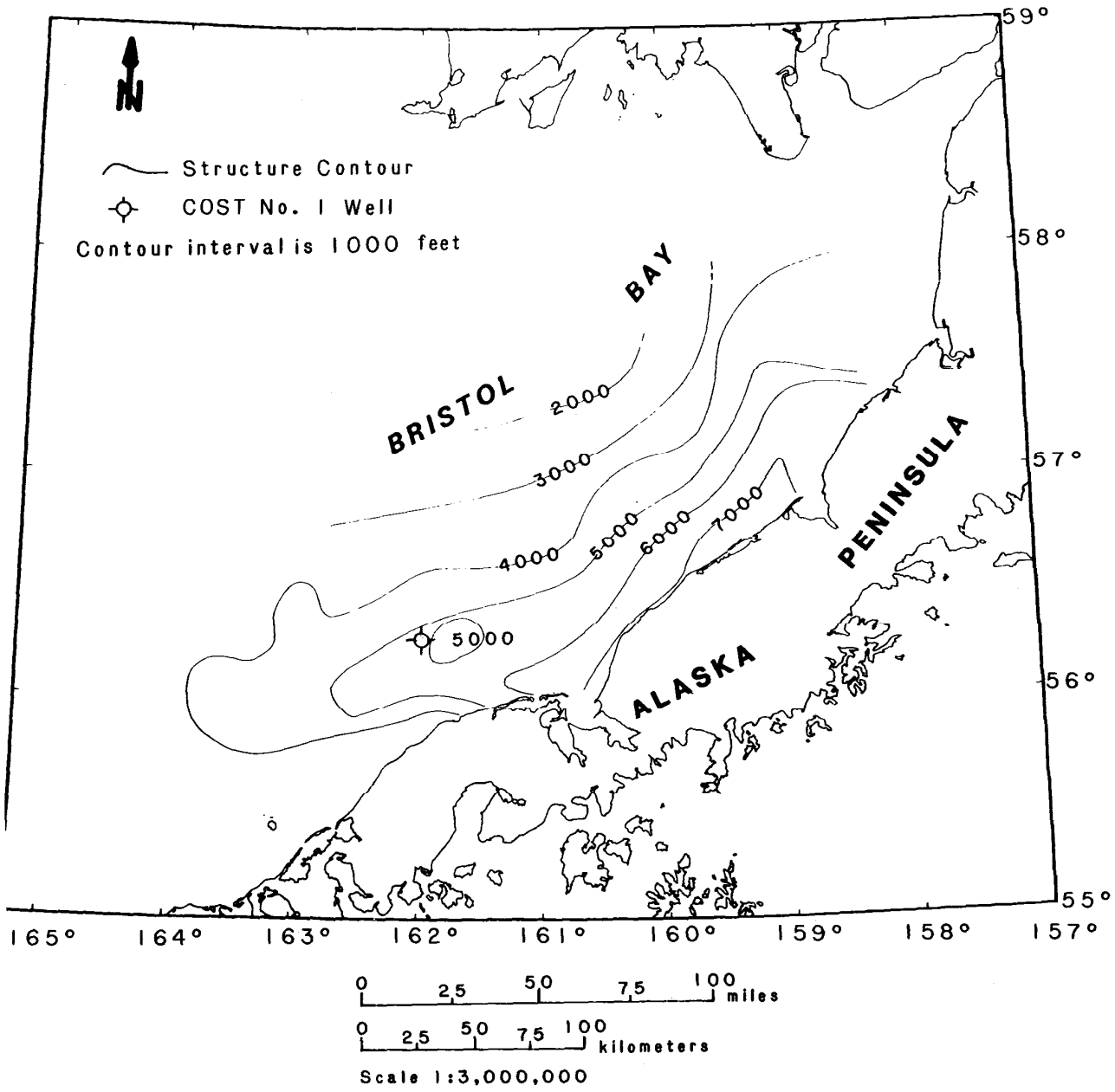

FIGURE 66. **Structure-contour map of horizon B (Oligocene).**

prodeltaic, clay-rich, bottomset beds deposited across an erosional unconformity that had previously exposed laterally varying lithologies.

SEISMIC SEQUENCE II

Seismic sequence II is composed of strata of early Pliocene to late Oligocene age. The strata have been grouped into three lithologic zones designated B-1 through B-3 (fig. 62). The sequence contains two seismic facies, one that corresponds to lithologic zone B-1, the other to lithologic zones B-2 and B-3. The base of seismic sequence II is defined by horizon B, a major, regional unconformity (figs. 62, 65, 66).

The upper seismic facies is characterized by reflections that are predominantly very low in amplitude and often discontinuous. On some seismic profiles this interval is almost acoustically transparent, whereas on others this interval contains irregularly occurring reflections that have conspicuously high amplitude and high continuity. The discontinuous nature of these reflections suggests a spatially and temporally variable depositional environment.

The transition from the upper to lower seismic facies of sequence II coincides with the boundary between lithologic zones B-1 and B-2 (fig. 62). This transition is marked by a downward increase in reflection amplitude and continuity. The lower seismic facies is characterized by a marked decrease in cycle breadth between reflections. This change in cycle breadth corresponds to a similar pattern change apparent on both the spontaneous potential (SP) and gamma ray well logs. In this facies, the SP and gamma ray responses are made up of distinct highs and lows that alternate at 50- to 150-foot intervals. This combination of log patterns generally indicates a section of well-sorted sand with intercalated clay-rich beds. The deposition of sand and clay in alternating 50- to 150-foot-thick stratigraphic units implies a cyclic alternation between high-energy and low-energy depositional environments, perhaps wave-dominated shoreface and tidal flat, or alternatively, between current-scoured and tranquil shelf settings. Microfossil data from the COST No. 1 well, which was drilled in the deepest part of the basin, favor a shelfal setting.

At the southwestern and northeastern ends of the basin, reflections at the bottom of the lower seismic facies onlap horizon B. This onlapping relationship indicates that a relative rise in sea level took place following the period of subaerial exposure that created the horizon B unconformity (figs. 62, 65). During the deposition of seismic sequence II, a steady influx of sediment that kept pace with basin subsidence and a eustatic rise in sea level would have produced a nearly stationary strandline relative to the COST well site. If the sedimentation rate fluctuated, as it probably did during the early and middle Miocene as a consequence of the cessation of Mishik arc volcanism (Wilson, 1985), the position of the strandline relative to the basin axis would have also fluctuated.

Landward and basinward excursions of the strandline in response to perturbations in the sedimentation rate of volcanigenic detritus would have been accompanied by lateral migrations of depositional environments. The depositional pattern resulting from such transgressions and regressions would show up on well log data as cyclic oscillations between high- and low-energy environments that are bounded by abrupt vertical transitions. This pattern matches those observed on the SP and gamma ray logs in the lower seismic facies of seismic sequence II and suggests that this model may represent a plausible interpretation of the depositional setting at that time.

On the sonic log at a depth of 4,110 feet below KB, interval velocities increase abruptly (fig. 57). On seismic profiles, this velocity increase is manifested by a continuous, concordant, high-amplitude reflection that can be traced throughout most of the North Aleutian Basin. A similar high-amplitude reflection has been recognized elsewhere in the Bering Sea (Scholl and Creager, 1973; Hein and others, 1978; Hammond and Gaither, 1983; and Turner and others, 1984c). Because of its characteristic mimicking of sea floor topography in those areas, it was termed a "bottom-simulating reflector" (BSR) by those investigators. In most of the North Aleutian Basin, the depth of this reflection ranges between 1.1 and 1.3 seconds two-way travel time, which is comparable to travel times reported for BSRs in other sedimentary basins underlying the Bering Sea shelf (Turner and others, 1984; Turner and others, 1986; and C.D. Comer, oral commun., 1986). In those basins, the cause of this reflection was attributed to the presence of gas hydrates or to a siliceous diagenetic zone. These phenomena are pressure and temperature dependent and temperature dependent, respectively, which accounts for the characteristic mimicking of sea floor topography and discordance with primary reflections produced by impedance contrasts related to original depositional processes. In the North Aleutian Basin, the origin of this reflection is problematic because where the sedimentary section mantles the top of buried basement features, the reflection remains concordant and rises in the section rather than cutting across primary reflections. This relationship indicates that in the North Aleutian Basin, this reflection is not produced by strictly depth-dependent diagenesis or gas-hydrate phase transformations, but, to some degree, is stratigraphically controlled.

Horizon B, which defines the base of seismic sequence II, is a regional unconformity that is represented at the COST No.1 well by a concordant reflection. Southwest of the COST well, a buried basement ridge (informally named the Black Hills ridge by Marlow and others (1980) because of its apparent structural connection with the Black Hills on the Alaska Peninsula) separates the North Aleutian and Amak Basins. Across the crest of this buried ridge at the southeastern end of North Aleutian Basin (fig. 65), and near the head of Bristol Bay at the northeastern end of the basin, horizon B represents the top of acoustic basement. Across the flanks of the Black Hills ridge, horizon B is an angular unconformity that truncates seismic sequences III, IV, and V where they onlap acoustic basement or each

other (fig. 65). Marlow and Cooper (1980) postulated a Cretaceous age for horizon B on the basis of the Jurassic and Cretaceous ages of rocks dredged from the Bering Sea continental slope and outer shelf. They also cited Burk (1965), who earlier reported that middle Cretaceous rocks are missing on the adjacent Alaska Peninsula. MMS interpretations assign a late Oligocene age to horizon B on the basis of the ages of overlying and underlying concordant strata at the COST well (fig. 62).

The time of formation of the horizon B unconformity, as determined from COST well data, coincides with the interpreted time of subduction of the Kula-Pacific spreading center in the mid-Tertiary. Grow and Atwater (1970) first speculated on the consequences of subduction of the Kula-Pacific spreading center at the Aleutian trench. They envisioned increased magmatic activity, uplift of the arc, and fragmentation of the Kula-Pacific ridge to be probable effects. DeLong and others (1978, 1980) expanded on the original ideas of Grow and Atwater (1970) and presented an alternative model which proposes that subduction of the Kula-Pacific spreading center beneath the Aleutian arc was accompanied by reduction or cessation of subduction-related magmatism followed by uplift and subaerial erosion of the arc. Cessation of magmatism would have been caused by the interaction of progressively younger and hotter oceanic crust with the thermal regime beneath the arc. Subaerial erosion would have been caused by uplift of the arc as it overrode progressively younger and consequently shallower oceanic crust of the Kula plate. On the basis of geologic data, those investigators estimated that in the Aleutian Islands west of Unalaska, subduction-related magmatism began to decline in the Eocene and that the age of the subsequent unconformity is approximately 30 million years before present (m.y.b.p.). Previously, Scholl and others (1975) reported that the Aleutian Ridge, which forms the base of the Cenozoic stratovolcanoes that compose the Aleutian arc, was not uplifted, folded, and faulted until middle and late Miocene time. Grow and Atwater (1970) inferred an early Miocene or post-early Miocene age for this unconformity in the central Aleutians. On the basis of micropaleontological data from the COST No. 1 well, the postulated Miocene age of this event appears to be too late.

Wilson (1985) proposed that because of the southwardly convex geometry of the Aleutian arc and the roughly east-west orientation of the Kula-Pacific spreading center, arc-related magmatism on the Alaska Peninsula would have ceased 5 to 10 million years later than it did in the Aleutian Islands. This delay would have been caused by the greater distance that the northwardly migrating Kula-Pacific spreading center would have had to travel between the time that it reached the central Aleutians and the time it began to be subducted beneath the Alaska Peninsula. A time lag of this magnitude in the timing of ridge-trench interactions along the southern margin of Alaska during the Tertiary was first postulated by Grow and Atwater (1970). Wilson substantiated his hypothesis with radiometric dates from intrusive and extrusive rocks from the peninsula that indicate that arc-related magmatism ceased in the early Miocene. Burk (1965) noted that upper Oligocene and lower Miocene strata are missing on

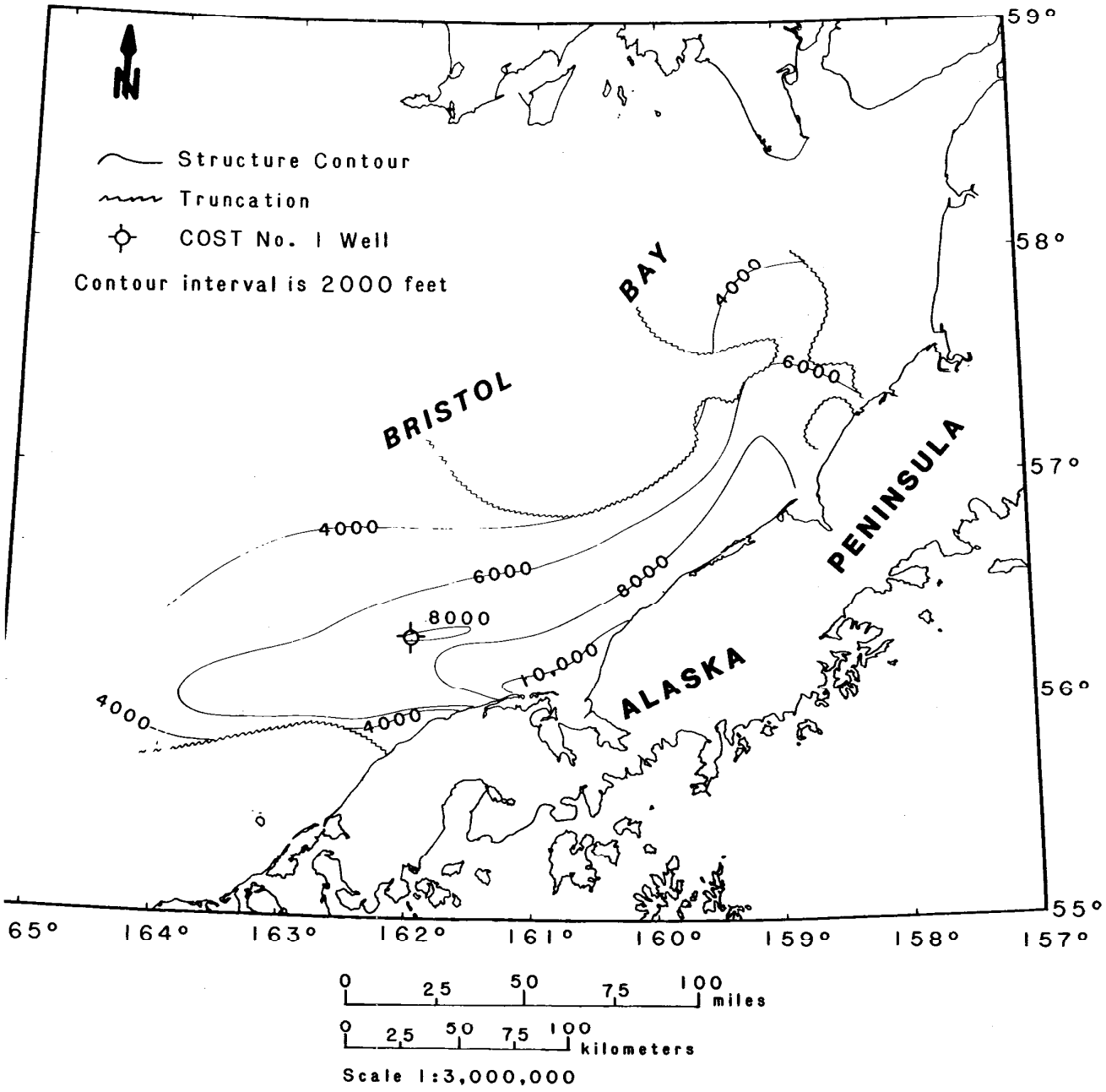

FIGURE 67. **Structure-contour map of horizon C (Oligocene).**

the Alaska Peninsula, which he interpreted to reflect uplift, deformation, and erosion. If the hypothesis of DeLong and others (1978, 1980) is correct, and if the decline in magmatism on the Alaska Peninsula reported by Wilson and the absence there of upper Oligocene and lower Miocene strata noted by Burk are due to the same phenomenon, then the age of the horizon B unconformity as determined from COST No. 1 well paleontologic data is compatible with the age predicted for an unconformity caused by the subduction of the Kula-Pacific spreading center.

In the model for ridge subduction proposed by DeLong and others (1978), as the ridge approaches the arc, the arc will be progressively uplifted and the sedimentary facies deposited on the crest of the arc will change from deep marine to shallow marine. As the arc subsides following passage of the ridge beneath it, this sedimentation pattern will be reversed. Presumably, a similar and causally related progressive change in the sedimentation pattern would also take place in the North Aleutian Basin behind the arc. This change would reflect both an adjustment in the depositional environment and changes in sediment texture and mineralogy caused by uplift and deep erosion of the primary source terrane of the basin. Lithologic data from the COST No. 1 well indicate that the quartz component of the sandstone framework matrix experienced a relative increase during the late Eocene and Oligocene followed by a relative decrease during the latest Oligocene, Miocene, and Pliocene (plate 1). This trend is mirrored by the volcaniclastic lithic component. Although part of the increase observed in the quartz lithic component is, no doubt, the result of less dilution by the volcaniclastic lithic component, some of the relative increase in the quartz contribution is interpreted to reflect erosion of the elevated arc. Also, an abrupt offset in the overall trend of sonic velocities, from lower velocities above to higher velocities below, is evident on the COST No. 1 well sonic log at the depth corresponding to horizon B (plate 1). This discontinuity is interpreted to reflect the erosion of shallower and less indurated strata at a time when shoaling of the continental margin as a consequence of ridge subduction resulted in the intensification of currents across the shelf.

SEISMIC SEQUENCE III

Seismic sequence III is composed of Oligocene strata that correspond to lithologic zones C1 and C2 (fig. 62). The upper and lower boundaries of this sequence are represented by horizons B and C, respectively (figs. 64, 65, 66, 67). Throughout much of the North Aleutian Basin, horizon B is a major regional unconformity. Horizon C represents an unconformity that appears to have formed during an Oligocene regression.

At the COST No. 1 well near the center of the basin, the transition from seismic sequence II to III is marked by a change in the character of the reflections from those of variable amplitude, cycle breadth, and continuity above, to reflections of moderate amplitude, uniform cycle breadth, and high local continuity below.

Within seismic sequence III, reflection amplitude decreases downward and the lower one-third of the sequence is nearly acoustically transparent. On seismic profiles across the flanks of the basin, the few faint reflections that can be discerned in the lower one-third of the sequence onlap horizon C (fig. 65). The onlapping of reflections in the lower one-third of the sequence is accompanied by a concomitant decrease in amplitude and continuity of reflections in the upper two-thirds. Thus, not only does the seismic character of the entire sequence change vertically, but the seismic character of the upper two-thirds of the seismic sequence also changes laterally.

At the COST well, the transparent nature of the lower one-third of the seismic sequence is produced by the acoustic homogeneity of the corresponding strata, namely terrestrial beds made up of poorly sorted to moderately well sorted, fining-upwards sequences of sandstone and cobble conglomerate. These sediments were shed into the basin during the period of erosion that culminated with the formation of an unmapped Oligocene unconformity. The correlative horizon of this unmapped unconformity intersects the COST No. 1 well at a depth of 6,385 feet below sea level, where there is also evidence of a lithologic break both in the core data and on the well logs. This unconformity is of limited areal extent and was not considered significant enough to represent a seismic sequence boundary. As sea level subsequently rose following deposition of the terrestrial beds, additional detritus shed from the degrading Black Hills ridge and ancestral Alaska Peninsula were deposited in an onlapping fashion onto that unconformity. A progressive change from a continental or transitional environment at the bottom to a more open marine environment at the top is suggested by the relative increase in reflection amplitude and continuity towards the top of the sequence as well as towards the center of the basin. This progressive change in depositional environments is corroborated by lithologic and paleontologic data from the COST well.

Horizon C represents an extensive mid-Tertiary unconformity. Northeast of the COST well it corresponds to the top of acoustic basement. As the Cenozoic stratigraphic sequence rises in the seismic section on seismic profiles collected across the northern flank of the Black Hills ridge, horizon C remains mostly concordant with the underlying reflections while overlying reflections progressively lap out against it (fig. 65). On the basis of paleontologic ages from the COST No. 1 well, horizon C is assigned a probable late Oligocene age. Paleoenvironments interpreted from microfossil assemblages from the well suggest that horizon C coincides with a regression. Accordingly, the broad, regional extent of the horizon C unconformity might be ascribed to its origin at a time which corresponds to a late Oligocene drop in global sea level that was recognized by Vail and others (1977).

SEISMIC SEQUENCE IV

Seismic sequence IV is made up of lower Oligocene and upper Eocene strata that correspond to lithologic zones D1 and D2

(fig. 62). The top of seismic sequence IV is defined, in different areas of the basin, by horizons B and C. The bottom of sequence IV is defined by horizon D (fig. 68). At the COST well, reflection continuity is high and amplitude is uniformly moderate to low. Throughout the rest of the basin, both amplitude and continuity are variable.

At some locations in the basin, horizon D unconformably overlies acoustic basement (fig. 65). At the COST well, horizon D is concordant, and several lines of evidence indicate that it represents a disconformity. These data include a difference in the type and degree of mineral alteration, abrupt changes in the character of the gamma ray and deep resistivity well logs, a change in sediment provenance, and a jump in the genetic potential (S1 + S2) of the interstitial kerogen (plate 2).

On seismic profiles through the deepest part of the North Aleutian Basin, the surface represented by horizon D rises over buried acoustic basement highs and descends into lows underlain by seismic sequence V (fig. 64). As the depth to horizon D fluctuates along these profiles, the acoustic characteristics of the reflections making up the overlying seismic sequence vary in a systematic manner. Reflections that correspond to strata that fill depressions underlain by seismic sequence V generally have a higher continuity and a more uniform amplitude than those that occur above acoustic basement highs. Where seismic sequence IV fills depressions, the continuity of the reflections remains high throughout the sequence, and amplitudes characteristically increase toward the top. In contrast, where seismic sequence IV overlies basement highs, reflection amplitude tends to be higher and continuity lower than in depressions. In depressions, the bottom-most reflections onlap horizon D. The presence of onlapping reflections and the lateral variations in reflection amplitude, continuity, and configuration indicate that a lateral transition between depositional environments existed at the time of deposition of seismic sequence IV.

Within depressions, the vertical transition from low amplitude and broad cycle breadth at the bottom to higher amplitude and narrower cycle breadth at the top reflects the change in depositional environments that accompanied a relative rise in sea level. This transition in acoustic characteristics is produced by an upward gradation in lithofacies from thick, homogeneous, continental or inner neritic beds at the bottom to more laterally continuous, middle neritic lithofacies higher in the sequence. A paralic environment at the base of the sequence is corroborated by lithologic data from correlative strata at the well which contain well-sorted sandstone, coal, broken mollusc shells, and inclined laminae. The neritic environment at the top is corroborated by the presence of finer grained sandstone, intact mollusc shells, horizontal burrows, and extensive bioturbation.

Southwest of the COST well, where seismic sequence IV onlaps the northern flank of the Black Hills ridge, reflections within the sequence are subparallel or wavy and demonstrate a wide range of

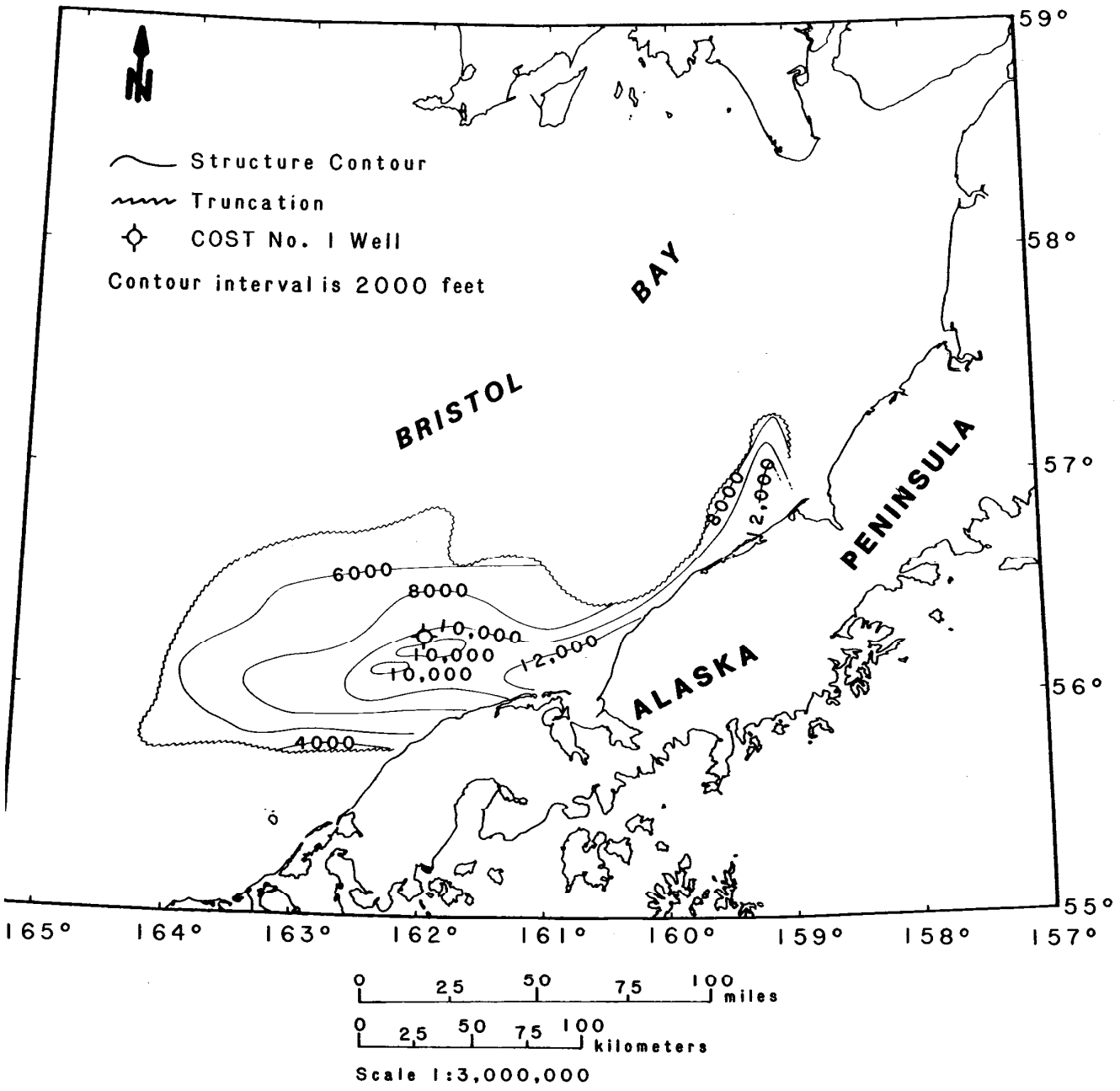

FIGURE 68. **Structure-contour map of horizon D (late Eocene).**

variation in both amplitude and continuity (fig. 65). These reflections are also associated with diffractions. Palynological data from the COST No. 1 well indicate that these strata are continental. The high amplitudes of some reflections may be caused by large impedance contrasts related to the occurrence of coal beds such as those sampled in correlative strata at the COST well. Southwest of the COST well, the top of sequence IV is characterized by a low angle of discordance between horizon C and the underlying reflections it truncates. This low-angle relationship may reflect the genesis of horizon C as a subaerial peneplain during a period of relative tectonic quiescence, rather than as an erosional remnant of penecontemporaneous deformation as is represented by horizon B.

SEISMIC SEQUENCE V

Seismic sequence V is made up of Eocene strata which contain a wide variety of lithologies that are subdivided into lithologic zones E, F, and G (fig. 62). The top of seismic sequence V is represented by horizon D; the base of the sequence is not discernible in much of the basin. At the COST well, horizon D is a disconformity, whereas at other locations in the basin it is an angular unconformity.

At the COST well, seismic sequence V fills a structural depression in acoustic basement. At that location, sequence V is composed of reflections that are distinguishable from those of the overlying sequence by their characteristically higher amplitude, lower continuity, and subparallel configuration. The high amplitude of these reflections is attributed to high acoustic impedance contrasts related to the presence of coal. Reflection continuity decreases towards the bottom of the depression, where the reflections become wavy. The base of sequence V in this depression is difficult to identify on seismic profiles because the coherent, high-amplitude, broad-cycle-breadth reflections that constitute the basin fill do not terminate abruptly against the margins of the depression, but rather merge laterally into similar but less coherent, high-amplitude, broad-cycle-breadth reflections that correspond to the surrounding acoustic basement. Although the base of the sequence cannot be precisely identified in the vicinity of the COST well, seismic data suggest that an additional 1.3 seconds of coherent, concordant reflections corresponding to approximately 7,000 feet of strata underlie horizon D. Lithologic, well log, and geochemical data indicate that significant discontinuities are present within seismic sequence V at the depths of 15,535 and 16,567 feet below sea level. However, distinct seismic horizons at those depths are not evident in the seismic reflection data.

The broad cycle breadth of reflections within sequence V can be attributed, in part, to attenuation of the higher frequencies of the source wavelet. However, this reflection characteristic also suggests that the strata represented by these reflections may be massively bedded. In some areas, the margins of these structural depressions are discernible, and the reflections that correspond to basin fill are "turned up" and appear to onlap the surrounding

acoustic basement. This onlapping relationship may have been exaggerated by postdepositional subsidence and compaction.

On seismic profiles throughout most of the basin, horizon D directly overlies acoustic basement. However, in several areas, isolated structural depressions in acoustic basement, similar to the one underlying the COST well site, are present beneath horizon D. These depressions are elongate and trend approximately east-west. On the basis of stratigraphic position and similarities in acoustic signature, the strata that fill these depressions are interpreted to be correlative with the Eocene strata at the COST well.

6. Well Log Interpretation and Lithostratigraphy

by

Gary C. Martin

A suite of wireline well logs (listed below) that were run in the North Aleutian Shelf COST No. 1 well by Schlumberger Ltd. were interpreted to provide data on the lithology and reservoir characteristics of the strata penetrated. The petrophysical information derived from logs was supplemented by sidewall and conventional core data, and descriptions of rock cuttings and hydrocarbon shows from lithology and formation evaluation (mud) logs. Petrographic reports prepared by AGAT Consultants, Inc. (1982 and 1983), were also integrated with the above data.

Log	Depth (feet) below Kelly bushing
Dual Induction Laterolog with Spherically Focused Log (DIL-SFL)	1,363 - 16,686
Compensated Formation Density Log (FDC)	1,363 - 16,696
Compensated Neutron - Formation Density Log (CNL-FDC)	1,363 - 16,696
Borehole-Compensated Sonic Log (BHC)	1,363 - 16,686
Long-Spaced Sonic Log (LSS)	1,200 - 16,545
Natural Gamma Ray Spectrometry Tool (NGT)	1,363 - 16,696
High-Resolution Dipmeter Tool (HDT) and Arrow Plot From CLUSTER Program	1,386 - 16,709

The logs listed above, with the exception of the LSS, NGT, and HDT logs, are displayed on plate 1, along with stratigraphic summaries of other geologic data. The well reached a total depth of 17,155 feet, but wireline logs were not run through the lower 446 feet of the well because of weather and operational problems.

The well penetrated a clastic sedimentary section of Cenozoic age. The lithologies present include sandstone, conglomerate, siltstone, mudstone, and coal. Deposition occurred primarily in shallow marine to coastal-plain paralic environments. The relative proportions of volcanic, metamorphic, and sedimentary clasts composing the lithic-grain fraction of the sandstones (pl. 1) indicate that the sediment was derived mainly from a volcanic terrane, especially the section below 10,400 feet. The composition of the volcanic rocks ranged from basalt to andesite. Sedimentary

and metamorphic clasts only represent significant amounts of the lithic-grain fractions above 10,400 feet, where together they locally account for more than 50 percent of the lithics. The increase in nonvolcanic detritus in sandstones above 10,400 feet probably resulted from the exposure and erosion of Mesozoic plutonic and sedimentary rocks that core and flank the Alaska Peninsula, and an influx of detritus from Paleozoic metamorphic rock to the north and northeast (Burk, 1965; Wilson, 1985; ACAT, 1982).

The retention of primary porosity and permeability in sandstones with burial depth in the well is primarily a function of lithic grain contents and compositions as reflected by sediment source areas. Plate 1 shows that the relative amount of mechanically and chemically stable quartz grains in a given sandstone correlates with the relative abundances of metamorphic and sedimentary grains in the lithic fraction of the sandstone. Below 10,400 feet in the COST well, the almost exclusively volcanic source terrane resulted in sandstones deficient in quartz in the grain framework. Compaction and diagenesis of unstable volcanic lithic and feldspar grains in this section of the well has largely destroyed the reservoir potential of the sandstones. Permeabilities measured from conventional cores below 10,400 feet are almost all less than 10 millidarcies (Lithology and Core Data chapter, table 7). The general trend of porosity reduction in sandstones (fig. 69) indicates that below about 10,400 feet, porosity is generally less than 25 percent and consists principally of microporosity in pore-filling clays and cement (Lithology and Core Data chapter, table 7). As a result, potential reservoir sandstones are primarily confined to the upper part of the well (above 10,400 feet).

LOG ANALYSIS METHODS

Wireline logging data were processed and analyzed by computer from Log Information Standard (LIS) formatted digital magnetic tapes. Data measurements and computations were performed at 0.5-foot depth increments. Prior to analysis, baseline drift on the Spontaneous Potential (SP) log was removed, the FDC bulk density and BHC sonic-travel-time data were converted to porosity, and core data were depth-shifted to match wireline data.

SP baseline drift was removed by shifting the data relative to a shale baseline SP response which was arbitrarily set to 0 millivolts (mv). Matrix density values used in converting bulk density to density porosity were obtained from the grain density data derived from laboratory measurements of conventional cores. Grain density values were averaged from a core taken within a lithologic zone or unit and used as the matrix density to calculate density porosity for that zone or unit. Matrix travel time used to calculate sonic porosity from sonic travel time was 55.5 microseconds per foot. Sonic porosity was corrected in shallow uncompacted sections of the well by a factor derived from travel times in adjacent shales or mudstones. The determination of effective porosity and permeability for evaluation of the reservoir

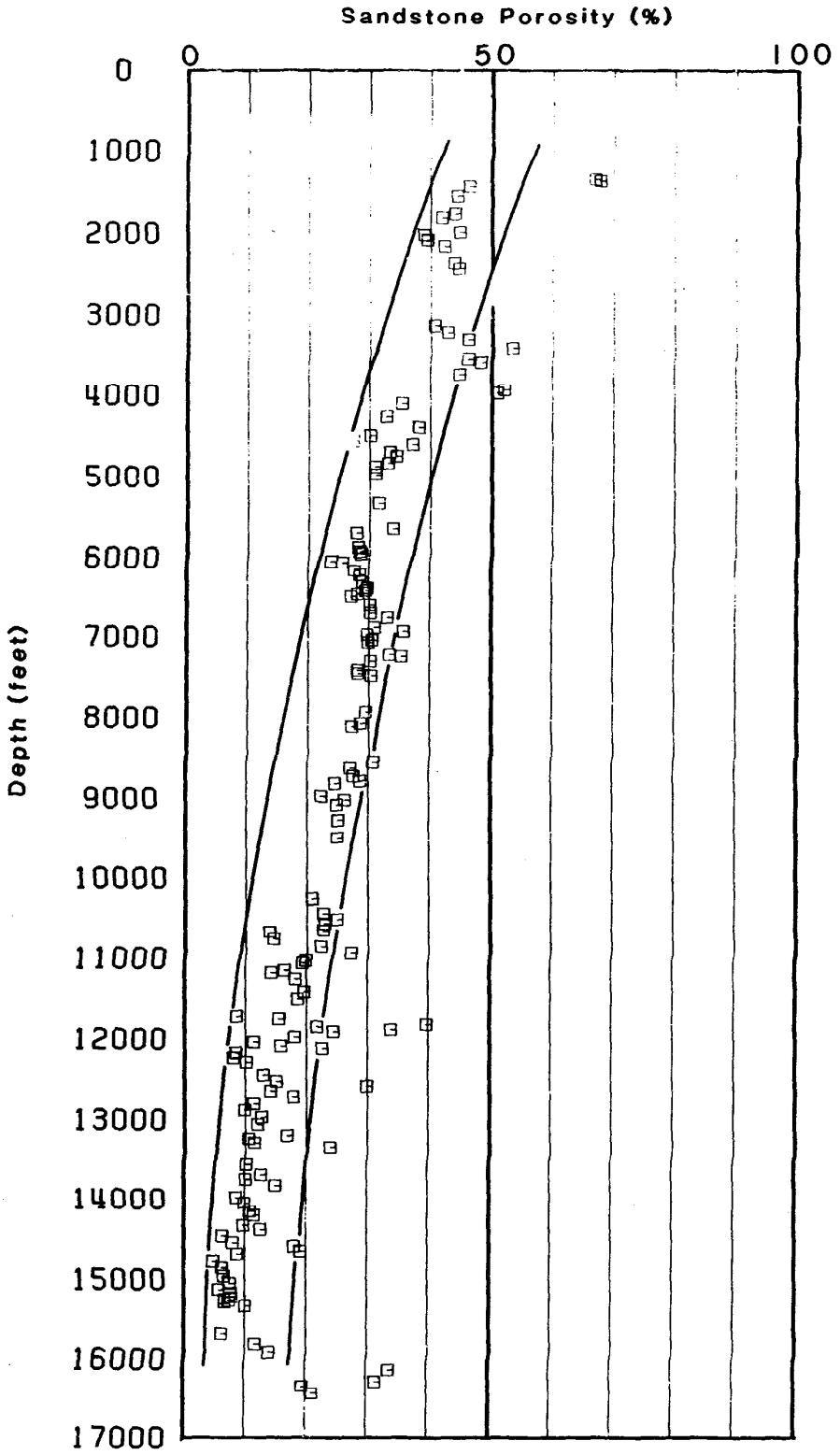

FIGURE 69. **Distribution of sandstone porosity with depth. Porosity calculated from density log data. Porosity uncorrected for shale effects.**

potential of sandstones in the COST well required an adjustment of the wireline data for shale effects. Standard methods for evaluating lithology and potential reservoir quality from the wireline logging data in the North Aleutian Shelf COST No. 1 well were hampered by the poor condition of the borehole and the lithic-rich character of the sandstones. The bit size and caliper traces (pl. 1) indicate that in many sections, the borehole was enlarged by caving to over 15 inches and was rough and irregular. Although the CNL, FDC, and BHC porosity logs are designed to compensate for borehole effects, they cannot fully correct for tool standoff effects in large, irregular holes. The CNL porosity log is most severely affected by borehole conditions. Because of this, analysis techniques that utilize neutron porosity were precluded in many sections of the well.

In addition to adverse borehole effects, the abundance of lithic detritus throughout the sediment size ranges resulted in little mineralogical difference between sandstones and mudstones. Because of this, radioactivity tools with log responses that are primarily a function of some aspect of mineralogy recorded little or no difference between sandstone and mudstone in many sections of the well. Therefore, standard log analysis techniques developed for sand-shale sequences in which the sandstones are composed mainly of quartz, and the mudstones or shales are composed mainly of clay minerals, do not yield valid results in the North Aleutian Shelf COST No. 1 well. For example, one of the most comprehensive methods for evaluating shaly sands is the technique of Poupon and others (1970), which is based upon statistical crossplots of neutron and density porosity. When this technique was employed for permeable sandstones above 10,400 feet in the COST well, excessively high shale and clay contents were indicated relative to the actual shale and clay observed in cores. In some cases the Poupon neutron-density technique failed to differentiate sandstone from shale.

The analysis technique which yielded reservoir data most consistent with core data used the SP log to identify sandstones and quantify sandstone shaliness, and the density log to calculate effective porosity. The results of computer-processed log interpretations of both the density-SP and Poupon neutron-density techniques are graphically compared with core, x-ray, and petrographic data in figures that accompany the discussion of the stratigraphic zones. Computer-processed results of the density-SP log analysis technique are listed in reservoir summary tables 8 to 13 that accompany the descriptions of the stratigraphic zones. A detailed description of the density-SP analysis is contained in the following section.

DENSITY-SP LOG ANALYSIS

The SP log response is primarily a function of the salinity contrast between the drilling-mud filtrate and formation water, and the presence of beds that are permeable to the borehole fluid (Schlumberger, 1972a). Since the SP phenomenon results from the movement of ions, it is controlled by permeability barriers that are

principally a result of grain size differences in sand-shale sequences rather than mineralogical contrasts. Therefore, the SP log is a good lithologic indicator of permeable sandstone versus impermeable lithologies such as shales, siltstones, and nonporous sandstones, irrespective of whether or not a mineralogic contrast exists between them. However, a sufficient salinity contrast between the formation water and drilling-mud filtrate must be present in order for the SP log to detect permeable beds.

Formation water salinities estimated from water resistivity determinations from the SP log and Pickett (1972) plots (fig. 70) in the upper 10,400 feet of the COST well range from about 13,000 to 30,000 parts per million (ppm) equivalent sodium chloride (NaCl). Drilling-mud-filtrate salinity at the time the SP log was run was 4,700 to 4,900 ppm equivalent NaCl. Static SP log deflections produced by these salinity contrasts are as much as 55 to 65 mv and are sufficient for lithologic discrimination.

In addition to using the SP log to identify permeable sandstones, it was also used to quantify sandstone shaliness. A permeable sandstone containing shale or clay will have a reduced SP deflection proportional to the volume of shale or clay it contains. An index of the shaliness from the SP log (SPI) was obtained from the equation

$$SPI=1-(SSPlog/SSP)$$

where: SSP = static SP deflection in clean sand
SSPlog = SP deflection in shaly sand.

However, other factors, such as thin beds, invasion anomalies, and hydrocarbon saturation can also decrease the SP in shaly sands (Schlumberger, 1972a). Therefore, the SPI represents an upper limit of shale or clay content. Because of this, the shale volume (VSHL) was not converted directly from the SPI, but was calculated from the equation

$$VSHL=0.083[2^{3.7SPI}-1]$$

(Asquith, 1982, p. 102). This equation is traditionally used to obtain shale volume from gamma ray log data in unconsolidated Tertiary sediments, but in this case it was used with the SP log data because it produced shale volumes which were in better agreement with the core data than the unaltered SPI.

After sandstone intervals were identified and the shaliness was estimated using SP log data, the apparent porosity obtained from the density log was corrected for shale effects to obtain effective porosity. Effective porosity (PHIE) was calculated by subtracting

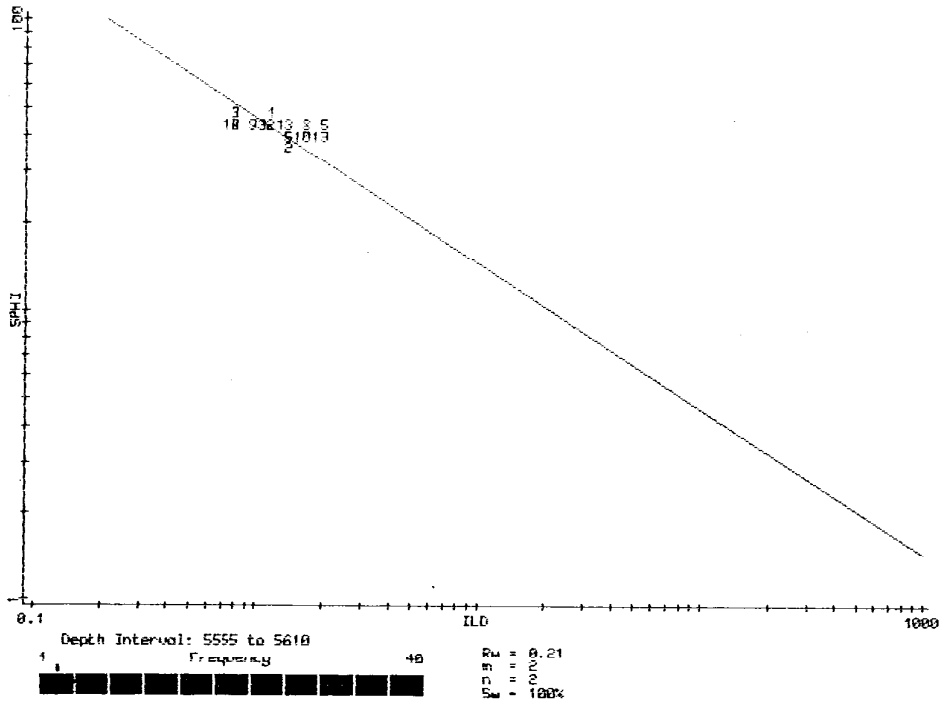

FIGURE 70. **Resistivity versus porosity Pickett crossplot (Pickett, 1972) from a water-wet clean sandstone at 5,555 feet. Formation water resistivity (RW) determined from intersection of trend line with 100% porosity. Number at plot point indicates frequency.**

the porosity component of shale from the apparent density porosity (DPHI) using the equation (Dresser Atlas, 1979)

$$PHIE=DPHI-VSHL[(RHOma-RHOsh)/(RHOma-RHOfl)]$$

where: RHOma = matrix density of the sandstone
RHOsh = bulk density of adjacent shale bed
RHOfl = fluid density
VSHL = shale volume

Effective porosity was calculated using data from the density tool rather than the sonic or neutron tool, or some combination, because apparent porosity from the density tool required the least correction for shale effects and produced the best fit with empirically determined core porosity. Crossplots of the three types of apparent log porosity versus core porosity from sandstone intervals (figs. 71, 72, and 73) illustrate the relative accuracies of the different apparent porosities. Neutron and sonic porosities read considerably higher than measured core porosities, and when linearly regressed, show poor fits. The density porosity, on the other hand, shows the best correlation of fit, and in the 20 to 35 percent porosity range reasonably approximates core porosity.

All of the porosity tools generally record an apparent porosity that is too high when shale is present in a sandstone, but the shale effects are generally smaller with the density tool. The density tool detects electron density, and its response is dependent on the bulk density of the rock and formation fluids. The density tool detects all the rock material in the sandstone, including all types of shale, and records an apparent density very close to the actual density. The principal source of error due to shaliness results from converting the density values from the log to density porosity. If the density of the shale contrasts strongly with the sandstone matrix density, then apparent density porosity will be in error. The magnitude of the error depends on the proportion of shale and its physical properties and manner of distribution in the sandstone. Assuming that the clays and other minerals composing the shales in a stratigraphic interval remain relatively constant, then the major factors affecting density porosity conversion will be the volume of shale and its manner of distribution. There are three basic ways shale can be distributed in a sandstone: as laminar, structural, and dispersed shale (fig. 74). The type of shale with the largest density contrast to the sandstone matrix is generally dispersed shale. This is because the laminar and structural shales are subjected to the same lithostatic pressure as the sandstone matrix (fig. 74), whereas dispersed shale is subjected only to hydrostatic pressure and therefore contains more bound water and a lower density (Schlumberger, 1972a, p. 91). Apparent density porosity is therefore mainly affected by only dispersed shale and, in contrast to sonic and neutron apparent porosities, which are affected by two or three types of shale, generally yields an apparent porosity close to the actual porosity.

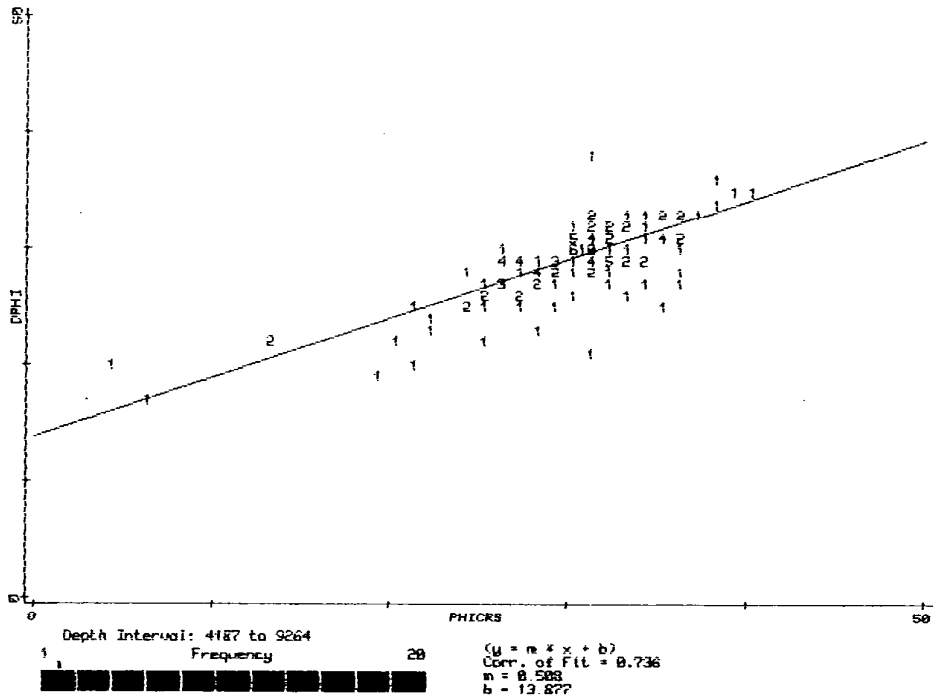

FIGURE 71. **Density porosity (DPHI) versus core porosity (PHICRS) crossplot and linear regression. Number at point indicates frequency.**

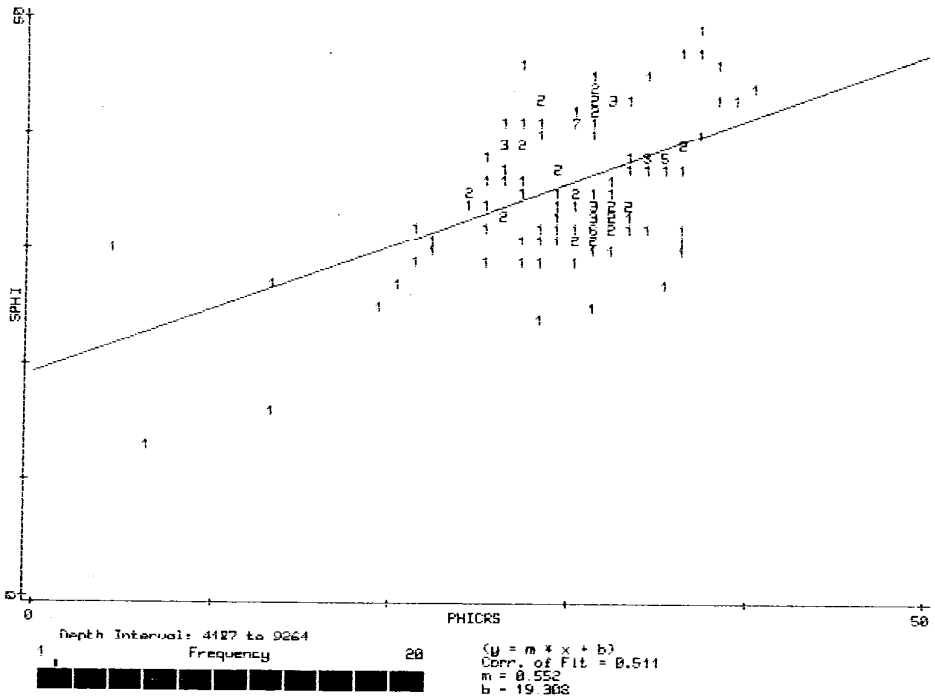

FIGURE 72. **Sonic porosity (SPHI) versus core porosity (PHICRS) crossplot and linear regression. Number at point indicates frequency.**

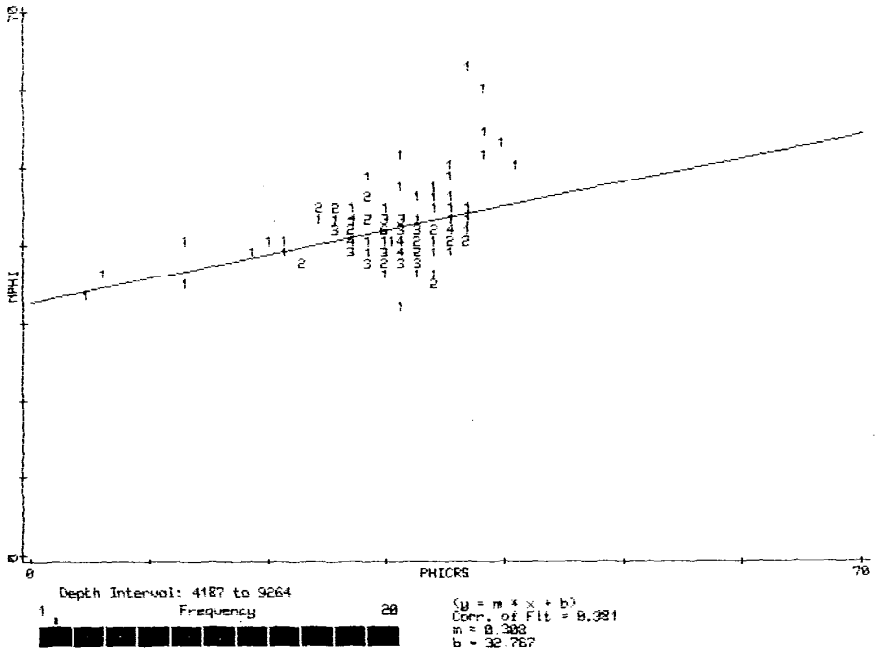

FIGURE 73. **Neutron porosity (NPHI) versus core porosity (PHICRS) crossplot and linear regression. Number at point · indicates frequency.**

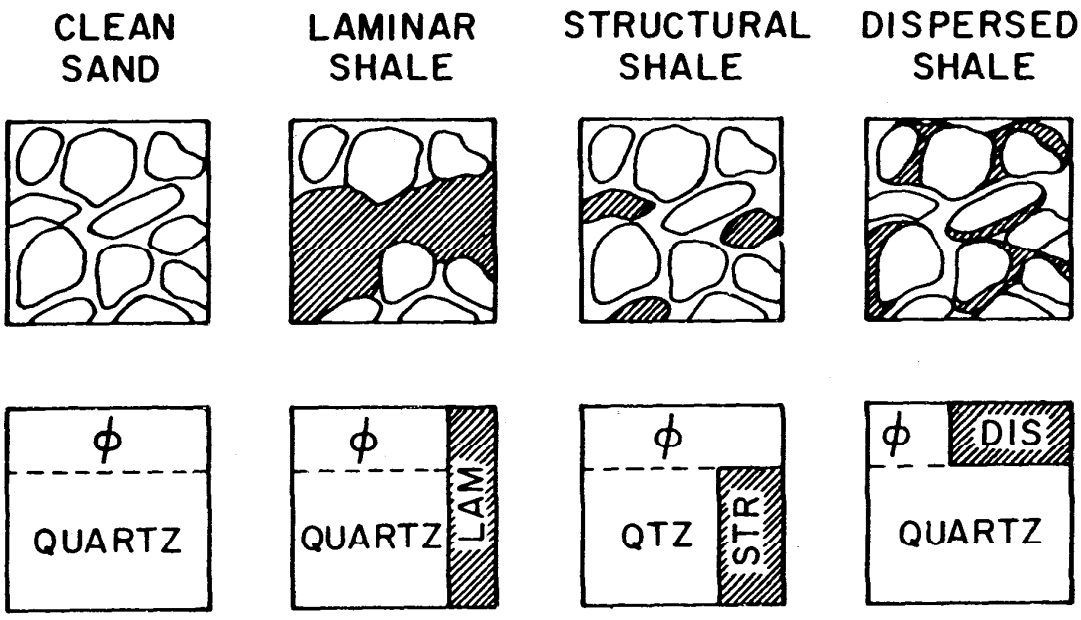

FIGURE 74. **Forms of shale classified by manner of distribution in formation. Pictorial representations above, volumetric representations below. ∅ represents porosity (after Schlumberger, 1972a, p. 91).**

The major form of shale detected in cores from the cleaner sandstones consisted of structural shale in the form of altered lithic clasts. The grain density of these lithic clasts was incorporated into the average sandstone matrix density used in converting density to apparent porosity by using laboratory analysis data from cores which contained these grains. Therefore, this component of shaliness should not introduce significant error in the apparent density porosity. However, for the shalier sandstones that were deposited in lower energy environments and contain dispersed and laminar shale in addition to structural shale, the apparent density porosity requires correction for the dispersed shale in order to obtain effective porosity. The core porosity in these shalier sandstones is also probably higher than actual effective porosity. This is suggested by the significantly lower effective porosities consistently indicated by petrographic analyses of shaly sandstones in this well (see Lithology and Core Data chapter). This same relationship between core and petrographic porosity was also observed in shaly sandstones in the Navarin Basin COST No. 1 well (Turner and others, 1984c, p.145). The apparent excess in core porosity measurements is attributed to two causes: (1) the measured core porosity detects a certain amount of shale microporosity which is permeable to the helium used in the analysis, and (2) the shrinkage of clays and loss of bound water in the core during the drying process artificially increases porosity by a small amount (Schlumberger, 1972a, p. 91). Therefore actual effective porosity will be lower than measured core porosity in shaly sandstones.

Permeability was estimated from the logs using the Wyllie-Rose (1950) relation:

$$KI^{1/2} = C(PHIE^3/SWirr)$$

where: KI = permeability index in millidarcies (md)
SWirr = water saturation of a zone at irreducible water saturation
C = constant based on fluid density (usually 79 for gas, and 250 for medium gravity oil)
PHIE = effective porosity

This general equation is empirical and based on frequently observed relations between porosity and permeability. In the COST well, there were no hydrocarbon zones at irreducible water saturation; consequently, values of SWirr could not be directly determined. However, estimates of probable values of SWirr, if hydrocarbons were present, can be calculated for cored intervals by substituting measured core permeabilities into the Wyllie-Rose equation and solving for SWirr. A probable value of SWirr was estimated in this way for each core in the COST well that contained permeable sandstone. The SWirr value thus obtained was used to calculate permeability from the logs for the remainder of the sandstones in the same stratigraphic zone or subzone from which the core was taken. Probable values of SWirr determined in this way for cores 2 through 8, assuming a fluid constant of C = 79, varied from 2 to 40 percent.

The validity of this permeability analysis is based on the assumptions that the petrophysical properties of the sandstones in a particular stratigraphic interval or zone remain relatively constant, that the core sampled a representative sandstone, and that the core permeabilities are relatively unaffected by the coring process and represent in situ permeability. In the shalier sandstone cores, the measured permeability may be too high for the same reasons that the core porosity is too high. Figure 75 is a crossplot of log-derived permeability versus core-derived permeability for cores 2 through 9, and gives an indication of the amount of variability encountered in the cored intervals. The data plot reasonably well along the diagonal line representing equal permeability, and the amount of scatter suggests most of the data is probably accurate to within an order of magnitude.

DESCRIPTION OF STRATIGRAPHIC ZONES

The North Aleutian Shelf COST No. 1 well is divided into 11 stratigraphic zones, each a unit of genetically related strata with similar lithologic and petrophysical properties. The zonation is based on wireline log characteristics, lithology (from cores and drill cuttings), seismic-sequence characteristics and boundaries, and biostratigraphic and paleobathymetric determinations. Each zone is designated by the letter of the seismic horizon which occurs at or near the base of the zone (pl. 1).

Summaries of reservoir quality are presented for each zone above 10,400 feet that contains permeable sandstone. Sandstone thickness and weighted averages of effective porosity, shale volume, and permeability (if the zone was cored) are given for sandstone intervals greater than 10 feet thick that contain shale interbeds no thicker than 3 feet. A minimum effective porosity cutoff of 10 percent and a maximum shale volume cutoff of 50 percent were employed in the reservoir quality summations. Figures showing lithology and logs of wireline porosity and permeability compared with the core porosity and permeability are presented for each zone containing permeable sands from which conventional cores were taken. Additional figures of quantitative determinations of lithology from x-ray diffraction and petrographic analyses are shown for comparison with log analyses.

Zone A (1,000 to 2,510 feet)

Rotary-drill-bit cuttings and sidewall cores from this zone contained poorly consolidated diatomaceous conglomerate or conglomeratic sandstone, siltstone, and mudstone of Pleistocene and Pliocene age. The microfossil assemblages indicate that the paleobathymetry varied from middle to outer neritic. The SP and gamma ray logs indicate that zone A is characterized by thinly interbedded conglomerates and sandstones to a depth of 2,105 feet. Thicknesses of individual beds in this interval are generally less than 20 feet and often less than 10 feet. Below 2,105 feet, the bedding sequence is more massive.

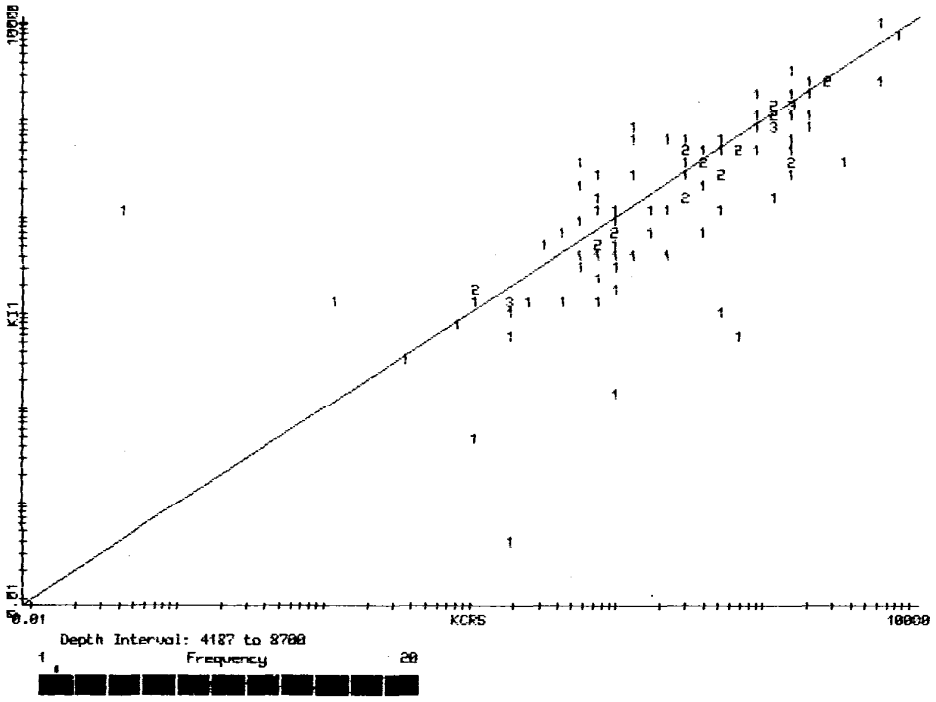

FIGURE 75. **Log-derived permeability (KI1) versus core permeability (KCRS) crossplot. Number at point indicates frequency. Diagonal line indicates line of equal permeability, KI1=KCRS.**

The abundance of volcanic clasts in the lithic fraction of sandstone in this zone (pl. 1) indicates that the source area was largely volcanic. A 3-foot-thick bed interpreted to be a welded or highly cemented tuff was identified on the logs at 2,213 feet. The logs indicate the bed is hard, dense, resistive, and anomalously radioactive. The NGT log records a high relative thorium content, which is typical of bentonites or volcanic tuffs (Fertl, 1979; Serra and others, 1980). The age and lithology of zone A are similar to and suggest equivalency with the volcaniclastic Milky River Formation of Brockway and others (1975) on the Alaska Peninsula.

The lower contact of this zone coincides with seismic horizon A, which marks the base of a seismic facies characterized by progradational clinoforms in the vicinity of the COST well and elsewhere in the basin. Along basement highs and basin margins, horizon A is an angular unconformity (see Seismic Stratigraphy chapter).

Because no conventional cores were cut in this zone, the log data could not be checked against core analyses. In addition, the borehole in most of the permeable intervals was enlarged beyond 15 inches by caving. Therefore, it is doubtful that meaningful log-derived analyses could have been obtained.

Zone B1 (2,510 to 4,110 feet)

Cuttings, cores, and wireline logs indicate that this interval consists of poorly consolidated sandstone, diatomaceous siltstone and mudstone, and lignite of Miocene to early Pliocene age. The sandstones are generally fine grained and rich in volcanic clasts, although ratios of metamorphic and sedimentary to volcanic lithic clasts gradually increase downward in the zone (pl. 1). The SP and gamma ray logs indicate that the sandstone occurs in massive beds, generally over 50 feet thick. Mudstones and siltstones are largely confined to the lower part of the zone, below 3,130 feet. Four lignite beds 2 to 3 feet thick were identified on logs between 3,130 and 3,310 feet, and lignite was reported in the cuttings from 3,000 to 3,915 feet. Microfossil assemblages indicate transitional (estuarine?) to middle neritic depositional environments, and the lignite beds indicate intermittent periods of nonmarine deposition.

The lower boundary of zone B1 is marked by an abrupt shift on the sonic and density logs from higher bulk density and sonic velocity below the boundary, to lower bulk density and sonic velocity above the boundary (pl. 1). These log shifts coincide with and are attributed to the presence of abundant diatoms in the sediment above the boundary. Similar wireline log shifts that coincide with the appearance of abundant siliceous atoms have been described in other Bering Sea COST wells. The origin of the relatively sharp boundary between diatomaceous and nondiatomaceous sediment in the Navarin Basin COST No. 1 well, for instance, was attributed to temperature-dependent diagenesis of the biogenic opal-A of the diatom tests below the boundary (Turner and others, 1984c). However, on seismic reflection profiles in the North Aleutian Basin, this boundary

coincides with a continuous, concordant, high-amplitude reflection traceable throughout most of the basin. The concordancy of the reflection in areas of dipping strata suggests that it marks a stratigraphic boundary, because a temperature-dependent diagenetic zone would be discordant (see Seismic Stratigraphy chapter). A stratigraphic origin is also suggested by the contrasting lithologies above and below the boundary in the COST well. Immediately below the boundary is a 115-foot-thick sandstone that marks the top of an overall regressive shelf sequence, whereas immediately above the boundary is a 100-foot-thick mudstone that represents a transgressive deposit. Thus, it is probable that the origin of the boundary is more a result of a proliferation of diatoms during deposition than a result of later diagenesis.

TABLE 8. Reservoir summary of log analysis of sandstones, stratigraphic zone B1: 2,510 to 4,110 feet.

Depth Interval (feet)	Sandstone Thickness (feet)	Sandstone Shaliness (% volume)	Porosity Apparent (%)	Porosity Effective (%)	Permeability Index (millidarcies)
2,511-2,643	132	31.2	50.1	32.6	(not calculated)
2,648-2,759	111	34.2	45.5	30.3	"
2,775-2,918	144	27.2	41.5	29.9	"
2,946-3,132	186	21.2	41.7	32.7	"
3,143-3,208	65	17.4	40.9	33.5	"
3,223-3,242	20	35.7	45.2	30.0	"
3,248-3,285	37	19.4	41.6	33.1	"
3,331-3,388	77	27.1	44.9	31.8	"
3,420-3,483	63	17.0	53.2	37.5	"
3,546-3,569	23	21.5	45.9	35.9	"
3,586-3,707	121	16.6	47.9	38.9	"
3,711-3,723	12	36.8	44.3	28.7	"
3,742-3,963	221	13.2	45.2	37.2	"
3,978-3,998	20	27.6	50.6	38.0	"
Total:	1,234	Mean: 22.7	45.2	33.9	

Table 8 presents a reservoir summary of the log-derived computer analysis of sandstones in zone B1. The only conventional core cut in zone B1 (core 1 at 3,391.3 to 3,393 feet) sampled a diatomaceous mudstone interval. Consequently, no core data from a sandstone interval were available to check or calibrate the log data, and no log-derived permeability was calculated for this zone. Much of the borehole was enlarged by caving in the sandstone intervals, so the accuracy of the porosity data is uncertain.

Zone B1 contains over 1,200 feet of sandstone in beds from 12 to 221 feet thick. The apparent porosity (DPHI) calculated from bulk density logs is very high, ranging from about 40 to 55 percent. These high porosities are probably a function of loose compaction and the presence of abundant diatomaceous material, which is highly

microporous. Effective porosity (PHIE) determined from apparent porosity (DPHI) and corrected for shale effects ranges from about 29 to 39 percent. It is uncertain, however, whether or not this analysis of effective porosity accounted for the effects of the abundant microporosity of the diatomaceous material on the density log.

Zone B2 (4,110 to 4,870 feet)

This zone consists of a sequence of sandstone, siltstone, and mudstone of Miocene age. Microfossil assemblages indicate deposition occurred in inner to middle neritic depths. Sandstone beds recorded on SP and gamma ray logs are generally thinner and contain more mudstone or siltstone interbeds than zone B1. The vertical sedimentary sequence consists of thin sandstone beds and low sand-to-shale ratios in the lower part of the zone, which grade upward to thicker sandstone beds and higher sand-to-shale ratios. Core 2 (4,191 to 4,200 feet) cut a sandstone from the upper part of the zone. The clay-rich, fine- to medium-grained, bioturbated sandstone contains horizontal and vertical burrows and whole pelecypod shells. The vertical sedimentary succession, taken with the core description, suggests that zone B2 represents an overall shoaling-upward, regressive shelf sequence. The lithic fraction of the sandstones (pl. 1) indicates that, in addition to detritus from volcanic sources, as much as 50 percent of the sediment was sourced from metamorphic and sedimentary terranes.

Data from core 2 were used to check and calibrate the logging data used in the computer-processed log analysis of potential sandstone reservoirs in zone B2. Core depths appeared to be shifted 5 feet high relative to the density log; therefore the core data were shifted 5 feet deeper to achieve a better fit with the density porosity trace (DPHI). The logs, core data, and computer-processed density-SP log analysis are shown in figure 76. Shaliness is indicated by the neutron and sonic porosity traces (NPHI and SPHI), which read considerably higher than the density and core porosity. The neutron porosity trace is off scale (over 50 percent) throughout most of the interval. Shaliness is also indicated by the gamma ray log (GR), which records only a small difference in deflection between the sand interval at 4,150 to 4,225 feet and the shale interval at 4,225 to 4,250 feet. The computer-processed bulk-rock analysis from the density-SP logs (fig. 76) indicates the sandstone contains about 20 to 30 percent shale. The log-derived permeability (KI1) was computed assuming a SWirr of 40 percent. There is considerable scatter between the core- and log-derived permeability in this shaly sand.

The bulk-rock analysis from this density-SP analysis is also shown in figure 77, where it is compared with the neutron-density log analysis and with x-ray and petrographic analyses of core 2. Because the sandstone contains abundant intergranular shale, the percentage of large effective pores is low. The grain framework determined by petrographic analysis consists of a roughly equal ratio of quartz and feldspar to lithics. The x-ray analysis (fig. 77) indicates

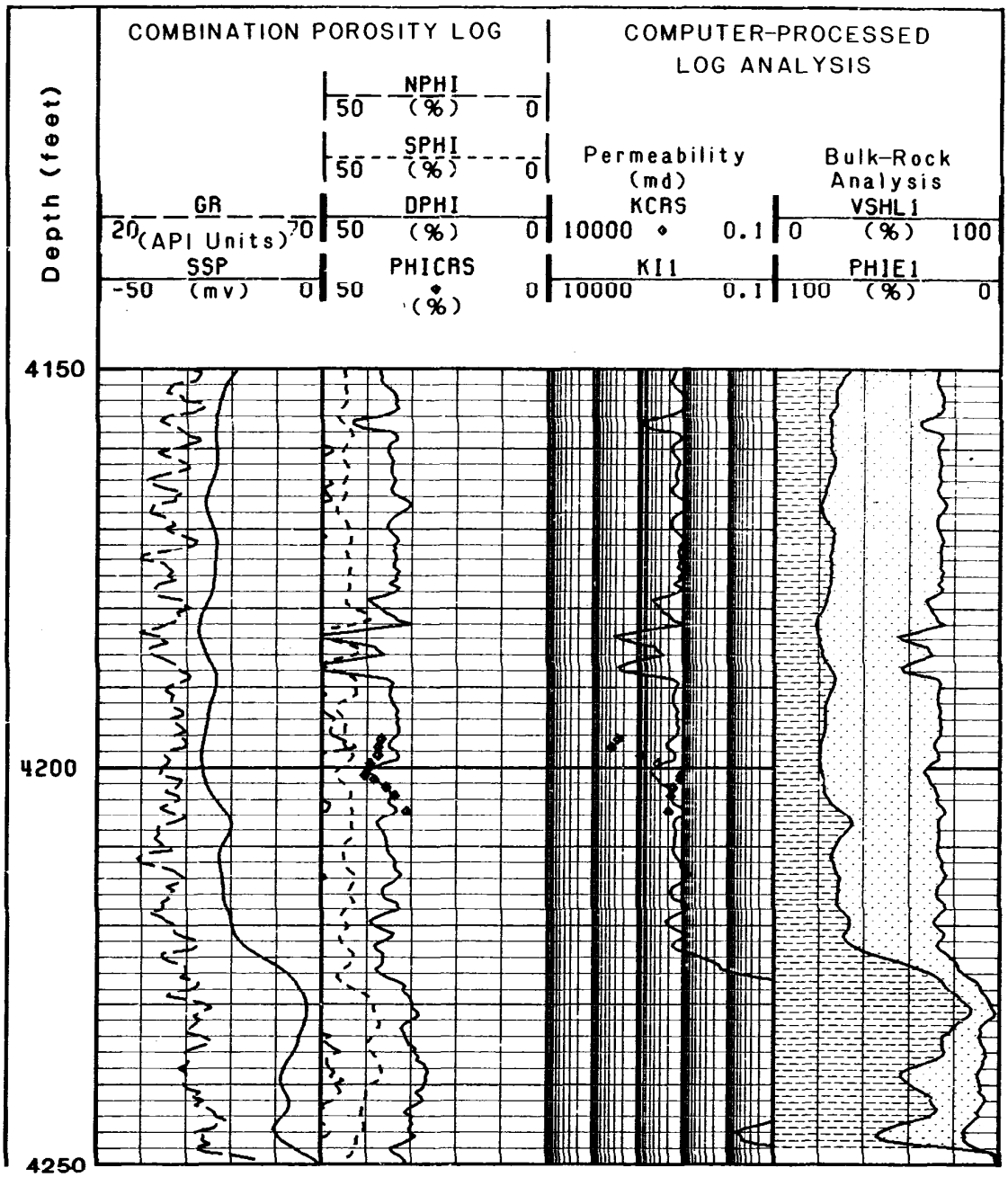

FIGURE 76. **Combination porosity log and computer-processed interpretation over the depth interval of core 2, stratigraphic zone B2. Core porosity (PHICRS) and permeability (KCRS) are plotted for comparison with log data. Computer bulk-rock analysis derived from SP and density logs. Core data depth-shifted 5.0 feet deeper relative to logs.**

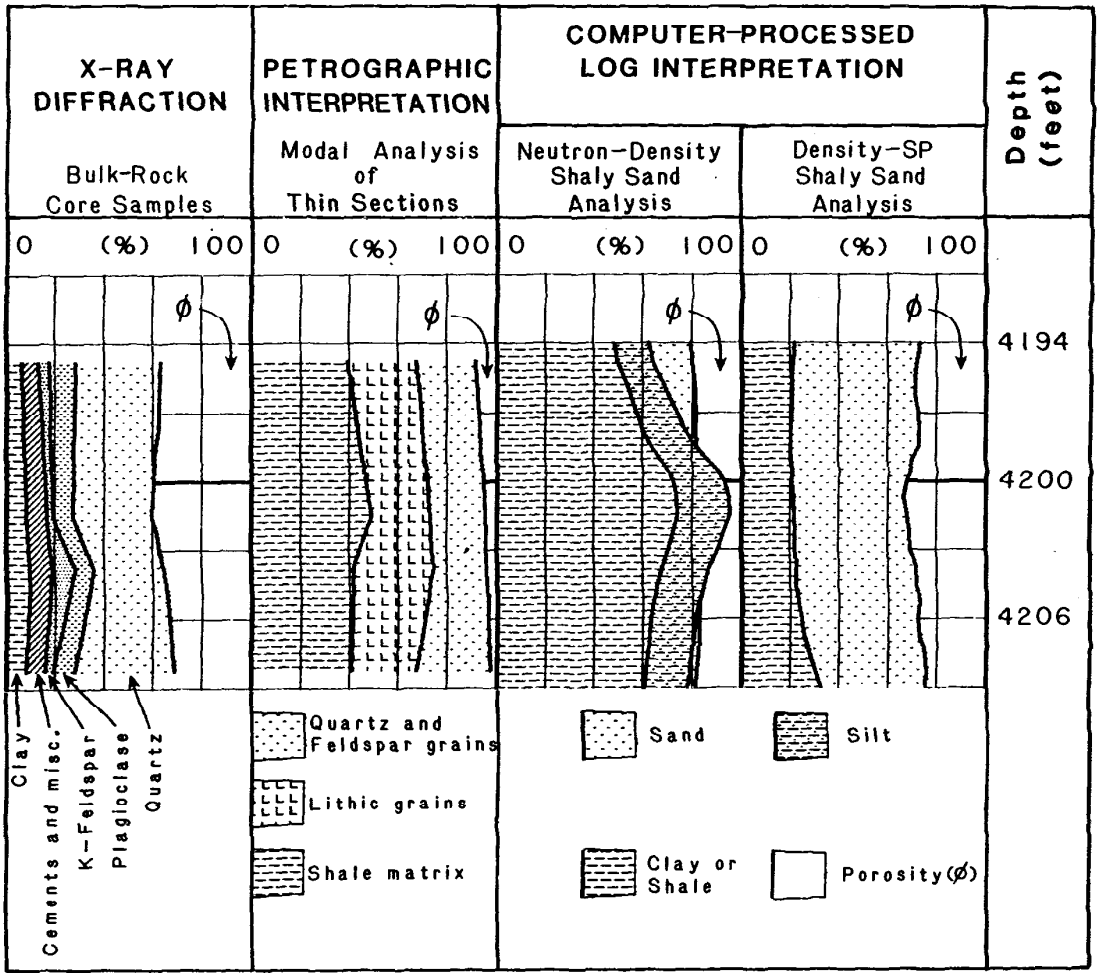

FIGURE 77. **Quantitative lithologic analyses of core 2, stratigraphic zone B2, from x-ray, petrographic and computer-processed log interpretations. X-ray and petrographic data from AGAT (1982). Porosity in x-ray analysis represents core porosity. Porosity in petrographic analysis is visually estimated effective porosity.**

relatively low contents of clay minerals, which suggests that the abundant shale indicated by the petrographic analysis consists in part of clay- to silt-sized particles of quartz and feldspar.

The neutron-density log analysis indicates excessive amounts of clay and silt relative to that indicated by the x-ray and petrographic analyses, and does not yield a valid interpretation. The neutron log was apparently adversely affected by the abundant shale and lithic-clast contents of the sand. The density-SP analysis corresponds more reasonably with the x-ray and petrographic data, and indicates relative sand and shale contents intermediate to those indicated by the x-ray and petrographic analyses. The large variance between contents of shale matrix in the petrographic interpretation and the clays and cements of the x-ray diffraction analysis is partly a function of the considerable fraction of microporosity which was included in the shale matrix in the petrographic interpretation. If this microporosity was deleted from the shale matrix and added to the porosity in the petrographic interpretation, the variance would probably be within the range expected for the two different techniques.

TABLE 9. Reservoir summary of log analysis of sandstones, stratigraphic zone B2: 4,100 to 4,870 feet.

Depth Interval (feet)	Sandstone Thickness (feet)	Sandstone Shaliness (% volume)	Porosity Apparent (%)	Porosity Effective (%)	Permeability Index (millidarcies)
4,110-4,224	114	26.8	35.4	27.4	16
4,267-4,313	46	22.5	30.9	24.1	7.6
4,322-4,365	43	34.5	34.1	23.8	7.1
4,395-4,484	89	17.3	37.8	31.4	37
4,504-4,538	34	17.8	30.0	24.5	8.4
4,617-4,661	44	24.7	37.4	30.0	28
4,705-4,732	27	30.1	33.4	24.3	8.0
4,745-4,785	40	26.6	34.4	26.3	13
4,851-4,863	12	30.3	35.2	26.0	12
Total:	449	Mean: 27.2	34.8	27.2	16

A summary of the results of the log-derived reservoir analyses of sandstones in zone B2 is presented in table 9. Zone B2 contains about 450 feet of sandstone in beds between 10 and 115 feet thick. Apparent porosity from the density log, which approximates core porosity, ranges from about 30 to 38 percent and averages about 35 percent for sandstones in the zone. Effective porosities in which shale microporosity has been removed range from 24 to 32 percent and average about 27 percent Log-derived permeabilities range from about 7 to 37 millidarcies (md), but the accuracy is somewhat uncertain in this zone, given the scatter exhibited between core and log permeability on figure 76.

Zone B3 (4,870 to 5,675 feet)

Zone B3 is characterized by sandstone beds or bed sets, generally over 50 feet thick, that are interbedded with thinner intervals of mudstone and siltstone typically 10 to 35 feet thick. Microfossil data indicate that this sequence is probably late Oligocene in age and was deposited in inner to middle neritic depths. Seismic horizon B, which coincides with the base of zone B3, is a regional unconformity in the North Aleutian shelf area. In the vicinity of the COST well, however, reflections above and below horizon B are concordant. The sonic log from the COST well records a significant offset in the trend of interval transit time (DT) at the depth of horizon B (pl. 1). The offset indicates a relatively abrupt increase in interval velocity, which implies that the rocks above and below the offset have had different burial histories and that horizon B probably represents a disconformity at the well site.

The sandstones of zone B3 are fine to medium grained and moderately to well sorted. The sandstone provenance, as in zone B2, is generally more than half volcanic, but does contain significant metamorphic and sedimentary fractions (pl. 1). The ratio of quartz to other sand grain types is slightly higher in this zone than in any of the overlying zones (pl. 1). The greater abundance of quartz sand is probably a result of a combination of higher depositional energies and greater sediment influxes from metamorphic and sedimentary terranes.

The higher quartz contents of these sands are related to the improvement in reservoir quality indicated by log and core data. The most significant departures in zone B3 reservoir characteristics from those of the overlying zones are lower shaliness and higher permeability. Average sandstone shaliness derived from SP log data is about 15 percent, and log-derived permeability averages over 800 md for the zone (table 10).

The data from core 3 used in calibrating and checking the log-derived analysis are shown in figure 78. Core depths were shifted 9 feet lower relative to the log depths to match a thin, calcite-cemented interval in the core with a resistive, high density spike on the logs. All three log porosity traces have smaller separations than in the previous cored interval (core 2), which indicates a smaller shale effect and cleaner sandstone. The lower shale content is reflected in the core permeabilities, which are generally in the 900- to 2,000-md range and are approximated quite well by the log-derived permeabilities (fig. 78). The log-derived permeability was calculated assuming a SWirr value of 5 percent. The cemented streak at 5,244.5 feet (fig. 78) has a much lower porosity and permeability than is indicated by the log analysis (the core permeability is less than 0.1 md and plots off the right scale of track 3). This is due to the higher matrix density of calcite cement and the averaging effect of the logging tool across the cemented interval, which is thinner than the resolution of the logging tool.

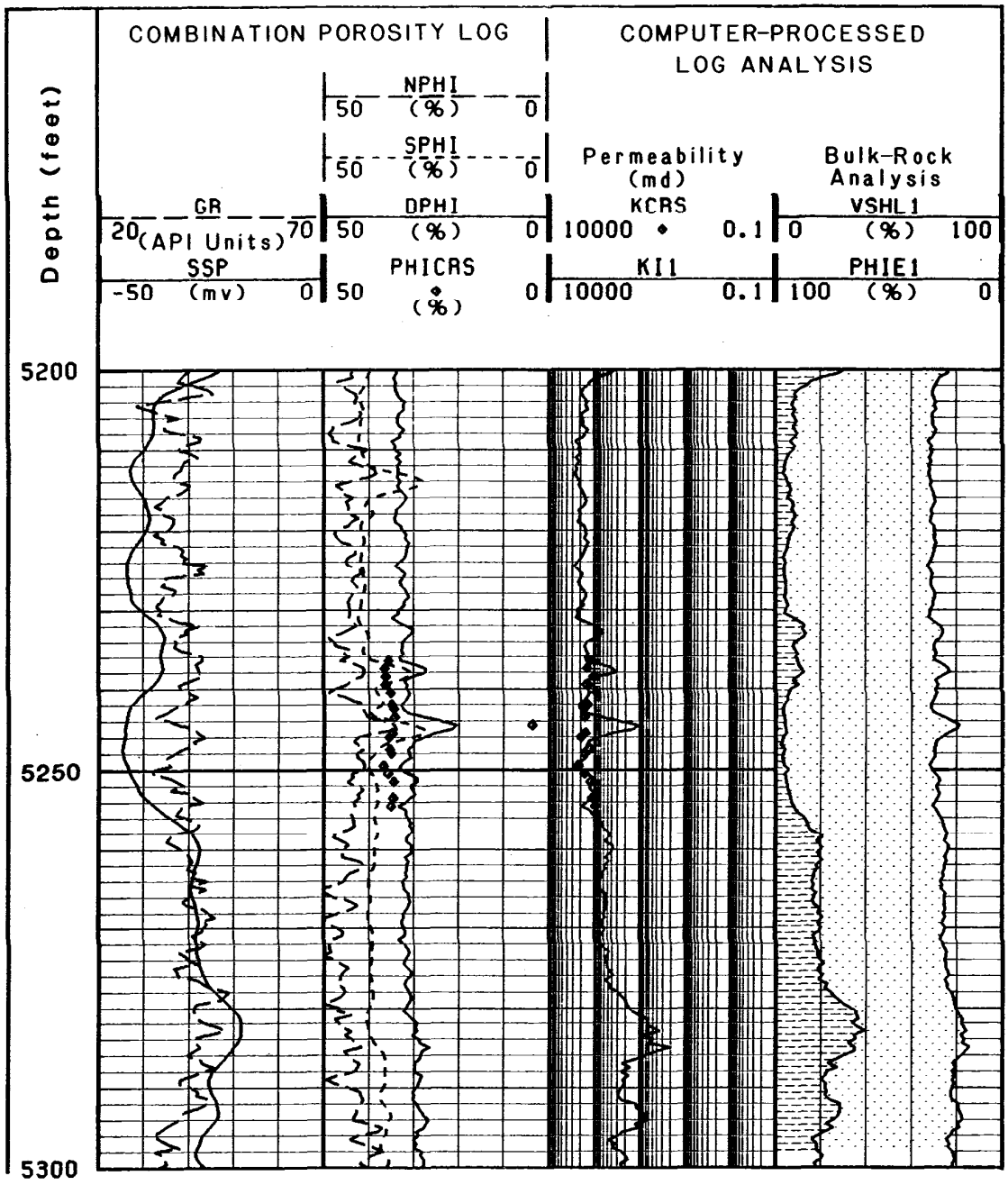

FIGURE 78. **Combination porosity log and computer-processed interpretation over the depth interval of core 3, stratigraphic zone B3. Core porosity (PHICRS) and permeability (KCRS) are plotted for comparison with log data. Computer bulk-rock analysis derived from SP and density logs. Core data depth-shifted 9 feet deeper relative to logs.**

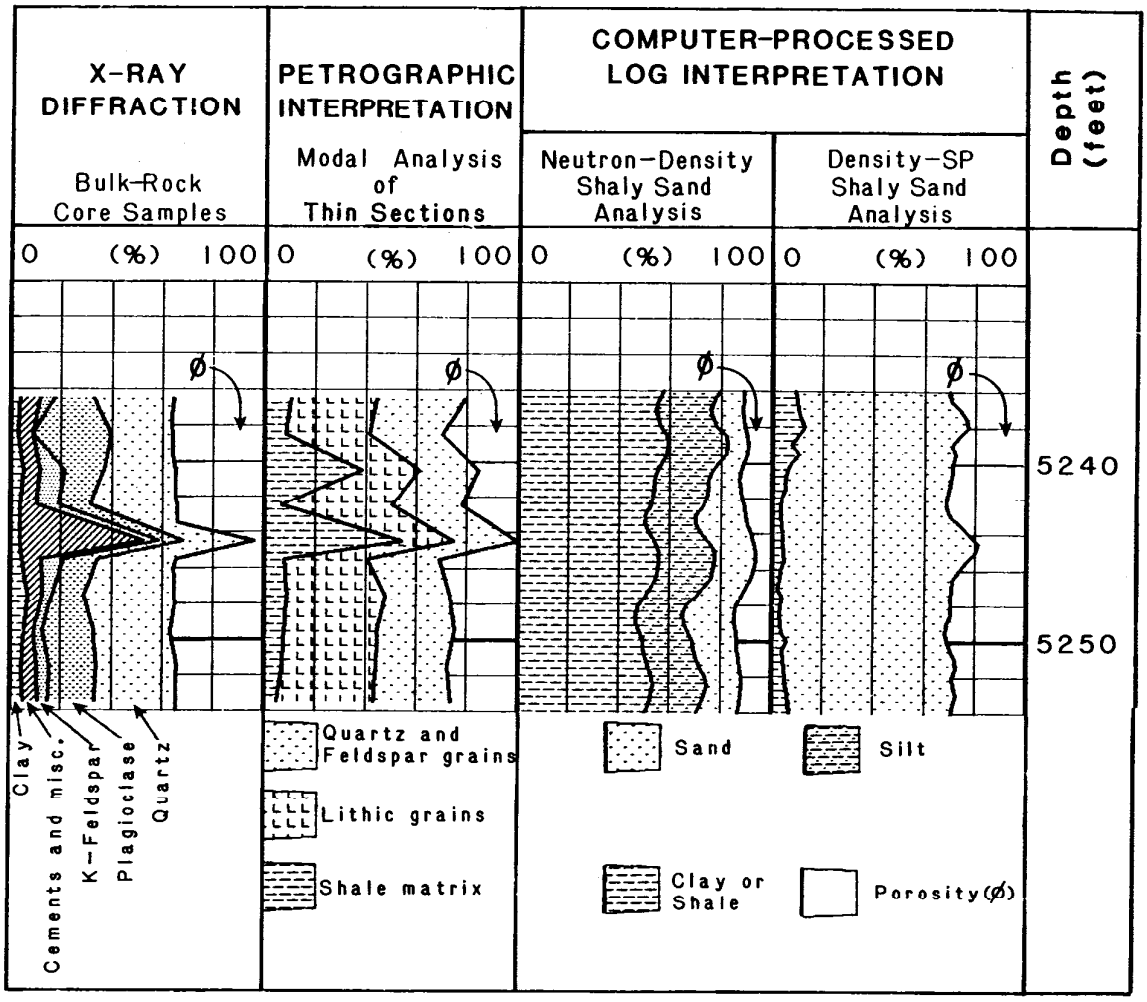

FIGURE 79. **Quantitative lithologic analyses of core 3, stratigraphic zone B3, from x-ray, petrographic and computer-processed log interpretations. X-ray and petrographic data from AGAT (1982). Porosity in x-ray analysis represents core porosity. Porosity in petrographic analysis is visually estimated effective porosity.**

TABLE 10. Reservoir summary of log analysis of sandstones, stratigraphic zone B3: 4,870 to 5,675 feet.

Depth Interval (feet)	Sandstone Thickness (feet)	Sandstone Shaliness (% volume)	Porosity Apparent (%)	Porosity Effective (%)	Permeability Index (millidarcies)
4,886-4,953	67	21.4	32.0	24.6	500
4,986-5,099	113	20.2	33.7	26.7	820
5,109-5,130	21	30.4	32.3	21.8	240
5,138-5,302	164	17.0	31.3	25.4	600
5,337-5465	128	10.8	30.4	26.7	820
5,473-5,506	34	15.5	32.7	27.2	910
5,527-5,617	90	9.4	36.0	32.3	2,600
5,647-5,672	25	6.4	34.9	32.2	2,500
Total:	642	Mean: 15.6	32.5	27.1	890

Lithologic analyses of core 3 are shown in figure 79. The bulk-rock analysis of track 4 in figure 78 is repeated in the same track of figure 79 (the density-SP analysis). As in the overlying interval of core 2, the density-SP analysis approximates the effective porosity and lithology determined from x-ray and petrographic analyses much better than the neutron-density analysis technique (fig. 79). The density-SP analysis indicates a clean sandstone with a shale content of 5 to 10 percent or less. This agrees well with clay content of the x-ray diffraction analysis, and generally well with the petrographic interpretation. Although the sandstone is relatively clean in terms of dispersed and laminar shale, the petrographic interpretation indicates that 50 percent or more of the sandstone grain framework is composed of lithic grains. Because this relatively shallow sandstone has not undergone extensive diagenesis or compaction, these shaly lithic grains have not been altered to the extent that they have adversely affected effective porosity and permeability. However, the neutron-density analysis detects these lithic grains as shale and apparently fails to differentiate them from dispersed and laminar shale types. As a result, it gives an overly pessimistic interpretation of lithology and reservoir characteristics.

Zone B3 contains a total of 642 feet of sandstone in beds between about 20 and 165 feet thick (table 10). The shaliness of these beds ranges from about 6 to 30 percent. Apparent porosity from the density porosity log ranges from about 30 to 36 percent and, when corrected for shale, yields effective porosity ranging from about 22 to 32 percent. The sandstones generally appear to have excellent reservoir potential, with permeabilities ranging from 240 to over 2,600 md.

Zone C1 (5,675 to 6,470 feet)

Zone C1 consists of a sequence of shaly sandstone, siltstone, and mudstone of probable late Oligocene age. The microfossil assemblage indicates a transitional to middle neritic depositional environment (pl. 1). The relatively high-amplitude, parallel and continuous reflectors on seismic profiles corresponding to this zone suggest a marine shelf depositional setting (see Seismic Stratigraphy chapter). The lower boundary of zone C1 coincides with a seismic horizon that represents an angular unconformity on the basin flanks. However, at the COST well, these strata are concordant and the horizon represents at most a paraconformity. The sediment provenance is similar to that of overlying stratigraphic zones B1, B2, and B3, that is, dominantly volcanic but with significant contributions from metamorphic and sedimentary terranes (pl. 1).

Sandstone beds in zone C1 are typically less than 50 feet thick, and the SP log deflections are suppressed because of shaliness (pl. 1). The average shaliness of sandstones in zone C1 (35 percent) is over twice that of overlying zone B3 (16 percent), which suggests a lower energy depositional environment. Core 4 (5,970 to 5,995.3 feet) sampled the lower portion of a 40-foot sandstone from near the middle of the zone which consisted of very poorly to moderately sorted, fine- to medium-grained, clayey sand. The core was extensively mottled and bioturbated and contained whole and broken pelecypod shells, scattered lithic pebbles, and disseminated carbonaceous detritus. The cored sandstone bed (fig. 80) grades upward from a mudstone composed of over 80 percent shale at the base of the bed (5,998 feet) to a relatively clean sandstone containing only 10 to 15 percent shale in the upper part of the bed (5,960 to 5,965). The porosity and permeability data show a concomitant gradual increase upward in the bed. The funnel-shaped log profile and vertical coarsening- and cleaning-upward sequence indicates a shoaling-upward depositional environment typical of deltaic distributary mouth bars, shoreface sands, and offshore bars or shelf sands (Scholle and Spearing, 1982). The disseminated carbonaceous detritus indicates proximity to shore and suggests a shoreface or distributary mouth bar environment.

The match between core and log porosity and permeability data in figure 80 is quite close, which suggests the computer-processed log analysis using the density-SP combination provides a reliable estimate of the sandstone reservoir characteristics for this zone. A comparison of lithologic analyses from the two log interpretation techniques with the x-ray and petrographic analyses (fig. 81) also indicates that the density-SP log interpretation provides the better estimate of lithology and reservoir character. The neutron-density log analysis grossly overestimates the clay and silt content, but in this instance, provides a relatively close approximation of the visual estimate of large pores from the petrographic analysis.

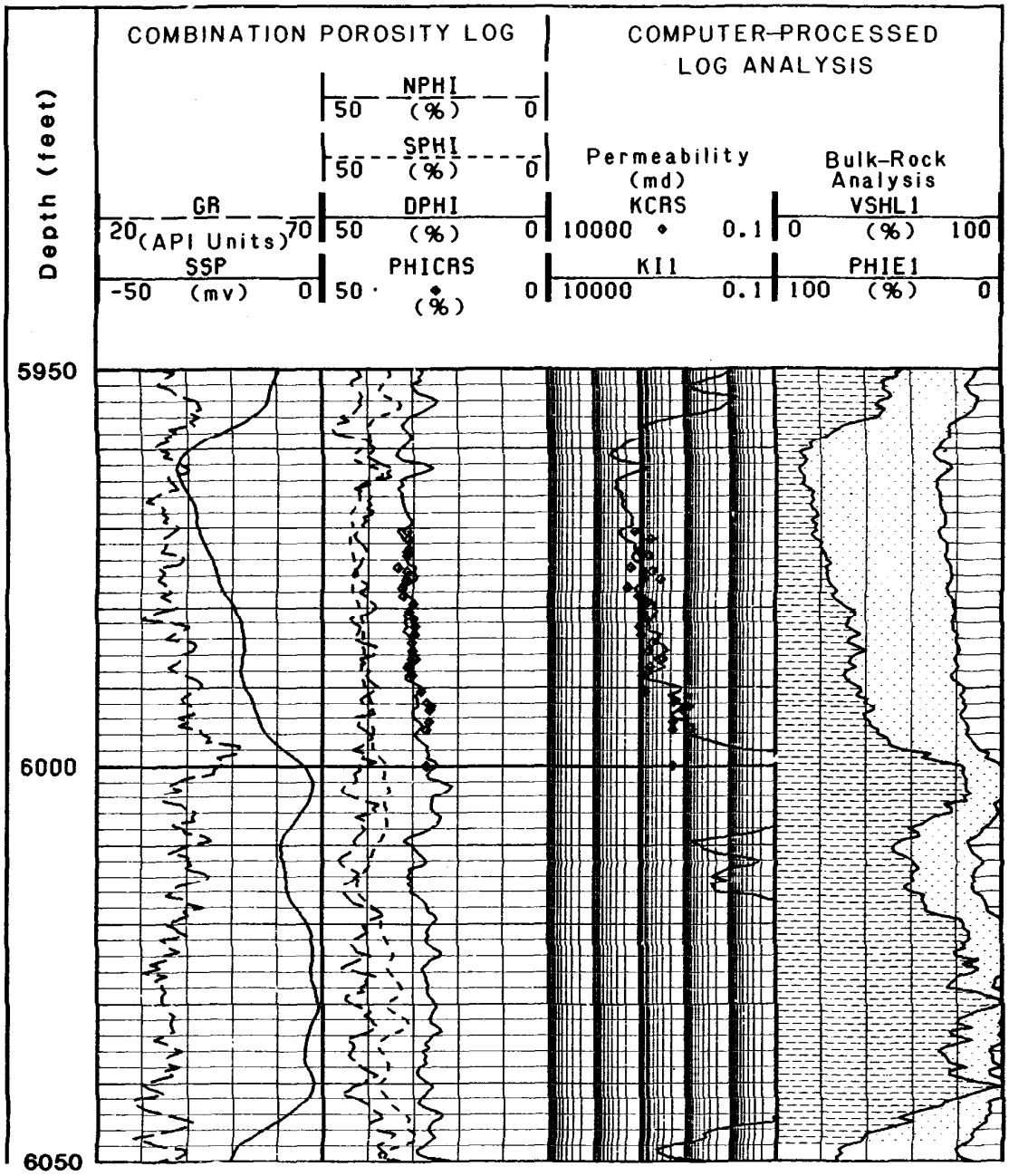

FIGURE 80. **Combination porosity log and computer-processed interpretation over the depth interval of core 4, stratigraphic zone C1. Core porosity (PHICRS) and permeability (KCRS) are plotted for comparison with log data. Computer bulk-rock analysis derived from SP and density logs.**

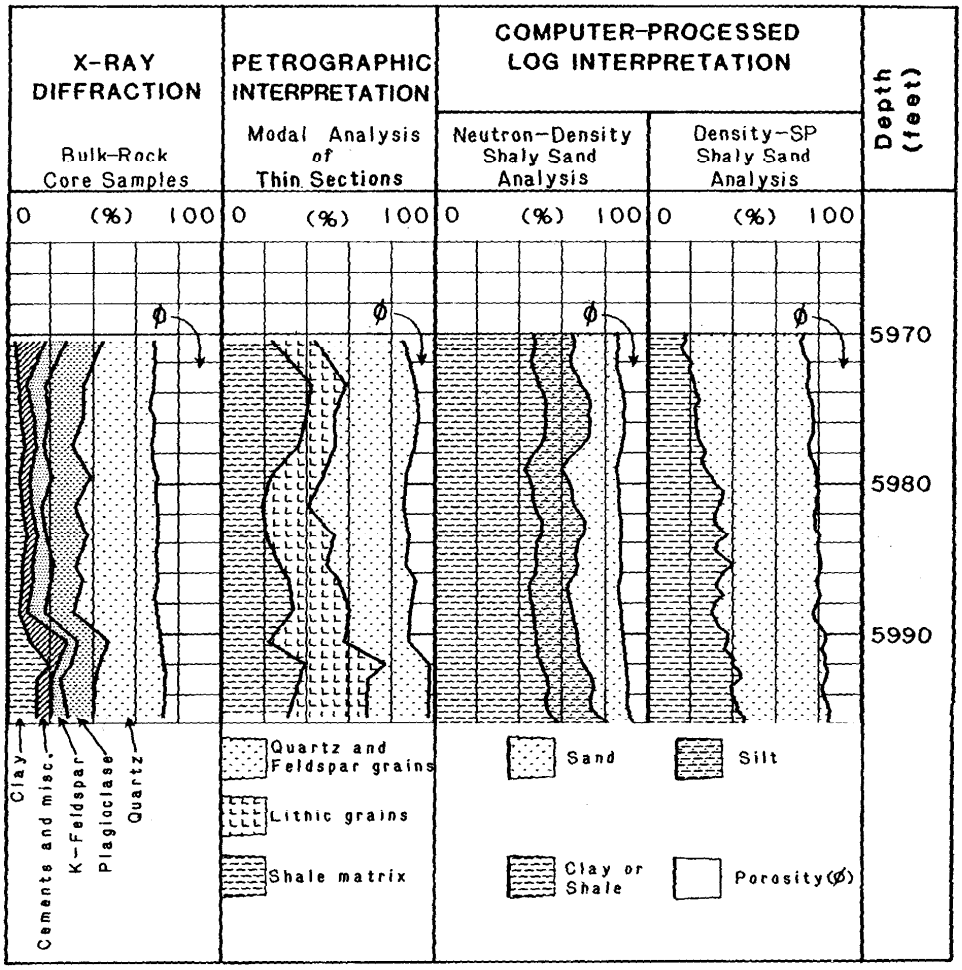

FIGURE 81. **Quantitative lithologic analyses of core 4, stratigraphic zone C1, from x-ray, petrographic and computer-processed log interpretations. X-ray and petrographic data from AGAT(1982). Porosity in x-ray analysis represents core porosity. Porosity in petrographic analysis is visually estimated effective porosity.**

TABLE 11. Reservoir summary of log analysis of sandstones, stratigraphic zone C1: 5,675 to 6,470 feet.

Depth Interval (feet)	Sandstone Thickness (feet)	Sandstone Shaliness (% volume)	Porosity Apparent (%)	Porosity Effective (%)	Permeability Index (millidarcies)
5,698-5,722	24	36.4	28.2	17.2	15
5,727-5,766	49	32.3	31.3	22.1	66
5,783-5,839	56	34.9	28.5	18.2	21
5,926-5,938	12	36.0	30.2	19.2	28
5,951-5,996	45	28.6	30.5	21.8	61
6,046-6,060	14	32.5	26.0	16.8	13
6,073-6,109	36	39.4	27.9	17.2	15
6,172-6,186	14	39.5	28.9	17.6	17
6,225-6,271	47	32.8	30.6	20.5	42
6,319-6,359	40	42.2	30.8	18.3	21
6,403-6,418	15	36.2	31.6	20.5	42
6,423-6,445	22	40.5	30.9	18.7	24
Total:	374	Mean: 35.3	29.8	19.4	30

Zone C1 contains a total of 374 feet of sandstone in beds between about 10 and 60 feet thick (table 11). These sandstones generally contain between 30 and 40 percent shale. Although apparent porosity is relatively high, generally about 30 percent, the effective porosity is considerably lower, about 19 percent. As a result, the permeabilities of these sandstones are lower than those of the overlying zone and average only about 30 md.

Zone C2 (6,470 to 7,900 feet)

The rocks of this zone consist largely of sandstone and shaly sandstone. Microfossil data indicate the rocks are of probable late Oligocene age and were deposited in transitional to nonmarine environments. The base of zone C2 coincides approximately with seismic horizon C, which, at least on the flanks of the basin, represents an unconformity. Seismic reflections in the lower third of seismic sequence III, corresponding to the strata of zone C2, lap onto horizon C on the flanks of the basin (see Seismic Stratigraphy chapter, fig. 65). At the COST well, no discordance is evident on seismic or well log data, so horizon C may represent a disconformity or paraconformity. The rocks of zone C2 consist of two distinct facies: one composed of thick, massive beds or sets of beds of relatively clean sandstone; the other composed of thinner, shaly sandstones interbedded with siltstone and mudstone, and locally, coal. The shaly sand facies, which is characterized by an interval of low-magnitude SP log deflections (pl. 1), occurs in the middle of the zone from 6,875 to 7,540 feet and divides the clean sand facies into two units, one at the top of the zone and one at the bottom.

On the average, the clean sand facies has a higher ratio of quartz to lithic grains than the sandstones of any other zone in the well (pl. 1). The relative abundance of quartz in the clean sand facies is a function of sediment provenance and depositional environment. Sediment derived from the volcanic terranes of the Alaska Peninsula is typically poor in quartz. The ratio of sedimentary and metamorphic clasts to volcanic clasts in the lithic-grain fraction of the sandstones in zone C2 (pl. 1) suggests that a higher percentage of the sediment was derived from sedimentary and metamorphic terranes than elsewhere in the well. Thus, sedimentary detritus richer in quartz was available for reworking during deposition of zone C2. Depositional energy was also a factor in determining the relative quartz content, because within zone C2 only the clean sand facies contain higher-than-typical contents. Assuming that the provenance remained relatively constant during deposition of both the clean and shaly sand facies of zone C2, the higher quartz contents in the clean sand facies are probably the result of the destructive abrasion and winnowing of softer lithic detritus in the higher energy depositional environments.

Core 5 (6,665 to 6,671 feet) sampled a sandstone from the upper unit of the clean sand facies. This was the only conventional core cut in zone C2, and the samples consisted mostly of unconsolidated fine- to coarse-grained sand. Because of the unconsolidated condition of the core samples, the accuracy of the porosity and permeability measurements is suspect. In addition, only three core measurements were obtained, which represents a rather small statistical sample for comparing with the log data. Consequently, the data from this core were used to calibrate logging data only for the upper unit of the clean facies. The log analysis of the shaly sand facies was calibrated using data from core 4 of stratigraphic zone C1, which contained a similar sandstone facies. The log analysis of the lower unit of the clean sand facies of this zone was calibrated using data from cores 6 and 7 of the underlying zone (D1), which appeared to contain relatively similar clean sandstones.

Porosity and permeability data from the logs and from core 5 are shown in figure 82. A probable SWirr value of 2.1 percent for calculating permeability from the logs was obtained from the Wyllie-Rose relation using core data. This is an unusually low value of SWirr; typical SWirr values for most reservoir rocks range from about 10 to 50 percent (Schlumberger, 1972a, p.100). The low value calculated for SWirr from the core data may be a result of artificially high permeability created as a result of fabric disruption of the friable sandstone during the coring process. Although the sandstones of the upper unit of the clean sand facies are porous and relatively coarse grained, and should therefore have good reservoir characteristics, the high permeabilities that were calculated from the logs (ranging from about 1,800 to 5,600 md) may be too optimistic.

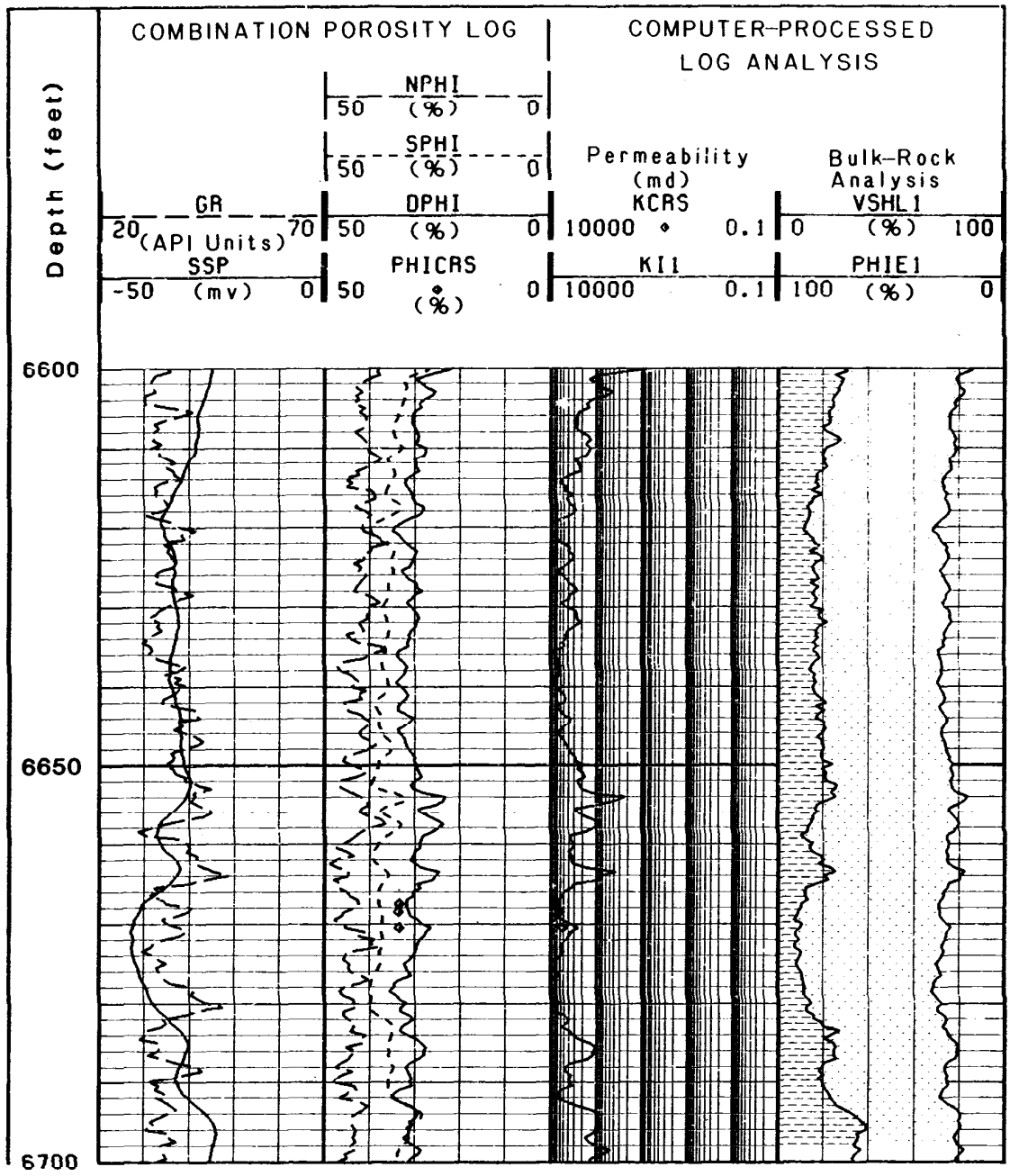

FIGURE 82. **Combination porosity log and computer-processed interpretation over the depth interval of core 5, stratigraphic zone C2. Core porosity (PHICRS) and permeability (KCRS) are plotted for comparison with log data. Computer bulk-rock analysis derived from SP and density logs. Core data depth-shifted 2 feet deeper relative to logs.**

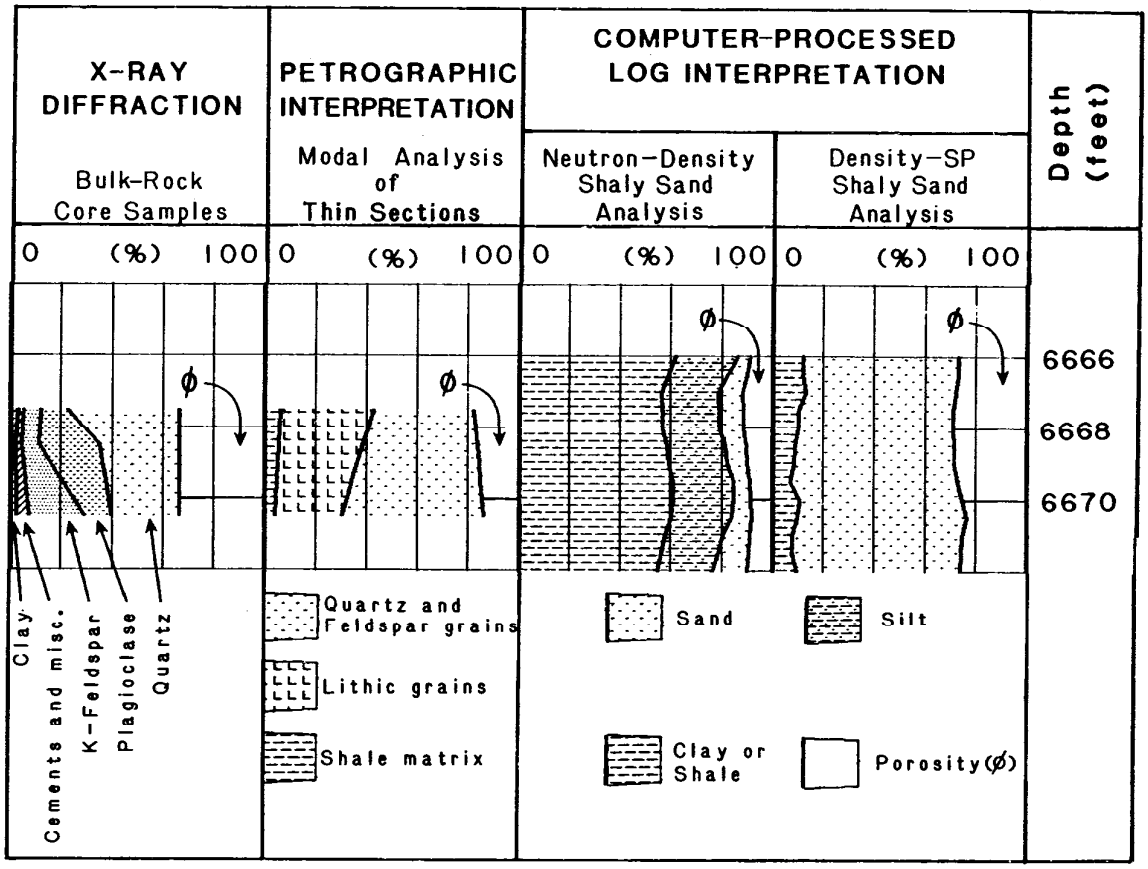

FIGURE 83. **Quantitative lithologic analyses of core 5, stratigraphic zone C2, from x-ray, petrographic and computer-processed log interpretations. X-ray and petrographic data from AGAT (1982). Porosity in x-ray analysis represents core porosity. Porosity in petrographic analysis is visually estimated effective porosity.**

TABLE 12. Reservoir summary of log analysis of sandstones, stratigraphic zone C2: 6,470 to 7,900 feet.

Depth Interval (feet)	Sandstone Thickness (feet)	Sandstone Shaliness (% volume)	Porosity: Apparent (%)	Porosity: Effective (%)	Permeability Index (millidarcies)
----- Clean Sand Facies, Upper Unit -----					
6,470-6,493	23	8.7	30.3	27.1	5,600
6,502-6,582	80	19.4	28.8	22.5	1,800
6,592-6,874	282	19.0	32.3	26.4	4,800
	---	----	----	----	-----
Total:	385	Mean: 18.5	31.6	25.7	4,000
----- Shaly Sand Facies -----					
6,891-6,905	14	35.1	31.4	20.8	46
6,939-7,035	89	37.5	32.7	21.6	58
7,044-7,058	15	25.2	30.8	22.9	82
7,074-7,182	109	32.8	30.2	20.7	44
7,191-7,204	14	44.5	33.2	19.9	35
7,230-7,242	13	42.3	34.1	21.5	56
7,249-7,333	84	38.1	32.9	21.5	56
7,411-7,447	36	39.2	28.9	17.4	16
7,460-7,517	57	36.7	29.9	18.6	23
7,523-7,536	13	31.0	29.9	20.3	40
	---	----	----	----	--
Total:	444	Mean: 36.2	31.4	20.7	44
----- Clean Sand Facies, Lower Unit -----					
7,541-7,768	227	23.7	32.5	25.1	1,600
7,773-7,810	37	19.2	28.9	24.2	1,300
7,830-7,885	55	22.5	28.6	23.8	1,100
	---	----	----	----	-----
Total:	319	Mean: 23.0	31.4	24.8	1,400

The lithologic analyses from the x-ray, petrographic, and computer-processed log interpretations, with the exception of the neutron-density analysis, all indicate that the sandstone contains only minor amounts of intergranular porosity-occluding shale or cements and that the framework is dominated by mechanically stable quartz and feldspar grains (fig. 83). Table 12 summarizes the sandstone reservoir characteristics of the three units of zone C2. The clean sand facies units each contain over 300 feet of excellent reservoir quality sandstone in beds ranging from 20 to 280 feet thick. Effective porosity in these units is over 22 percent and permeability, if the log-derived analysis is accurate, is over 1,000 md. By contrast, permeabilities in the shaly sand facies are lower by one or two magnitudes and range from 16 to 82 md.

Zone D1 (7,900 to 9,555 feet)

This interval contains conglomeratic sandstone, sandstone, siltstone, mudstone, and coal. The probable early Oligocene microfossil assemblages indicate a transitional to nonmarine environment, except near the top of the zone, where inner neritic to transitional conditions are indicated (pl. 1). Zone D1 contains a more heterogeneous vertical sequence of lithofacies and a higher proportion of mudstone and siltstone than any of the other Oligocene stratigraphic zones. The heterogeneous lithology and greater abundance of mudstone is reflected by the higher activities of the sonic and density logs and the positive shift of the SP log shale baseline (pl. 1). The variable mix of lithofacies and lower sand-shale ratio is probably a result of fluctuating depositional energies, which are typical of coastal-plain paralic environments.

Below seismic horizon C, which marks the approximate contact of zones C2 and D1, there is a significant overall downward increase in the abundance of volcanic lithic grains relative to sedimentary and metamorphic grains in the framework of sandstones (pl. 1). Accompanying this shift is a downward reduction in quartz content of the sandstones and a decrease in effective porosity and permeability (table 13). This rapid deterioration of reservoir quality is apparently related to the increase in chemically and mechanically unstable volcanic lithic grains, which are more susceptible to compaction and diagenesis with increasing burial depth.

Data from cores 6 and 7 were used in checking and calibrating the log analyses of sandstones in the upper part of zone D1 (7,900 to 8,240 feet), as well as in the lower unit of zone C2 (7,540 to 7,900 feet). The density porosity trace (DPHI) closely approximates the core porosity over most of the cored interval, but the log-derived permeability corresponds with core permeability only in the clean sandstone interval from 8,082 to 8,098 feet (fig. 84). The match of log to core permeability is poor in the interval above 8,082 feet, where the lithology consists largely of shaly sandstone with clay-rich laminae. However, these intervals of very shaly sandstone were excluded from the sandstone reservoir analyses in tables 12 and 13 because they were interpreted as nonreservoir rock by the computer-processed log analysis as a result of their high shale contents.

Petrographic analyses indicate that the clean sandstone interval in core 7, like the clean sand facies of zone C2, contains a high fraction of mechanically stable quartz and feldspar grains (fig. 85). Most of the effective porosity is apparently in the form of large, unoccluded intergranular pores, because the effective porosity calculated from the density-SP analysis is nearly equivalent to that of the visually estimated mesoporosity (large pores) of the petrographic interpretation (fig. 85). It is significant that only in this quartz- and feldspar-rich interval does the neutron-density log analysis yield results more nearly in agreement with the other analyses. This indicates that it is principally the lithic grains

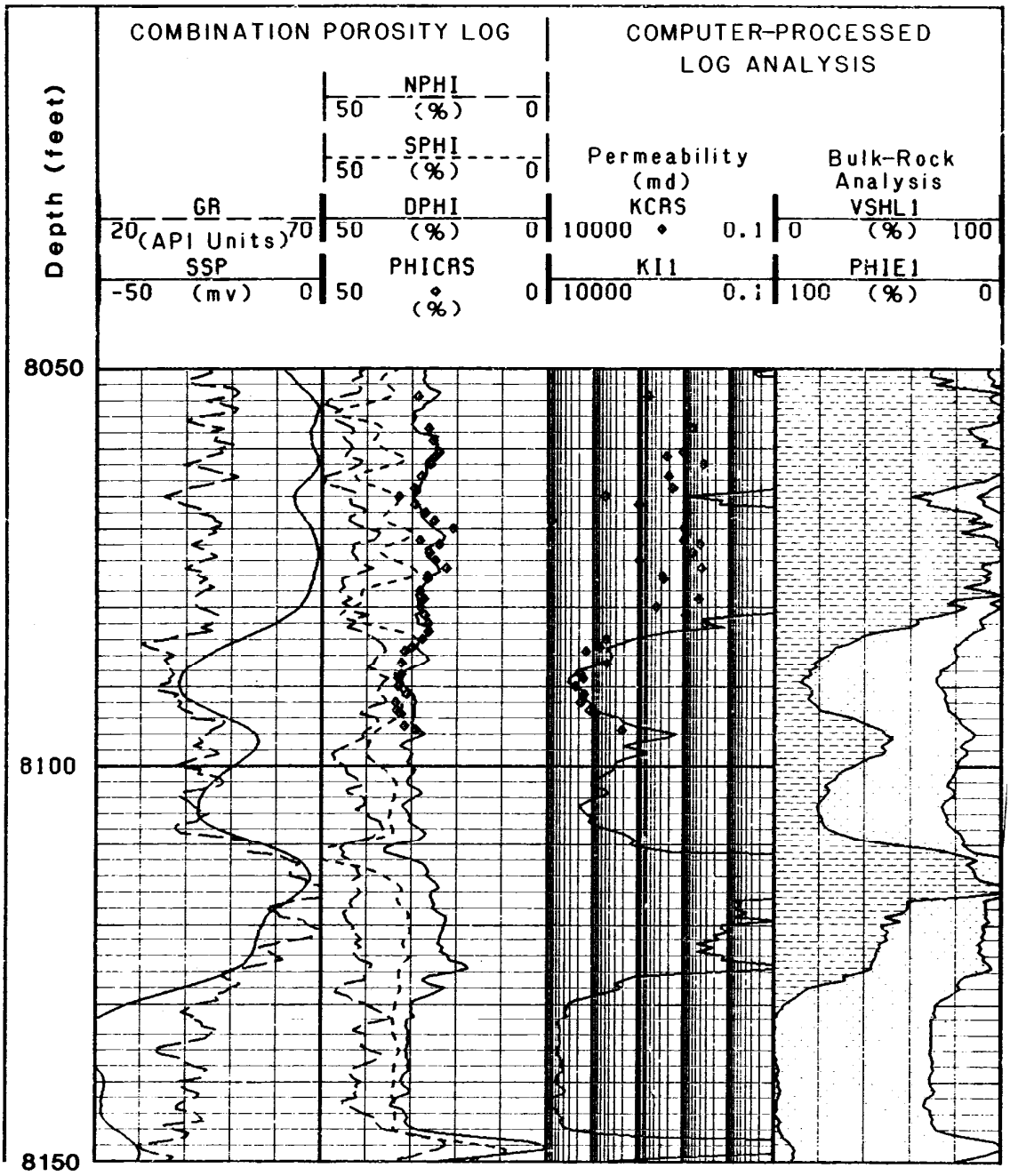

FIGURE 84. **Combination porosity log and computer-processed interpretation over the depth interval of cores 6 and 7, stratigraphic zone D1. Core porosity (PHICRS) and permeability (KCRS) are plotted for comparison with log data. Computer bulk-rock analysis derived from SP and density logs. Core data depth-shifted 2.5 feet deeper relative to logs.**

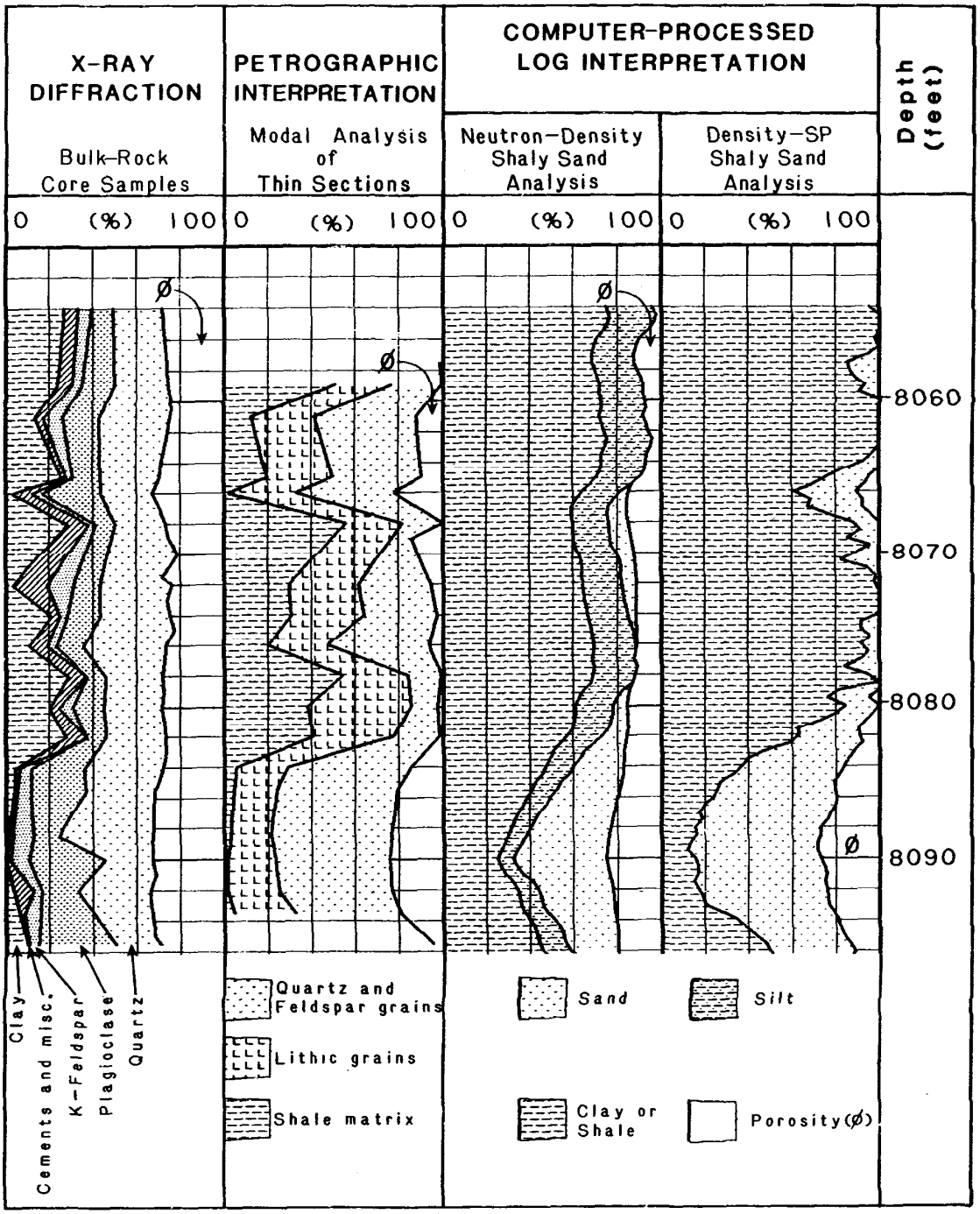

FIGURE 85. **Quantitative lithologic analyses of cores 6 and 7, stratigraphic zone D1, from x-ray, petrographic and computer-processed log interpretations. X-ray and petrographic data from AGAT (1982). Porosity in x-ray analysis represents core porosity. Porosity in petrographic analysis is visually estimated effective porosity.**

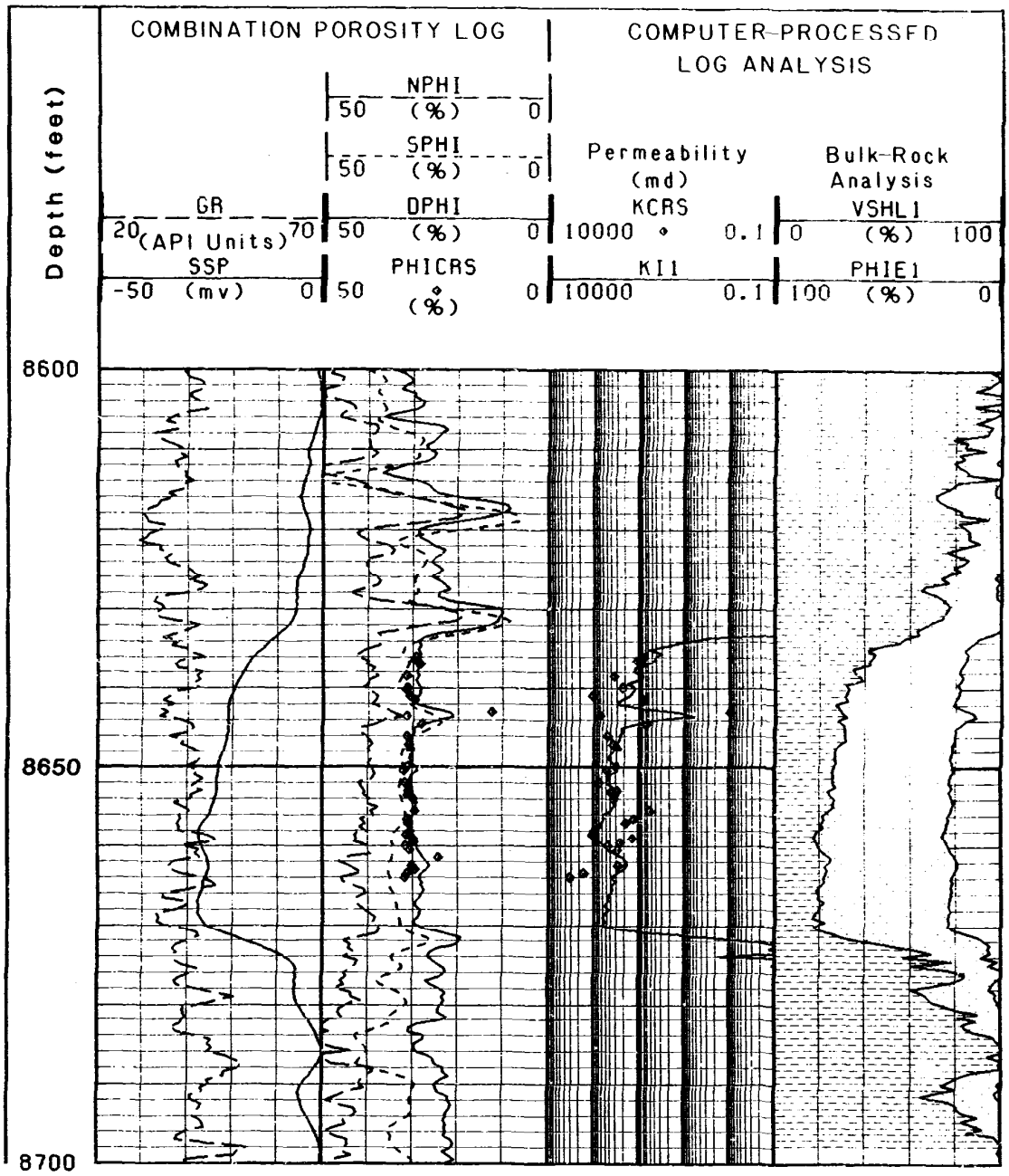

FIGURE 86. **Combination porosity log and computer-processed interpretation over the depth interval of core 8, stratigraphic zone D1. Core porosity (PHICRS) and permeability (KCRS) are plotted for comparison with log data. Computer bulk-rock analysis derived from SP and density logs. Core data depth-shifted 7 feet lower relative to logs.**

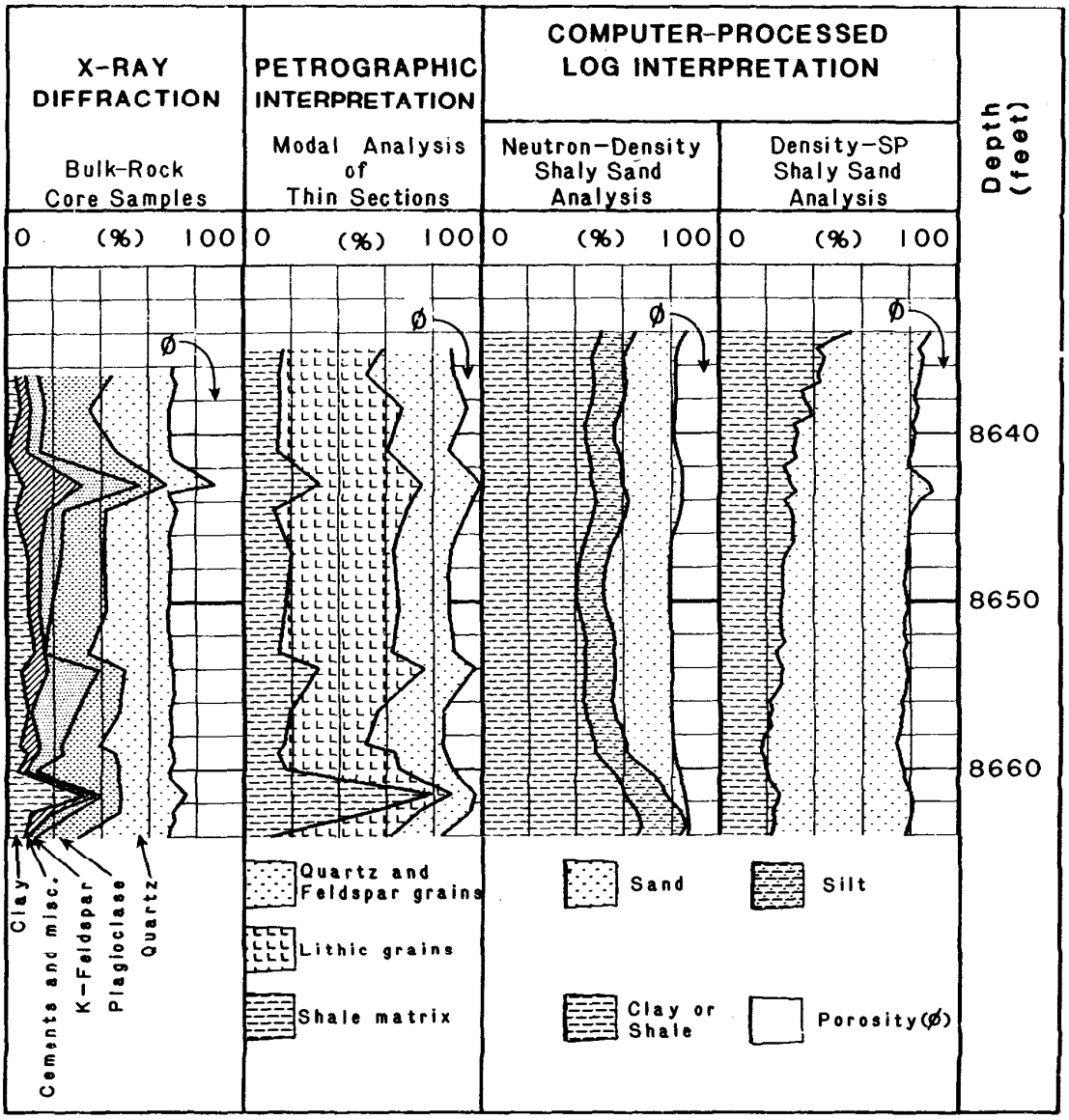

FIGURE 87. **Quantitative lithologic analyses of core 8, stratigraphic zone D1, from x-ray, petrographic and computer-processed log interpretations. X-ray and petrographic data from AGAT (1982). Porosity in x-ray analysis represents core porosity. Porosity in petrographic analysis is visually estimated effective porosity.**

in these sandstones that are adversely affecting this type of analysis.

Data from core 8 were used in checking and calibrating the log analyses for sandstones in the lower three-quarters of zone D1 (8,240 to 9,555 feet). The vertical profile of the sandstone bed (fig. 86) indicates a relatively sharp basal contact, with gradually upward-increasing shale contents and decreasing porosity. The core consisted of a granule to pebble conglomerate that fines upward to coarse- to fine-grained sandstone. The sedimentary structures consist of graded beds containing basal scours, cross-bedding, and low-angle inclined to wavy laminae. This fining-upward vertical succession of lithofacies is characteristic of fluvial point-bar deposits (Cant, 1982; Allen, 1970), which tend to generate bell-shaped SP curves similar to that of figure 86 (Bernard and others, 1970).

In this sandstone, both the sonic and density logs provided a generally good approximation of core porosity. The log-derived permeability roughly approximates that of the core, although considerable scatter in the core data is evident. The petrographic analysis (fig. 87) indicates that the sand composition is dominated by lithic clasts. As a result, the neutron-density analysis overestimates clay and silt content, although it does provide a good estimate of relative quartz and feldspar sand-grain content and yields effective porosity close to that of the density-SP analysis.

TABLE 13. Reservoir summary of log analysis of sandstones, stratigraphic zone D1: 7,900 to 9,555 feet.

Depth Interval (feet)	Sandstone Thickness (feet)	Sandstone Shaliness (% volume)	Porosity Apparent (%)	Porosity Effective (%)	Permeability Index (millidarcies)
7,949-7,981	32	33.2	31.9	21.0	300
8,083-8,109	27	27.9	29.7	20.8	280
8,126-8,231	105	11.4	29.1	25.1	880
8,563-8,575	12	26.5	32.6	23.8	640
8,634-8,671	37	26.8	28.9	20.4	250
8,790-8,807	17	28.4	30.7	21.2	320
8,823-8,870	47	29.0	26.5	17.2	91
9,031-9,042	11	29.0	29.0	19.9	220
9,093-9,107	14	44.5	27.6	12.7	15
Total:	302	Mean: 23.4	29.3	21.5	350

Core 9 (9,255 to 9,265 feet) was not used in the log analysis of this zone because it sampled an interval of interbedded lenticular sandstone and claystone containing bedding units too thin for accurate resolution by the well logs and volumetrically too small for inclusion as prospective reservoir rock.

Zone D1 contains over 300 feet of sandstone in beds over 10 feet thick (table 13). The reservoir quality appears generally good to excellent except in the lower part of the zone. The log-derived permeabilities are generally over 200 md and appear reasonably accurate on the basis of the match with the core permeabilities. Most of the sandstone is in relatively thin beds, however, and only one bed, in the upper part of the zone, is over 50 feet thick.

Zone D2 (9,555 to 10,380 feet)

This zone contains a sequence of siltstone, claystone, and shaly sandstone of early Oligocene to late Eocene age. Relatively low activities on the resistivity and SP log traces, particularly below 10,000 feet, suggest a uniform, massively bedded, homogeneous lithology (pl. 1). The SP log displays a near baseline response over most of the interval, which indicates that the zone contains no significant thickness of permeable lithology. A small-magnitude SP deflection across a sandstone bed at the base of the zone (10,320 to 10,355 feet) suggests that the bed contains some permeability, but about half of core 11 (Lithology and Core Data chapter, fig. 17) from this sandstone is relatively impermeable (less than 5 md), which indicates that the bed contains relatively thin zones of permeability.

Microfossils from this zone indicate a paleobathymetry ranging from inner to middle neritic, except near the base of the zone between 10,250 and 10,380 feet, where a shallower, transitional environment is indicated. Core 11 from this shallow-water facies sampled a moderately to well sorted, medium- to coarse-grained sandstone that contained abundant mollusc shell fragments and low-angle inclined and ripple laminations. Overall, the vertical succession of lithofacies and biofacies in this zone suggests a transgressive marine-shelf sequence.

The base of zone D2 coincides with seismic horizon D, which in some areas of the North Aleutian Basin overlies acoustic basement and represents an unconformity. At the well site, however, reflections above and below horizon D are concordant, and the dipmeter log data indicate no angular discordance in structural dip. The abrupt changes in wireline log character and sediment provenance (pl. 1) and the marked increase in diagenetic alteration of the sandstones below horizon D suggest that although concordant, it probably represents a disconformity at the COST well. Seismic reflections corresponding to stratigraphic zones D1 and D2 (seismic sequence IV) exhibit a lateral change in character to lower continuity and higher amplitudes where horizon D overlies acoustic basement (Seismic Stratigraphy chapter). This suggests that where stratigraphic zones D1 and D2 overlie basement, they probably represent a nonmarine facies of the neritic to transitional deposits encountered at the well site.

Zone D2 was the lowest stratigraphic interval in the COST well to receive significant influxes of relatively quartz-rich detritus from sedimentary and metamorphic terranes. Below this depth, the source terranes were almost exclusively volcanic. The appearance in

the late Eocene of significant amounts of nonvolcanic lithic clasts in zone D2 sediments probably reflects the erosion of previously buried Mesozoic plutonic and sedimentary rocks that core and flank the Alaska Peninsula and influxes of metamorphic detritus from Paleozoic exposures to the north and northeast (Burk, 1965; Wilson, 1985; AGAT, 1982).

Zone E (10,380 to 15,620 feet)

This zone consists of a complexly interbedded sequence of volcaniclastic sandstones and conglomerates, siltstones, mudstones, and abundant coals of Eocene age. Microfossils indicate that the rocks represent nonmarine deposits except at the top of the zone (above 10,740 feet), where transitional to inner neritic deposition occurred. Lithic clasts in the sandstones of this zone are almost entirely of volcanic origin (pl. 1), which indicates that the sediment provenance of this zone is almost exclusively volcanic.

The variable lithology and complex interbedding of this zone are reflected on wireline logs by the high activity and large-scale deflections of most of the curves (pl. 1). However, the SP log displays only small-magnitude deflections from baseline, and resistivity logs record little or no curve separations, which suggests that the sandstones are impermeable. This is corroborated by analyses of cores from this zone (Lithology and Core Data chapter, table 3) which indicate very low permeabilities. The lack of effective porosity and permeability is linked to the volcanic provenance of the sediments. The mechanically and chemically unstable volcanic lithic clasts which compose these sandstones have undergone extensive ductile deformation and diagenetic alteration, and the pore space is largely filled with authigenic cements and deformed grains.

The boundary between zones E and F may represent an unconformable surface. There is a very large shift on the gamma ray log at this contact (pl. 1), and anomalies in thermal maturity trends (see Organic Geochemistry chapter) at this depth suggest that some of the stratigraphic section has been removed by erosion. The unconformity, if present, is a disconformity, as no angular discordance is evident on the dipmeter log.

Overlying the possible unconformable surface is a relatively massive sandstone that, for this zone, has a relatively large SP log deflection, which suggests it has some permeability. High values on the resistivity log suggest it may contain hydrocarbons (pl. 1). Abundant dull yellow-gold fluorescence reported in drill cuttings also indicates the presence of hydrocarbons. Water saturations determined from a resistivity-versus-porosity crossplot (fig. 88) indicate that as much as 50 percent of the pore space of this sandstone may contain hydrocarbons. However, the accuracy of this determination of hydrocarbon saturation is uncertain because it is dependent on an accurate determination of formation water resistivity (RW). The lack of the SP log response throughout most of the zone, and the unusual formation characteristics of these volcaniclastic

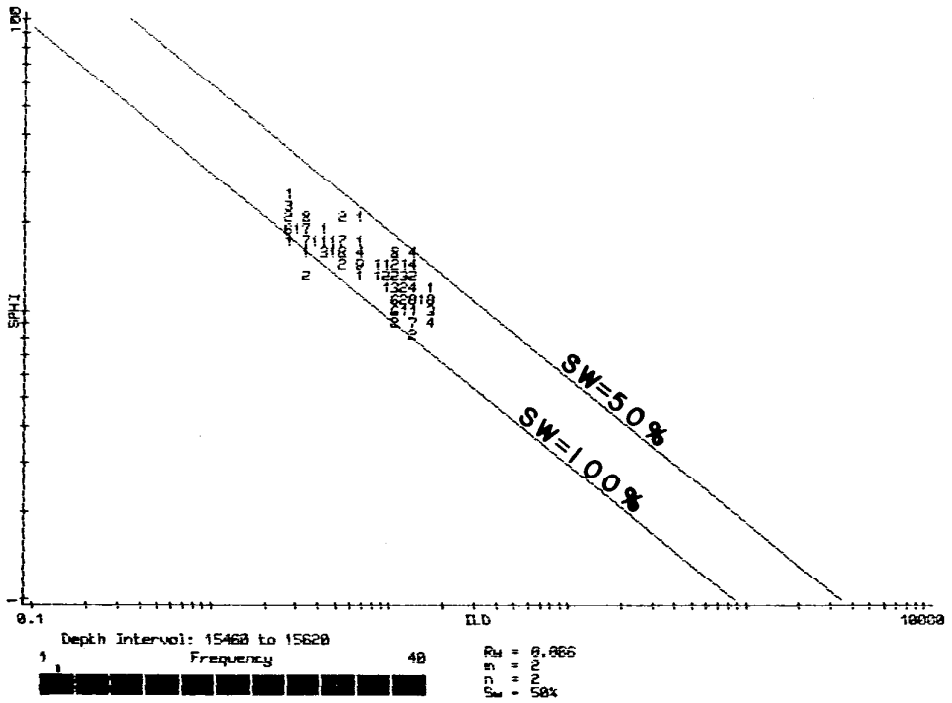

FIGURE 88. **Resistivity (ILD) versus sonic porosity (SPHI) Pickett crossplot (Pickett, 1972) from the basal sandstone of stratigraphic zone E.**

rocks, make the determination of RW using standard techniques and parameters uncertain.

Zone F (15,620 to 16,652 feet)

Zone F consists of volcaniclastic conglomerates, sandstones, siltstones, mudstones, and volcanic tuffs of Eocene age. The most notable difference between this zone and the overlying zone E is the much lower gamma ray log response in zone F, particularly in shaly intervals, where the response is as much as 90 gamma API units lower. The Natural Gamma Spectrometry log indicates that the reduction in radioactivity is due to an abrupt decrease in thorium and a more gradual decrease in potassium which occur at the boundary of zone E and F. The thorium content in the lower part of zone E generally ranges from 3 to 9 ppm, but in the upper part of zone F it ranges only from 1 to 4 ppm. All thorium compounds are insoluble and have limited mobility during diagenesis (Serra and others, 1980, p. 9). Therefore, unless thorium has been concentrated in zone F in residual minerals as a result of alteration and weathering or depositional winnowing, the difference in thorium contents between zones E and F probably signifies a difference in provenance.

Hydrocarbon shows consisting of gas peaks on the mud log and oil stain and fluorescence in drill cuttings were encountered below 16,130 feet. Identification of lithology in this interval on the wireline logs is difficult because of the lack of any SP log response and the overall low radioactivity recorded in both sandstone and shale intervals on the gamma ray log. The drill cuttings from the interval containing hydrocarbon shows consisted predominantly of silty claystone and shale containing calcite-filled fractures. The hydrocarbons are inferred to have been produced from the fractures.

Zone G (16,652 to 17,155 feet)

Lithologically, zone G is similar to zone F, except that zone G also contains thin coal beds and a 20-foot section of diabase(?) from 16,680 to 16,700 feet. Zone G is apparently unconformably overlain by zone F. The dipmeter log indicates that strata above 16,652 feet dip 3^{o} to 6^{o} east-southeast; between 16,652 and 16,700 feet, a few scattered dips suggest that the strata in zone G dip 40^{o} to 60^{o} east-southeast. The angular discordance suggested by the dipmeter log is confirmed by bedding attitudes in cores 18 and 19 (near horizontal in core 18 of zone F, inclined approximately 20^{o} in core 19 of zone G). It is unknown if these steeper dips continue below 16,722 feet because no dipmeter or other logs were run below about 16,700 feet. It is possible that the angular discordance represents only local deformation adjacent to the diabase(?) intrusive. However, this appears unlikely because the subjacent rocks of core 19 show little evidence of deformation other than inclined bedding.

7. Paleontology and Biostratigraphy

by

John A. Larson

The biostratigraphy and paleoecology of the North Aleutian Shelf COST No. 1 well were determined by detailed analysis of microfossil assemblages contained in samples recovered from the well. The microfossils included foraminifera, diatoms, silicoflagellates and ebridians, marine and terrestrial palynomorphs, calcareous nannofossils, ostracodes, and rare Radiolaria. The samples examined consisted of rotary-drill-bit cuttings (ditch samples) collected at 30-foot intervals from 1,380 feet to the total depth of 17,155 feet, along with numerous sidewall cores (SWC) and 19 conventional cores (CC). In addition, processed samples, slides, and reports prepared for the COST well participants by Biostratigraphics (1983) were examined, interpreted, and integrated into this report. Discrepancies between the biostratigraphy of this report and the consultants' conclusions may be due to interpretive differences or differences in emphasis on the various groups of biostratigraphic indicators.

The Minerals Management Service biostratigraphic interpretations also include analyses of megafossils recovered from conventional cores (Marks, 1983; Dilcher, 1983) and ostracode studies by Elisabeth Brouwers of the U.S. Geological Survey (written commun., 1985). The analysis of the foraminifera and interpretation and synthesis of other biostratigraphic and geologic data were done by the author. Analysis and interpretation of siliceous microfossils was done by Donald L. Olson of MMS.

The biostratigraphy is discussed in the order in which the strata were encountered in the well. The biostratigraphy of the Pleistocene, Pliocene, and late Miocene is based primarily on diatoms, with supporting evidence from foraminifera. The MMS siliceous microfossil zonation for this portion of the well is shown in figure 89. Calcareous nannofossils and palynomorphs were important for determining the biostratigraphy of the Oligocene, with some support from foraminifera, while palynomorphs were the most important group in the Eocene. The MMS interpretation of the biostratigraphy and paleobathymetry of the well is shown in figure 90. Fossil occurrences are listed as highest and lowest occurrences in the well to avoid the potential confusion of references to first and last occurrences. Data from conventional cores are regarded as the most reliable, followed by sidewall cores, both of which are given more weight in the interpretation than data

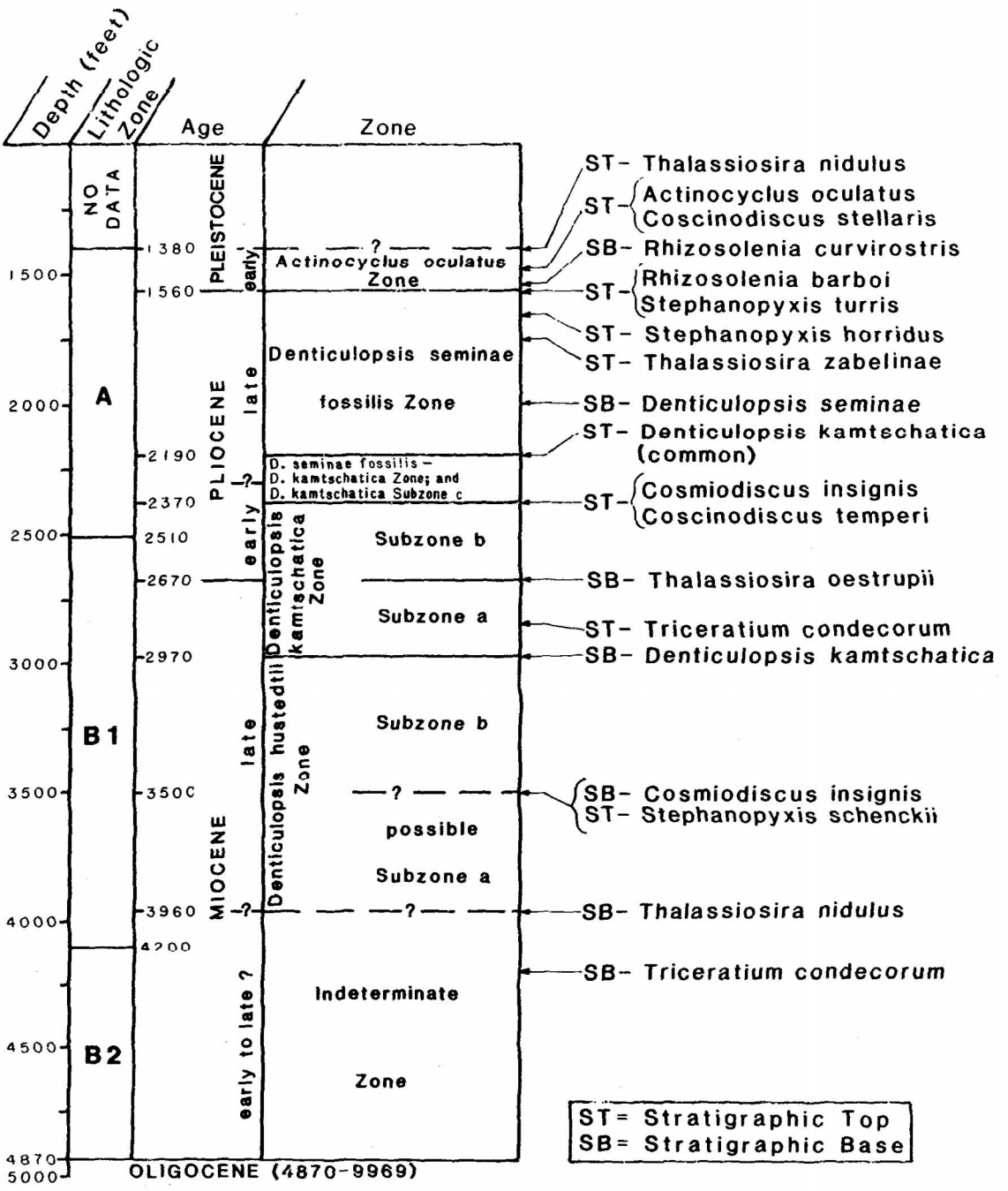

FIGURE 89. **Summary of siliceous-microfossil biostratigraphic zones, North Aleutian Shelf COST No. 1 well. Zonation after Barron, 1980.**

from cuttings. The lithologic, seismic, and geochemical data referred to here are discussed in more detail in the appropriate chapters of this report.

Paleoenvironmental determinations were based on interpretations of both microfossils and macrofossils. Paleoclimatological interpretations were based on spore and pollen suites and, to a lesser extent, on foraminifera, siliceous microfossils, ostracodes and molluscs. Paleobathymetric determinations were primarily based on foraminiferal evidence, but dinoflagellates and marine organisms such as molluscs, echinoids, ophiuroids, bryozoans and cirripeds were also considered in the analysis. Lithological, sedimentological, and well log data were also utilized. Fluvial, lacustrine, and paludal environments are classified as nonmarine (continental). Transitional environments include brackish-water marshes, estuaries, and hypo- and hypersaline lagoons. Paleoenvironments for sediments deposited under marine conditions are expressed in terms of bathymetry (fig. 90) and are divided into inner neritic (0 to 60 feet), middle neritic (60 to 300 feet), outer neritic (300 to 600 feet), and upper bathyal (600 to 1,500 feet).

The biostratigraphy of the upper part of the well is defined primarily on the basis of diatom distributions from cuttings averaged over 90-foot intervals (Biostratigraphics, 1983) or taken from the top 30 feet of each 90-foot interval (MMS), and from sidewall cores and conventional cores. Siliceous microfossils, including diatoms, are scarce and poorly preserved below 3,960 feet. Below 4,200 feet, diatoms are very rare and appear to be mostly caved specimens. Neogene age determinations are primarily based on the diatom zonation scheme of Barron (1980). However, this well presented particular problems in diatom zonation in that a large portion of the diagnostic species used in the zonations proposed by Barron (1980), Koizumi (1973, 1977), and Schrader (1973) were absent. Several of the biostratigraphic determinations are based on diatom species that have established age ranges, but have not been designated as key species by the authors of the major zonation schemes. Therefore, the diatom zonation of the upper part of the well must be considered provisional.

PLEISTOCENE

The uppermost sampled part of the well (1,380 to 1,560 feet) is probable early Pleistocene in age and is assigned to Barron's (1980) Actinocyclus oculatus Zone (fig. 89). This zonation is based on the highest observed occurrences of Actinocyclus oculatus and Pseudopyxilla americana at 1,470 feet, and Coscinodiscus stellaris at 1,480 feet (SWC). Other species whose highest occurrences might indicate a slightly younger age appear at 1,380 feet (Rhizosolenia curvirostris, Thalassiosira nidulus), but their actual highest stratigraphic occurrences cannot be determined because of the lack of samples from higher in the well. The base of the Actinocyclus oculatus Zone is placed at 1,560 feet on the basis of the highest

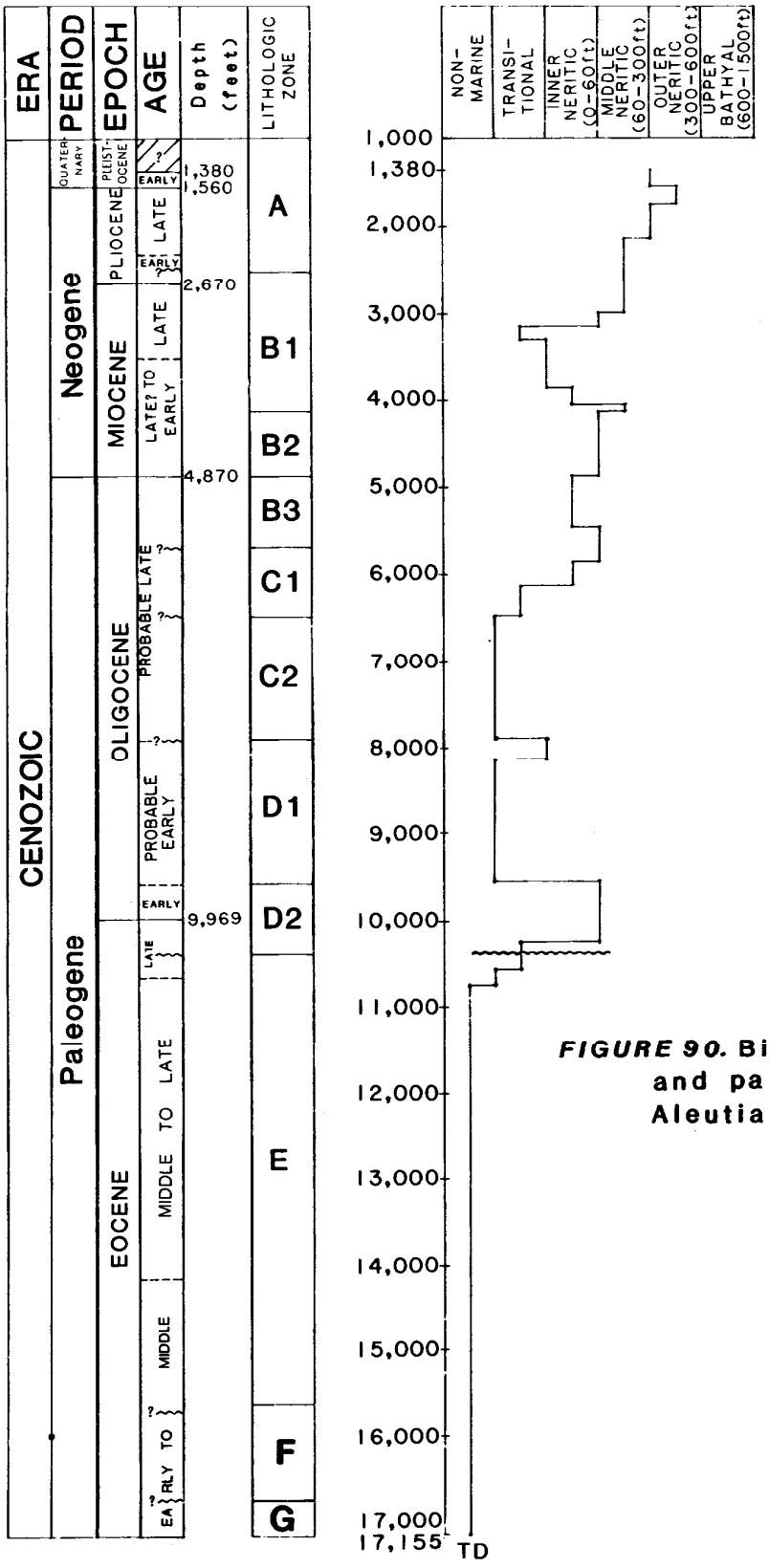

FIGURE 90. **Biostratigraphic summary and paleobathymetry, North Aleutian Shelf COST No.1 well.**

occurrence of Rhizosolenia barboi and Stephanopyxis turris in the underlying zone, and on the lowest occurrence of Rhizosolenia curvirostris at 1,545 feet (SWC). Other Pleistocene species present in this interval include Actinocyclus curvatulus, Actinocyclus divisus, Biddulphia aurita, Porosira glacialis, Rhizosolenia hebetata, Thalassiosira gravida, and Thalassiosira nidulus. Numerous siliceous microfossils having long or undefined biostratigraphic ranges are also present in this part of the well. These include species of the genera Actinoptychus, Arachnoidiscus, Bacteriosira, Coscinodiscus, Cymbella, Denticulopsis, Dicladia, Distephanus, Eunotia, Fragillaria, Grammatophora, Melosira, Navicula, Nitzschia, Parathranium, Rhaphoneis, Rhizosolenia, Stephanopyxis, Tetracyclus, Thalassionema, Thalassiosira, and Thalassiothrix.

The foraminifera in the Pleistocene part of the well comprise a typical high-latitude, cold-water shelf assemblage. There were no age-diagnostic species observed. The foraminiferal assemblage includes Buccella frigida, Buccella tenerrima, Cassidulina teretis, Cibicides aff. C. mckanni, Dentalina spp., Elphidiella oregonense, Elphidium bartletti, Elphidium clavatum, Elphidium incertum, Glabratella sp., Lenticulina nikobarensis, Protoelphidium orbiculare, Quinqueloculina sp., Vaginulina sp., and Uvigerina juncea. The planktonic species Globigerina bulloides and Globigerina quadrilatera are present in a sidewall core at 1,545 feet. Echinoderm and molluscan fragments were also found in the early Pleistocene interval.

The pollen-spore assemblage from this interval includes undifferentiated bisaccates, Betulaceae, Malvaceae, Alnipollenites sp., Deltoidospora sp., Juglanspollenites sp., Laevigatosporites sp., Liquidambarpollenites sp., Osmundacidites sp., Sphagnumsporites sp., and Tsugaepollenites sp. The dinoflagellate assemblage includes rare, recycled Jurassic forms and Tectatodinium pellitum. The latter species is included by Bujak (1984) in his Pliocene Impagidinium pacificum zone (Bering Sea and northern North Pacific Ocean), but has been reported elsewhere to range higher in the section (Lentin and Williams, 1985; Helby and others, 1984).

No ostracodes or calcareous nannofossils were recovered from this part of the well. Poorly preserved spongodiscid radiolarians were found at 1,545 feet (SWC). *These are probably reworked.*

Environment

Data from the Pleistocene sediments indicate middle to outer neritic deposition in relatively cold water (fig. 90).

PLIOCENE

The Pliocene section extends from 1,560 to 2,670 feet and is defined and subdivided primarily on the basis of diatom distributions. Seismic horizon A, at 2,510 feet, marks the boundary between lithologic zones A and B1. It is a conformable surface at

the well, but is unconformable toward the landward edge of the basin, where it can be correlated with the base of a prograding clastic wedge that may be equivalent to the Pliocene Milky River Formation on the Alaska Peninsula. This horizon is not a discernible biostratigraphic discontinuity at the well.

The interval from 1,560 to 2,190 feet is late late Pliocene in age and is assigned to the Denticulopsis seminae var. fossilis Zone of Barron (1980). The top of this zone is based on the highest stratigraphic occurrences of Rhizosolenia barboi and Stephanopyxis turris, both late Pliocene indicators, at 1,560 feet. The highest occurrences of Stephanopyxis horridus (1,650 feet) and Thalassiosira zabelinae (1,760 feet) and the lowest occurrences of Denticulopsis seminae (1,980 feet in SWC, 2,010 feet in cuttings) also occur in this interval. The base of the interval (2,190 feet) is placed at the top of the underlying zone. Other species with highest stratigraphic occurrences in the interval include Ammodochium rectangulare, Chaetoceros radicans, Coscinodiscus pustulatus, Dicladia pylea, Nitzschia fossilis, Rhaphoneis angularis, Stephanopyxis inermis, Thalassiosira antiqua, Thalassiosira aff. T. convexa, and Xanthiopyxis ovalis. The remaining assemblage is similar to that of the early Pleistocene, with the addition of species of Actiniscus, Cestodiscus, Cocconeis, Diploneis, Entopya, and Trochosira.

A combined early late to late early Pliocene assemblage ranging from the Denticulopsis seminae fossilis/Denticulopsis kamtschatica Zone to Denticulopsis kamtschatica Subzone c occurs in the interval from 2,190 to 2,370 feet. The top of the Denticulopsis seminae fossilis/Denticulopsis kamtschatica Zone is identified by Barron (1980) as the highest stratigraphic occurrence of common Denticulopsis kamtschatica. However, this species is not common in the well, so its highest continuous occurrence (2,190 feet) is the marker that is used here to fix the top of the Denticulopsis seminae fossilis/Denticulopsis kamtschatica Zone. There were no species indicating the base of the Denticulopsis seminae fossilis/ Denticulopsis kamtschatica Zone or the top of the underlying Denticulopsis kamtschatica Subzone c found in the well. These intervals were combined into a grouped interval extending downward to the top of the next underlying zone. Because the division of early and late Pliocene is defined by Barron (1980) to be at the top of the Denticulopsis kamtschatica Subzone c, and because this subzone could not be defined precisely in the well, the boundary between early and late Pliocene was estimated to be at about 2,285 feet, midway in the combined Denticulopsis seminae fossilis/Denticulopsis kamtschatica and Denticulopsis kamtschatica Subzone c interval defined here. The siliceous microfossil assemblage in this combined zone is similar to that of the zone above, with the addition of species of Dictyocha, Ebriopsis, Lithodesmium, Sceptroneis, and Stephanodiscus.

The sequence from 2,370 to 2,670 feet is early Pliocene in age and represents Denticulopsis kamtschatica Subzone b. The top of this interval is defined by the highest occurrence of Coscinodiscus insignis and Coscinodiscus temperi (2,370 feet). The base of the

interval (top of Miocene) is placed at the lowest contiguous occurrence of Thalassiosira oestrupii (2,670 feet). Other species with highest stratigraphic occurrences in this interval include Actinocyclus ingens and Lithodesmium minisculum. The remainder of the siliceous microfossil assemblage is similar to the assemblage in the zone above, with the addition of species of Archaeomonas, Cymatosira, Endictya, Hemiaulus, Pseudoammodochium, Pseudopyxilla, Pterotheca, and Tabellaria.

Ostracodes recovered from isolated intervals throughout the well were analyzed and identified by Elisabeth Brouwers (written commun., 1985). Ostracodes found in the late Pliocene part of the section include Acanthocythereis dunelmensis at 1,620 feet and Rabilimis ?septentrionalis at 1,650 and 1,680 feet. Both of these species have ranges of Pliocene to Pleistocene. Palmenella sp., occurring at 1,770 feet, and Semicytherura n. sp. A, at 2,010 feet, range from late Miocene to Pliocene. These species support a Pliocene age and indicate a middle shelf depositional environment. No ostracodes were found in the early Pliocene part of the section.

The foraminifera in the Pliocene section represent a high-latitude, cold-water assemblage similar to that found in the overlying early Pleistocene section. Faunal abundance decreases downward, and foraminifera are extremely rare in the early Pliocene section. Additional species found in the section include Cassidulina transluscens, Cibicides cf. C. perlucidus, Cibicides cf. C. suppressus, Guttulina cf. G. sadoensis, Nonion labradoricum, Nonionella labradorica, Pseudopolymorphina spp., Quinqueloculina agglutinata, Trifarina angulosa, and Vaginulina cf. V. striate. One specimen of Globigerina sp. was found at 1,680 feet. No planktonic foraminifera were recovered below this depth. Bivalve, gastropod, echinoid, bryozoan, and ophiuroid fragments, along with fish teeth and bone fragments, were found in the late Pliocene section. They are much less common in the early Pliocene section.

The Pliocene spore and pollen assemblage is similar to the early Pleistocene assemblage. Additional forms that appear in the late Pliocene section include mainly Polypodiaceae and Taxodiaceae, along with rare Compositae, Lycopodiumsporites sp., Salix sp., Taurocusporites segmentatus, Tiliaepollenites sp., and Ulmipollenites sp. The early Pliocene section contains Pterocaryapollenites sp., along with rare Boisduvalliapollenites clavatites, Callialasporites trilobatus, and Caryapollenites simplex.

The dinoflagellate assemblage in the late Pliocene section includes only Tasmanaceae, Tectatodinium pellitum, and some rare, recycled Cretaceous and Eocene specimens. Tectatodinium pellitum has been noted by Bujak (1984) in Pliocene age samples from DSDP Leg 19 in the Bering Sea. Additional dinoflagellate species in the early Pliocene section include Membranilarnacia sp. and ?Operculodinium sp.

No calcareous nannofossils or Radiolaria were observed in the Pliocene section.

Environment

Sediments of the Pliocene section were deposited in a shelf environment under cold-water conditions. On the basis of diatom and foraminifera populations, paleodepths in the late Pliocene are estimated to be middle to outer neritic. Even though foraminifera are rare in the early Pliocene section, large numbers of diatoms and moderate dinoflagellate populations indicate a probable middle neritic environment.

MIOCENE

The interval from 2,670 to 4,870 feet is Miocene in age. The late Miocene is defined by diatom distributions, and the base of the Miocene is defined by the highest occurrence of calcareous nannofossils of Oligocene age. Additional evidence for a Miocene age comes from foraminifera, dinoflagellates, and ostracodes.

The section is late Miocene from 2,670 to 2,970 feet (Denticulopsis kamtschatica Subzone a). The top of the interval is based on the lowest continuous occurrence of Thalassiosira oestrupii (2,670 feet) and the highest occurrence of Triceratium condecorum (2,850 feet). The base of the interval is defined here by the lowest continuous occurrence of Denticulopsis kamtschatica (2,970 feet). The lowest continuous occurrence of Thalassiosira gravida fossilis at 2,850 feet also indicates a late Miocene age. This interval also includes the highest occurrences of species of Aulacodiscus, Cladogramma, Cocconeis, Endictya, and Stauroneis.

Biostratigraphics (1983) placed the top of the Miocene at 3,210 feet on the basis of the highest occurrence of thick-walled specimens of the diatom Stephanopyxis turris, a form that they have used as an uppermost Miocene marker in several wells in the Bering Sea. They also found Triceratium condecorum no higher than 3,210 feet in the well. However, because Triceratium condecorum was observed in MMS samples extending up to 2,850 feet, and because its extinction is considered to have occurred in the late Miocene (Schrader, 1973; Koizumi, 1977), the top of the Miocene was placed higher in this study. Specimens of Triceratium condecorum above 3,210 feet do not appear to be recycled. Stephanopyxis turris (thick-walled form) was not observed above 3,210 feet and apparently did not continue into the latest Miocene at this location, perhaps because of local ecological constraints. The distribution and significance of the thick-walled form of Stephanopyxis turris in the late Miocene is still under study.

The interval from 2,970 to 3,500 feet is provisionally assigned to the late Miocene Denticulopsis hustedtii Subzone b. The top of this interval is defined by the lowest contiguous occurrence of Denticulopsis kamtschatica, which defined the base of the overlying subzone. The base is defined by the lowest occurrence of Cosmiodiscus insignis at 3,500 feet (SWC). Although the lowest occurrence of this species is regarded by Barron (1980) as being

within Subzone b, rather than as the basal subzone boundary marker, it is placed at the lower boundary of the subzone here because there are no highest or lowest occurrences of Subzone b or upper Subzone a marker species found below this depth. The highest occurrences of Stephanopyxis schenckii and Dictyocha pseudofibula at 3,500 feet (SWC) also indicate a late Miocene age. This interval also contains the highest occurrences of species of Diploneis and Pinnularia.

The interval from 3,500 to 3,960 feet is probable late Miocene in age, possibly within the Denticulopsis hustedtii Subzone a. The top of the subzone is placed at the lowest occurrence of Cosmiodiscus insignis, which was used to define the base of the subzone above. The base of the subzone is placed at the lowest occurrence of Thalassiosira nidulus (3,960 feet). The highest occurrence of Distephanus pseudocrux (3,570 feet) also supports a late Miocene age. The highest occurrences of species of Pseudopodosira also occur in this interval.

Below 3,960 feet, diatom distributions are too sparse and generalized to provide a basis for further zonation. The occurrence of Triceratium condecorum at 4,199 feet (CC) indicates a middle to late Miocene age. Below 4,200 feet, siliceous microfossils are extremely rare, and no further age determinations were made using this group.

Rare ostracodes were found at scattered intervals in the Miocene section. These include Normanicythere n. sp. A (4,080 feet) indicating a Miocene age, and "Hemicythere" sp. (4,740 feet) indicating a probable Miocene age. Both are indicative of a shelf environment.

Foraminifera are very rare high in the Miocene section and include possibly caved specimens of Elphidium clavatum and Cassidulina californica. Bivalve, gastropod, and fishbone fragments are present. Below 3,900 feet, foraminifera are present in moderate numbers. Species in this part of the section include Elphidiella cf. E. hannai, Elphidium sp., Elphidium cf. E. bartletti, Elphidium clavatum, Elphidium cf. E. incertum, Oolina sp., Polymorphina sp., Protoelphidium cf. P. orbiculare, Pyrulina sp., Quinqueloculina bellatula, and Sigmomorphina cf. S. pseudoschencki. The presence of Porosorotalia cf. P. clarki at 4,050 feet supports a Miocene age. Bivalve, gastropod, and echinoid fragments, along with barnacle, bryozoan, and fishbone fragments, are scattered throughout the middle and lower parts of the Miocene section.

The spore and pollen assemblage in the Miocene section is similar to that of the Pliocene, but also includes the highest occurrences of Onagraceae, Caryapollenites sp., Cicatricosisporites sp., Diervillapollenites echinata, Juglanspollenites sp. (3,298 feet, SWC), Multicellaesporites sp., Tiliaepollenites crassipites, and Triporopollenites sp. In addition, a sample at 4,195.3 feet (CC) yielded specimens of Ericipites ericoides, Selaginella sp. A, and Verrucatosporites favus, all of which are considered to be of probable Miocene age (Bujak-Davis Group, written commun., 1985).

Also present in this sample are Laevigatosporites ovatus, Pterocaryapollenites stellatus, Selaginella perinata, Tsugaepollenites igniculus, and Tsugaepollenites viridifulminipites.

Dinoflagellates are present sporadically throughout the Miocene interval. The assemblage includes Baltisphaeridium sp., Lejeunia fallax (3,390 feet), Lejeunecysta hyalina (3,840 feet), Lejeunecysta cf. L. paratenella, Operculodinium sp. 2, and some rare, recycled Jurassic forms. Although Lejeunecysta fallax has been considered to be a middle Miocene species, Bujak (1984) has noted its occurrence in late Miocene to Pliocene age sediments in DSDP Leg 19 samples from the Bering Sea. Tasmanaceae, thick-walled spherical algae bodies of uncertain affinity, are also present in this section.

With the exception of the lowermost part, the Miocene section is barren of calcareous nannofossils. Species present near the base of the section (4,740 feet) include Coccolithus pelagicus, Dictyococcites sp., and Reticulofenestra aff. R. pseudoumbilica.

One Radiolarian, Stylodictya validispina, was identified from a conventional core sample at 3,392.8 feet.

Environment

Although foraminifera are scarce in the upper part of the Miocene section (2,670 to 3,130 feet), abundant diatoms, frequent bivalve, gastropod, and echinoid fragments, and rare barnacle and fishbone fragments are present, indicating deposition under open marine, probably middle neritic depths. Below this, from 3,130 to 3,310 feet, conditions were transitional, with intervals containing rare marine microfossils interspersed with coal-bearing deposits. From 3,310 to 3,900 feet, rare microfossils indicate transitional to inner neritic conditions. Foraminifera and rare dinoflagellates indicate that the lower part of the Miocene section, from 3,900 to 4,870 feet, was deposited at inner to middle neritic depths.

Bottom-Simulating Reflectors

Turner and others (1984c) found evidence linking the downward disappearance of siliceous microfossils in the late Miocene section of the Navarin Basin COST No. 1 well (apparently due to the dissolution of the opaline silica making up the microfossils and its reprecipitation in other mineral forms) with a seismic horizon resembling a Bottom-Simulating Reflector, or BSR (Scholl and Creager, 1973; Hein and others, 1978), in the Navarin Basin. Other COST wells in the Bering Sea (the St. George Basin COST No. 1 and No. 2 wells and the Norton Basin COST No. 1 and No. 2 wells) also show a downward disappearance of diatoms in the Miocene section. However, these disappearances cannot be shown to coincide directly with proven BSR's because seismic reflectors in the area parallel a flat-lying sea floor, so that the characteristic cross-cutting relationship between a BSR and relief features in conventional seismic reflectors could not develop. In the North Aleutian Shelf COST No. 1 well, the near-total disappearance of siliceous microfossils in the upper part of

the Miocene section (4,100 feet) corresponds with an abrupt increase in sonic velocity and bulk density on the well logs, and roughly coincides with a relatively prominent horizontal seismic reflector (see Seismic Stratigraphy chapter). Although evidence at the COST well indicates that this horizon may be a diagenetic surface, its lateral equivalent on seismic data records is essentially parallel both to the sea floor and to all the other seismic reflectors in the upper part of the North Aleutian Shelf stratigraphic sequence. Because of this, there is no definitive indication that this horizon is in fact a BSR. As was the case in well data and seismic panels from the Norton and St. George Basins, a BSR-like horizon may well be present, but cannot be unequivocally substantiated.

OLIGOCENE

The section from 4,870 to 9,969.3 feet (CC) is Oligocene in age (fig. 90). The top of this interval is defined by calcareous nannofossil occurrences, the base by the highest occurrence of Eocene dinoflagellates. An early Oligocene sequence in the lowermost part of the interval, below 9,555 feet, is also defined by dinoflagellate occurrences. In addition to zonations based on biostratigraphic evidence, the Oligocene section is subdivided into several sequences on the basis of seismic evidence. The divisions occur at apparently conformable horizons in the well that become angular unconformities on the flanks of the basin. The first of these is seismic horizon B, at 5,675 feet, which corresponds to the boundary between lithologic zones B3 and C1 (see fig. 62, Seismic Stratigraphy chapter; fig. 90; and Plate 1). It is followed by a structurally less significant seismic horizon at 6,470 feet that exhibits only limited, local angular unconformity toward the basin margins. A third horizon, seismic horizon C, occurs at 7,900 feet, about midway in the Oligocene section, and marks the boundary between lithologic zones C2 and D1. Horizon C may correspond to the large mid-Oligocene sea level drop (base of third-order cycle TO2.1) described by Vail and others (1977). Accordingly, horizon C is used here to divide the Oligocene into probable late and probable early sections (fig. 90). This division yields roughly the same proportions of early and late Oligocene section as are seen in the St. George Basin COST No. 1 and No. 2 wells (Turner and others, 1984a, b), where the division of the Oligocene section was based on calcareous nannofossil data.

The top of the Oligocene section is placed at 4,870 feet, where well logs indicate a lithologic change. The paleontological top of the Oligocene is defined by the occurrence of the calcareous nannofossils Dictyococcites bisectus and Dictyococcites scrippsae? within the interval from 4,830 to 4,920 feet. Both of the above species are known to range from the late middle Eocene into the late Oligocene (Bukry, 1973, 1975), where the highest occurrence of Dictyococcites bisectus marks the top of the Dictyococcites bisectus Subzone, which forms the upper half of the Sphenolithus ciperoensis Zone (Bukry, 1975). This part of the section is referred to here as probable late Oligocene in age. Both Dictyococcites cf. D. bisectus and Dictyococcites scrippsae also occurred in the late Oligocene

section of the St. George Basin COST No. 2 well (Turner and others, 1984b). Calcareous nannofossils are scarce throughout the remainder of the Oligocene section, with additional occurrences restricted to Cyclicargolithus floridanus at 5,010 feet and Coccolithus pelagicus at 5,460 feet.

The sparse dinoflagellate population at the top of the Oligocene section is similar to that of the Miocene assemblage. From 5,010 to 6,000 feet a more abundant assemblage is present, including Cribroperidinium sp., Cordosphaeridium sp., Deflandria sp., Hystrichokolpoma rigaudiae, Spiniferites spp., and Paralecaniella indentata. Below 6,000 feet, the dinoflagellate assemblages are similar, but relatively sparse past 7,900 feet, into the probable early Oligocene section. A more diverse population of early Oligocene age appears below 9,510 feet and includes Paralecaniella indentata, Phthanoperidinium cf. P. alectrolophum, Phthanoperidinium sp., Phthanoperidinium amoenum, and Phthanoperidinium comatum.

The Oligocene spore and pollen assemblage is similar to that of the Miocene, with several additional species. In the probable late Oligocene assemblage, these include Castanea sp., Dicellaesporites sp., Diporisporites sp., Faguspollenites sp., Nyssapollenites sp., Nyssapollenites cf. N. spinosa, Quercus sp., Rugaepollis fragillis, Tiliaepollenites sp., Tiliaepollenites vessipites, and Vitreisporites pallidus. In addition, a sample at 5,230.3 feet (CC) yielded Cicatricosisporites sp. The probable early Oligocene section, below 7,900 feet, contains the highest occurrences of Appendicisporites sp. (8,073.9 feet, CC), Ilexpollenites sp., Involutisporites sp., Microthyriacites sp., Schizosporis cf. S. reticulatus, and Sernapollenites sp. Below 9,555 feet, Jussiaea sp., Retitricolpites sp., and Tricolpites sp. are also present.

Late Oligocene foraminiferal populations are very similar to those in the early Miocene, except that the late Oligocene specimens often exhibit a slight change in preservation, with a more burnished, tan appearance. Additional species present in the late Oligocene include Buccella sp., Cassidulina cf. C. crassipunctata, Cibicides cf. C. evolutus, Cibicides cf. C. fletcheri, Cribrononion sp., and Quinqueloculina cf. Q. sachalinica. Rotalia beccarii (equivalent to Ammonia japonica and varieties) occurs consistently in the section below 5,130 feet. This species has been noted in the Oligocene section of all of the other Bering Sea COST wells, although in at least one well, the Navarin Basin COST No. 1, it ranged upward into the early Miocene (Turner and others, 1984c). Foraminifera are very rare to absent in the late Oligocene section below 6,120 feet, but reappear down section at 7,900 feet, at the top of the probable early Oligocene interval. Species present below 7,900 feet include Elphidiella cf. E. hannai, Elphidium cf. E. incertum, Elphidium sp., Haplophragmoides sp., and Rotalia beccarii. Also present in the consultants' sidewall and ditch samples were specimens of "Caucasina" sp. The generic assignment for these specimens was difficult because of their small size and poor preservation, and it is possible that these specimens might belong to the genus Buliminoides (R. Boettcher, Micropaleo Consultants, Inc., personal

commun., 1986). Foraminifera are rare to absent between 8,190 and 9,570 feet in the early Oligocene section. They appear once again at 9,570 feet and continue to the base of the Oligocene at 9,969 feet. The assemblage in this deeper interval consists of Cribrononion aff. C. roemeri (9945.6 feet, CC), Elphidiella cf. E. hannai, Elphidiella katangliensis, Haplophragmoides sp., and Pseudoglandulina inflata.

In situ ostracodes are rare in the Oligocene section. Echinocythereis n. sp., which ranges in age from ?Oligocene to Miocene, was found at 9,660 feet (E. Brouwers, written commun., 1985).

Marine molluscs were identified in conventional core samples from the late Oligocene section. These included the bivalves Macoma nasuta (5,979.3 feet, CC), Cyclocardia sp. (5,981.7 feet, CC), and the gastropod Turritella? sp. (5,993.0 feet, CC) (Marks, 1983). These macrofossils indicate a probable temperate environment. Bivalve and gastropod fragments are present in cuttings throughout the late Oligocene section, but are rare between 7,020 and 7,900 feet. Echinoid fragments and rare ophiuroid and barnacle fragments are present in the upper part of the late Oligocene section, but are absent in the lower part. Coal is present in cuttings from below 7,530 feet. A neritic bivalve, Anomia? sp., was found in the early Oligocene section in a conventional core sample at 9,962.6 feet (Marks, 1983). Bivalve fragments are present in cuttings from 7,900 to 8,430 feet, missing from 8,430 to 9,570 feet, and present again from 9,570 feet to the base of the Oligocene section (9,969 feet). Coal fragments, observed below 7,900 feet throughout the probable early Oligocene section, are less common in the early Oligocene section below 9,510 feet.

Environment

The depositional environment of the late Oligocene section is inner to middle neritic from 4,870 to 6,120 feet. Below this depth, nonmarine to transitional environments are present to the base of the late Oligocene at 7,900 feet. A regressive event at 7,900 feet, possibly corresponding to a major mid-Oligocene regression (the base of third-order cycle TO2.1 noted by Vail and others, 1977), was postulated on the basis of seismic and well log data. Paleontological evidence for this sea level change is not definitive, but the paleoenvironments are more marine immediately below this depth.

The early Oligocene depositional environment is transitional to inner neritic from 7,900 to 8,190 feet. Very sparse fauna indicate nonmarine to transitional environments below this from 8,190 to 9,555 feet. From 9,555 feet to the base of the early Oligocene section (9,969 feet), the depositional environment is inner to middle neritic. Mineralogical evidence indicates another possible environmental change in the early Oligocene part of the section at 8,380 feet. At this depth, an upward increase of quartz content in the section indicates changes in provenance and/or climate (see sandstone framework mineralogy column, Plate 1).

EOCENE

The section from 9,969.3 feet (CC) to the bottom of the well (17,155 feet, TD) is Eocene in age. Age determinations in the upper part of the Eocene section are based mainly on dinoflagellates, with support from calcareous nannofossils. Age determinations in the lower part of the section are based on spore and pollen occurrences. The sediments are late Eocene in age from 9,969 to 10,659 feet, middle to late Eocene from 10,659 to 14,100 feet, and early to middle Eocene from 14,100 to 17,155 feet (TD).

The dinoflagellate assemblage in the upper part of the Eocene section is quite similar to that of the early Oligocene, but contains additional species supporting a late Eocene age. The top of the Eocene is placed at the highest occurrence of Deflandria cf. D. wetzelii (9,969.3 feet, CC). The highest occurrences of Adnatosphaeridium reticulense at 9,978.1 feet (CC) and Areosphaeridium diktyoplokus at 9,982.2 feet (CC) further support an Eocene age (Williams and Bujak, 1977; Bujak, 1984). Additional dinoflagellates in the late Eocene section include Achomosphaera alcicornu, Achomosphaera ramulifera, Cordosphaeridium exilurmum, Deflandria cf. D. phosphoratica, Deflandria saggitula, Glaphyrocysta exuberans, Glaphyrocysta sp., Lejeunecysta granosa, Phthanoperidinium sp., and Phthanoperidinium cf. P. levimurum. Apectodinium homomorphum, an early to middle Eocene species considered by some to range into the late Eocene (Helby and others, 1984, class discussion), occurs at 10,328.9 feet (CC). There are also a few recycled Cretaceous and Paleocene forms present. The spore and pollen assemblage is similar to that of the early Oligocene, with the addition of Lycopodiumsporites annotinoides and a slight increase in Caryapollenites sp., Deltoidospora sp., and Juglanspollenites sp.

The base of the late Eocene (10,659 feet, SWC) is marked by the occurrence of Reticulofenestra reticulata, a calcareous nannofossil that occurs in the late Eocene Discoaster barbadiensis Zone (Bukry, 1973). This is the deepest occurrence of calcareous nannofossils in the well, and the lowest indicator of late Eocene age.

The late Eocene section includes an unconformity at 10,380 feet. This surface coincides with the boundary between lithologic zones D2 and E (fig. 90), and is denoted by discernible changes in lithology and well log character (see Well Log Interpretation and Lithostratigraphy chapter). The unconformity is also marked by an abrupt change in the character of seismic reflections recorded from an equivalent depth on nearby seismic profile data. Dipmeter data from the well and seismic data from the surrounding vicinity indicate that strata above and below the unconformity are flat lying and parallel, forming a probable paraconformity. The seismic data further show that this surface develops into an angular unconformity at the flanks of the basin (see the discussion of horizon D, Seismic Stratigraphy chapter). The hiatus at the unconformity does not appear to be of great duration because a comparison of microfossil assemblages collected from above and below this horizon fails to indicate a significant lapse of time.

The section from 10,659 to 14,100 feet is probably middle to late Eocene in age. Rare specimens of Paralecaniella indentata at 11,844 feet (SWC) are the only dinoflagellates present. The pollen assemblage is essentially the same as that in the overlying section, with the addition of Caprifolipollenites sp. and a slight increase in Tiliaepollenites sp. New elements in the assemblage are principally spores, including several that indicate an Eocene age (Rouse, 1977; Elsik, 1981; Helby and others, 1984; Bujak, 1984). The spore assemblage includes Alternoseptites sp., Chaetosphaerites sp., Ctenosporites wolfei, Dicellaesporites sp., Fusiformisporites sp. A (Rouse, 1977), Microthyriacites sp., Multicellaesporites sp., Multicellaesporites sp. B (Rouse, 1977), Pesavis tagluensis, Psiladiporites sp., Striadiporites sp., and Punctodiporites sp. A (Rouse, 1977). A lacustrine algal spore, Pediastrum sp., occurs at 12,166 feet (SWC). Samples from 12,630.6 and 12,631.0 feet (CC) also yielded leaf imprints of Metasequoia sp., Cercidiphyllum sp., and betuloid leaves of the Alnus-Carpinus-Corylus group (Dilcher, 1983). Similar leaves have been observed in Paleocene to Eocene age sediments on Ellesmere Island, Canada.

From 14,100 to 17,155 feet (TD), the sediments are probable early to middle Eocene in age on the basis of pollen and spore assemblages. The primary basis for this age assignment is the occurrence of Pistillipollenites mcgregorii at 14,100 feet. This species is generally regarded as an early Eocene form (Biostratigraphics, 1983), but it has been recorded in sediments possibly as young as middle Eocene in British Columbia and the Canadian Arctic (Rouse, 1977). The pollen assemblage is otherwise similar to that of the overlying section, with the exception of a decline in the abundance of Tsugaepollenites, and the addition of Bombacaceae, Tetracolpites sp. (16,029.0 feet, CC), and Momipites sp. (16,715.0 feet, CC). The spore assemblage contains the same elements as the overlying section, with the addition of Acanthotriletes sp. (12,630.4 feet, CC), Striadiporites sp., Rugubivesiculites sp., and Concavissimisporites verrucosus. Pediastrum sp. occurs at 16,620 feet. A conventional core sample at 16,715 feet also yielded Diporisporonites sp., Microsporonites sp., Pluricellaesporonites sp., and Striadiporites cf. S. sanctaebarbarae (Bujak-Davies Group, written commun., 1985). In addition, a conventional core sample at 16,705.2 feet yielded a betuloid leaf fragment of the Alnus-Carpinus-Corylus group (Dilcher, 1983).

The boundary between lithologic zones E and F (at 15,620 feet in the early to middle Eocene section) appears to be an unconformity. This interpretation is based primarily on an abrupt lithologic change apparent on well logs and a slight increase in thermal maturity of organic constituents in the sediments (see the Well Log Interpretation and Lithostratigraphy chapter and the Organic Geochemistry chapter). The quality of seismic data from this depth is too poor to permit a basin-wide correlation of this horizon. Comparisons of microfossils from above and below this probable unconformity do not indicate any significant time hiatus at this level.

Another apparent unconformable surface, a probable angular unconformity, is indicated lower in the early to middle Eocene section, where abruptly steeper dips are encountered at the boundary between lithologic zones F and G (16,652 feet). These steep dips were observed down to 16,722 feet, where well log data ends, and they may continue to the bottom of the well (see Well Log Interpretation and Lithostratigraphy chapter). As with the possible unconformity at 15,620 feet, seismic reflectors at this depth are not resolvable with the current data. This makes the full lateral extent of the surface encountered at 16,652 feet in the COST well impossible to determine at the present time. Also, an angular unconformity such as this might be expected to mark a relatively significant time hiatus. However, microfossils recovered from the steeply dipping interval below the unconformity fail to establish an age any older than early to middle Eocene, and suggest that the erosional hiatus was a relatively brief one. Accordingly, the interval from 16,652 feet to TD is assigned an early to middle Eocene age in concordance with the age of the sediments above that depth (fig. 90). Microfossils are relatively sparse and non-diagnostic below the unconformity, however, and the possibility of an older age in this lower interval cannot be totally disregarded.

The foraminiferal assemblage is generally sparse in the late Eocene section. With the exception of relatively frequent specimens of Cribrononion aff. C. roemeri, all other occurrences are rare. Other species present include Cibicides conoides, Dentalina sp., Elphidiella sp., Elphidium cf. E. incertum, Elphidium aff. E. minutum, Elphidium sp., Globobulimina affinis, Globobulimina sp., Haplophragmoides sp., ?Textularia sp., and Pseudoglandulina cf. P. inflata. Foraminifera are very rare in the middle to late Eocene part of the section. No foraminifera were recorded below 10,740 feet, except for very rare, probably caved specimens.

Rare echinoid fragments and pyritized diatoms occur in the late Eocene section but are not present below 10,200 feet. Molluscan shell fragments are common in the late Eocene section and are increasingly numerous below 10,410 feet. Conventional core samples taken at 10,326.2, 10,328.6, and 10,333.3 feet yielded Ostrea (Crassostrea) sp., which indicates a temperate to warm marine environment (Marks, 1983). In the early to middle Eocene section, molluscan fragments are rare below 10,650 feet. They are essentially absent below 10,830 feet, indicating a more terrestrial environment in the underlying parts of the Eocene section.

Radiolaria are extremely rare in the Eocene section of the well, occurring only in three samples from the middle to late Eocene section. Unidentified, altered radiolarians were observed in sidewall core samples at 10,730 and 10,829 feet, while Cenosphaera? sp. was observed in cuttings at 11,670 feet. No in situ ostracodes were observed in the Eocene section.

Radiometric age date analysis (potassium-argon, whole-rock) was done on three samples from the early to middle Eocene part of the section (Teledyne Isotopes, 1983). These analyses yielded a mixture

of age estimates. A volcanic pebble to boulder(?) conglomerate with siltstone matrix recovered from conventional core fragments at 16,016.2 to 16,016.6 feet yielded an age of 31.6 ± 2.0 million years (early Oligocene). The discrepancy between biostratigraphic and radiometric ages in this sample may be explained by possible removal of radiometric decay products due to alteration of the original rocks, resulting in an underestimation of the absolute age. Petrologic studies of the COST well (see Lithology and Core Data chapter) have indeed indicated considerable alteration of volcanic rock fragments in lithologic zones E, F, and G (fig. 90). Devitrified, amygdaloidal volcanic fragments from a ditch sample at 16,670 feet yielded an age of 40.5 ± 10.3 million years (late middle Eocene). "Salt and pepper" textured diabasic (intrusive?) fragments from cuttings at 16,690 to 16,700 feet yielded an age of 47.1 ± 18.3 million years (middle Eocene). These latter two samples roughly correspond to biostratigraphic age estimates.

Environment

On the basis of dinoflagellate and foraminifera data, the depositional environment between 9,969 and 10,230 feet is inner to middle neritic. Environments are transitional down to 10,590 feet, with oysters (Ostrea) at 10,326 to 10,333 feet (CC) indicating temperate to warm, marine to transitional conditions. An unconformity at 10,380 feet suggests a brief erosional, possibly emergent, episode. Between 10,590 and 10,830 feet, bivalve fragments, very rare, poorly preserved radiolarians, and coal fragments indicate transitional to nonmarine conditions. From 10,830 to 17,155 feet (TD), nonmarine conditions are indicated by the lack of marine macro- and microfossils, by abundant pollen and spores, by the presence of Pediastrum sp., a lacustrine algae (at 12,166 feet (SWC) and 16,620 to 16,800 feet), and by persistent occurrences of coal fragments. A possible erosional or nondepositional surface, identified in geochemical and well log data, is present at 15,620 feet. An apparent angular unconformity at 16,652 feet is interpreted to indicate a relatively brief episode of erosion.

CORRELATION

Bering Sea COST wells

The Neogene and Quaternary section of the North Aleutian Shelf COST No. 1 well is similar to that of the other Bering Sea COST wells (Turner and others, 1983a,b; 1984a,b,c). The Neogene biostratigraphy of all of these wells is based primarily on siliceous microfossils, which usually provide an effective zonation down to a depth of about 3,500 feet, generally into the late to late middle Miocene part of the section. Below this depth, the abundance of siliceous microfossils decreases drastically, possibly due to the effects of pressure- and temperature-dependent diagenetic dissolution.

Ostracodes have proved biostratigraphically and paleoecologically useful in the Neogene section of several of the

wells, as they were in the Pliocene of the North Aleutian Shelf COST No. 1 well. Neogene palynological zonations are not yet well developed in the Bering Sea, but some spore occurrences were useful in dating the Miocene section. Calcareous nannofossils have generally been of limited usefulness in the Neogene section of the Bering Sea. Their Neogene occurrences in the North Aleutian Shelf COST No. 1 well are restricted to the lower part of the Miocene section.

A synthesis of data from the distributions of benthic foraminifera, marine and terrestrial palynomorphs, ostracodes, and rare siliceous microfossils and calcareous nannofossils has been successfully used for the general dating and correlation of the middle to early Miocene section in the Bering Sea. In the North Aleutian Shelf COST No. 1 well, the highest occurrences of benthic foraminifera such as Porosorotalia cf. P. clarki provide a probable correlation with the Miocene of other Bering Sea COST wells (the two Norton Basin COST wells and the Navarin Basin COST well; Turner and others, 1983a, b, 1984c) and with the Miocene of Sakhalin Island, USSR (Voloshinova and others, 1970; Gladenkov, 1980).

Paleogene correlations in the Bering Sea are based on dinoflagellates, spores, calcareous nannofossils, and foraminifera. The Paleogene microfossils of the Bering Sea stratigraphic section, particularly the foraminiferal assemblage, appear to resemble those of the Kamchatka Peninsula and Sakhalin Island in the northeastern USSR (Turner and others, 1984c; Gladenkov, 1980).

The late Oligocene section of the North Aleutian Shelf COST No. 1 well was defined by occurrences of calcareous nannofossils, as was the case in the two St. George Basin COST wells. In the Navarin Basin and Norton Basin COST wells, on the other hand, the top of the Oligocene was defined by dinoflagellate occurrences. The uppermost late Oligocene section of the North Aleutian Shelf COST No. 1 well contains a sparse, nondiagnostic dinoflagellate assemblage that is very similar to the early Miocene assemblage overlying it. This population disappears slightly below the top of the Oligocene section, and dinoflagellates do not appear again in the well until the early Oligocene.

Some species of benthic foraminifera have been found in the Oligocene section of several of the Bering Sea COST wells (Turner and others, 1983a, b; 1984a, b, c) and may have some potential for correlation. Among these is Rotalia cf. R. beccarii (Ammonia japonica varianta), which occurs in the Oligocene of the North Aleutian Basin COST No. 1 well and all the other Bering Sea COST wells, although it does extend into the early Miocene of the Navarin COST No. 1 well. Pseudoglandulina cf. P. inflata is found in the Oligocene section of the North Aleutian Shelf COST No. 1 well, the Navarin Basin COST No. 1 well, and the Norton Basin COST No. 1 well. Caucasina? sp. appears in the Oligocene of the North Aleutian Shelf COST No. 1 well, and various species of Caucasina were also noted in both of the Norton Basin COST wells (Turner and others, 1983a, b). Porosorotalia clarki, which occurs in the Miocene of the North

Aleutian Basin COST No. 1 well, the Navarin Basin COST No. 1 well, and the two Norton Basin COST wells (Turner and others, 1983a, b; 1984c), is also present in the late Oligocene section of the latter three wells and the St. George Basin COST No. 2 well (Turner and others, 1984b). No planktonic foraminifera were identified in the Oligocene section of the North Aleutian Shelf COST No. 1 well. This contrasts with the Navarin Basin COST No. 1 well, where planktonic species were rare but relatively diverse in the early Oligocene (Turner and others, 1984c).

The lower diversity and general sparseness of benthic foraminiferal assemblages throughout the Oligocene section of the North Aleutian Shelf COST No. 1 well, especially in the middle part of the section, suggest that the Oligocene depositional environments here were shallower than in the other Bering Sea COST wells. Although the Oligocene section of the Norton Basin COST No. 2 well was also shallow, foraminiferal diversity there appears to be higher, indicating a more marine environment (Turner and others, 1983b).

The upper part of the Eocene section of the North Aleutian Shelf COST No. 1 well is defined on the basis of dinoflagellate and calcareous nannofossil occurrences. Below the late Eocene part of the section, all marine microfossils disappear and nonmarine depositional environments are present throughout the remainder of the well. In this lower part of the section, biostratigraphic control is provided by characteristic Eocene fungal spore assemblages and by pollen. A dinoflagellate species that is potentially useful for late Eocene correlations in the Bering Sea area is Areosphaeridium diktyoplokus, which first occurs in the North Aleutian Shelf COST No. 1 well at 9,982.2 feet (CC). This species, which was also found in the late Eocene of the Navarin Basin COST No. 1 well (Turner and others, 1984c), has been noted in the literature as a late Eocene species in the Bering Sea (Bujak, 1984), and as a late middle to late Eocene species in offshore eastern Canada (Williams and Bujak, 1977). Spore assemblages that were useful for assigning an Eocene age to the nonmarine section below 10,689 feet in the North Aleutian well are also present in the transitional to nonmarine Eocene section of the Norton Basin COST No. 2 well (Turner and others, 1983b). Species common to the two wells include Ctenosporites wolfei, Dicellaesporites sp., Pesavis tagluensis, Punctodiporites sp., and Striadiporites sp. This spore assemblage is not well represented in other Bering Sea COST wells, perhaps because the Eocene paleoenvironments of these wells tend to be more marine. Pistillipollenites mcgregorii, the pollen that helped define the top of early to middle Eocene in the North Aleutian Shelf COST No. 1 well, was not observed in the other Bering Sea COST wells, except for the St. George Basin COST No. 1, where recycled specimens appear in the Neogene section.

Foraminifera are restricted to the upper (late) part of the Eocene section in the North Aleutian Shelf COST No. 1 well, where they form a low-diversity assemblage of generally shallow-shelf genera, mostly without notable biostratigraphic correlation value. One exception may be the most common species present in the earliest

Oligocene and the late Eocene section, Cribrononion aff. C. roemeri. This species also appears in late Eocene shallow-water sediments of the St. George Basin COST No. 1 well (Turner and others, 1984a). It has not been observed in the rest of the Bering Sea COST wells, where either slightly deeper water or shallower, transitional to nonmarine environments are present in this part of the section.

Generally shallow environments seem to be common in the Eocene section of the Bering Sea COST wells. Shallow-water to nonmarine environments characteristic of the late Eocene and the early to late Eocene parts of the North Aleutian Shelf COST No. 1 well are also found in the Norton Basin COST No. 2 well, the upper part of the late Eocene section in the St. George Basin COST No. 1 well, and in the Oligocene or older (possible Eocene) portion of the St. George Basin COST No. 2 well (Turner and others, 1983b; 1984a, b). A nonmarine environment is also indicated for the abbreviated section of possible Eocene or older sediments in the Norton Basin COST No. 1 well (Turner and others, 1983a). The exceptions to this general Eocene shallowness are the outer neritic to upper bathyal environments of the late middle Eocene section in the Navarin Basin COST No. 1 well and the middle to late Eocene portion of the St. George Basin COST No. 1 well (Turner and others, 1984a, c). From the Bering Sea COST wells, it appears that the Eocene paleoenvironment of the Bering Sea shelf consisted mostly of shallow seas to low emergent terrain, with local basins undergoing episodes of deeper water deposition.

The North Aleutian Shelf COST No. 1 well bottomed in early to middle Eocene strata. Although it appears from seismic data that there may be a sedimentary section below this in the basin, little can be inferred concerning it. Dredge sample and seismic data indicate the possibility of local deposits of older Eocene and Paleocene sediments in the Navarin Basin area (Turner and others, 1984c), and it is possible that some of these older Tertiary sediments may be locally present to the south in deeper parts of the North Aleutian and St. George Basins. In fact, recycled Paleocene dinoflagellates were found in the Eocene section of the North Aleutian Shelf COST well. Mesozoic age rocks may also be present deeper in the North Aleutian Shelf section. Early Cretaceous to Late Jurassic sedimentary rocks were encountered at depth in the St. George Basin COST No. 2 well (Turner and others, 1984b), and similar sediments may extend eastward at depth into the North Aleutian Shelf area. Recycled Cretaceous dinoflagellates were found in the Eocene section of the North Aleutian Shelf COST well.

The Alaska Peninsula

Correlations of the North Aleutian Shelf COST No. 1 well with formations to the south on the Alaska Peninsula are not clear because of the absence of fine-scale biostratigraphic resolution onshore. Onshore biostratigraphic work is generally made difficult by the prevalence of shallow-water to nonmarine, nonfossiliferous siltstones, sandstones, and volcaniclastic sediments throughout most of the Cenozoic section. At present, biostratigraphic control onshore is provided principally by molluscan fossils from outcrop

samples, with meager support coming from sparse foraminifera, ostracode, or other fossil data in outcrop and well samples. Correlation from onshore to the North Aleutian Shelf COST No. 1 well is further complicated by the incompletely defined lateral and vertical extent and interrelationships of onshore formations. In addition, the quality of the seismic profiles used to tie onshore formations to offshore seismic reflection data is relatively poor, and seismic correlations are accordingly difficult. Nevertheless, some very tentative correlations were attempted.

The lower parts of lithologic zone A in the North Aleutian COST No. 1 well consist of volcanic-rich sands of early to late Pliocene age. On seismic sections, this interval (seismic sequence I; see Seismic Stratigraphy chapter) correlates in a shoreward direction with a progradational sequence that may be the seaward extension of the volcaniclastics of the onshore Milky River Formation, also generally considered to be of Pliocene age (Brockway and others, 1975). Lithologic zone B1, immediately below this horizon at the well, consists of cleaner, quartzose sands of early Pliocene and Miocene age. These sands may be an offshore neritic facies correlative with the relatively quartz-rich, tidally deposited Miocene Bear Lake Formation found onshore (Nilsen, 1985; Burk, 1965; Brockway and others, 1975). Poor onshore biostratigraphic control and uncertain onshore to offshore seismic correlations, along with the distance of the well from shore and the attendant possibility of at least partially different sedimentary sources at the well, make direct correlations of onshore formations with the well difficult below the upper parts of this sequence.

8. Geothermal Gradient

by

Tabe O. Flett

A temperature gradient for the North Aleutian Shelf COST No. 1 well was computed using maximum-reading thermometers which recorded bottom hole temperatures (BHT) from logging runs 1, 2 and 3. Because of an early advance of sea ice in the Bering Sea, it was necessary to plug and abandon the well before drill stem tests could be conducted, so formation fluid temperatures are not available. No logs were obtained from 16,692 feet to total depth. Additionally, no temperatures were recorded on the first logging run for the repeat formation tester (RFT), and on the second and third logging runs, the recorded temperatures remained a constant 70 °F, which suggests an instrument failure. No high-resolution temperature logs were run. As a consequence, it was necessary to derive an average geothermal gradient from BHT values using the method suggested by Fertl and Wichman (1977).

True formation temperatures were estimated from each logging run by extrapolating BHT measurements obtained from successive log suites to a static formation temperature. This analytical extrapolation is accomplished by applying a linear regression to BHT observations versus the logarithm of the expression

$$\frac{dt}{t + dt}$$

where for each measurement, dt = time (in hours) after mud circulation stopped and t = mud circulation time (in hours) at the logging point prior to logging. The true static formation temperature was estimated by projecting the line extrapolated from this ratio and the BHT observations to

$$\frac{dt}{t + dt} = 1$$

The technique is based on the observation that temperature rise after mud circulation has stopped is similar to static pressure buildup and may therefore be analyzed in a similar manner (Fertl and Wichman, 1977). The procedure is illustrated in figure 91 for logging run 3. Because t equals 27 hours in this instance, the projected formation temperature may be a bit low. Very long circulation time (in excess of a day) would lead to static temperature estimates that are lower than the true static formation temperature (Fertl and Wichman, 1977).

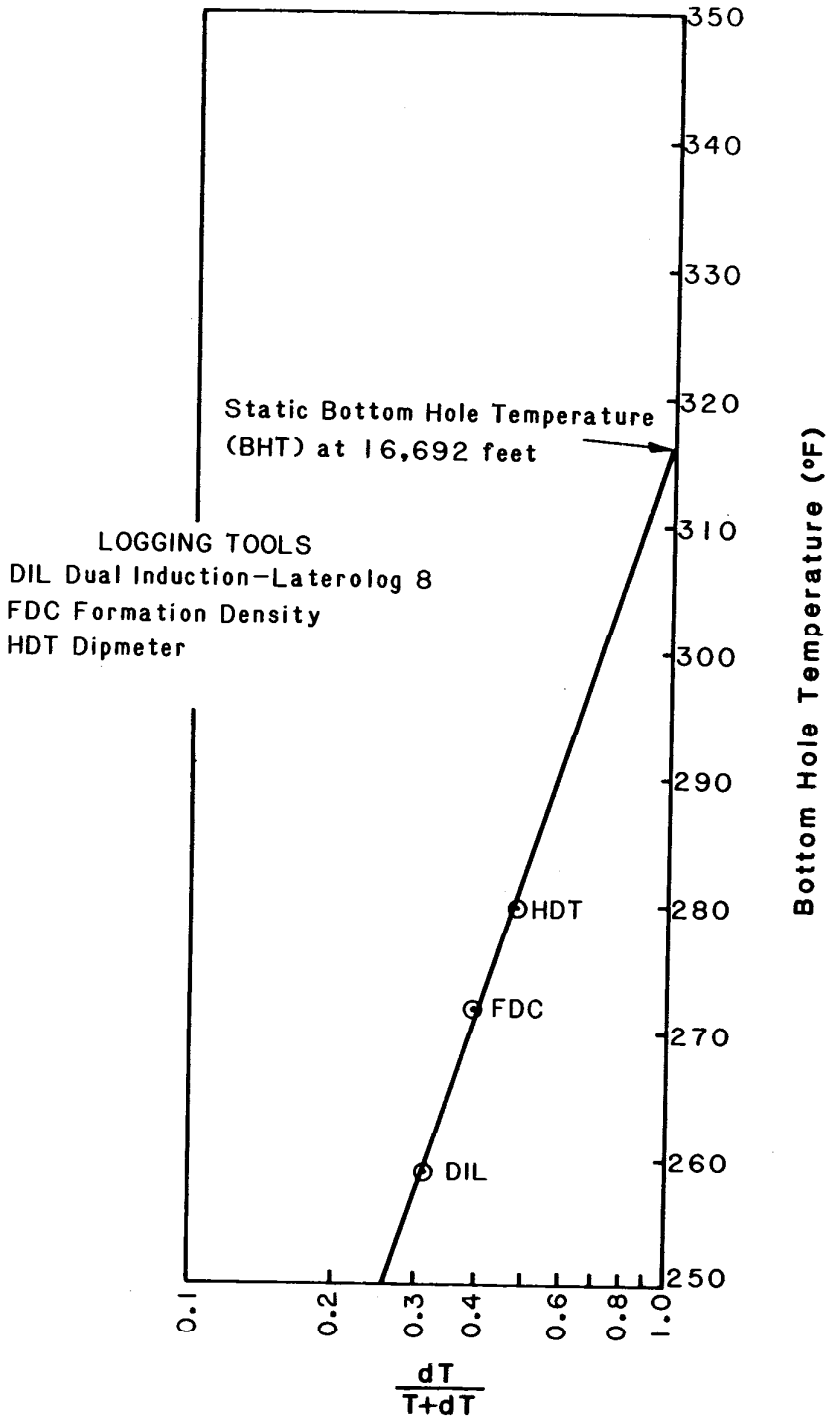

T equals circulating time in hours and
dT equals elapsed time after circulation stopped.

FIGURE 91. **Graph showing the extrapolation of bottom hole temperatures (BHT) to determine static BHT for logging run 3, North Aleutian Shelf COST No. 1 well.**

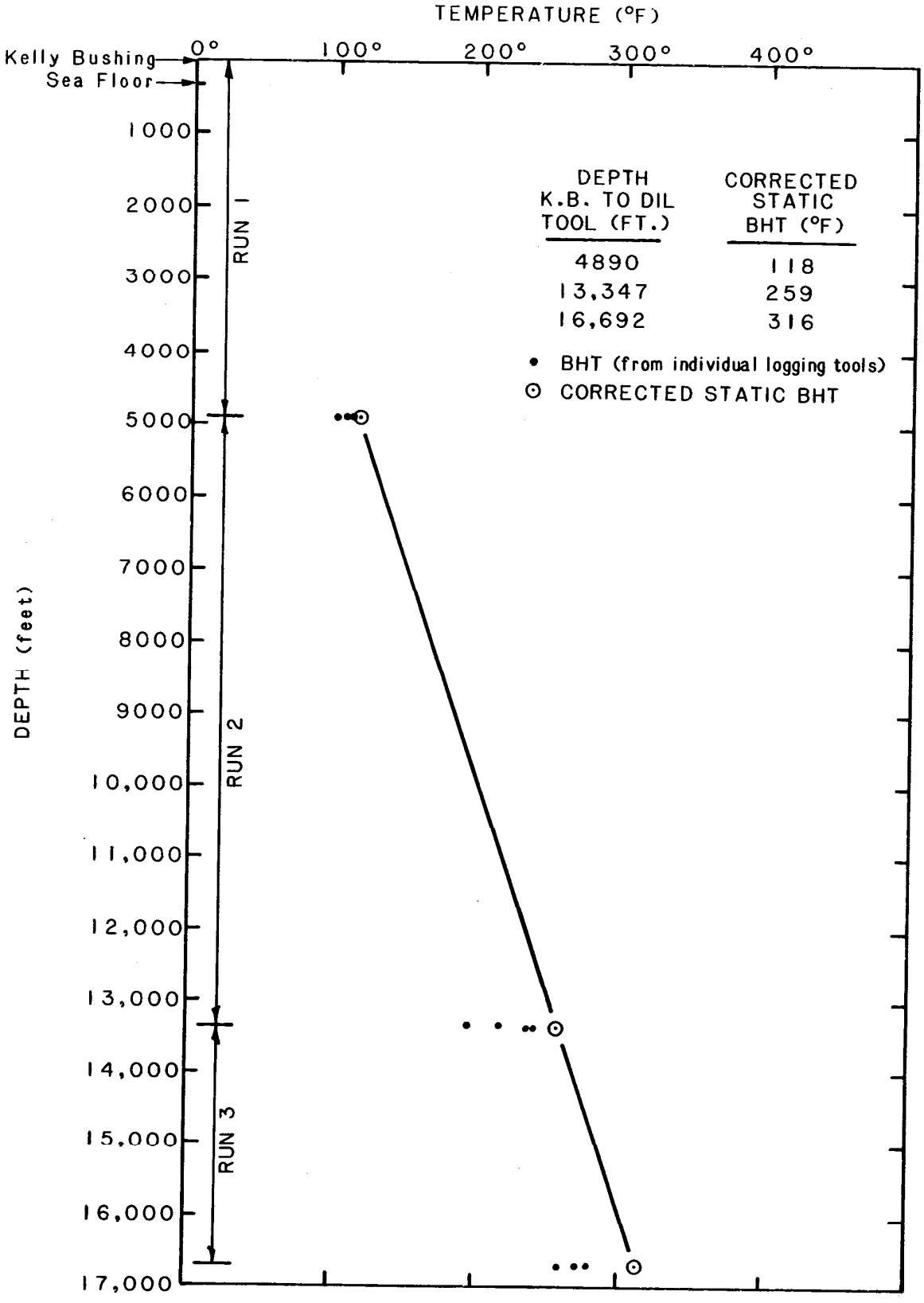

FIGURE 92. **Temperature gradient for the North Aleutian Shelf COST No. 1 well.**

An average temperature gradient was computed using corrected BHT values from the three logging runs (fig. 92) by means of a least squares linear regression. The linear function derived from these points has an average thermal gradient of 1.7 ^{o}F per 100 feet (31 ^{o}C per kilometer). This average gradient applies to the interval between 4,890 and 16,700 feet.

It is commonly observed that in clastic areas, overpressured zones are characterized by high geothermal gradients (Gretener, 1982). An overpressured zone occurs between 11,285 and 16,085 feet (see Abnormal Formation Pressure chapter). Detailed temperature data might well reveal a higher temperature gradient in this zone that the average gradient does not reveal.

The average thermal gradient computed from BHT values (fig. 92), when projected to the sea floor, predicts a temperature of about 36 ^{o}F (2 ^{o}C). Temperatures at the sea floor probably fluctuate with time because of changes in the circulation of seawater and seasonal variations in temperature. Observed water temperatures near the sea floor ranged from 41 ^{o}F (5.0 ^{o}C) on September 18, 1982, to 37 ^{o}F (2.8 ^{o}C) on January 10, 1983 (EG & G Environmental Consultants, 1983). It is reasonable to assume that sea floor temperatures probably remain generally within this range.

Estimates of temperature gradients are permissible only if the gross lithology of the section is known and can be taken into consideration. Detailed lithology is available to TD in this well, but in view of the limited temperature data available, it would be prudent to regard the computed temperature gradient and estimated temperatures (plate 2) with some caution.

9. Organic Geochemistry

by

Tabe O. Flett

INTRODUCTION

The ARCO North Aleutian Shelf COST No. 1 Well was drilled slightly north of the depocenter in the North Aleutian Basin at approximately 162° W. It provides a reasonably complete stratigraphic sample of potential source rocks in the basin and permits a preliminary estimate of the thermal maturity throughout the basin. However, the possibility of lateral facies changes or changes in thermal regimen elsewhere in the basin is recognized, and conclusions drawn from data derived from this single well must be considered somewhat speculative. All depths in this chapter are measured from the Kelly bushing, which was 85 feet above mean sea level (logger's depth) and 359 feet above the sea floor.

Organic geochemical analyses approved by ARCO were performed on canned cuttings samples, sidewall cores, conventional core samples, and four canned mud samples. The total time elapsed from the actual sampling at the well to analysis in the laboratory did not exceed 1 month, with an average period of 18 to 20 days, according to ARCO representative P. Barker (oral commun., January 1986). Zephiran was added to the canned cuttings samples as a bactericide. No evidence that bacterial methane evolved in canned samples was reported.

Canned cuttings collected at 60-foot intervals were sampled for headspace gas by Robertson Research (U.S.), Inc. (Dow, 1983), and the samples were analyzed for light (C_1-C_6+) hydrocarbons using gas chromatography. The cuttings were then washed, described, and a representative sample was analyzed for total organic carbon content (TOC) in a Leco carbon analyzer. Samples with at least 0.3 weight percent TOC were then further analyzed with Rock-Eval pyrolysis (technique summarized in appendix 4). Sidewall cores taken at about 100-foot intervals, plus representative plugs and chips from 19 conventional cores, were analyzed in the same manner, except that the light-hydrocarbon analysis was not included. Kerogen isolation was performed on cuttings and sidewall cores selected at approximately 300-foot intervals and from each conventional core. These samples were analyzed for vitrinite reflectance (R_o), spore coloration index (SCI), and elemental composition. A few samples contained insufficient kerogen for elemental analysis. Soxhlet extraction, elution chromatography, and saturate-fraction gas chromatography were performed on conventional core samples. Soxhlet extraction with

dichloromethane was performed on 50-gram samples for 18 hours. The asphaltenes were precipitated from hexane and the hexane-soluble fraction was separated into saturates, aromatics, and NSO compounds on a silica-alumina chromatographic column by successive elutions with hexane, benzene, and benze-methanol solvents, respectively. The saturate fraction in the C_{15} to C_{40} range was analyzed with a Perkin-Elmer, Sigma 3 gas chromatograph fitted with a 12-foot $NaNO_3/LiNO_3/KNO_3$ eutectic column. The chromatograph was programmed from 40 to 360 ^{o}C at 12 ^{o}C per minute using helium carrier gas at a rate of 25 milliliters per minute.

Preliminary analyses were performed independently by Exploration Logging, Inc., of U.S.A. (Exlog) on wet, canned cuttings collected at 60-foot intervals, plus a limited number of conventional core, sidewall core, and mud samples. Total organic carbon content (TOC) was determined using a Leco furnace, and the organic material was evaluated by Rock-Eval pyrolysis. Because pyrolysis results can really only be compared on a relative basis, and because procedural differences may yield slightly different numerical results (Hunt, 1979), only the more extensive analyses performed by Robertson Research (Dow, 1983) are included in this report. Exlog TOC values are shown on plate 2 at about 500-foot intervals to demonstrate the reproducibility of the measurements. All the data are on file with the Minerals Management Service and are available for public examination at the MMS Field Operations Office in Anchorage, Alaska.

ORGANIC CARBON

A minimum organic content of at least 0.5 percent for noncarbonate rock is generally believed to be necessary to generate sufficient petroleum for expulsion into a potential reservoir (Hunt, 1979; Tissot and Welte, 1984). Most source rocks, according to Hunt, contain from 1 to 2 percent organic carbon plus several hundred parts per million (ppm) hydrocarbon. Additionally, the amount of organic carbon required to generate significant amounts of petroleum varies with the type of organic matter from which it was derived, because this determines the amount of hydrogen available to combine with the carbon.

Total organic carbon content (TOC) from cuttings, sidewall, and conventional cores is displayed on plate 2. TOC values from 1,500 to approximately 2,500 feet are less than 0.5 percent. This interval corresponds roughly to stratigraphic zone A. From about 2,500 to 4,000 feet (stratigraphic zone B1), TOC values are erratic, ranging generally from 0.5 to 3.0 percent. Samples analyzed from this interval contained both coal and wood fibers. Between 4,000 and 8,000 feet (stratigraphic zones B_2, B_3, C_1, and C_2), the TOC values remain erratic and range generally between 0.1 and 1.0 percent. From 8,000 to 9,500 feet (stratigraphic zone D1), coal and carbonaceous material are present in many samples and TOC values range from less than 0.1 percent to nearly 7.0 percent. From 9,500 to about 10,400 feet (stratigraphic zone D2), the samples are predominantly sandstone, and most TOC values are less than 0.9 percent. From

10,400 to 13,291 feet (the top half of stratigraphic zone E), TOC values are as high as 50 percent and very erratic. TOC values less than 0.1 percent are indicated on plate 2 by arrows along the margin of the organic carbon profile. A sample from conventional core 14 (12,262.4 feet) contained 60 percent bituminous coal, and the remaining 40 percent consisted of shale which contained coal laminations. TOC for this sample is 35.89 percent, which reflects the presence of coal. At depths greater than 13,291 feet, sidewall cores are not available and the averaging effect of the blending of cuttings in samples is apparent in the analyses. Coal is present in samples from 13,291 to about 15,700 feet and TOC values are as high as 19 percent, but the variation in the TOC values from cuttings is markedly less than the variation for conventional core samples. The analyses of samples from conventional core 16 (14,167.4 to 14,186.2 feet), however, indicate that the organic carbon content remains high. A casing point occurs at 13,280 feet (logger's depth), but the consistently high TOC values, and the occurrence of significant amounts of coal in conventional core samples below the casing point, suggest that caving has not introduced significant amounts of coal into cuttings obtained below the casing point. From about 15,700 to 16,800 feet (the greater part of stratigraphic zone F), TOC values range from about 0.7 to nearly 2.8 percent. No coal was reported from conventional core samples, and only minor amounts of coal, possibly caved, occurred in cuttings from this interval. From 16,800 to 17,155 feet (TD), TOC values are generally between 5 and 10 percent and coal is again present in the cuttings samples.

The total organic carbon content is high throughout most of the sediments penetrated by this well. However, the organic carbon is, for the most part, associated with coal. It appears from TOC data that the noncoaly shale sequence between 16,020 and 16,800 feet may offer the best hydrocarbon source potential of all the sequences sampled in the well. The coal-bearing sediments that exhibit high organic carbon contents elsewhere in the well are not considered to represent suitable sources for significant amounts of hydrocarbons.

DESCRIPTION OF KEROGEN

The results of reflected-light petrography, the hydrogen index from pyrolysis, and the hydrogen-to-carbon ratio from the elemental analyses performed by Robertson Research (Dow, 1983) are presented as well profiles in figure 93. Transmitted light microscopy is not addressed in this report, but it is available from the MMS Field Operations Office in Anchorage, Alaska. Three petrographic classes of kerogen plus amorphous material, a subgroup within the exinite or liptinite category, were reported by Robertson Research (Dow, 1983). They are:

1. Amorphous (algal or structureless matter)
2. Exinite (herbaceous, lipid-rich relics)
3. Vitrinite (woody and humic components)
4. Inertinite (hard, carbon-rich, nonreactive, brittle particles)

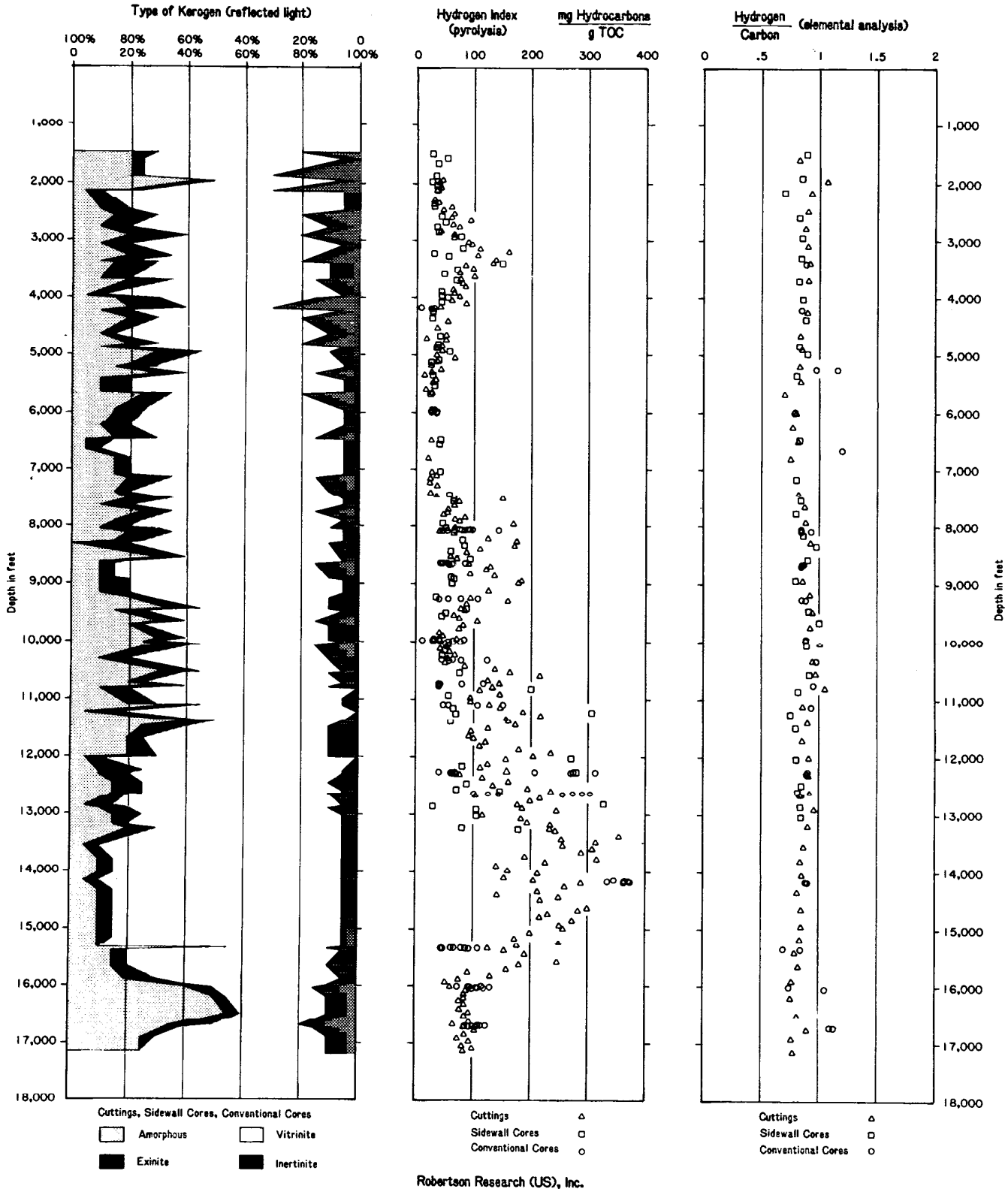

FIGURE 93. **Classification of organic matter.**

This page was intentionally left blank.

A comparison of visual percentage estimates of kerogen types with chemical data on a large number of samples has shown that kerogen assemblages with less than a sum of about 35 percent of amorphous material plus exinite tend to be gas prone, whereas oil sources usually contain over 65 percent of these two maceral types (Dow and O'Connor, 1982).

Kerogen has been separated into three types on the basis of its elemental composition as plotted on a Van Krevelen diagram or as plotted on a modified Van Krevelen diagram constructed from Rock-Eval pyrolysis data (Van Krevelen, 1961; Tissot and Welte, 1984). On a modified Van Krevelen diagram, the three kerogen types fall into three compositional fields (fig. 94). The composition of each kerogen type changes with progressive maturation along the evolution paths illustrated in figure 94. Appendix 2 contains additional information about this system of kerogen classification. From the surface to about 15,700 feet, the visual kerogen is dominantly of the vitrinite group macerals. A high vitrinite content is also suggested by relatively low hydrogen-to-carbon (H/C) ratios (from elemental analysis). Within this interval, H/C ratios range from slightly less than 1.0 near the surface to about 0.75 at total depth, reflecting a normal loss of hydrogen associated with burial and progressive diagenetic and catagenetic alteration. Unaltered type III kerogen characteristically exhibits an initial H/C ratio of about 1.0, which decreases to about 0.3 as the kerogen matures (Hunt, 1979).

The hydrogen index ($(S_2/TOC)100$) from pyrolysis appears to vary with the coal content of the coal-bearing zones associated with high TOC values (fig. 93 and plate 2). Dow (1983) noted a correspondence between TOC and S_2 values and stated that some of the coaly samples that exhibit high hydrocarbon indices also contain bitumen-saturated vitrinite. Bitumen has been demonstrated to influence both the maximum temperature and the size of the S_2 pyrolysis response (Clementz, 1979). All of the plotted analyses with hydrogen indices in excess of 150 contained generous amounts of coal. These data suggest that the kerogen assemblage in strata from the sea floor to about 15,700 feet is made up largely of vitrinite group macerals composed of type III gas-prone organic material.

Between 15,700 and 17,155 feet (TD), the proportion of amorphous material plus exinite increases to a maximum of 60 percent at 16,500 feet (cuttings sample). Significantly, only 5 percent of the kerogen in this sample consisted of structured relics that could be identified as exinite; 55 percent were structureless, or "amorphous." Unaltered sapropelic kerogen typically yields an H/C ratio of about 1.4 to 1.7 (Hunt, 1979). The hydrogen index from pyrolysis of sapropelic kerogen may exceed 600. However, these values progressively decrease with increasing maturation. The amorphous-rich samples between approximately 16,000 and 17,000 feet generally yielded H/C ratios of only 0.75, and hydrogen indices no greater than 130. The geochemical data therefore appear to conflict with the visual kerogen data. The thermal maturity of the sediments is near optimum for the generation of petroleum (mean random vitrinite

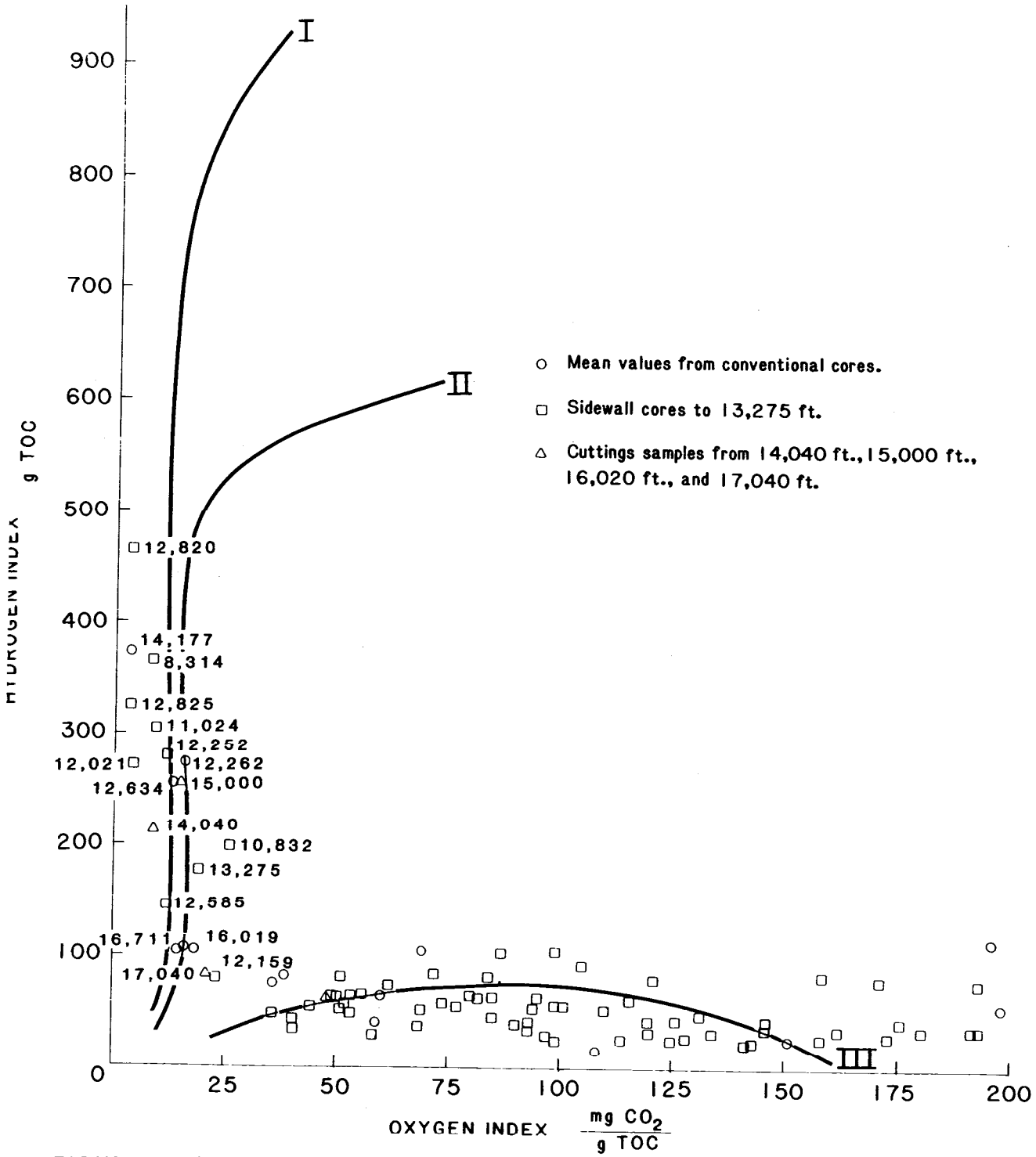

FIGURE 94. **Modified Van Krevelen diagram. Data from Rock Eval pyrolysis of sidewall cores and mean values from conventional cores analyzed by Robertson Research (U.S.), Inc.**

reflectance approaching 1.0 percent). Hydrogen indices at this level of maturity are more characteristic of a type III rather than a type I or type II kerogen (Demaison, 1981). Several conventional core samples between 16,000 and 17,000 feet exhibit anomalous H/C ratios (1.06 to 1.12), which may be attributed to the presence of the solid bitumen noted by Dow (1983). Dow further suggests that at least part of the "amorphous" fraction of the kerogen assemblage is actually degraded, finely divided vitrinite, or low-yield, oxidized amorphous material with very low oil-generating potential. Precipitation or absorption of dissolved or colloidal organic matter such as humic acid can also result in structureless, "amorphous," organic matter having very little petroleum potential (Tissot and Welte, 1984). Any of these factors may have contributed to the discrepancy between the geochemical and visual kerogen data. It is likely that the organic matter between 15,700 and 17,155 feet (TD) is also a type III, gas-prone kerogen composed mostly of vitrinite group macerals or macerals having chemical properties very similar to vitrinite.

The variation in the content and properties of the organic material in the section above 15,700 feet contrasts greatly with that in deeper parts of the well. Above 15,700 feet, TOC values, S_2 values, and the hydrogen indices are extremely variable. Coal is a conspicuous component of the sediments, and coal petrography generally yields a vitrinite content of about 80 percent. Below 15,700 feet, both the TOC and the hydrogen indices are lower in value, and the statistical variation within the data is much smaller. Coal does not become a significant fraction of the samples until below 16,680 feet (plate 2). There is a marked reduction in petrographically identified vitrinite group macerals from about 16,000 to 17,000 feet, where "amorphous," or structureless, organic matter represents the most common kerogen present. This abrupt change in the chemistry and petrographic character of the kerogen may indicate a change in the organic source, the provenance, or the depositional setting.

THERMAL MATURITY

Various parameters were used to evaluate the level of thermal maturity of the carbon-bearing sediments from the North Aleutian Shelf COST No. 1 well. Profiles of maturation parameters, including mean random vitrinite reflectance (R_o), spore coloration index (SCI), kerogen fluorescence intensity, carbon preference index (CPI), and T_2-max, are plotted on figure 95.

Dow (1983) reported that few significant problems were experienced that interfered with the evaluation of R_o. High-rank recycled organic matter, occasional oxidized vitrinite, solid bitumen, pseudovitrinite, and caved material were encountered in some cuttings samples, but the abundance of terrestrially derived kerogen in most samples provided ample vitrinite for examination. Because many good unimodal reflectance histograms were obtained, Dow (1983) considered R_o to be the most reliable indicator of thermal maturity for this well. Although the R_o limits for the oil generation zone

vary slightly with kerogen composition, there is general agreement that the lower threshold occurs at an R_o value of about 0.6 percent for humic kerogen and that the upper threshold extends to about 1.3 or 1.35 percent (Dow, 1977; Hunt, 1979; Tissot and Welte, 1984). In the North Aleutian Shelf COST No. 1 well, R_o values increase to 0.6 percent at about 12,700 feet and reach a maximum value of 1.1 percent at 17,143 feet (the lowermost sample). A projection of the R_o values to greater depth suggests that R_o will exceed 1.4 percent at about 20,000 feet. Crude oil is unlikely to be preserved beyond this level of maturity.

From the sea floor to a depth of 15,368.5 feet (conventional core 17), the R_o values define a continuous, nearly linear curve, which suggests that any discontinuities which may be present in the stratigraphic column do not represent great hiatuses in time or thermal history. Between the core sample at 15,368.5 feet and a cuttings sample at 15,900 feet, there is an abrupt increase in R_o, which Dow (1983) interpreted to represent an unconformity. An alternative explanation for the R_o discontinuity is that cuttings in the interval from the casing point at 13,280 feet to the core sample at 15,368.5 feet were contaminated by cavings from immature coal seams in the open hole below the casing point. This may have suppressed the mean R_o values obtained from these cuttings. No sidewall cores were obtained below 13,291 feet, but two conventional cores (16 and 17) from 14,179.1 and 15,368.5 feet yielded R_o values that agree with the data from cuttings. This suggests that caving was not a severe problem, and that the R_o discontinuity recognized by Dow (1983) is not an aberration of the data.

Robertson Research personnel also studied spore and pollen slide preparations in transmitted light. A value ranging from 1 to 10 was assigned as a spore coloration index (SCI) on the basis of the color of the specimen. These colors, which range from "straw to pale yellow" for SCI=1, to "glassy black/graphitized" for SCI=10, reflect the degree of thermal maturity reached by the organic particles in the sediment sample. The technique is an adaptation of Staplin's (1969) thermal alteration index. The threshold for peak oil generation typically corresponds to an SCI value of about 3.6 and the "oil floor" occurs at about an SCI value of 7.4, according to the correlation diagram for indicators of thermal maturity published by Robertson Research (Dow, 1983).

Unfortunately, the SCI data are of poor quality because of an abundance of recycled or oxidized organic matter and because of discoloration caused by bituminous material. For these reasons, and perhaps due to the subjectivity of color perception by the observer, the SCI profile does not agree favorably with R_o or other maturity data. It is apparent from figure 95 that the SCI data place the catagenetic zone at a shallower depth than do other indicators of thermal maturity. The SCI data do suggest an increase in the rate of change of the thermal maturity in cuttings between 15,660 and 15,900 feet, which corresponds to the discontinuity observed in the R_o data.

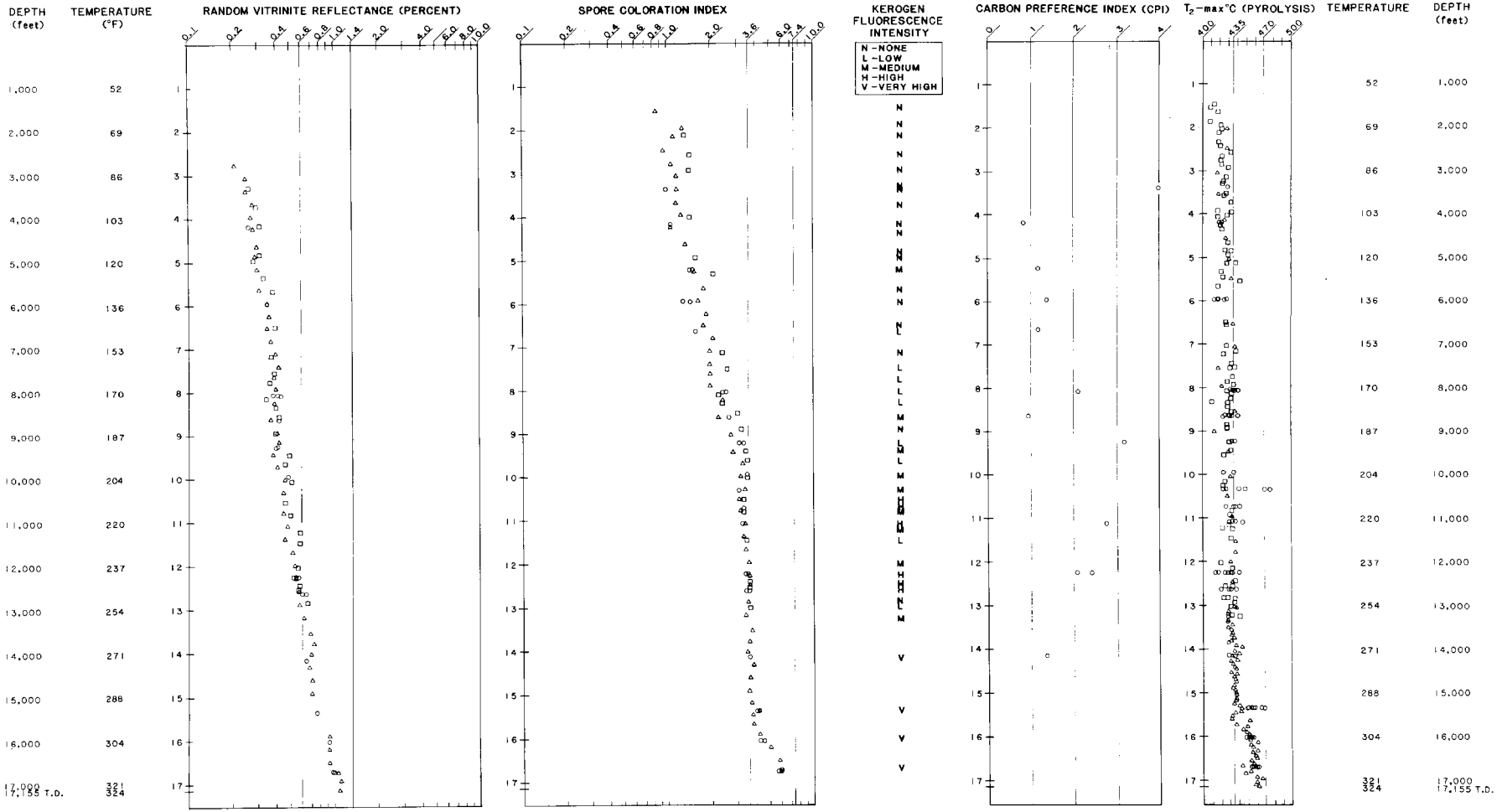

FIGURE 95. **Indicators of thermal maturity. △cuttings, □sidewall cores, ○conventional cores.**

This page was intentionally left blank.

Coal petrographers have observed that bitumens, petroleum-like substances, form from liptinites and vitrinites. Bituminization, the first coalification jump, corresponds with the most prolific phase of crude oil formation in petroleum source rocks. It occurs in the R_o range from about 0.5 percent to about 1.3 percent (Stach and others, 1982). Radke and others (1980) observed that several dramatic changes in coal rank trends occur at about 0.9 percent R_o. They suggest that the coincidence of changes in liptinite and vitrinite fluorescence with changes in the yield and composition of soluble organic matter (bitumens) at near equal stages of thermal maturity is the result of a common cause. They interpreted this common cause to be the shift from predominantly generating to predominantly degrading chemical reactions, such as the dealkylation of aromatics and the cracking of alkanes. According to the Radke study, vitrinite fluorescence increases to a maximum at an R_o of about 1.0 percent, after which it decreases radically. In the subject well, the fluorescence of vitrinite reaches very high levels as R_o values approach 1.0 percent (fig. 95). Samples from this COST well do not exceed an R_o value of 1.1 percent, and kerogen fluorescence remains very high to the deepest data point at 17,143 feet.

Radke and others (1980) also observed that in coals, the odd-even predominance of n-alkanes from C_{15+} bitumen extracts, as expressed by the CPI_{25-31} (appendix 3), exhibits a gradient change between R_o values of 0.9 and 1.0 percent. Typically, the CPI from terrestrially derived bitumen declines from high values and approaches 1.0 asymptotically as thermal maturity rises to 0.9 or 1.0 percent R_o.

Robertson Research (Dow, 1983) computed CPI values using the original Bray and Evans (1961) formula, CPI_{24-34} (see appendix 3), to a maximum depth of 14,170.1 feet (conventional core 16). At this depth, the CPI_{24-34} had decreased to 1.35 from a maximum of 3.96 in shallower strata (fig. 95). Several inferences may be drawn from this CPI trend:

1. R_o should be somewhat less than 0.9 percent when the CPI has decreased to 1.35. For the conventional core sample from 14,179.1 feet, an R_o value of 0.64 percent was obtained. This indicates a close similarity between the level of thermal maturity of the kerogen and that of the heavy hydrocarbon extract at this depth.

2. Stach and others (1982) state that fluid bitumen (crude oil) is expelled from kerogen at levels of thermal maturity where CPI values decline below 1.3. At 14,180 feet, potential source beds are just approaching the level of maturity at which significant amounts of petroleum would be released if suitable kerogen were present.

3. Waxes formed by land plants contain more odd-numbered normal paraffin chains in the C_{27}, C_{29}, and C_{31} range, and in thermally immature shales, these constituents commonly produce CPI_{24-34} values well in excess of 1.0 (Hunt, 1979). CPI values from basins off southern California typically range from 2.5 to 5 (Hunt, 1979). CPI values that range up to 3.96 (fig. 95) in the subject well suggest that the $C_{15}+$ extract in this interval was derived from a terrestrial source.

Gas chromatograms of $C_{15}+$ saturate-fraction hydrocarbons (fig. 96) verify an increase in maturity of the extract in the vicinity of 15,368.5 feet (core 17). The paraffins from 14,179.1 feet (core 16) exhibit a distinct bimodal distribution with a large population of long chain molecules. These long chain paraffins are thought to be derived from terrestrial or brackish-water plants rather than from a marine source.

Barker (1974), Claypool and Reed (1976), and Espitalié and others (1977) have suggested that T_2-max, the temperature in degrees Centigrade at which maximum evolution of thermal hydrocarbons occurs during pyrolysis (see summary of method in appendix 4), can be used to characterize the degree of thermal maturation of kerogen. These measurements can be influenced by the instrumentation and technique of the testing laboratory, the rate of heating, the type of kerogen, the presence of recycled or oxidized organic matter, downhole contamination, and the presence of solid bitumen (Tissot and Welte, 1984; Dow, 1983). Shallow samples in this well are believed to exhibit spuriously high levels of maturity due to the presence of recycled organic matter. Conversely, deeper, organic-rich, coal-bearing samples with solid bitumen contents probably have yielded spuriously low T_2-max values (Clementz, 1979).

Pyrolysis was performed on cuttings, sidewall cores, and conventional cores by both Exlog and Robertson Research. The T_2-max profile in figure 95 was constructed from Robertson Research data. Their procedure is calibrated in such a manner that T_2-max values between 435 and 470 ^{o}C are obtained when the kerogen is at its most favorable level of maturity for the formation of crude oil. The onset of the oil-generating zone is difficult to identify in the T_2-max data from this well, but most samples below about 11,400 feet have T_2-max values greater than 435 ^{o}C.

There is a fair degree of correlation among the various indicators of thermal maturity. Due to the presence of abundant humic kerogen throughout the stratigraphic column in this well, R_o measurements appear to represent the most reliable indicator of thermal maturity. A zone of thermal maturity sufficient for oil generation probably occurs between 12,700 and 20,000 feet at the well site. This assumes that overmature Mesozoic "basement" rocks do not occur within that interval. The R_o profile is continuous from near the surface to 15,368.5 feet, which indicates that deposition was more or less continuous. Between 15,368.5 and 15,900 feet, there is

a maturity anomaly which may represent an unconformity. The unconformity is tentatively placed at 15,620 feet on the basis of data from the gamma ray log.

HYDROCARBON SOURCE POTENTIAL

Plate 2 presents representative sample descriptions and profiles of selected geochemical data which address the ability of the potential source rocks to generate hydrocarbons. The abbreviations in the sample descriptions are listed in appendix 1. Appendix 4 contains a brief description of the pyrolysis technique. Peters (1986) provides detailed guidelines for the interpretation of pyrolysis data.

The organic carbon content of samples from the COST well, as previously noted, appears to vary largely in response to the coal content of the samples. Dow (1983) identified four coal-bearing zones associated with high TOC values (2,600 to 4,200 feet, 7,500 to 9,700 feet, 13,000 to 15,700 feet, and 16,800 to 17,150 feet). Dow further recognized a positive correspondence between TOC and the pyrolytic response (S_2) of the kerogen in these coal-bearing intervals.

Studies by Claypool and Reed (1976) indicate that the S_2 peak from pyrolysis is approximately proportional to the organic carbon content and that the S_1 peak is directly proportional to the concentration of extractable $C_{15}+$ hydrocarbons of a source rock sample. The sum S_1+S_2 has been termed the genetic potential by Tissot and Welte (1984) because it accounts for both the type and abundance of organic matter. Table 14 summarizes the threshold values used for evaluating the oil and gas potential of source rocks.

TABLE 14. Suggested threshold values for genetic potential (S_1+S_2) from pyrolysis (from Tissot and Welte, 1984).

Genetic Potential $S_1 + S_2$ (ppm)	Hydrocarbon Source Rock Potential
Less than 2,000	No oil; some potential for gas.
2,000 to 6,000	Moderate source rock.
Greater than 6,000	Good source rock.

The genetic potential profile on plate 2 was constructed from Robertson Research data. Most values in excess of 2,000 ppm fall within Dow's coal-bearing zones and rise and fall parallel to the TOC values. The interval from approximately 10,700 to 13,000 feet, though not identified by Dow (1983) as a coal-bearing zone, yielded many samples for analysis that contained significant amounts of coal. A sample from 12,262.4 feet (conventional core 14), for example,

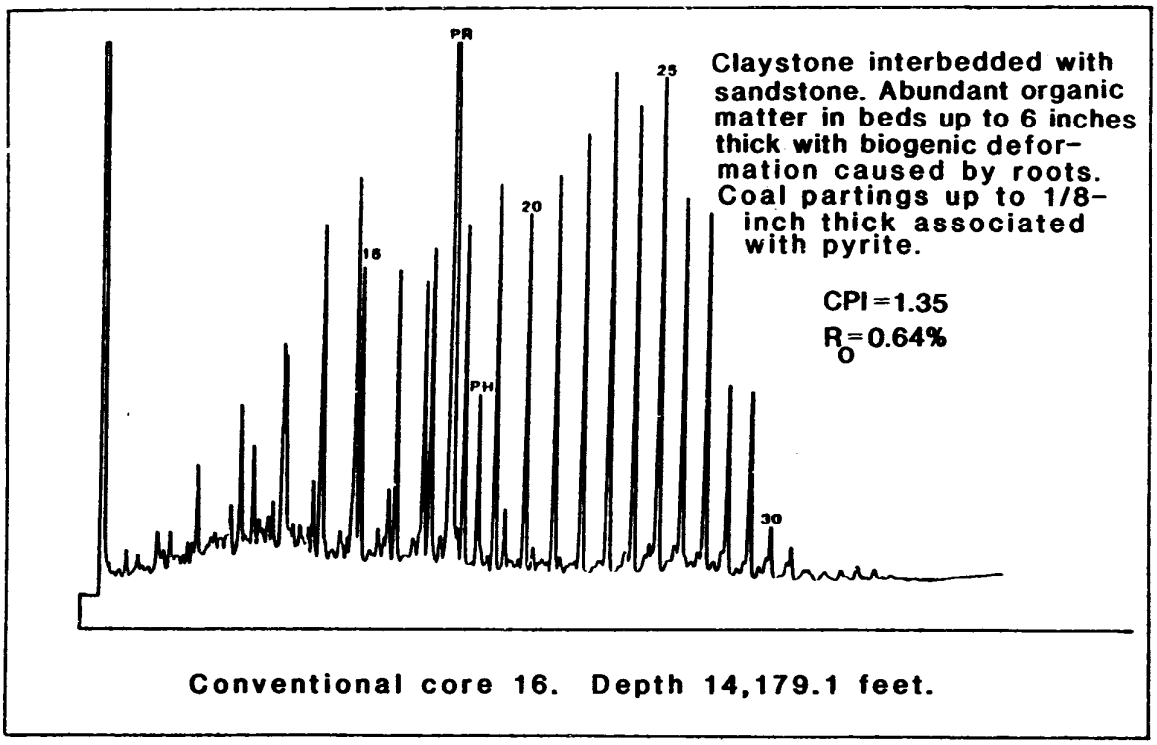

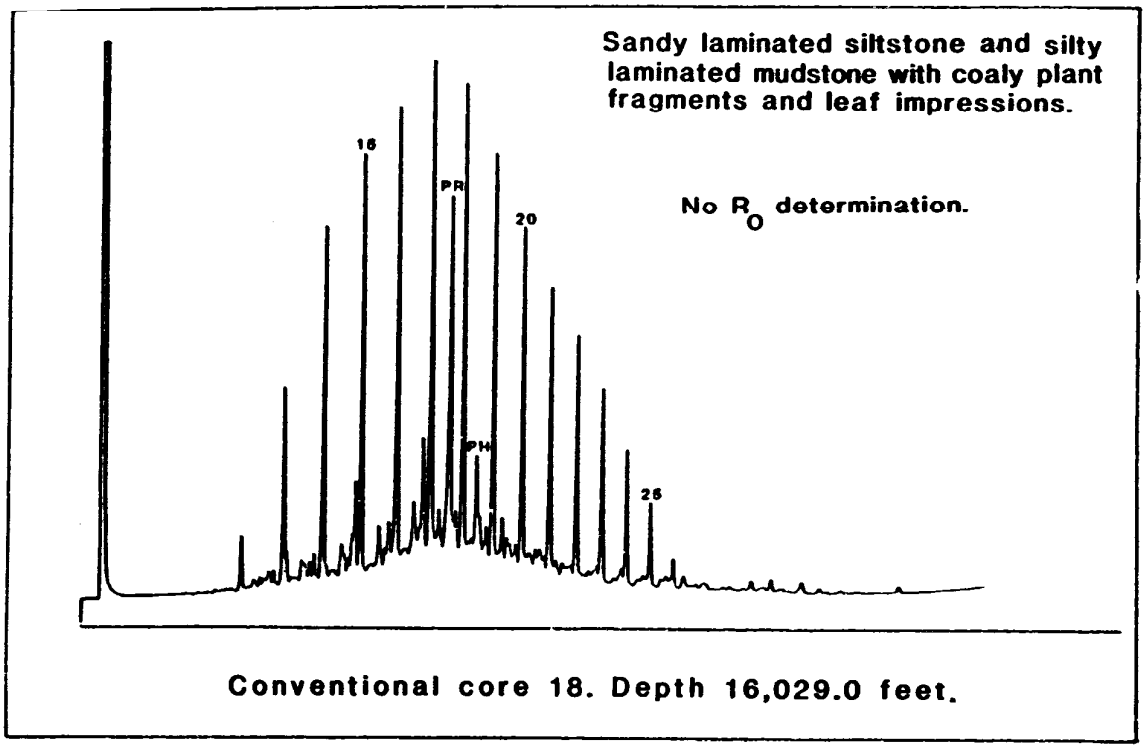

FIGURE 96. Gas chromatograms of C_{15+} saturate fraction hydrocarbon. (Extract and R_o data from Robertson Research (U.S.) Inc. Lithologic descriptions from AGAT Consultants, Inc.)

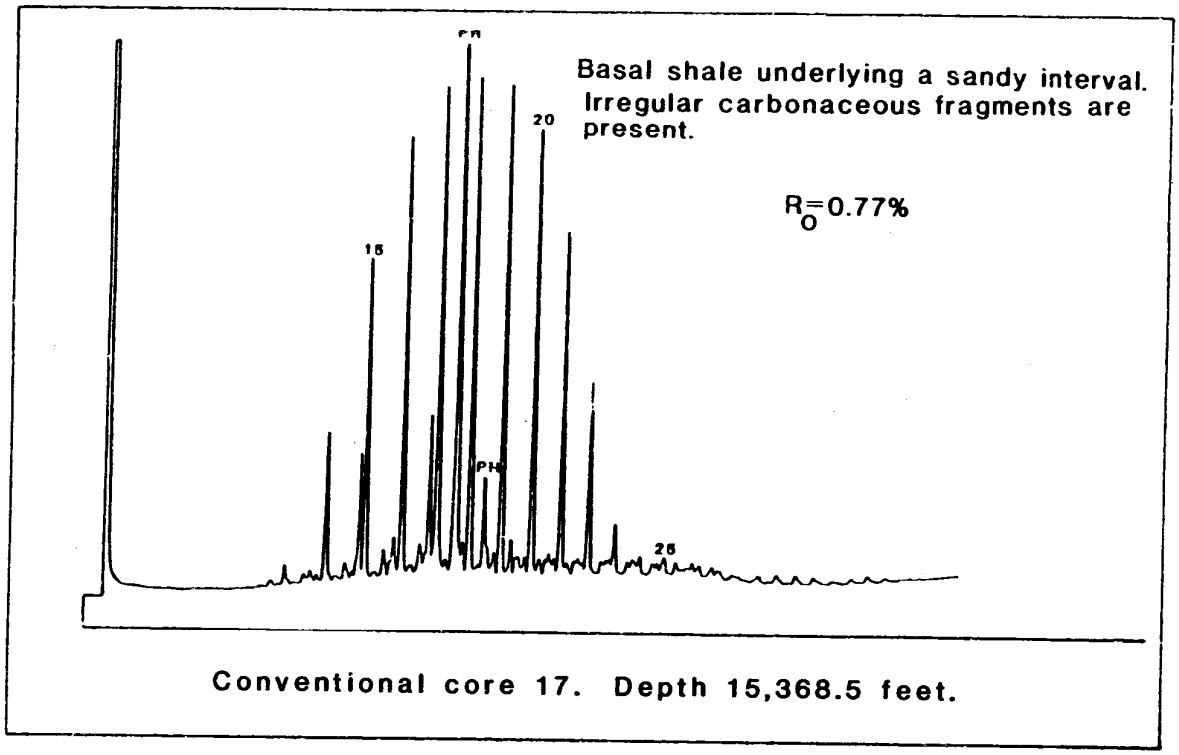

Conventional core 17. Depth 15,368.5 feet.

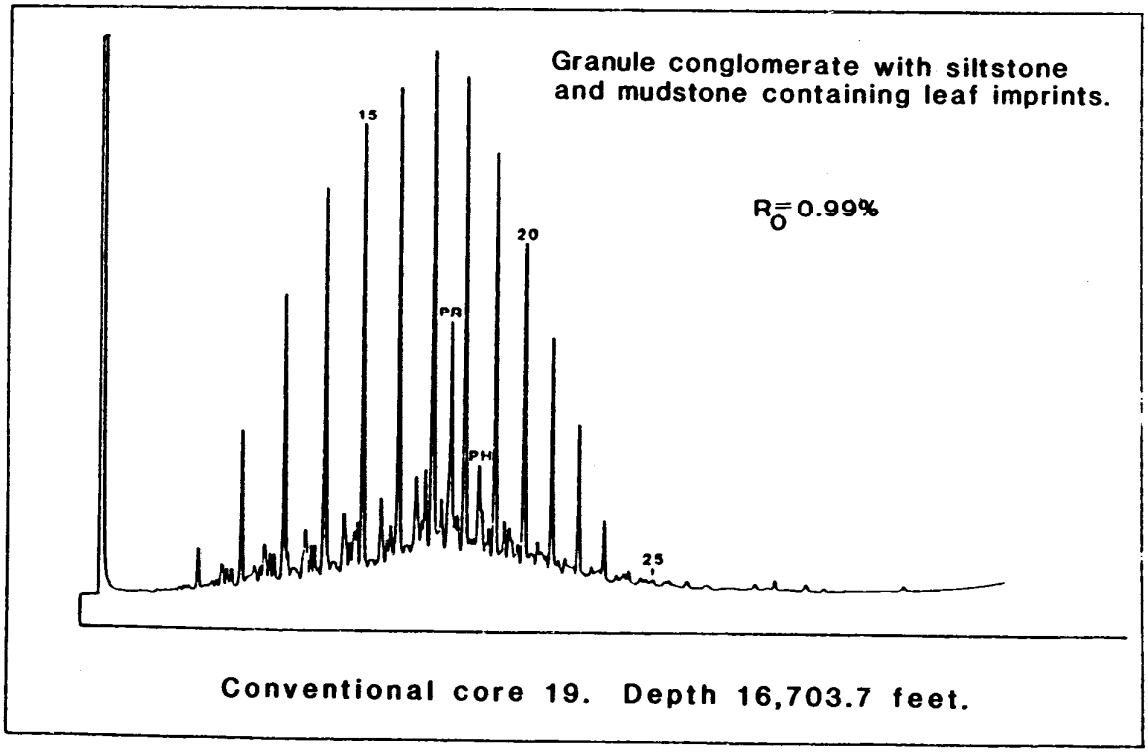

Conventional core 19. Depth 16,703.7 feet.

***FIGURE* 96. (cont.)**

contained 60 percent bituminous coal. Between 16,020 and 16,800 feet, the samples contain significant amounts of shale and mudstone but virtually no coal. TOC values range from 0.9 to 2.75 percent, but nearly all fall between 1 and 2 percent. The genetic potential of these samples is generally about 2,000 ppm, with one value as high as 4,055 ppm (depth 16,707.5 feet, conventional core 19). Because the genetic potentials of this interval are not an artifact of high S_2 values related to coal content, the data suggest that the interval may be considered a moderate source bed sequence.

The transformation ratio, $S_1/(S_1+S_2)$, is generally regarded as an indicator of thermal maturity (Barker, 1974; Claypool and Reed, 1976; Espitalié and others, 1977). Peters (1986) suggests that the oil generative window should fall approximately between $S_1/(S_1+S_2)$ values of 0.1 and 0.4. In this well, the transformation ratio is relatively constant and less than 0.1 down to a depth of 15,620 feet (the postulated unconformity); for deeper samples, it increases to values that range mostly between 0.1 and 0.2. Two anomalous transformation ratio peaks occur at 16,380 and 16,620 feet (0.413 and 0.400. respectively). Below 16,620 feet, the ratio drops back down to about 0.2. The anomalous peaks at 16,380 and 16,620 feet appear to coincide with changes in organic composition (occurrence of migrated oil?) rather than thermal maturity anomalies. Thermal maturity does not regress with depth except where intrusives occur within a bedded sequence. No intrusives were identified in the well. Furthermore, in the interval where the transformation ratio reaches 0.4, R_o values are only 0.9 or 1.0 percent. Peters (1986) indicates that R_o values of 1.3 or 1.4 percent are typically associated with transformation ratios as high as 0.4. It is possible that the high transformation ratios are the result of migrated light hydrocarbons or bituminous material. The transformation ratio peaks approximately coincide with zones of hydrocarbon shows (elevated gas in the drilling fluids) noted during the drilling of the well.

The peaks in $S_1/(S_1+S_2)$ values also correlate with peaks in the volume of headspace gas (per unit weight of kerogen carbon) and in the wetness of this gas. The headspace gas is the free gas found in cans of cuttings that has evolved after sample collection. It is sampled and analyzed before further sample processing. The wetness peak occurs across the interval 15,720 to 16,800 feet, and corresponds to a peak in headspace gas volume from 16,200 to 16,688 feet.

Continuous analysis of drilling-mud gas was performed by Exlog using a catalytic flame ionization detector that measured the total hydrocarbon content of the drilling mud. The background value generally ranged around 10 units (5 units equal 1.0 percent methane in air). Two zones, 16,165 to 16,315 feet and 16,800 to 16,985 feet, contained levels of mud gas an order of magnitude above this background. Gas chromatography indicated that these hydrocarbons were composed largely of methane. Robertson Research (U.S.), Inc., analyzed four canned samples of drilling mud which were collected coincident with the maximum mud gas levels that were encountered at

total depth. They reported that the gas was composed primarily of light (C_1 to C_5) hydrocarbons especially rich in methane, and that the composition of the mud gas was similar to that of the headspace gas recovered from canned cuttings samples from below 12,000 feet.

C_{15}+ hydrocarbon values and bitumen-to-TOC ratios are erratic throughout most of the well, but overall they appear to increase slightly below 16,000 feet. Relatively high bitumen-to-TOC ratios at 9,982.0 feet (conventional core 10) and 10,326.4 feet (conventional core 11) are due to low TOC values. The high ratio at 12,634.4 feet (conventional core 15) is due to a significant amount of extractable bitumen, up to 2,290 ppm. This sample contained 10 percent bituminous coal. None of the samples analyzed produced bitumen-to-TOC ratios in excess of 0.20. Values in excess of 0.20 would be abnormal and might indicate the presence of migrated bitumen (Tissot and Welte, 1984).

Traces of petroleum (gas peaks on the mud log and oil stain and fluorescence in drill cuttings) occur in the high-TOC, "amorphous" kerogen interval between 16,000 and 17,000 feet. However, it is unclear whether these hydrocarbons have been generated in situ by these relatively lean source rocks or if they migrated to the well site from a remote source. Because of the low permeability of these rocks, it appears unlikely that the hydrocarbons could have migrated from a very distant source.

Throughout the rest of the well above 16,000 feet, the presence of predominantly type III kerogen, plus the predominance of light alkanes in both headspace gas from cuttings and gas from drilling mud, suggests that all potential source beds penetrated by the North Aleutian Shelf COST No. 1 well are gas prone.

SUMMARY AND CONCLUSIONS

The North Aleutian Shelf COST No. 1 well penetrated 17,155 feet of Tertiary sedimentary rock containing mostly type III, humic, gas-prone kerogen derived from terrestrial or nearshore sources. Type III kerogen is the product of Demaison's (1981) "type C" organic facies. Table 15 compares the geochemical characteristics of a "type C" organic facies with the characteristics of sediments from about 10,500 to 11,000 feet in the well.

A "type C" organic facies is typically the product of a mildly oxic depositional environment and may include both marine and nonmarine sediments, slope and rise deposits, and exinitic coals. Sediments deposited and preserved in this type of environment tend to be gas prone but may produce petroleum condensate. The organic material sampled in this well appears to be a very good example of a type III kerogen from a "type C" organic facies. Only minor amounts of exinite occur, either in coal or as disseminated kerogen. The abundant amorphous kerogen recovered from samples from between 16,000 and 17,000 feet contains very little hydrogen, and it is believed to have been derived from vitrinite-group rather than exinite-group

macerals. Anomalously high amounts of organic carbon and pyrolytic hydrocarbons are associated with coal and solid bitumen. The interval with the greatest source potential for petroleum is the predominantly shale and mudstone sequence between 16,020 and 16,800 feet. The TOC and $C_{15}+$ hydrocarbon content suggest modest source rock quality, and the genetic potential ($S_1 + S_2$) from pyrolysis is generally moderate to low within this interval.

TABLE 15: Geochemical characteristics of Demaison's "type C" organic facies and analogous values from the North Aleutian Shelf COST No. 1 well. Coal-bearing samples are excluded.

	Type C Organic Facies (R_o = 0.5%)	COST No. 1 Well (R_o = 0.5%)
H/C	0.8 to 1.0	0.82 to 0.98
Hydrogen Index	25 to 125	55 to 79
Oxygen Index	50 to 200	62 to 523

Sufficient thermal maturity for the generation of crude oil exists below about 12,700 feet, and at this site, degeneration of liquid hydrocarbons due to thermal cracking (the "oil floor") probably does not occur at depths less than 20,000 feet. Minor oil shows and thermogenic gas were encountered in the North Aleutian Shelf COST No. 1 well below 15,700 feet. Methane, probably of biogenic origin, was present above 2,500 feet.

A maturity anomaly which may represent an unconformity occurs between 15,368.5 and 15,900 feet. An abrupt drop in the gamma ray log response at 15,620 feet may mark the position of this unconformity.

10. Abnormal Formation Pressure

by

Kirk W. Sherwood

INTRODUCTION

The presence of abnormal formation pressures in the North Aleutian Shelf COST No. 1 well was first suggested by operational problems encountered while drilling the deepest parts of the well. Exlog (Exploration Logging (USA) Inc., 1983) reported in their operational summary that rising background gas, trip gas, and connection gas were observed in the drilling fluids while drilling below 15,915 feet (subsea depth). Increased mud weights, up to 13.0 pounds per gallon (ppg), were required to control the movement of gas into the wellbore. Frequent flow checks on drilling breaks, however, found no evidence of significant incursion of fluids into the wellbore. Nevertheless, each trip below 16,115 feet produced abundant cavings of splintery pressured shale, which required reaming each time the wellbore was re-entered. Along with the rising gas content of the mud, the wellbore instability suggested the existence of an underbalanced condition in the wellbore. Splintery shale cavings had also been noted at 11,345 feet, which suggested that an overpressured sequence had also been penetrated in shallower parts of the well (Exlog, 1983).

An analysis of wireline log acoustic data and interval velocities calculated from the borehole velocity survey (see Velocity Analysis chapter) subsequently documented the presence of a significant velocity inversion in the part of the well below 10,000 feet (fig. 58). This velocity inversion was thought to result from a major lithologic change (abundant low-velocity coal) and perhaps the presence of abnormal formation pressure. Because of the potential effect of a thick sequence of overpressured rock on seismic interpretation throughout the basin, and because of the potential hazard that excess formation pressures present to drilling operations, a study of the overpressuring phenomenon was undertaken.

DIRECT PRESSURE MEASUREMENTS

Only a limited number of direct measurements of formation pore fluid pressure are available for the North Aleutian Shelf COST No. 1 well. Formation pressures can be measured directly through conventional drill stem production tests or wireline devices such as the Schlumberger Repeat Formation Tester (RFT). Although no drill

stem tests were conducted in the North Aleutian Shelf COST No. 1 well, three RFT surveys were conducted, with a total of 35 pressure measurements attempted. Of these 35 attempts, only 8 tests were successful; the remaining 27 tests either encountered impermeable formation or failed to obtain a proper seal. The results of the 8 successful tests are tabulated below.

TABLE 16. RFT pressure tests.

	MD	TVD	SSD	PSI	PSI/FOOT	EMW(ppg)
1.	2,830	2,830	2,745	1,200	0.437	8.422
2.	4,115	4,115	4,030	1,769	0.439	8.461
3.	4,878	4,878	4,793	2,103	0.439	8.461
4.	5,113	5,113	5,028	2,212	0.440	8.480
5.	6,675	6,675	6,590	2,893	0.439	8.461
6.	8,089	8,089	8,004	3,495	0.437	8.422
7.	8,660	8,659	8,574	3,749	0.437	8.422
8.	9,295	9,294	9,209	4,059	0.441	8.500

Where MD = measured depth, in feet, from Kelly bushing
TVD = true vertical depth, in feet, from Kelly bushing
SSD = subsea depth, in feet
PSI = formation pressure, in pounds per square inch
PSI/FOOT = pressure gradient, in pounds per square inch per foot
EMW(ppg) = equivalent mud weight, in pounds per gallon

The RFT data are also summarized in the pressure plot of figure 97. All data points cluster very close to an average gradient of 0.439 pounds per square inch per foot (psi/foot) or 8.45 ppg equivalent fluid density, and none of these measurements identify any abnormally pressured strata anywhere in the part of the well above 9,209 feet (SSD). A pore pressure gradient of 0.439 psi/foot suggests relatively fresh formation water, as pure freshwater yields a hydrostatic gradient of 0.433 psi/foot. A somewhat higher average gradient of 0.452 psi/foot was measured in the Navarin Basin COST No. 1 well (Sherwood, 1984, p. 170). A brine gradient of 0.468 psi/foot typifies normally pressured wells in the Gulf of Mexico province (McClure, 1977, p. AP-2). In the North Aleutian Shelf COST No. 1 well, no direct pressure measurements were obtained in the deeper section where operational difficulties suggested the possible presence of abnormal pore pressure.

INDIRECT PRESSURE EVALUATION

In the absence of direct pressure data, wireline well logs which measure physical properties such as electrical conductivity, acoustic transmission velocity, and density may be employed to obtain an estimate of formation pore pressure. Empirical observations have established that the resistivity (inverse of electrical

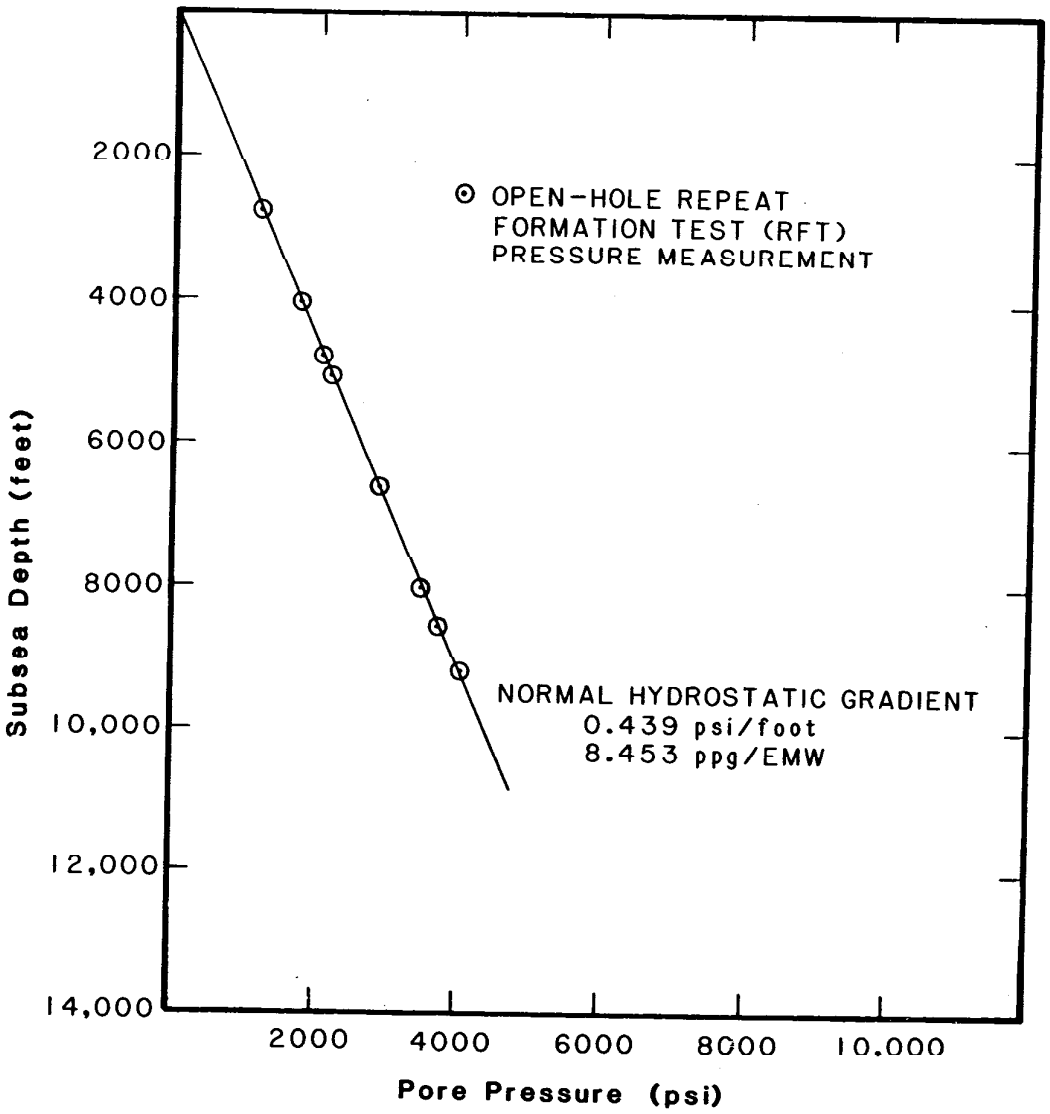

FIGURE 97. **Plot of formation pore pressure versus subsea depth for North Aleutian Shelf COST No. 1 well. The pressure measurements above 9209 feet collectively define an average "normal" hydrostatic gradient of 0.439 psi/foot, shown as a line in the diagram above. A gradient of 0.433 psi/foot is considered normal for fresh water. (EMW=equivalent mud weight.)**

conductivity), acoustic velocity, and density of sediments rise progressively and systematically with depth of burial (Hottmann and Johnson, 1965). The changes in these physical properties are attributed primarily to tighter particle packing, greater interparticle bonding, and the introduction of pore-occluding chemical cements. Collectively, these processes result in a decrease in porosity and the expulsion of pore fluids. In zones of abnormal pore pressure, these processes are reversed or arrested because of confinement or retention of pore fluids, resulting in excess pore pressure, increased porosity, and reduced formation rigidity and shear strength. The alteration of rock properties within overpressured zones is reflected in the physical measurements obtained by wireline logs. In depth profiles of resistivity, interval velocity, and density, an abnormally pressured zone is manifested by a reversal or deviation from the trends observed in the overlying normally compacted sequence. This effect is observed within most rock types, but varies most systematically with pore pressure in shales. For this reason, shale is the lithology most often analyzed in pore pressure studies.

Empirical studies, such as the pioneering paper by Hottmann and Johnson (1965), have conclusively demonstrated that the anomalous physical properties of overpressured shales can be quantitatively related to actual pore fluid pressures. This report utilized a set of shale evaluation curves formulated by McClure (1977) after empirically derived curves for analysis of seismic data previously published by Pennebaker (1968a; 1968b). Empirical curves for pressure evaluation have also been published by Hottmann and Johnson (1965), MacGregor (1965), and Wallace (1965).

Shale Conductivity

Electrical conductivity data for shales in the North Aleutian Shelf COST No. 1 well are presented in figure 98A. Shale conductivities remain relatively constant throughout the depth interval from 1,400 to 7,000 feet. Conductivities decrease progressively with increasing depth from 7,000 to 11,500 feet, where a sharp reversal, or increase in shale conductivity, is found. From 12,000 feet to the deepest logged part of the well (16,600 feet), shale conductivities, though highly erratic, decrease progressively with depth. Pressure evaluation curves were fitted to this data set by sliding the curves vertically along a match (overlay matched to data plot) at the 2,000 millimhos per meter (MMOS) line until the curve for "normal" compaction (identified as the 8.5-ppg curve) coincided with the deepest zone (8,574 to 9,209 feet) in which normal pressure gradients were measured by RFT tests.

Shale conductivities at depths above 6,000 feet depart markedly from the normal compaction curve and suggest that these strata are overcompacted. However, density and velocity data do not corroborate an overcompacted condition for strata in this interval (figs. 98C, 98D). The anomalously low conductivity of shales in the upper part of the well is most likely attributable to the presence of low-salinity formation fluids. Examples of this commonly observed effect

in both onshore and offshore wells are illustrated by Fertl (1976, figs. 5.36, 5.38, and 5.43). The source of the freshwater is unknown, although it may, in some cases, represent invasion of aquifers by meteoric water. Through log analysis, Gary Martin of the Minerals Management Service (written commun., 1986) estimated pore water salinities to be 13,000 parts per million (ppm) at 2,200 feet, gradually rising with depth to 30,000 ppm (approximately that of seawater) at a depth of 6,000 feet. The presence of relatively fresh pore fluids in the upper part of the well is also confirmed by the relatively low hydrostatic gradient (0.439 psi/foot) obtained from analysis of RFT data.

Between 11,500 and 12,000 feet, shale conductivities rise markedly, suggesting a pronounced increase in pore fluid volume, and, probably, pore pressure. This conductivity anomaly may also stem in part from the fact that fluids retained in overpressured zones are commonly more saline than those in the overlying, normally compacted sequence (McClure, 1977, p. I-18). However, elevated salinities are not a universal condition of overpressured zones. Examples where overpressured zones contain relatively fresh pore fluids (in contrast to saline fluids in the overlying, normally compacted sequence) are illustrated by Fertl (1976, p. 194-5, figs. 5.16, 5.17). The analysis in figure 98A indicates that maximum pore pressure gradients occur from 11,500 to 12,600 feet. Here, the pressure evaluation curves suggest equivalent fluid densities of 16 to 17 ppg (0.83 to 0.88 psi/foot). Within the zone from 12,600 to 16,000 feet, shale conductivities suggest moderately elevated pore pressure gradients which progressively decline with depth. Below 16,000 feet, shales appear to be normally pressured.

Shale Velocity

Shale velocities (inversely portrayed as travel time) are summarized in figure 98C. In the interval from 1,400 to 10,600 feet, shale velocities progressively increase with depth along a normal compaction profile, represented by a regional, composite compaction curve compiled from normally compacted shales in three Bering Sea wells (Navarin COST No. 1; St. George COST No. 1; St. George COST No. 2).

In the interval from 10,600 to 11,200 feet, shale velocities are anomalously high, possibly suggesting the presence of a caprock. Apparent overcompaction in this depth interval is corroborated by conductivity and density data (figs. 98A, 98D). Such zones of abnormal hardness or cementation are often found directly above zones of abnormal pore pressure (Fertl, 1976, p. 226, fig. 5.44). Caprock zones are commonly highly cemented, and associated mudrocks are typically described as "hard, limey shale." In fact, AGAT (1983) reports that conventional core 12, taken in the depth interval from 10,645 to 10,655 feet (SSD), consists largely of well-cemented mudstones containing up to 47 percent siderite and calcite (predominantly siderite). Conventional core 13, taken in the depth interval from 11,000 to 11,020 feet (SSD), contains sandstones and

conglomerates which are thoroughly cemented in thin, discrete zones by calcite.

In the interval from 11,200 to 12,200 feet, shale velocities decrease dramatically, suggesting the presence of abnormally high pore pressures. Below this sharp reversal, from 12,200 to 16,600 feet, shale velocities are somewhat erratic, but progressively rise with increasing depth. Pressure evaluation curves were fitted to this data set by sliding the curves vertically (matched at the 100 microseconds/foot line) until the "normal" compaction curve (labeled 8.5 ppg) coincided with the regionally derived Bering Sea composite compaction curve, as shown in figure 98C.

The anomalous shale velocities in the interval from 11,200 to 16,600 feet correspond to equivalent fluid densities as high as 17 ppg (0.88 psi/foot). The top of the overpressured zone is placed at 11,200 feet on the basis of the shale velocity analysis. An interval velocity curve derived from a vertical seismic profile (see Velocity Analysis chapter) with a 200-foot sample interval identifies the top of a major velocity reversal at approximately 10,000 feet. However, the low interval velocities in the interval from 10,000 to 11,200 feet appear to result from the presence of low-velocity coals. Shale velocities indicate that abnormal pressure gradients up to 15.5 ppg fluid density equivalent are present from 14,500 feet down to 16,000 feet. Shale velocity data suggest more moderate pore pressures below 16,000 feet, ranging between 12 and 14 ppg, and conductivity and density data suggest that the shales below 16,000 feet are normally compacted. It appears from a consensus of all data that a practical "floor" for the zone of abnormal pressure lies at approximately 16,000 feet (SSD).

Shale Density

Shale densities obtained from wireline logs are presented in figure 98D. Similar to the trend observed in the shale velocity data, shale densities progressively increase with depth along a normal compaction profile (the 8.5-ppg curve) from 1,400 to 11,200 feet. Between 11,200 and 11,800 feet, shale densities decrease abruptly, and although highly erratic, gradually increase with depth from 11,800 to 16,600 feet. The pressure evaluation curves suggest that equivalent pore pressure gradients as high as 18 ppg (0.93 psi/foot) or higher may be present within the zone of anomalously low shale densities. At approximately 16,000 feet, shale densities return to normal values, and the strata below 16,000 feet appear to be normally pressured.

In summary, an analysis of the wireline log data indicates that a major zone of abnormal pore fluid pressure exists in the approximate depth interval from 11,200 to 16,000 feet (SSD) in the North Aleutian Shelf COST No. 1 well. Within this zone, an analysis of shale properties using empirical pressure evaluation curves indicates that pore fluid pressure gradients up to, and possibly locally exceeding, 0.88 psi/foot (17 ppg) are present. RFT and

wireline log data indicate that normal pore pressure gradients are present above 11,200 feet and below approximately 16,000 feet (SSD).

Drilling Exponent

As the North Aleutian Shelf COST No. 1 well was drilled, Exlog continuously monitored formation pore pressure through iterative calculation of a normalized drilling exponent (or "Nx"). The fundamental assumption underlying the "drilling exponent" method of pressure evaluation is that the rate of penetration is directly dependent upon the differential pressure at the rock face in contact with the drill bit. A high differential pressure aids the drilling process because the shear strength of the rock is lowered and the percussive impact of the teeth of the drill bit detaches greater quantities of rock from the drill face. Penetration rates commonly increase dramatically when overpressured zones are encountered because the rising pore pressure increases the differential between formation pressure and the pressure exerted by the column of drilling fluid (mud). A rapid increase in drill rate in a lithologically monotonous sequence is often the earliest warning that an overpressured zone has been entered.

Lithology and several variables associated with drilling operations (including, for example, mud weight, viscosity, bit weight, bit type, bit dullness, bit jets, rotation rate, hole size, downhole drill assembly, etc.), however, also can markedly affect penetration rate. The drilling exponent method of pressure evaluation attempts to account for the collective effects of the numerous known geological and operational variables on the penetration rate in order to calculate a theoretical "normalized" rate against which the actual drill rate may be compared. Drill rates in excess of the normalized rate are considered to represent evidence of an overpressured condition, and the drill rate anomaly may be quantitatively related to formation pressure. An excellent summary of the basic method is found in Jorden and Shirley (1966). Specific details of the technique used by Exlog are published in Exlog manuals MS-156 and MS-196.

The results of the Exlog pore pressure computations (shown as equivalent fluid density) are summarized in figure 98E. A dashed line at 8.45 ppg on the left side of the plot represents the actual hydrostatic gradient above 9,209 feet as derived from RFT measurements. Casing points and leak-off fracture gradients are posted on the right side of the diagram. Nx-derived equivalent fluid densities in the interval from 5,000 to 9,000 feet suggest modest overpressuring, but actual pressure measurements within this zone do not corroborate the Nx pressure estimates. No Nx pressure anomaly was detected at 11,200 feet, where wireline log data identify the top of the major zone of abnormal pore pressure. A minor Nx anomaly was noted beginning at 14,000 feet, and rapidly increasing pore pressures were identified below 16,000 feet, where wireline log analysis places the base of the overpressured zone. As noted, significant sloughing of splintery shale cavings into the wellbore began to occur while drilling below 15,900 feet. However, the shale

velocity analysis (and corroborative analyses of conductivity and density data) suggests that this material was probably coming from the interval between the 9 5/8-inch casing shoe at 13,195 feet (logger's subsea depth) and the base of the overpressured zone at 16,000 feet. It is not known why Exlog's Nx-derived pressure calculations failed to recognize the top of the overpressured zone. The stratigraphic column between 10,000 and 15,600 feet is predominantly sandstone, coal, and siltstone. Shale is relatively sparse, but becomes a common lithology below 16,000 feet. Perhaps the extreme variation in lithology (hence, drillability) within the sequence below 10,000 feet masked the less dramatic effect of overpressure on penetration rates.

PRESSURE PLOT

A plot of pore pressure versus depth is presented in figure 99A. Only direct pressure measurements are plotted for the normally pressured interval from 2,745 to 9,209 feet. Below 9,300 feet, the plotted values represent apparent pore pressures that were calculated from equivalent fluid density values established by the analysis of shale velocities (fig. 98C). Shale velocity data were used preferentially over the other analyses because they exhibit the least scatter, and, within the normally pressured interval, conform closely to a regionally derived compaction curve. Fertl (1976, p. 210) recommends the use of shale velocities for quantitative pressure analysis on the grounds that the sonic log "is relatively unaffected by changes in hole size, formation temperature, and formation salinity." Figure 99A also shows values for bottom hole dynamic circulating mud pressure. These values were calculated from estimates of equivalent circulating density ("ECD") provided by Exlog (1983, appendix C). The normal hydrostatic gradient established by the RFT data is posted as a dashed line, and a typical lithostatic gradient of 1.0 psi/foot is shown as a solid line on the right. Abnormally high pore pressures typically plot to the right of the normal gradient, and, in instances of extreme overpressuring, may plot along the lithostatic gradient. At 11,200 feet, the calculated pore pressures in this well deviate from the normal gradient and progressively shift with increasing depth toward the lithostatic gradient. Near the bottom of the well, estimated pore pressures decline abruptly and begin to approach mud column pressures and normal hydrostatic pressures.

According to this analysis, pore pressures began to exceed mud column pressures at an approximate depth of 11,500 feet. From this depth down to the 9 5/8-inch casing point at 13,195 feet (SSD), the well was drilled in an underbalanced condition. Furthermore, below 11,700 feet, pore pressures had increased so dramatically that the pore pressure gradients at the bottom of the hole began to exceed the leak-off fracture gradient (13.1 ppg) established near the 13 3/8-inch casing shoe at 4,779 feet (SSD). Had the well experienced any significant flow from a zone of permeability below 11,700 feet, the mud weight that would have been required to control the flow could have fractured the formation in the open hole near the 13 3/8-inch

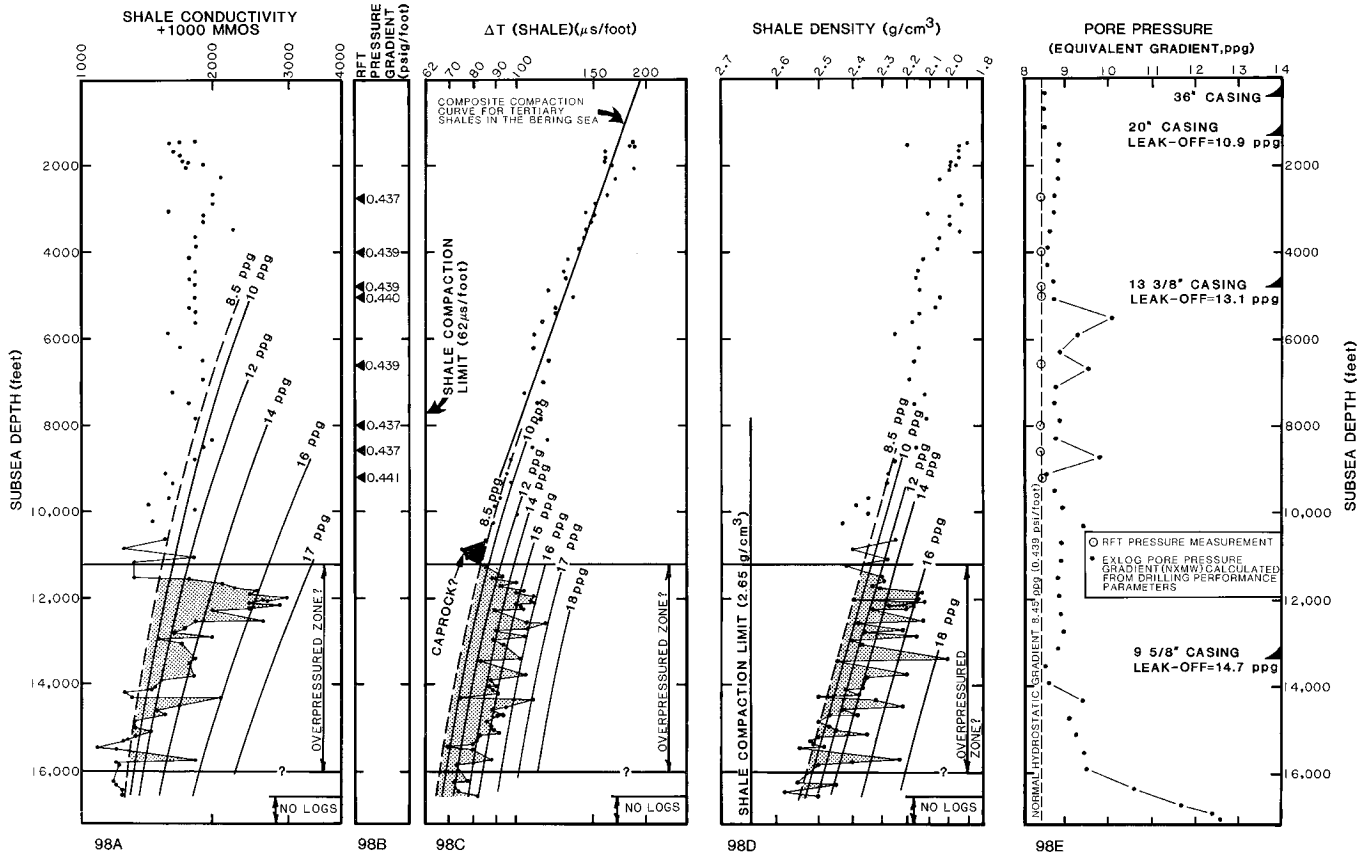

FIGURE 98.

A. Shale conductivity versus subsea depth for the North Aleutian Shelf COST No. 1 well. The zone of over-pressure (high conductivity) between 11,200 and 16,000 feet is shown as a stippled area.

B. Pressure gradients versus subsea depth as obtained from Repeat Formation (RFT) tests.

C. Shale interval travel time (inverse of velocity) versus subsea depth for the North Aleutian Shelf COST No. 1 well. The zone of abnormal pore pressure (low velocity or high travel time) between 11,200 and 16,000 feet is shown as a stippled area. A possible caprock zone is also identified between 10,700 and 11,200 feet. A composite normal compaction curve for Tertiary shales in the Bering Sea (adapted from Sherwood, 1984) is also shown.

D. Shale density (wireline log) versus subsea depth for the North Aleutian Shelf COST No. 1 well. The zone of abnormal pore pressure (low density) between 11,200 and 16,000 feet is shown as a stippled area.

E. Pore pressure estimates from drilling parameters versus subsea depth for the North Aleutian Shelf COST No. 1 well. Pore pressure estimates were calculated by Exploration Logging Inc., concurrent with the drilling of the well. No significant overpressure was noted until approximately 16,000 feet. Casing points and leak-off fracture gradients are also posted along with pore pressure gradients obtained from RFT tests.

This page was intentionally left blank.

casing shoe. Subsequent loss of mud into this newly created fracture in the upper part of the hole, coupled with flow from a deeper horizon, would have resulted in a condition known as downhole blowout. At 13,195 feet, where the 9 5/8-inch casing was set, pore pressure gradients were approximately 16 ppg, or 3 ppg in excess of the fracture gradient at the top of the open hole. Once the 9 5/8-inch casing was in place, nearly half of the overpressured zone was isolated from the mud column, and the existing hole was completely protected. However, the leak-off fracture gradient established just below the 9 5/8-inch casing was only 14.7 ppg. When drilling was resumed below the 9 5/8-inch casing, the mud weight was only 9.7 ppg, or roughly 6 ppg underbalanced relative to formation pore pressure gradients. In this part of the well, pressure estimates also indicate that pore pressure gradients were 1.3 ppg in excess of the 14.7 ppg fracture gradient near the 9 5/8-inch casing shoe. As was the case when the upper part of the overpressured zone was drilled, the potential existed for flow from a deep permeable zone accompanied by mud loss into an induced fracture near the 9 5/8-inch casing shoe.

No permeable strata or natural fracture zones were encountered, however, and the underbalanced condition only resulted in an incursion of minor amounts of gas (possibly derived from coal beds) into the wellbore. As noted above, wellbore instability problems developed while drilling below 15,900 feet (Exlog, 1983), but were partially controlled by raising the mud weight. The mud weight was eventually raised to 13.0 ppg at a depth of 17,155 feet (MD), where abandonment operations were commenced in response to encroaching ice. At that time, circulation was ceased for 48 hours. Mud solids settled during that period of time, and a quantity of 18.7-ppg mud was subsequently circulated out of the bottom of the hole (Exlog, 1983). When circulation was resumed, a mud loss was incurred, suggesting that the formation had been fractured somewhere in the open hole beneath the 9 5/8-inch casing.

The stratigraphic column for the North Aleutian Shelf COST No. 1 well is shown in figure 99B. The overpressured zone appears to be confined entirely to rocks of Eocene age. Much of the overpressured interval lies within lithologic zone E, but appears also to extend a few hundred feet down into lithologic zone F. Lithologic zone F unconformably overlies steeply-dipping, normally-pressured strata of lithologic zone G. Lithologic zone E consists of volcaniclastic sandstones and conglomerates, siltstones, coals, and mudstones deposited in nonmarine and inner neritic settings (see Well Log Interpretation and Lithostratigraphy chapter). Lithologic zone F consists of mudstones, siltstones, volcaniclastic sandstones and conglomerates, coals, and tuffs.

The top of the overpressured zone lies several hundred feet below seismic horizon D, which corresponds to the top of lithologic zone E (fig. 99B). The overpressured zone lies entirely within seismic sequence V. Reflections within seismic sequence V are characterized by high amplitudes, broad cycle breadth, and relatively moderate continuity, and differ markedly in appearance from those in overlying sequences (fig. 62, Seismic Stratigraphy chapter).

The contrasting acoustic character of this seismic sequence may, in part, be due to the presence of excess pore pressures. This seismic sequence, as noted previously, is further characterized by a major velocity inversion (fig. 58, Velocity Analysis chapter).

POSSIBLE CAUSES OF OVERPRESSURE

Abnormal pore pressures may develop in response to a variety of geological processes. Rapid sedimentary loading of uncompacted rocks which are unable to efficiently expel pore fluids from a steadily shrinking void system is probably the most common cause of abnormal pore pressure. This is supported by the observation that most overpressured sequences are found in relatively young basins characterized by rapid subsidence and deposition. Rapid uplift and nonequilibration of pressured strata, tectonic activity, fault seals, or supercharging by oil or gas columns also may create abnormal pore pressure conditions (Fertl, 1976, p. 23). Burst (1969) related overpressure to three separate stages, or major pulses, of water mobilization and expulsion during the progressive burial and diagenesis of shales. Powers (1967), Burst (1969), and Bruce (1984) suggested that thermally controlled diagenesis of clays (illitization of smectites) can generate excess free pore water which may result in abnormal pore pressures in thick shale sequences. Abnormal pore pressures in the lower part of the Navarin Basin COST No. 1 well have been attributed to this process (Sherwood, 1984, p. 189-190). Jones (1969) argued that abnormal pore pressures may develop by osmotic processes across shales which behave as semi-permeable membranes. Aquathermal pressuring, or thermal expansion of confined pore fluids, may also be a cause of abnormal pore pressure (Barker, 1972). Diagenetic destruction of framework grains and the collapse of the skeletal fabric of the rock was suggested as a possible cause of overpressure in diatomites at shallow depths in the Navarin Basin COST No. 1 well (Sherwood, 1984, p. 188).

In the North Aleutian Shelf COST No. 1 well, existing data do not clearly identify any single, traditionally recognized process which may have led to the formation of abnormal pore pressures in lithologic zones E and F. Lithologic zone E, as noted above, consists largely of sandstone, conglomerate, siltstone, coal, and shale. Shale is relatively sparse in lithologic zone E, and it seems unlikely that shale dewatering or diagenesis could have contributed significant volumes of fluid to the pore system of lithologic zone E. Furthermore, the vertical distribution of clays, as illustrated in figure 99C, does not identify any apparent trend of illitization of smectites with depth; in fact, smectites are fairly common throughout the well (fig. 99D). The zeolites clinoptilolite and heulandite disappear near the top of the overpressured interval (fig. 99D), and water released by dissolution of zeolites could have contributed some quantity of fluids to the pore system. However, zeolites represent only a minor constituent (less than 5 percent) of the sediments in this well. Chlorite is the dominant phyllosilicate below 12,300 feet (figs. 99C, 99D) and, to some extent, may have

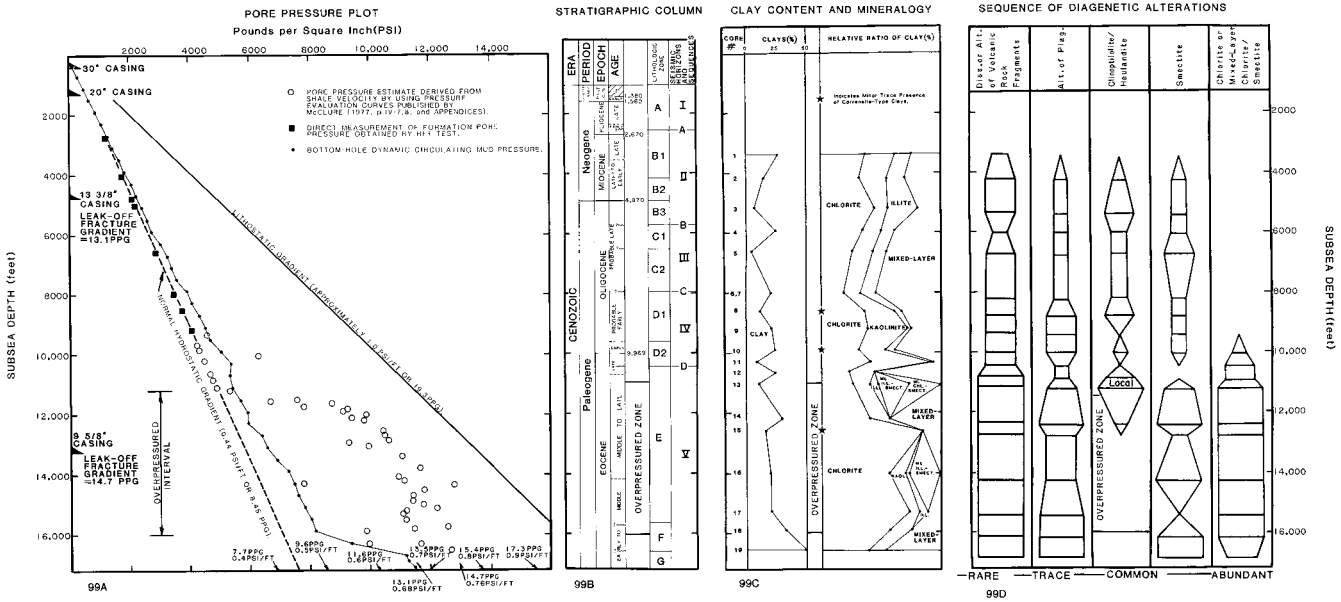

FIGURE 99.

A. Pore pressure plot incorporating RFT data and pore pressure estimates based upon shale velocity data.

B. Stratigraphic column summarizing major time, lithologic, and seismic sequences for the North Aleutian Shelf COST No. 1 well.

C. Clay content and mineralogy of cores from North Aleutian Shelf COST No. 1 well. Adapted from AGAT(1983, vol. 1, fig. 7).

D. Sequence and relative abundance of some major diagenetic alterations in the North Aleutian Shelf COST No. 1 well. Adapted from AGAT (1983, vol. 1,fig. 6).

This page was intentionally left blank.

formed at the expense of more hydrous clay minerals, thereby releasing fluids of dehydration into the pore system.

Petrographic studies conducted by Lynch (see Lithology and Core Data chapter) and AGAT (1983) indicate that the Eocene sandstones in the North Aleutian Shelf COST No. 1 well are typically much richer in volcanic rock fragments than sandstones in the overlying sequences. AGAT (1983) reported that sandstones in lithologic zone E are almost entirely composed of volcanic rock fragments. At depths greater than 10,000 feet, the volcanic rock fragments are extensively replaced by a fine-grained aggregate of diagenetic clays and other minerals (fig. 99D). The geochemical transformation of these formerly rigid volcaniclastic grains to a ductile, clay-rich material has caused a virtual collapse of the structural framework of these rocks in response to overburden pressure. Petrographic observations reveal that these ductile grains have flowed into adjacent pores, resulting in the complete destruction of the original pore system. The pore-filling material created by this mechanical process is termed pseudomatrix. AGAT (1983) described this process as the single most significant agent of porosity destruction within sandstones below 10,000 feet in the North Aleutian Shelf COST No. 1 well. The loss of structural integrity of the rock fabric and concomitant wholesale loss of pore volume would logically place a greater share of the total overburden (lithostatic) weight on the pore fluids trapped within the sandstones, thus resulting in a condition of excess pore pressure. This process is conceptually similar to that suggested for development of overpressure in diatomites in the Navarin Basin COST No. 1 well (Sherwood, 1984, p. 188), where thermally controlled diagenetic destruction of siliceous microfossils apparently led to the collapse of the solid rock framework. The available evidence indicates that a similar process, that is, diagenetic softening and structural collapse of volcaniclastic framework grains in the sandstones of lithologic zones E and F, represents the most probable cause of the abnormal pore pressures observed in the North Aleutian Shelf COST No. 1 well.

SUMMARY

Analysis of shale properties as measured by wireline logs has identified a major zone of abnormally high pore pressure between 11,200 and 16,000 feet (subsea depth) in the North Aleutian Shelf COST No. 1 well. The overpressured zone occurs within seismic sequence V and lithologic zones E and F. No direct pressure measurements were obtained within the overpressured zone. Analysis of shale properties using empirical pressure evaluation curves suggests that hydrostatic gradients as high as 0.88 psi/foot (17 ppg equivalent density) exist within this zone. Much of the overpressured zone was drilled in an underbalanced condition, but because of the impermeability of the strata, no significant incursion of formation fluid or gas into the wellbore occurred during drilling operations.

Sandstones, conglomerates, siltstones, coal, and minor shale compose the bulk of the overpressured zone. Petrographic analysis indicates that these sandstones were almost completely composed of volcanic rock fragments which are now largely replaced by clay. These altered grains have deformed in a ductile manner during compaction, and nearly all pores are now filled with pseudomatrix. Structural collapse of replaced framework grains and extrusion of altered grains into adjacent pore space have destroyed virtually all mesoporosity in sandstones of the overpressured zone. This process is considered to be the most likely cause for the development of excess pore pressure in the North Aleutian Shelf COST No. 1 well.

11. Geologic Hazards and Shallow Geology

by

Peter J. Hoose

GEOLOGIC HAZARDS

Potentially hazardous sea floor and shallow subbottom conditions were identified (Hoose and others, 1984) from publicly available data collected in 1981 by Marine Technical Services, Inc.; in 1980 by Fugro, Inc. (Ertec Western, Inc., 1983); in 1976 by the U.S. Geological Survey; and in 1976 by Petty Ray Geophysical. Most of the data collected during these surveys were limited to that part of the North Aleutian Basin Planning Area south of latitude 56°30'. Geological aspects of the North Aleutian Basin Planning Area that are potentially hazardous to hydrocarbon exploration and production are seismicity, sea floor faulting, shallow gas-charged sediment, volcanic activity, and sea floor scouring by bottom currents.

Seismicity

The Alaska Peninsula-Aleutian arc is one of the world's most active seismic belts in terms of both the number of events and the total amount of energy released. This belt is part of a nearly continuous zone of seismicity, tectonism, and volcanic activity that rings the Pacific Ocean and reflects the tectonic interactions between mobile lithospheric plates. In southeastern Alaska, tectonic interaction between the Pacific and North American plates takes place along the Queen Charlotte-Fairweather fault system, where right-lateral strike-slip faulting is taking place. In southcentral Alaska and along the Aleutian arc, tectonic interaction involves subduction of the Pacific plate beneath the North American plate. This process is responsible for the seismicity, tectonics, and volcanic activity that are characteristic of the region.

Earthquakes in and around the North Aleutian Basin Planning Area can be grouped into three categories based on their size, depth of focus, and cause. These categories are (1) earthquakes that occur within the Benioff zone as a direct consequence of the subduction process; (2) earthquakes that occur as part of a swarm related to volcanic eruptions; (3) and earthquakes that occur behind the arc at relatively shallow depths. The greatest seismic risk is posed by the first category: large-magnitude, thrust-type earthquakes that occur at shallow depths in the Benioff zone.

Minister and Jordan (1978) and Chase (1978) calculated that the long-term average rate of plate convergence along the Aleutian subduction zone is 7.7 centimeters per year. Most of the accumulated elastic strain associated with this convergence is relieved during great earthquakes, those earthquakes with surface wave magnitudes (Ms) greater than 7.8 (McCann and others, 1980). Studies of the aftershock zones of large earthquakes (Sykes, 1971; Pulpan and Kienle, 1979; Sykes and others, 1980) and of regional and local geologic trends (Fisher and others, 1981) have revealed that the tectonic margin of southern Alaska is segmented into discrete blocks that respond individually to subduction-related tectonics. Between 1938 and 1979, convergence between the Pacific and North American plates was accommodated by seven earthquakes of magnitude 7.6 or larger (Davies and others, 1981). These earthquakes ruptured most of the interface between these plates and accordingly relieved the accumulated elastic strain along almost the entire plate margin from British Columbia to the western Aleutians. Significantly, however, the rupture zones of these events failed to include the tectonic block that forms the subduction zone immediately south of the North Aleutian Basin Planning Area. This tectonic block, the Shumagin seismic gap, has not experienced a large earthquake since sometime between 1899 and 1903 (Davies and others, 1981). Consequently this area is a likely site for a future large earthquake. Because of its proximity to the North Aleutian Basin Planning Area, a large earthquake within the Shumagin seismic gap poses a significant threat to hydrocarbon exploration and production facilities.

McNutt and Beavan (1981) and Pulpan and Kienle (1979) discuss seismicity associated with volcanic eruptions on the Alaska Peninsula south and east of the North Aleutian Basin Planning Area. Earthquakes associated with eruptions of Pavlof Volcano tend to be small (magnitude 1 or less), high-frequency events that occur in swarms (McNutt and Beavan, 1981). Pulpan and Kienle (1979) attribute earthquake swarms to hydrofracturing at shallow depths beneath volcanic centers. Earthquakes that precede volcanic eruptions elsewhere in the world have been as large as, but rarely greater than, magnitude 5.5. These latter data suggest that the low-magnitude seismicity observed at Pavlof Volcano may not be representative.

Data compiled by Davies (1981) in the North Aleutian Basin Planning Area south of latitude 56° and east of 165° longitude indicate that for the period from 1937 through 1978, 18 shallow-focus (less than 75 kilometers) earthquakes were detected. These events ranged in magnitude from 3.40 to 5.75.

Earthquakes are capable of causing damage to permanent structures directly by ground shaking, fault displacement, or surface warping, and indirectly by ground failure, sediment consolidation, or tsunami inundation. The severity of destruction caused by ground shaking is a function of the amount of acceleration, amount of displacement, direction of motion, frequency content, duration of motion, thickness of unconsolidated sediment, and geometry of the sedimentary basin. Generally, a structure built on nonfractured

bedrock or on well-consolidated sediment will experience less damage from ground motion than one built on a sediment deposit that is loose, fine grained, water saturated, or thick. Studies of the effects of the March 27, 1964, great Alaskan earthquake revealed that the intensity of seismic shock and the resulting damage to manmade structures were greatest in areas underlain by thick deposits of unconsolidated sediment, particularly where they were water saturated (Foster and Karlstrom, 1967; Plafker and others, 1969).

In the event that a large earthquake occurs in the Benioff zone adjacent to the planning area, substantial regional uplift or subsidence might occur which could have a major impact on permanent facilities located on the Alaska Peninsula and within the planning area. Surface deformation associated with the March 27, 1964, earthquake centered in Prince William Sound extended 500 miles along the trend of the Aleutian arc-trench system (Plafker, 1965). This earthquake, which had a magnitude (Mw) of 9.2 (Kanamori, 1977), uplifted parts of Montague Island by as much as 30 feet and produced tectonic subsidence in parts of the Kenai and Chugach Mountains of more than 6 feet. Adjustments in elevation of this scale are capable of submerging dock facilities or uplifting them beyond the reach of high tide, such as occurred in Cordova, Alaska, during the 1964 earthquake. Ground failure effects associated with earthquakes can include slumps, landslides, submarine slides, sediment liquefaction, and sediment consolidation.

Sea Floor Faulting

Marlow and Cooper (1980), Gardner and Vallier (1981), and Hoose and others (1984) discussed the presence of faults in the North Aleutian Basin Planning Area. Most faults in the planning area south of latitude 56°30' are part of the North Amak fault zone, an eastward extension of the St. George graben (Hoose and others, 1984). Within this zone, most faults do not reach the sea floor but terminate at subseafloor depths ranging from 100 to 950 feet. Faults that do reach the surface are manifested by sea floor sags rather than abrupt scarps. Shallow seismicity indicates that some of these faults are presently active. These faults may be capable of disrupting bottom-founded structures, especially pipelines, and could act as conduits for shallow gas. Faults that do not extend to the sea floor and hence appear to be inactive may still pose a hazard because they represent planes of weakness in older strata that could become reactivated during a large earthquake.

Gas-Charged Sediment

Acoustic anomalies which may represent gas-charged sediment are present in parts of the North Aleutian Basin Planning Area (Hoose and others, 1984). The origin of the gas is probably the microbial decay of organic-rich sediment, particularly peat accumulations, deposited subaerially in depressions exposed during low-sea-level stillstands. Most anomalies occur within 24 to 82 feet of the sea floor, but some occur as deep as 200 feet. The possibility that gas-charged sediment may be present is significant because on

continental shelves elsewhere it has been associated with sea floor instability, sediment overpressuring, and reduced sediment shear strength (Whelan and others, 1976; Nelson and others, 1978).

Volcanic Activity

The North Aleutian Basin Planning Area is susceptible to hazards caused by volcanic activity because of its proximity to the Aleutian volcanic arc. Forty-nine volcanoes are located in the Aleutian arc between the planning area and Attu Island at the end of the Aleutian chain 900 miles to the west. Of these volcanoes, 28 have erupted historically, 21 of them during this century. Volcanoes in this arc are andesitic. Accordingly, their eruptions tend to be violent and are characterized by both ash and lava production. Lava flows, mud slides, bombs, floods, ash fall, noxious fumes, poisonous gases, acid rain, earthquake swarms, lightning strikes, and nuée ardente associated with these eruptions can be hazardous locally. Radio interference, acid rain, and ash fall can be hazardous over extended distances.

Volcanic eruptions are capable of generating large volumes of ash that can be carried long distances in highly mobile flows and by winds. Miller and Smith (1977) described ash flow deposits around Aniakchak and Fisher Calderas on the Alaska Peninsula that were laid down by mobile flows which traveled distances as great as 30 miles and breached obstacles as high as 1,600 feet. The horizontal distance traveled by these flows was limited by the ocean, so this distance should not be considered an indication of maximum mobility. The Katmai eruption of 1912 produced a large volume of ash which blanketed Kodiak Island, 100 miles to the east, with as much as 1 foot of air borne material (Wilcox, 1959). The ash caused considerable damage to communities downwind of Katmai owing to the abrasive action of the particles and the corrosiveness of the ash-produced acid (AEIDC and ISER, 1974). The wide-ranging extent of ash fallout was demonstrated in 1953 and 1976 when wind-borne ash from eruptions of Mt. Spurr and Augustine Volcano reached Anchorage, 80 and 180 miles downwind, respectively. In the southern Bering Sea, the direction of the prevailing wind changes seasonally: southerly and southwesterly winds predominate during the summer and northeasterly winds predominate during the winter (Ertec Western, Inc., 1983). Due to this seasonal wind pattern, volcanoes outside of the planning area as well as proximal volcanoes on the Alaska Peninsula have the potential to deposit ash within the planning area.

Bottom Currents

Sediment erosion and deposition on the sea floor can be hazardous to oil drilling and production structures and to undersea pipelines as a consequence of loading due to burial and the modification of sea floor topography which can undermine structural supports. Hebbard (1959, 1961) reported currents with tidal and nontidal components as strong as 85 centimeters per second (cm/sec) and 5 cm/sec, respectively. Kinder and Schumacher (1981) measured a weak coastal current with a mean northeasterly flow of 1 to 5 cm/sec

and scaler speeds of up to 34 cm/sec. This coastal current is part of a wind-driven, nongeostrophic, counterclockwise gyre that occupies Bristol Bay. High-resolution seismic profiles that indicate the presence of four types of current-generated bedforms (sediment waves, scour depressions, ripple marks, and megaripples) (Hoose and others, 1984) and direct current measurements and visual observations (B. Molnia, oral commun., 1984) confirm that the sea floor near the well site is being raked by bottom currents.

Sediment waves have been identified in only one locality in the planning area. These bedforms are relatively large features with crest to trough heights of as much as 12 feet. They occur at the crest of and downcurrent from a 46-foot rise in sea floor topography, which suggests that they formed in response to a stationary internal wave on the lee side of the rise. Flood (1978) invoked a similar cause to explain the presence of sediment waves on the Blake-Bahama Outer Ridge.

In some nearshore parts of the planning area, bottom currents have eroded parallel, evenly spaced, linear scour depressions 30 to 80 feet wide and approximately 30 feet apart. Within these depressions, currents have winnowed away fine sediment, leaving a coarse lag deposit which shows up on side-scan sonographs as dark (highly reflective) stripes across a light (poorly reflective) nonscoured sea floor. In some areas, the sediment composing these lag deposits is incorporated into ripples. Scour depressions are rarely observed as individual features. They usually occur in small zones containing three or more depressions or in extensive fields which contain many individual depressions and cover up to 200 square miles. Megaripples are often found associated with scour depressions. These features occupy the sea floor between scour depressions and have wavelengths of 20 to 80 feet.

SHALLOW GEOLOGY

Repeated Quaternary glaciations produced dramatic sea level fluctuations that created complex sedimentation patterns across the North Aleutian shelf. In the vicinity of the COST No. 1 well, water depths range from 250 to 290 feet, and the sea floor is relatively flat and featureless (Hoose and others, 1984). Three miles southeast of the well, the sea floor rises from a depth of 260 feet to 200 feet over a distance of three miles. This increase in sea floor gradient, which occurs relatively abruptly compared to the remainder of the planning area, occurs across a linear zone that trends parallel to the modern coastline. This feature, together with several submerged linear ridges that trend parallel to it 25 miles further offshore, represents an ancient, submerged, beach-barrier island complex. The depth range of these features suggests that they may correspond to the minus-184-foot late Pleistocene sea level stillstand determined by Sterns (1974) from Hawaiian data; the minus-164-foot to minus-230-foot stillstand range interpreted by Knebel and others (1974) for the period 16,000 to 17,000 years before present (B.P.); or the minus-

230-foot global lowstand at 14,800 year B.P. recognized by Morner (1971) on the basis of European data.

In the vicinity of the well, the sea floor sediment is predominantly dark-gray, relatively well sorted, fine sand. The sea floor is underlain by 50 to 85 feet of Holocene and upper Pleistocene sand, sandy silt, and silty clay (Hoose and others, 1984). Estimates of the average Holocene sedimentation rate range from less than 1 centimeter (cm) per 1,000 years (yr) (Ertec Western, Inc., 1983) to 30 cm per 1,000 yr (Gershanovich, 1968). Askren (1972) estimated an average Holocene sedimentation rate on the inner shelf of 9 cm per 1,000 yr.

Site-Specific Shallow Geology

The shallow geology and potential geologic hazards in the vicinity of the well site were identified from a site-specific survey conducted by Nekton, Inc. (1980b). At the well site, the sea floor is underlain by 72 feet of unconsolidated Holocene and late Pleistocene sediment. The sea floor within 3,000 feet of the well site is generally flat and featureless. Three thousand feet south of the drill site lies a series of sedimentary features which occur as part of a field that mantles the crest of a 20-foot-high sea floor swell. Nekton called these features megaripples, or ribbons of coarse sand. More likely, they are scour depressions that were identified elsewhere in the planning area in a later study (Hoose and others, 1984). Using a video camera, Nekton also observed ripple marks with wavelengths up to approximately 20 inches.

The site-specific survey revealed no faults near the drill site. It did, however, identify two zones of acoustic "wipe out" near the alternate drill site (3 miles southwest of the primary site). Such zones usually indicate the presence of gas-charged sediment. The origin of the gas is probably microbial decay of organic-rich sediment that was deposited during a low sea level stillstand. The gas is probably under normal or near-normal pressure.

12. Environmental Considerations

by

Allen J. Adams

ARCO Exploration Company, as operator for itself and other participants, submitted a letter to the Minerals Management Service (MMS) office (formerly Conservation Division, USGS) dated June 18, 1981, for the proposed drilling of a deep stratigraphic test well (DST) in the North Aleutian Basin of the Alaska Outer Continental Shelf (OCS). Documents prepared in support of this proposal included a Drilling Plan, an Environmental Report (Woodward-Clyde Consultants, 1981), an Oil Spill Contingency Plan (OSCP). and a Coastal Zone Consistency Certification. Site-specific biological surveys and shallow-drilling-hazards surveys at the primary and alternate sites were required to document environmental conditions before approval of the geological and geophysical (G&G) permit application for the well. The primary and alternate sites are located 79 miles north-northeast and 75 miles north, respectively, of Cold Bay, Alaska. ARCO followed the requirements set forth in the Code of Federal Regulations (30 CFR Part 251) in submission of an application for a G&G Permit for this well.

A deep stratigraphic test well is drilled for the acquisition of geological and engineering data in order to determine the potential for hydrocarbon generation and retention within a proposed lease sale area. Such wells are commonly drilled off-structure and are not intended to locate hydrocarbon accumulations. The North Aleutian Shelf deep stratigraphic test, designated the North Aleutian Shelf COST No. 1 well by the operator, was drilled off-structure. The information gathered from this test well was used to evaluate the hydrocarbon potential of the area covered by the North Aleutian Basin Lease Sale originally scheduled for January 15, 1986.

As part of the permit application review process, an Environmental Assessment (EA) under the National Environmental Policy Act (NEPA) directive was prepared (Lowry, 1981). An EA serves as a decision-making document to determine if the proposed action is or is not a major Federal action significantly affecting the quality of the human environment (in the sense of NEPA, Section 102(2)(C)) and is designed to ensure documented consideration of environmental values in relation to geology, meteorology, oceanography, biology, and socioeconomics. An EA includes a description of the proposed action, a description of the affected environment, environmental consequences, alternatives to the proposed action, unavoidable adverse environmental effects, and controversial issues.

GEOLOGY

The North Aleutian Basin is an east-west elongate structural depression on the Bering Sea shelf that was associated with the formation of the Aleutian arc system. The basin contains late Mesozoic and Cenozoic marine and nonmarine flat-lying sediments.

Site-specific shallow-drilling-hazards surveys covering the proposed primary and alternate sites, conducted in accordance with 30 CFR 250.34 requirements, showed near-surface reflectors to be horizontal and featureless (Nekton, Inc., 1980b). Two "acoustically turbid" zones, which are considered to be indicators of shallow gas, were identified at the alternate site. Water depths varied from 72 meters at the primary site to 84 meters at the alternate site. The bottom relief is due to strong bottom currents generated by extreme tides and severe storms, which have created sand waves, sediment ribbons, and ripples over the survey area.

The geologic hazards addressed by EA AK 81-4 include shallow gas, faulting, seismicity, sediment instability, volcanism, abnormal pressure, and hydrogen sulfide. The shallow-drilling-hazards survey indicated the presence of shallow gas at the alternate site. Shallow gas, usually biogenic in origin, was neither anticipated nor encountered at the primary location.

No shallow faults were identified in the hazards survey conducted by Nekton (1980b).

Concerns about seismicity in the area have focused on the Shumagin seismic gap, a segment of the North Pacific plate boundary along the eastern Aleutian arc which has not ruptured in a great earthquake since at least 1899 to 1903 (Davies and others, 1981). A great earthquake has a magnitude of 7.8 or greater on the Richter scale. An earthquake in the North Aleutian shelf area could cause liquefaction or mass movement. However, the topography of the sites was nearly flat, so mass movement would not be expected to occur. Substrate liquefaction was also considered unlikely, but if it did occur, the effects would be limited to anchors, wellhead, blowout preventer stack, or riser connections. An earthquake of sufficient magnitude to cause liquefaction, although unpredictable, was considered to be unlikely during drilling operations. No seismicity-related problems occurred during the drilling of the well.

The North Aleutian Basin could be affected by a large volcanic explosion. Such an event was considered unlikely during operations. Even if a major eruption had occurred, only minor ashfall would have affected the sites because of their distance from shore.

Abnormal pressure was not expected at either drill site, and well location, design, and safety procedures were designed to alleviate potential adverse conditions that could result from abnormal pressure. Accumulation of high-pressure hydrocarbons at depth was considered unlikely because the well was drilled off-structure (however, see Abnormal Formation Pressure chapter).

Drill rig monitoring systems able to detect the presence of hydrogen sulfide gas, H_2S, were in place. Proper precautions were taken in accordance with an H_2S Contingency Plan prepared by the operator and approved by MMS. No H_2S problems were encountered.

METEOROLOGY AND OCEANOGRAPHY

Most of the Bering Sea lies in subarctic latitudes and a cyclonic atmospheric circulation predominates in the region. Cloudy skies, moderately heavy precipitation, and strong surface winds characterize the marine weather. Weather is controlled by high pressure in the Pacific and Arctic Oceans and over Siberia, which results in the Aleutian low. In the North Aleutian shelf area, currents up to 1.3 knots per hour may occur. Generally, the flow is northwesterly through Unimak Pass, northeasterly along the Alaska Peninsula nearshore, and easterly in the north because of the affects of the southern edge of the Bristol Bay gyre. Wave heights greater than or equal to 3 meters can be expected 27 percent of the time in January, 31 percent in February, 34 percent in March, 18 percent in April, 8 to 12 percent from May through September, 20 percent in October, 36 percent in November, and 29 percent of the time in December (Brower and others, 1977). The well site is ice free from May through December, with less than 25 percent coverage from January through April. The amount of ice coverage in the area is highly dependent on wind velocity, duration, and direction.

Because limited meteorological and oceanographic data were available, the operator was required to collect meteorological, oceanographic, and performance data, pursuant to OCS Order No. 2, to aid in future operations in the area. During set-up and drilling operations, climatic and sea-state conditions were monitored to ensure that local conditions did not exceed rig tolerances or jeopardize human safety. Winds, barometric pressure, air and water temperatures, waves, and currents were monitored. All environmental data collected during the drilling of this well are available from the MMS Field Operations office in Anchorage, Alaska.

BIOLOGY

The Bering Sea shelf, particularly the Bristol Bay area, is one of the most biologically productive areas of the North American OCS. Several of the world's largest known concentrations of commercial fish and shellfish (salmon, king and Tanner crab, shrimp, and various groundfish) occur in the area. Twenty-five species of marine mammals, including seals, walrus, sea otters, and whales are present in the Bristol Bay area. In addition, vast marine bird populations are present (current estimates indicate about 27 million birds seasonally present, with some colonies of over one-half million individuals).

The surrounding coastal habitats (estuaries and wetlands, riparian shrub-thickets, rocky bluffs and cliffs, and local spruce

hardwood communities) also support abundant faunal and floral populations.

Site-Specific Survey

A site-specific marine biological survey was designed by MMS and other Federal and State agencies to provide biological data at both the primary and alternate COST well sites. Through the use of underwater video and photographic documentation, plankton tows, sediment and infaunal sampling, and trawling, ARCO (Nekton, 1980a) determined the relative abundance and types of organisms present in various habitats. Both day and night surveys were conducted from August 3 to August 7, 1980. The results are summarized as follows:

Otter Trawls

Demersal (bottom-dwelling) fish were the dominant component of trawl catches at both sites, accounting for at least 95 percent of the total individuals and 70 percent by weight of the trawl catch. Both the number and weight of fish were greater at the primary site than the alternate site. The yellowfin sole, Limanda aspera, was the dominant species, accounting for at least 90 percent of the total number of fish in each trawl. The walleye pollock, Theragra chalcogramma, which has been taken in large numbers in the Bering Sea, was collected in very low numbers at both sites, as were the other fish species.

Epibenthic invertebrates, including the commercially important Tanner crab, Chionoecetes bairdi, and the red king crab, Paralithodes camtschatica, were collected in low numbers at both sites.

Underwater Television and Photography

Demersal fish and epibenthic invertebrates observed on video recordings were similar at both sites, with yellowfin sole the most abundant species observed. The epibenthic community observed in bottom photographs is similar at both sites with the exception of unidentified bivalves, which were more abundant at the alternate site. Bottom composition and topography were also similar at the two sites.

Benthic Infauna

The alternate site supported more taxa (84 compared to 78) but a lower density (820 compared to 1,033 individuals per square meter) than the primary site. The greater number of taxa at the alternate site was primarily due to a higher number of polychaete annelid (bristleworms) taxa (39 compared to 32). Annelids and echinoderms were the numerically dominant taxa at both

sites, followed by arthropods, molluscs, and protistids (Foraminifera). The sand dollar, Dendraster excentricus, was the most abundant taxon at both sites, accounting for roughly 30 percent of the total organisms. The second most abundant taxon differed between sites: the polychaete Spiophanes bombyx at the primary site, and several species of the amphipod Paraphoxus at the alternate site.

Plankton

Species composition, relative abundance of organisms, and total number of organisms per cubic meter were similar at the two sites, as was expected considering their close spatial proximity and the well-mixed water column. Copepods were the most abundant taxa at both sites, accounting for 43 to 65 percent of the total organisms.

Several species of the chaetognath (arrow worm) Sagitta accounted for 23 to 27 percent of day samples and 12 to 27 percent of night samples at both sites. Decapod crustaceans (crabs and shrimp) accounted for 11 to 14 percent of day samples and euphausids (shrimp-like crustaceans) 9 to 15 percent. At night, euphausids accounted for 16 to 31 percent of the total number of organisms.

Fish eggs were generally observed in low numbers except in day samples at the alternate site, where they represented 12 percent of the total number of organisms. Larvae of the yellowfin sole and walleye pollock were recorded in similar numbers at both sites, accounting for less than 1 percent of the total number of organisms observed.

Diel (twice daily) vertical migration was observed at both sites, as indicated by higher abundances in the upper stratum at night.

Birds and Mammals

The Northern Fulmar, Fulmaros glacialis, was the must abundant bird at both sites. The total number of bird species observed at the primary site (13) was greater than at the alternate site (6). Dall porpoise, Phocoenaoides dalli, were the only mammals observed at either site and were more abundant at the primary site.

The biological survey indicated that the area supported no unique habitats or species that would require rejection or modification of the drilling program. It was determined that normal operations at either of the two sites would not adversely affect the

environment. No additional biological resources were discovered during the drilling operations. No adverse impacts on existing biological resources were apparent from well activities.

Endangered Species, Marine Mammals, and Birds

Many endangered species transit or use the planning area seasonally. Gray whales pass through primarily along the coast on their way to the Chirikof Basin summer feeding area. Fin and humpback whales may be present in the area, but occur primarily along the shelf break to the west. Sei, blue, Pacific right, and sperm whales are rarely seen in the area. Bowhead whales may be present at the ice front. The principal species of marine mammals in the area are Stellar's sea lions, sea otters, harbor seals, Pacific walrus, and gray whales. Other marine mammals present year round or seasonally include killer whales, harbor and Dall porpoise, northern fur and harbor seal, northern sea lion (in ice-free waters), and other walrus (at the ice front).

Southern Bristol Bay is an important nesting, migrational staging, and wintering area for many avian species. The world's entire population of black brant gathers seasonally in the vicinity of Izembek Lagoon. Stellar's eider and other waterfowl reside year round in coastal waters and occasionally in broken-ice leads. The Aleutian Canada goose may also stage at Izembek Lagoon during the migration to winter feeding grounds (U.S. National Marine Fisheries Service, 1981).

A letter was received from the National Marine Fisheries Service (NMFS), included as an attachment to the EA, recommending stipulations to be carried out in concert with the Alaska OCS Orders. NMFS recommended minimum approach distances for air and surface support craft, gave guidelines for reinitiation of consultation, and recommended continued cetacean research.

Fisheries

The planning area provides important habitat for many species, some of which form the basis of existing or potential commercial fisheries (crabs, salmon, clams, pollock, cod). The area is known to be of tremendous importance to the reproduction of red king crab, which spawn from the nearshore subtidal zone to depths of 300 feet. The major portion of the red king crab population gathers in the area in early spring to mate, release larvae, and molt. Larvae released in this area are carried northeast into Bristol Bay, where they settle, increase in size, and eventually provide recruitment to Bering Sea king crab populations. The area also is believed to be important to the reproduction of Tanner crab, since large concentrations of mature females are found there during the spring and summer. Numerous species of groundfish (Pacific halibut, yellowfin sole, rock sole, sablefish, pollock, flathead sole, and Pacific cod) utilize the area as a nursery. It is likely that the

area is also important to other species as a spawning area or nursery.

The in-migration route of the majority of Bering Sea sockeye salmon, which constitute the largest salmon stock in the world, passes through the planning area. Both juvenile and adult salmon of all five Pacific species (sockeye, chinook, coho, pink, and chum) spend a portion of their lives as residents of the Bering Sea shelf.

CULTURAL RESOURCES

It was determined that archeological surveys would not be required for the well sites because they were located in a low-probability area for cultural resources. If the TV transects, side-scan sonar, or magnetometer surveys had indicated unexplained anomalies, a review of the data would have been performed by a qualified marine archeologist. No anomalies were detected.

DISCHARGES INTO THE MARINE ENVIRONMENT

Past studies on the disposition and effects of routine discharges from offshore oil and gas activities indicate that such discharges are not likely to significantly affect the marine environment. The applicant disposed of drill cuttings and waste drilling mud (containing bentonite and barite) into the ocean in compliance with MMS and Environmental Protection Agency (EPA) regulations. Bentonite is a continuous additive to drilling mud, and barite is added as necessary for increasing mud weight. Bentonite and barite are insoluble, nontoxic, and inert. Other additives may be used in minor concentrations under special conditions. These other additives would be either nontoxic or chemically neutralized in the mud or upon contact with seawater. Liquid wastes, including treated sewage, gray water, and some drilling by-products were discharged in accordance with regulations set forth by the EPA.

CONTINGENCY PLAN FOR OIL SPILLS

Procedures for preventing, reporting, and cleaning up oil spills were addressed in the OSCP, which was part of the Drilling Plan. The OSCP listed the equipment and material available to the permittee and described the capabilities of such equipment under different sea and weather conditions. The plan also included a discussion of logistical support and identified specific individuals and their responsibilities in implementing the OSCP. Two response levels were organized: an on-site oil spill team and an onshore support organization. The on-site oil spill team was structured to provide immediate containment and cleanup capability for operational spills that may result from the transfer of fuel oil, and to initiate containment actions for larger uncontrolled spills. The onshore support organization was organized to provide additional equipment and manpower for large spills, if they occurred.

One thousand feet of containment boom, an oil spill skimmer, sorbents, oil storage containers, dispersants, collectants, and chemical application equipment were located on the drilling vessel. Several oil spill training drills were conducted to ensure familiarization with this equipment by each on-site oil spill team. The operation had access to additional oil spill response equipment located at onshore staging points. The OSCP also identified additional equipment that was available from other response organizations, contained agreements to commit these resources, and requirements for obtaining the equipment.

As part of the EA process, the proposed deep stratigraphic test well program was submitted for comments to the appropriate Federal and State agencies, as well as to other interested parties. Responses were included as part of the EA. On the basis of the EA, on October 26, 1981, the Deputy Conservation Manager, Alaska Region, with the concurrence of the Conservation Manager, signed a Finding Of No Significant Impact (FONSI) on ARCO's proposed action, determined that an Environmental Impact Statement (EIS) was not required, and issued a notice to this effect. Coastal Zone Management consistency from the State was obtained on September 17, 1981, before approval of the Application for Permit to Drill by the District Supervisor. The Office of the Deputy Conservation Manager (now Regional Supervisor, Field Operations) consequently issued a letter to ARCO approving their Drilling Plan and issuing a G&G Permit. The EA and FONSI documents are available for review in the public file in the office of the MMS Regional Supervisor, Field Operations, Anchorage, Alaska.

Summary

by

Ronald F. Turner

The ARCO North Aleutian Shelf COST No. 1 Well, located approximately 200 miles northeast of Dutch Harbor, Alaska, was drilled to a depth of 17,155 feet. The water depth at the well site was 285 feet. Drilling operations commenced on September 8, 1982, and the well was abandoned on January 14, 1983. Four strings of casing were set during drilling: 30-inch casing at 459 feet; 20-inch casing at 1,358 feet; 13 3/8-inch casing at 4,865 feet; and 9 5/8-inch casing at 13,287 feet. The drilling fluid for the first 1,370 feet was seawater and gel; the drilling mud used thereafter varied from 8.7 ppg to 13.0 ppg at TD.

As required by 30 CFR 251, the operator (ARCO) filed a Drilling Plan, Environmental Report, Oil-Spill Contingency Plan, and Coastal Zone Consistency Certification. In addition, the MMS required a geohazards survey, geotechnical survey, and site-specific biological survey. The zooplankton, infauna, epifauna, vagile benthos, and pelagic fauna were collected and analyzed. Particular emphasis was placed on protecting local and migratory marine mammals and avifauna. Waste discharges into the environment were minimal, nontoxic, and in compliance with Federal environmental protection regulations.

Although seafloor instability and gas-charged sediments are major geologic hazards in the North Aleutian Basin Planning Area, the well was drilled in an area not affected by these potential impediments. The area is also subject to severe seismicity. Wireline log data clearly identify a potentially dangerous zone of abnormal formation pore pressure from 11,200 to 16,300 feet. Log analysis methods for assessing abnormal pressures are discussed at some length in the Abnormal Formation Pressure chapter.

Nineteen conventional cores, 442 sidewall cores, and well cuttings collected at 30-foot intervals were analyzed for organic geochemistry, paleontology, lithology, porosity, and permeability. Stratigraphic units in the well were defined on the basis of microfossil content, lithology, seismic reflection data, and well log characteristics. The stratigraphic section was divided into 11 lithostratigraphic zones on the basis of lithology and well log characteristics. Five seismic sequences were delineated in the North Aleutian Basin, each representing a conformable unit of strata bounded by unconformities or their correlative conformities. The well penetrated Pleistocene (1,380 to 1,560 feet), Pliocene (1,560 to

2,670 feet), Miocene (2,670 to 4,870 feet), Oligocene (4,870 to 9,969 feet), and Eocene (9,969 to 17,150 feet) age strata.

Overall, the reservoir quality is modest, particularly below 10,400 feet. However, some good potential reservoirs are present in zones B1, B2, B3, C2, D1, and D2.

Sufficient thermal maturity for the generation of crude oil exists below 12,700 feet. The sediments penetrated by the well contained primarily type III, humic, gas-prone kerogen derived from terrestrial or nearshore sources. The best potential source rocks encountered in the well were between 16,020 and 16,800 feet. Minor oil shows and thermogenic gas were encountered below 15,700 feet.

Appendix 1. Abbreviations for Lithologic Descriptions Used in Plate 2

(Excerpted from Mitchell and Maher, 1957)

arg	argillaceous
bit	bitumen, bituminous
blk	black
brn	brown
calc	calcite, calcareous
carb	carbonaceous
cht	chert
cly	clay, clayey
clyst	claystone
cmt	cement, cemented
cr	coarse, coarsely
f	fine, finely
fos	fossil, fossiliferous
frag	fragment, fragmental
fri	friable
frs	fresh
glau	glauconite, glauconitic
gn	green
gr	grain, grained
gy	gray
hd	hard
ig	igneous
intbd	interbedded
intr	intrusion, intrusive
lam	laminated
lig	lignite, lignitic
ls	limestone
lstr	luster
lt	light, lighter
m	medium
mas	massive
mdst	mudstone
mica	mica, micaceous
mtx	matrix
pyr	pyrite, pyritized
qtz	quartz
sd	sand
sdy	sandy
sft	soft

sh	shale
shy	shaly
sl	slight, slightly
sltst	siltstone
slty	silty
ss	sandstone
tr	trace
tuf	tuffaceous
v	very
vf	very fine
vgt	variegated
volc	volcanics
wh	white

Appendix 2. Chemical Classification of Kerogen

Van Krevelen (1961) characterized coal by plotting the elemental ratios of H/C versus the ratios of O/C. These diagrams were later used to classify kerogen and were termed Van Krevelen diagrams by Tissot and Welte (1984). Early investigators believed that there were good correlations between the hydrogen index (from pyrolysis) and the elemental H/C ratio, and between the oxygen index (from pyrolysis) and the elemental O/C ratio (Tissot and Welte, 1984). They plotted the hydrogen index versus the oxygen index in the same way that Van Krevelen had plotted elemental ratios of H/C versus O/C. This new plot was termed a modified Van Krevelen diagram (fig. 94). For various reasons (see Peters, 1986), the correspondence between elemental data and pyrolysis data may be poor. Note the contrast between the hydrogen indices and the elemental H/C data on figure 93. In spite of this problem, it is possible to use this method to describe the chemical evolution of a kerogen as it reacts to increasing temperature through time.

Hunt (1979) described the basic chemical differences between the three kerogen types defined on the Van Krevelen diagram and the modified Van Krevelen diagram in the following way:

Type I kerogen:	Mostly normal and branched paraffins with some naphthenes and aromatics.
Type II kerogen:	Predominantly naphthenes and aromatics.
Type III kerogen:	Largely polycyclic aromatic hydrocarbons and oxygenated functional groups plus some paraffin waxes.

Appendix 3. Carbon Preference Index

The Carbon Preference Index (CPI) is the ratio of odd- to even-numbered, heavy (greater than 24), normal ("n") paraffins in a sample of organic matter, crude oil, or sediment. The CPI_{24-34} originally defined by Bray and Evans (1961) and used by Robertson Research (U.S.) Inc., in their report for the North Aleutian Shelf COST No. 1 well (Dow, 1983) is calculated as follows:

$$CPI_{24-34} = 1/2 \left(\frac{C_{25}+C_{27}+C_{29}+C_{31}+C_{33}}{C_{24}+C_{26}+C_{28}+C_{30}+C_{32}} + \frac{C_{25}+C_{27}+C_{29}+C_{31}+C_{33}}{C_{26}+C_{28}+C_{30}+C_{32}+C_{34}} \right)$$

A modified CPI_{25-31} was used by Radke and others (1980) in their study of soluble organic matter in coals. This index was not calculated for the samples analyzed for this report, but it is comparable to the original Bray and Evans index, and is mentioned in comparative discussions in this report. The Radke index is calculated as follows:

$$CPI_{25-31} = 1/2 \left(\frac{C_{25}+C_{27}+C_{29}+C_{31}}{C_{24}+C_{26}+C_{28}+C_{30}} + \frac{C_{25}+C_{27}+C_{29}+C_{31}}{C_{26}+C_{28}+C_{30}+C_{32}} \right)$$

(where C_{25}, C_{26}, etc., are expressed as mole percentages).

Bray and Evans (1965) observed that CPI values found in recent sediments are typically greater than those in ancient sediments. Even smaller CPI values commonly are obtained for crude oils. CPI values and odd/even ratios for other paraffin chain groups may be used for source rock evaluation, but complexities arise in the interpretation of these data because these kinds of ratios vary with thermal maturity, initial composition, and paraffin groups considered. Marine organisms, for example, preferentially synthesize odd carbon chains only in the low (less than C_{24}) paraffin chain group. As a result, the CPI_{24-34} of purely marine sediments is normally close to 1.0 regardless of the level of thermal maturity of the sediment. Land plants preferentially synthesize odd-chain hydrocarbon waxes up to C_{37}, and, consequently, their CPI_{24-34} values range up to about 20. Any appreciable contribution of organic materials from a terrestrial source will therefore yield CPI_{24-34} values for the sediments considerably greater than 1.0. The odd/even

predominance of paraffin extracts in most source beds gradually disappears with increasing thermal maturity. This is manifested as a decline in CPI values to minimum values which fall within the crude oil range from 0.9 to 1.3. Such values are commonly reached where thermal maturity corresponds to R_o values of approximately 1.0 percent (Radke and others, 1980). The actual range and rate of decline of CPI values depends upon the original organic material, the maturity gradient, and the molecular range of the paraffins used to compute the CPI. More detailed information on the use of CPI data can be found in Bray and Evans (1961; 1965), Hunt (1979, p. 302-310), and Radke and others (1980).

Appendix 4. Pyrolysis Method

Pyrolysis is performed by heating whole-rock samples at a predetermined rate in an inert atmosphere. Free or adsorbed hydrocarbons present in the rock are volatilized first at a moderate temperature. As the temperature increases, pyrolysis of kerogen generates hydrocarbons and hydrocarbon-like compounds from organic material in the rock sample. Finally, oxygen-bearing volatiles such as carbon dioxide and water are evolved. Relative amounts of the evolved hydrocarbons are measured by a flame ionization detector and quantities of oxygen-bearing compounds by a thermal conductivity detector. These measurements are usually reported in weight-to-weight ratios of evolved gas to rock sample and are abbreviated by the symbols S_1, S_2, and S_3, respectively. The temperature T_2-max, in degrees centigrade, is the temperature at which the maximum evolution of pyrolytic hydrocarbons (the S_2 peak) occurs.

T_2-max is generally regarded as a measure of thermal maturity, as is the transformation ratio $S_1/(S_1+S_2)$. The hydrogen index is (S_2/TOC) 100 and the oxygen index is (S_3/TOC) 100. They are normally reported in milligrams of gas per gram of organic carbon, and are used to identify the type of kerogen in source beds. The genetic potential (S_1+S_2) is a measure of the amount of petroleum that kerogen can generate during burial if it is subjected to an adequate temperature during a sufficient interval of time. For a more detailed treatment of this procedure see Tissot and Welte (1984) or Peters (1986).

References

AGAT Consultants, Inc., 1982 and 1983, Reservoir quality study, ARCO North Aleutian Shelf COST No. 1 well: Denver, Colorado, AGAT Consultants, Inc., 7 v. Report prepared for ARCO Exploration Company [available for inspection at U.S. Minerals Management Service, Field Operations Office, Anchorage, Alaska].

Allen, J. R. L., 1970, Studies in fluviatile sedimentation: A comparison of fining-upwards cyclothems, with special reference to coarse-member composition and interpretation: Journal of Sedimentary Petrology, v. 40, p. 298-323.

AEIDC and ISER, 1974, The Western Gulf of Alaska, a summary of available knowledge: prepared by the Arctic Environmental Information and Data Center (AEIDC) and the Institute of Social and Economic Research (ISER), University of Alaska; published by the U.S. Bureau of Land Management, Marine Minerals Division, 559 p.

Anstey, N. A., 1977, Seismic interpretation: The physical aspects: Boston, International Human Resource Development, 625 p.

Askren, D. R., 1972, Holocene stratigraphic framework, southern Bering Sea continental self: University of Washington, unpublished MS thesis, 104 p.

Asquith, G. B., 1982, Basic well log analysis for geologists: Tulsa, Oklahoma, American Association of Petroleum Geologists, p. 215.

Banik, N. C., 1983, Velocity anisotropy of shales and depth anomalies in the North Sea, in 53rd Annual International Society of Exploration Geophysicists Meeting. Sept. 11-15, Expanded Abstracts with Bibliographies: Tulsa, Oklahoma, p. 540-542.

Banik, N. C., 1984, Velocity anisotropy of shales and depth estimation in the North Sea basin: Geophysics, v. 49, p. 1411-1419.

Barker, C., 1972, Aquathermal pressuring, role of temperature in development of abnormal pressure zones: A.A.P.G. Bulletin, v. 56, no. 10, p. 2068-2071.

Barker, C., 1974, Pyrolysis techniques for source-rock evaluation: A.A.P.G. Bulletin, v. 58, no. 11, p. 2349-2361.

Barron, J. A., 1980, Lower Miocene to Quaternary diatom biostratigraphy of Leg 57, off northeastern Japan, Deep Sea Drilling Project, in Initial reports of the Deep Sea Drilling Project, v. 56, 57, part 2: National Science Foundation (U.S. Government Printing Office), p. 507-538.

Beck, M. E., Jr., 1980, Paleomagnetic record of plate-margin tectonic processes along the western edge of North America: Journal of Geophysical Research, v. 85, p. 7115-7131.

Biostratigraphics Consulting Micropaleontology, 1983, ARCO North Aleutian Shelf COST No. 1 Well, Bering Sea, Alaska: Ventura, California, Biostratigraphics, a unit of McClelland Engineers, 6 parts, 139 p.

Bray, E. E., and Evans, E. D., 1961, Distribution of n-paraffins as a clue to recognition of source beds: Geochimica et Cosmochimica Acta. v. 22. p. 2-15.

Bray, E. E., and Evans, E. D., 1965, Hydrocarbons in non-reservoir-rock source beds: A.A.P.G. Bulletin, v. 49, no. 3, p. 248-257.

Brockway, R., Alexander, B., Day, P., Lyle, W., Hiles, R., Decker, W., Polshi, W., and Reed, B., 1975, Bristol Bay region, stratigraphic correlation section, southwestern Alaska: The Alaska Geological Society, P.O. Box 1288, Anchorage, Alaska 99510, 1 oversized sheet.

Brower, W. H., Diaz, H. F., Prechtel, H. S., Searby, H. W., and Wise, J. L., 1977, Climatic Atlas of the outer continental shelf waters and coastal regions of Alaska, vol. 2, Bering Sea. AEIDC Publication B-77, Alaska Environmental Information and Data Center, University of Alaska, Anchorage.

Brown, L. F., Jr., and Fisher, W. L., 1982, Seismic stratigraphic interpretation and petroleum exploration: A.A.P.G. Continuing Education Course Note Series No. 16: Tulsa, Oklahoma, American Association of Petroleum Geologists, 186 p.

Bruce, C. H., 1984, Smectite dehydration--its relation to structural development and hydrocarbon accumulation in northern Gulf of Mexico Basin: A.A.P.G. Bulletin, v. 68, no. 6, p. 673-683.

Bujak, J. P., 1984, Cenozoic dinoflagellate cysts and acritarchs from the Bering Sea and Northern Pacific, DSDP Leg 19: Micropaleontology, v. 30, no. 2, p. 180-212.

Bukry, D., 1973, Low-latitude coccolith biostratigraphic zonation, in Initial reports of the Deep Sea Drilling Project, v. 15: National Science Foundation (U.S. Government Printing Office), p. 685-703.

Bukry, D., 1975, Coccolith and silicoflagellate stratigraphy, northwestern Pacific Ocean, Deep Sea Drilling Project, Leg 32, in Initial reports of the Deep Sea Drilling Project, v. 32: National Science Foundation (U.S. Government Printing Office), p. 677-692.

Burk, C. A., 1965, Geology of the Alaska Peninsula - island arc and continental margin: Geological Society of America Memoir 99, 250 p.

Burst, J. F., 1969, Diagenesis of Gulf Coast clayey sediments and its possible relation to petroleum migration: A.A.P.G. Bulletin, v. 53, no. 1, p. 73-93.

Cant, D. J., 1982, Fluvial facies models and their application, in Schoole, P. A., and Spearing, E., eds., Sandstone depositional environments: Tulsa, Oklahoma, American Association of Petroleum Geologists, p. 115-137.

Chase, C. G., 1978, Plate kinematics: the Americas, East Africa, and the rest of the world: Earth and Planetary Science Letters, v. 37, p. 355-368.

Claypool, G. E., and Reed, P. R., 1976, Thermal-analysis technique for source rock evaluation: Quantitative estimates of organic richness and effects of lithologic variation: A.A.P.G. Bulletin, v. 60, no. 4, p. 608-626.

Clementz, D. M., 1979, Effect of oil and bitumen saturation on source-rock pyrolysis: A.A.P.G. Bulletin, v. 63, no. 12, p. 2227-2232.

Coney, P. J., Jones, D. L., and Monger, W. H., 1980, Cordilleran suspect terranes: Nature, v. 288, p. 329-333.

Cooper, A. K., Marlow, M. S., and O'Brien, T., 1982, Sonobuoy seismic data collected during 1982 in the Bering Sea: U.S. Geological Survey Open-File Report 82-635, one roll of microfilm.

Cooper, A. K., Marlow, M. S., and Scholl, D. W., 1977, The Bering Sea --a multifarious marginal basin, in Talwani, M., and Pitman, W. C., eds., Island arcs, deep sea trenches and back-arc basins, Maurice Ewing Series, v. 1: Washington, D.C., American Geophysical Union, p. 437-450.

Cooper, A. K., Scholl, D. W., and Marlow, M. S., 1976, Plate tectonic model for the evolution of the eastern Bering Sea basin: Geological Society of America Bulletin, v. 87, p. 1099-1126.

Core Laboratories, Inc., 1983, Core analysis report for ARCO Alaska, Inc., North Aleutian Shelf COST No. 1 well, North Aleutian Shelf Alaska: Dallas, Texas, 1 v.

Creager, J. S., Scholl, D. W., and others, 1973, Initial Reports of the Deep Sea Drilling Project, v. 19: National Science Foundation (U.S. Government Printing Office), 913 p.

Davies, J. N., 1981, Seismic and volcanic risk [in the St. George basin and adjacent Aleutian arc], section 3.5 in Hameedi, M. J., ed., Proceedings of a synthesis meeting, the St. George basin environment and possible consequences of planned offshore oil and gas development, Anchorage, Alaska, April 28-30, 1981: U.S. Department of Commerce, NOAA, Outer Continental Shelf Environmental Assessment Program (OCSEAP), and U.S. Bureau of Land Management, p. 46-48.

Davies, J., Sykes, L., House, L., and Jacob, K., 1981, Shumagin seismic gap, Alaska Peninsula: history of great earthquakes, tectonic setting, and evidence for high seismic potential: Journal of Geophysical Research, v. 86, p. 3821-3855.

DeLong, S. D., Fox, P. J., and McDowell, F. W., 1978, Subduction of the Kula Ridge at the Aleutian Trench: Geological Society of America Bulletin, v. 89, p. 83-95.

DeLong, S. D., Fox, P. J., and McDowell, F. W., 1980, Subduction of the Kula Ridge at the Aleutian Trench, Reply: Geological Society of America Bulletin, p. 1, v. 90, p. 700-702.

Demaison, G. J., 1981, Stratigraphic aspects of source bed occurrence: the organic facies concept, in Geochemistry for geologists, short course notes: Dallas, Texas, American Association of Petroleum Geologists, p. 101.

Dilcher, D., 1983, Plant megafossils from core samples, a report prepared for ARCO Oil and Gas Company: preliminary reports and summary: Bloomington, Indiana, 6 p.

Dix, C. H., 1955, Seismic velocities from surface measurements: Geophysics, v. 20, p. 68-86.

Dow, W. G., 1977, Kerogen studies and geological interpretations: Journal of Geochemical Exploration, v. 7, no. 2, p. 79-99.

Dow, W. G., 1983, Geochemical analysis of North Aleutian Shelf, COST No. 1 well, Alaska Report No. 823/135: Houston, Texas, Robertson Research (U.S.), Inc., 315 p. [report prepared for ARCO].

Dow, W. G., and O'Connor, D. J., 1982, Kerogen maturity and type by reflected-light microscopy applied to petroleum exploration, in How to assess maturation and paleotemperatures, SEPM Short Course No. 7: Tulsa, Oklahoma, Society of Economic Paleontologists and Mineralogists, p. 133-157.

Dresser Atlas, 1979, Log interpretation charts: Houston, Texas, Dresser Industries, Inc., 108 p.

EG&G Environmental Consultants, 1983, North Aleutian COST well, meteorological and oceanographic monitoring program, v. 1: Waltham, Massachusetts, 293 p. [available from U.S. Minerals Management Service, Anchorage, Alaska].

Elsik, W. C., 1981, Fungal palynomorphs: notes for a palynology short course, October 1981, under the auspices of Louisiana State University at Baton Rouge, Louisiana, 242 p.

Ertec Western, Inc., 1983, Seafloor geologic hazards on the Northern Aleutian shelf: Report prepared for the Outer Continental Shelf Environmental Assessment Project, National Oceanic and Atmospheric Administration by Ertec Western, Inc. [available from NOAA, 3777 Long Beach Blvd., Long Beach, California 90807], 2 volumes, 29 pl., 309 p.

Espitalié, J., Laporte, J. L., Madec, M., Marquis, F., Boutefeu, A., 1977, Methode rapide de caracterisation des roches mers, de leur potentiel petrolier et de leur degre d'evolution: Revue de l'Institute Francais Petrolier, v. 32, p. 23-42.

EXLOG (Exploration Logging (USA), Inc.), 1983, Final operational report, ARCO Alaska, Inc., North Aleutian Shelf COST Well No. 1, September 1982 to January 1983: Anchorage, Alaska [available from U.S. Minerals Management Service].

Fertl, W. H., 1976, Abnormal formation pressures: Developments in Petroleum Science, 2: New York, N.Y., Elsevier, 382 p.

Fertl, W. H., 1979, Gamma ray spectral data assists in complex formation evaluation: Transactions Society of Professional Well Log Analysts 6th European Evaluation Symposium, London, England, p. 61.

Fertl, W. H., and Wichman, P. A., 1977, How to determine static BHT from well log data: World Oil, v. 184, no. 1, p. 105-106.

Fisher, M. A., Bruns, T. R., and Von Huene, R., 1981, Transverse tectonic boundaries near Kodiak Shelf, Alaska: Geological Society of America Bulletin, v. 92, p. 10-18.

Flood, R. D., 1978, Studies of deep-sea sedimentary microtopography in the North Atlantic Ocean: unpublished Ph.D. dissertation, Woods Hole Oceanographic Institute - Massachusetts Institute of Technology Joint Program in Oceanography, 395 p.

Folk, R. L., 1968, Petrology of sedimentary rocks: Austin, Texas, Hemphill. Cited in AGAT Consultants, Inc., 1982 and 1983.

Folk, R. L., 1970, Petrology of sedimentary rocks: Austin, Texas, Hemphill. Cited in AGAT Consultants, Inc., 1982 and 1983.

Folk, R. L., 1974, Petrology of sedimentary rocks: Austin, Texas, Hemphill, 182 p.

Foster, H. L., and Karlstrom, T. N. V., 1967, Ground breakage and associated effects in the Cook Inlet area, Alaska, resulting from the March 27, 1964, earthquake: U.S. Geological Survey Professional Paper 543-F, 28 p.

Gardner, J. V., and Vallier, T. L., 1981, Faulting in outer continental shelf of southern Bering Sea: A.A.P.G. Bulletin, v. 65, no. 9, p. 1568-1573.

Geological Society of America, 1970, Rock color chart: Boulder, Colorado, 10 p.

Gershanovich, D. E., 1968, New data on geomorphology and recent sediments of the Bering Sea and Gulf of Alaska: Marine Geology, v. 6, p. 281-296.

Gladenkov, Y. B., 1980, Stratigraphy of marine Paleogene and Neogene of northeast Asia (Chukotka, Kamchatka, Sakhalin): A.A.P.G. Bulletin, v. 64, no. 7, p. 1087-1093.

Gretener, P.E., 1982, Geothermics: using temperature in hydrocarbon exploration, Short course, AAPG Annual Meeting, San Francisco, California, 1981, Education Course Note Series, no. 17: Tulsa, Oklahoma, American Association of Petroleum Geologists, 170 p.

Grittner, S.F., 1983, Ice surveillance program to support the North Aleutian Shelf COST Well No. 1: Anchorage, Alaska, ARCO Alaska, Inc. [available from U.S. Minerals Management Service, Anchorage, Alaska].

Grow, J. A., and Atwater, T., 1970, Mid-Tertiary tectonic transition in the Aleutian Arc: Geological Society of America Bulletin, v. 81, p. 3715-3722.

Hammond, R. D., and Gaither, J. R., 1983, Anomalous seismic character--Bering Sea shelf: Geophysics, v. 48, p. 590-605.

Hebbard, J. F., 1959, Currents in the southeastern Bering Sea and possible effects on king crab larvae: U.S. Fish and Wildlife Service, Special Scientific Report--Fisheries no. 293.

Hebbard, J. F., 1961, Currents in the southeastern Bering Sea: International North Pacific Fisheries Committee, Bulletin no. 5, p. 1-15.

Hein, J. R., Scholl, D. W., Barron, J. A., Jones, M. G., and Miller, J., 1978, Diagenesis of late Cenozoic diatomaceous deposits and formation of the bottom-simulating reflector in the southern Bering Sea: Sedimentology, v. 25, p. 155-181.

Helby, R. J., Kidson, E. J., Stover, L. E., and Williams, G. L., 1984, Survey of dinoflagellate biostratigraphy, 16th Palynology Short Course, September 1984, with taxonomical notes and range charts, Hartax Inc., Baton Rouge, Louisiana, 250 p.

Hoare, J. M., 1961, Geology and tectonic setting of lower Kuskokwim-Bristol Bay region, Alaska: A.A.P.G. Bulletin, v. 45, no. 5, p. 594-611.

Hoose, P. J., Ashenfelter, K. A., Lybeck, L. D., and House, M. J., 1984, Prelease investigation maps of the North Aleutian shelf, Bering Sea, Alaska: U.S. Minerals Management Service, MMS Map Series 84-0002, 5 sheets.

Horsefield, B., and Douglas, A. G., 1980, The influence of minerals on the pyrolysis of kerogens: Geochimica et Cosmochimica Acta, v. 44, p. 1119-1131.

Hottmann, C. E., and Johnson, R. K., 1965, Estimation of formation pressures from log-derived shale properties: Journal of Petroleum Technology (June 1965), p. 717-722.

Hunt, J. M., 1979, Petroleum geochemistry and geology: San Francisco, California, W. H. Freeman, 617 p.

Jones, P. H., 1969, Hydrodynamics of geopressures in the northern Gulf of Mexico Basin: Journal of Petroleum Technology, v. 21, p. 802-810.

Jones, D. L., Irwin, W. P., and Ovenshine, A. T., 1972, Southeastern Alaska--a displaced continental fragment?: U.S. Geological Survey Professional Paper 800-B, p. B211-B217.

Jones, D. L., McKevett, E. M., and Plafker, G., 1970, Speculations on late Mesozoic tectonic history of part of southern Alaska: A.A.P.G. Bulletin, v. 54, no. 12, p. 2489.

Jones, D. L., and Silberling, N. J., 1979, Mesozoic stratigraphy--the key to tectonic analysis of southern and central Alaska: U.S. Geological Survey Open-File Report 79-1200, 41 p.

Jorden, J. R., and Shirley, O. J., 1966, Application of drilling performance data to overpressure detection: Journal of Petroleum Technology, v. 18, p. 1387-94.

Kaarsberg, E. A., 1959, Introductory studies of natural and artificial argillaceous aggregates by sound propagation and x-ray diffraction methods: Journal of Geology, v. 67, p. 447-472.

Kanamori, H., 1977, The energy release in great earthquakes: Journal of Geophysical Research, v. 82, p. 2981-2987.

Kinder, T. H., and Schumacher, J. D., 1981, Circulation over the continental shelf of the southeastern Bering Sea: in Hood, D. W., and Calder, J. A., eds., The eastern Bering Sea shelf: oceanography and resources, v. 1: U.S. Department of Commerce, p. 53-75.

Knebel, H. J., Creager, J. S., and Echols, R. J., 1974, Holocene sedimentary framework, east-central Bering Sea, continental shelf, in Herman, Y., ed., Marine geology and oceanography of the Arctic Seas: New York, N.Y., Springer-Verlag, 397 p.

Koizumi, Itaru, 1973, The late Cenozoic diatoms of sites 183-193, Leg 19, Deep Sea Drilling Project, in Supko, P. R., ed., Initial reports of the Deep Sea Drilling Project, v. 19: National Science Foundation (U.S. Government Printing Office), p. 805-855.

Koizumi, Itaru, 1977, Diatom biostratigraphy in the North Pacific region, in Saito, T., and Ujiie, H., eds., Proceedings of the First International Congress on Pacific Neogene Stratigraphy, Tokyo, Japan, 1976: Tokyo, Japan, Kaiyo Shuppan, p. 235-253.

Lentin, J. K., and Williams, G. L., 1985, Fossil dinoflagellates: index to genera and species: Dartmouth, Nova Scotia, Bedford Institute of Oceanography, 451 p.

Levin, F. K., 1978, The reflection, refraction, and diffraction of waves in media with an elliptical velocity dependence: Geophysics, v. 43, p. 528-537.

Lowry, P. L., 1981, OCS environmental assessment, EA No. AK-81-4: [unpublished report issued by] U.S. Geological Survey, Conservation Division, Anchorage, Alaska, 90 p. [Available for inspection at U.S. Minerals Management Service, Field Operations Office, Anchorage, Alaska.]

Lyle, W. M., Morehouse, J. A., Palmer, I. F., Jr., and Bolm, J. G., 1979, Tertiary formations and associated Mesozoic rocks in the Alaska Peninsula area, Alaska, and their petroleum-reservoir and source-rock potential: State of Alaska, Division of Geological and Geophysical Surveys, Geologic Report no. 62, 65 p.

MacGregor, J. R., 1965, Quantitative determination of reservoir pressures from conductivity log: A.A.P.G. Bulletin, v. 49, no. 9, p. 1502-1511.

Mancini, E. A., Deeter, T. M., and Wingate, F. H., 1978, Upper Cretaceous arc-trench gap sedimentation on the Alaska Peninsula: Geology, v. 6, p. 437-439.

Marks, J. G., 1983, Molluscan fossils from second Alaska deep test: a report for ARCO Oil and Gas Company, preliminary reports and summary: Englewood, Colorado, 11 p.

Marlow, M. S., and Cooper, A. L., 1980, Mesozoic and Cenozoic structural trends under the Bering Sea shelf: A.A.P.G. Bulletin, v. 64, no. 12, p. 2139-2155.

Marlow, M. S., and Cooper, A. K., 1983, Wandering terranes in southern Alaska: the Aleutian microplate and implications for the Bering Sea: Journal of Geophysical Research, v. 88, p. 3439-3446.

Marlow, M. S., McLean, H., Cooper, A. K., Vallier, T. L., Gardner, J. V., McMullin, R., and Lynch, M. B., 1980, A preliminary summary of regional geology, petroleum potential, environmental geology, and technology for exploration and development for proposed OCS Lease Sale 75, Northern Aleutian shelf, Bering Sea, Alaska: U.S. Geological Survey Open-File Report 80-653, 54 p.

Marlow, M. S., Scholl, D. W., and Cooper, A. L., 1977, St. George basin, Bering Sea shelf: a collapsed Mesozoic margin: in Talwani, M., and Pitman, W. C., eds., Island arcs, deep sea trenches and back-arc basins, Maurice Ewing Series, v. 1: Washington, D.C., American Geophysical Union, p. 211-220.

Marlow, M. S., Scholl, D. W., Cooper, A. K., and Buffington, E. C., 1976, Structure and evolution of the Bering Sea south of St. Lawrence Island: A.A.P.G. Bulletin, v. 60, no. 2, p. 161-183.

McCann, W. R., Perez, O. J., and Sykes, L. R., 1980, Yakataga gap, Alaska, seismic history and earthquake potential: Science, v. 207, p. 1309-1314.

McClure, L. J., 1977, Drill abnormal pressure safely, short course by L. J. McClure: Houston, Texas, p. 114.

McLean, H., 1979a, Tertiary stratigraphy and petroleum potential of Cold Bay-False Pass area, Alaska Peninsula: A.A.P.G. Bulletin, v. 63, no. 9, p. 1522-1526.

McLean, H., 1979b, Sandstone petrology: Upper Jurassic Naknek Formation of the Alaska Peninsula and coeval rocks on the Bering shelf: Journal of Sedimentary Petrology, v. 49, p. 1263-1267.

McNutt, S. R., and Beavan, R. J., 1981, Volcanic earthquakes at Pavlof Volcano correlated with the solid earth tide: Nature, v. 294, no. 5842, p. 615-618.

Miller, T. P., and Smith, R. L., 1977, Spectacular mobility of ash flows around Aniakchak and Fisher Calderas, Alaska: Geology, v. 5, p. 173-176.

Minister, J. B., and Jordan, T. H., 1978, Present-day plate motions: Journal of Geophysical Research, v. 83, p. 5331-5354.

Mitchell, J. G., and Maher, J. C., 1957, Suggested abbreviations for lithologic descriptions: A.A.P.G. Bulletin, v. 41, no. 9, p. 2103-2107.

Mitchum, R. M., Jr., Vail, P. R., and Sangree, J. B., 1977, Seismic stratigraphy and global changes of sea level, part 6: stratigraphic interpretation of seismic reflection patterns in depositional sequences, in Payton, C. E., ed., Seismic stratigraphy--applications to hydrocarbon exploration: American Association of Petroleum Geologists Memoir 26, p. 117-133.

Monger, J. W. H., Souther, J. H., and Gabrielse, H., 1972, Evolution of the Canadian cordillera: American Journal of Science, v. 272, p. 577-602.

Morner, N. A., 1971, Eustatic changes during the last 20,000 years and a method for separating the isostatic and eustatic factors in an uplifted area: Paleogeography, Paleoclimatology, Paleoecology, v. 9, p. 153-181.

Nekton, Inc., 1980a, Biological survey, proposed continental offshore stratigrapher test No. 1, North Aleutian shelf, Alaska: San Diego, California, 1 v. Prepared for ARCO Oil and Gas Company, Anchorage, Alaska. [Available for inspection at U.S. Minerals Management Service, Field Operations Office, Anchorage, Alaska.]

Nekton, Inc., 1980b, Shallow drilling hazards survey, proposed continental offshore stratigraphic test No. 1, North Aleutian shelf, Alaska: San Diego, California, 1 v. Prepared for ARCO Oil and Gas Company, Anchorage, Alaska. [Available for inspection at U.S. Minerals Management Service, Field Operations Office, Anchorage, Alaska.]

Nelson, C. H., Hopkins, D. M., and Scholl, D. W., 1974, Cenozoic sedimentary and tectonic history of the Bering Sea, in Hood, D. W., and Kelley, E. J., eds., Oceanography of the Bering Sea: Fairbanks, Alaska, University of Alaska, Institute of Marine Science, Occasional Publication no. 2, p. 485-516.

Nelson, C. H., Kvenvolden, K. A., and Clukey, E. C., 1978, Thermogenic gases in near-surface sediments of Norton Sound, Alaska, in Proceedings 10th Offshore Technology Conference, Houston, Texas, p. 2623-2633.

Nilsen, T. H., 1985, Sedimentology of tidally deposited Miocene Bear Lake Formation, Alaskan Peninsula (abst.): A.A.P.G. Bulletin, v. 69, no. 4, p. 673.

Patton, W. W., Jr., 1973, Reconnaissance geology of the northern Yukon-Koyukuk province, Alaska: U.S. Geological Survey Professional Paper 774-A, 17 p.

Pennebaker, E. S., Jr., 1968a, An engineering interpretation of seismic data: Society of Petroleum Engineers of AIME, Special Paper no. 2165, 43rd AIME Fall Meeting, Houston, Texas, p. 1-12.

Pennebaker, E. S., Jr., 1968b, Detection of abnormal pressure formations from seismic field data: American Petroleum Institute, paper no. 926-13-C, p. 184-191.

Peters, K. E., 1986, Guidelines for evaluating petroleum source rock using programmed pyrolysis: A.A.P.G. Bulletin, v. 70, no. 3, p. 318-329.

Pickett, G. R., 1972, Practical formation evaluation: Golden, Colorado, G. R. Pickett, Inc.

Plafker, G., 1965, Tectonic deformation associated with the 1964 Alaska earthquake: Science, v. 148, p. 1675-1687.

Plafker, G., 1969, Tectonics of the March 27, 1964, Alaskan earthquake: U.S. Geological Survey Professional Paper 543-I, 74 p.

Plafker, G., Kachadoorian, R., Eckel, E. B., and Mayo, L. R., 1969, Effects of the earthquake of March 27, 1964, on various communities: U.S. Geological Survey Professional Paper 542-G, 50 p.

Poupon, A., Clavier, C., Dumanoir, J., Graymard, R., and Misk, A., 1970, Log analysis of sand-shale sequences--a systematic approach: Journal of Petroleum Technology, v. 22, p. 867-881

Powers, M. C., 1967, Fluid-release mechanisms in compacting marine mudrocks and their importance in oil exploration: A.A.P.G. Bulletin, v. 51, no. 7, p. 1240-54.

Pulpan, H., and Kienle, J., 1979, Western Gulf of Alaska seismic risk, in Proceedings 11th Offshore Technology Conference, Houston, Texas, p. 2209-2218.

Radke, Matthias, Schaffer, R. G., Leythaeuser, Detlev, and Teichmuller, Marlies, 1980, Composition of soluble organic matter in coals: relation to rank and liptinite fluorescence: Geochimica et Cosmochimica Acta, v. 44, p. 1787-1800.

Reed, B. L., and Lanphere, M. A., 1973, Alaska-Aleutian Range batholith: geochronology, chemistry, and relation to circum-Pacific plutonism: Geological Society of America Bulletin, v. 84, p. 2583-2610.

Robertson Research (U.S.), Inc., see Dow, 1983.

Rouse, G. E., 1977, Paleogene palynomorph ranges in western and northern Canada, in Elsik, W. C., ed., Contributions of stratigraphic palynology (with emphasis on North America): v. 1, Cenozoic palynology: Association of Stratigraphic Palynologists Contribution Series no. 5 A, p. 48-65

Russ, T., Roche, J., and Ayers, D., 1983, Geochemical final well report, ARCO Exploration Company, North Aleutian Shelf COST Well No. 1: Anchorage, Alaska, Exploration Logging, Inc. (USA). 38 p. [available from U.S. Minerals Management Service, Anchorage, Alaska].

Sangree, J. B., and Widmier, J. M., 1977, Seismic stratigraphy and global changes of sea level, part 9: seismic interpretation of clastic depositional facies, in Payton, C. E., ed., Seismic stratigraphy, applications to hydrocarbon exploration: American Association of Petroleum Geologists Memoir 26, p. 165-184.

Schlumberger Well Services, Inc., 1972a, Log interpretation manual, vol. 1, principles: Houston, Texas, Schlumberger, 113 p.

Schlumberger Well Services, Inc., 1972b, Log interpretation charts: Houston, Texas, Schlumberger, 108 p.

Schlumberger Well Services, Inc., 1974, Log interpretation manual, vol. 2, applications: Houston, Texas, Schlumberger 116 p.

Scholl, D. W., Alpha, T. R., Marlow, M. S., and Buffington, E. C., 1975, Plate tectonics and the structural evolution of the Aleutian-Bering Sea region: Geological Society of America Memoir 151, p. 1-13.

Scholl, D. W., Buffington, E. C., and Hopkins, D. M., 1968, Geologic history of the continental margin of North America in the Bering Sea: Marine Geology, v. 6, p. 297-330.

Scholl, D. W., and Creager, J. S., 1973, Geologic synthesis of Leg 19 (DSDP) results, far North Pacific and Aleutian Ridge, and Bering Sea, in Supko, P. R., ed., Initial reports of the Deep Sea Drilling Project, v. 19: National Science Foundation (U.S. Government Printing Office), p. 897-913.

Scholle, P. A., and Spearing, D., eds., 1982, Sandstone depositional environments: American Association of Petroleum Geologists Memoir 31, 410 p.

Schrader, Hans, 1973, Cenozoic diatoms from the northeast Pacific, Leg 18, in Kulm, L. D., and von Heune, R., eds., Initial reports of the Deep Sea Drilling Project, v. 18: National Science Foundation (U.S. Government Printing Office), p. 673-797.

Serra, O., Baldwin, J. L., and Quirein, J. A., 1980, Theory and practical application of natural gamma-ray spectroscopy: Society of Professional Well Log Analysts Paper Q, 30 p.

Sharma, G. D., 1979, The Alaskan shelf: New York, N.Y., Springer-Verlag, 498 p.

Sherwood, K. W., 1984, Abnormal formation pressure, in Turner, R. F., ed., Geological and operational summary, Navarin Basin COST No. 1 well, Bering Sea, Alaska: U.S. Minerals Management Service, OCS Report MMS 84 0031, p. 167 192.

Stach, E., Machowsky, M. Th., Teichmuller, M., Taylor, G. H., Chandra, D., and Teichmuller, R., 1982, Stach's textbook of coal petrology: Berlin, West Germany, Gebruder Borntraeger, 535 p.

Staplin, F. L., 1969, Sedimentary organic matter, organic metamorphism, and oil and gas occurrence: Bulletin of Canadian Petroleum Geology, v. 17, p. 47-66.

Sterns, H. T., 1974, Submerged shorelines and shelves in the Hawaiian Islands and a revision of some of the eustatic emerged shorelines: Geological Society of America Bulletin, v. 85, p. 795-804.

Stone, D. B., and Packer, D. R., 1979, Paleomagnetic data from the Alaska Peninsula: Geological Society of America Bulletin, v. 90, p. 545-560.

Sykes, L. R., 1971, Aftershock zones of great earthquakes, seismicity gaps, earthquake prediction for Alaska and the Aleutians: Journal of Geophysical Research, v. 76, p. 8021-8041.

Sykes, L. R., Kisslinger, J. B., House, L., Davies, J. N., and Jacob, K. H., 1980, Rupture zones of great earthquakes in the Alaska-Aleutian arc 1784-1980: Science, v. 210, p. 1343-1345.

Teledyne Isotopes, 1983, Analysis of samples submitted for K-Ar age determination: Report for ARCO Oil and Gas Company, preliminary reports and summary: Westwood, New Jersey, 2 p. [available from U.S. Minerals Management Service, Anchorage, Alaska].

Tissot, B. P., and Welte, D. H., 1984, Petroleum formation and occurrence: New York, N.Y., Springer-Verlag, 699 p.

Turner, R. F., Bolm, J. G., McCarthy, C. M., Steffy, D. A., Lowry, Paul, and Flett, T. O., 1983a, Geological and operational summary, Norton Sound COST No. 1 well, Norton Sound, Alaska: U.S. Geological Survey Open-File Report 83-124, p. 83-124.

Turner, R. F., Bolm, J. G., McCarthy, C. M., Steffy, D. A., Lowry, Paul, Flett, T. O., and Blunt, David, 1983b, Geological and operational summary, Norton Sound COST No. 2 well, Norton Sound, Alaska: U.S. Geological Survey Open-File Report 83-557, 154 p.

Turner, R. F., McCarthy, C. M., Comer, C. D., Larson, J. A., Bolm, J. G., Banet, A. C., Jr., and Adams, A. J., 1984a, Geological and operational summary, St. George Basin COST No. 1 well, Bering Sea, Alaska: U.S. Minerals Management Service, OCS Report MMS 84-0016, 105 p.

Turner, R. F., McCarthy, C. M., Comer, C. D., Larson, J. A., Bolm, J. G., Flett, T. O., and Adams, A. J., 1984b, Geological and operational summary, St. George Basin COST No. 2 well, Bering Sea, Alaska: U.S. Minerals Management Service, OCS Report MMS 84-0018, 100 p.

Turner, R. F., McCarthy, C. M., Steffy, D. A., Lynch, M. B., Martin, G. C., Sherwood, K. W., Flett, T. O., and Adams, A. J., 1984c, Geological and operational summary, Navarin Basin COST No. 1 well, Bering Sea, Alaska: U.S. Minerals Management Service, OCS Report MMS 84-0031, 245 p.

Turner, R. F., Martin, G. C., Flett, T. O., Steffy, D. A., 1985, Geologic report for the Navarin Basin Planning Area, Bering Sea, Alaska: U.S. Minerals Management Service, OCS Report MMS 85-0045, 156 p.

Turner, R. F., Martin, G. C., Risley, D. E., Flett, T. O., Steffy, D. A., and Lynch, M., 1986, Geologic report for the Norton Basin Planning Area, Bering sea, Alaska: U.S. Minerals Management Service, OCS Report MMS 86-0033, 179 p.

Uhrig, L. F., and Van Melle, F. A., 1955, Velocity anisotropy in stratified media: Geophysics, v. 20, p. 774-779.

U.S. Fish and Wildlife Service, 1980, Resource report--North Aleutian shelf (Sale 75). [Available for inspection at U.S. Minerals Management Service, Field Operations Office, Anchorage, Alaska.]

U.S. National Marine Fisheries Service, 1980, Living marine resources and commercial fisheries relative to potential oil and gas development in the northern Aleutian shelf area (tentative sale No. 75): [Unpublished report by NMFS--Northwest and Alaska Fisheries Center (Seattle), Auke Bay Laboratory (Alaska), and Alaska Region. Available for inspection at U.S. Minerals Management Service, Field Operations Office, Anchorage, Alaska.]

U.S. National Marine Fisheries Service, 1981, Section 7 consultation, North Aleutian shelf, 3 p. [Letter dated April 28, 1981, from NMFS to U.S. Geological Survey, Conservation Division, Alaska. Available for inspection at U.S. Minerals Management Service. Field Operations Office, Anchorage, Alaska.]

Vail, P. R., Mitchum, R. M., Jr., and Thompson, S., III, 1977, Seismic stratigraphy and global changes of sea level, part 4, global cycles of relative changes of sea level, in Payton, C. E., ed., Seismic stratigraphy, application to hydrocarbon exploration: American Association of Petroleum Geologists Memoir 26, p. 83-97.

Van Krevelen, D. W., 1961, Coal: New York, N.Y., Elsevier, 514 p.

Voloshinova, N. A., Kuznetsova, V. N., and Leonenko, L. S., 1970, Neogene Foraminifera of Sakhalin: proceedings of the All Union Petroleum Scientific Research, Geological Exploration Institute: Translated from Russian; prepared for the Smithsonian Institution and National Science Foundation by Saad Publications (Translations Division), Karachi, Pakistan; TT 76-53241; 3 v., 608 p. [Available in English from the National Translations Center.]

Wallace, W. E., 1965, Application of electric-log-measured pressures to drilling problems and a new simplified chart for well site pressure computation: Log Analyst, v. 6, p. 26-28.

Wallace, W. K., 1983, Major lithologic belts of southwestern Alaska and their tectonic implications: Geological Society of America, Abstracts and Program, v. 15, p. 406.

Wallace, W. K., and Engebretson, D. C., 1984, Relationships between plate motions and Late Cretaceous to Paleogene magmatism in southwestern Alaska: Tectonics, v. 3, p. 295-315.

Whelan, T., Coleman, J. M., Roberts, H. A., and Suhayda, J. N., 1976, The occurrence of methane in recent deltaic sediments and its effect on soil stability: International Association of Engineering Geologists Bulletin, v. 14, p. 55-64.

Wilcox, R. E., 1959, Some effects of recent volcanic ash falls with special reference to Alaska: U.S. Geological Survey Bulletin 1028-N, p. 409-476.

Williams, G. L., and Bujak, J. P., 1977, Cenozoic palynostratigraphy of offshore eastern Canada, in Contributions of stratigraphic palynology (with emphasis on North America): v. 1, Cenozoic palynology, W. C. Elsik, ed., Association of Stratigraphic Palynologists Contribution Series No. 5A, p. 14-47.

Wilson, F. H., 1985, The Meshik arc--an Eocene to earliest Miocene magmatic arc on the Alaska Peninsula: State of Alaska, Department of Geological and Geophysical Surveys, Professional Report 88, 14 p.

Woodward-Clyde Consultants, 1981, Environmental report for North Aleutian COST No. 1: [prepared for] ARCO Alaska, Inc., Anchorage, Alaska, 55 p. [Available for inspection at U.S. Minerals Management Service, Field Operations Office, Anchorage, Alaska.]

Wyllie, M. R. J., and Rose, W. D., 1950, Some theoretical considerations related to the quantitative evaluations of the physical characteristics of reservoir rock from electric log data: Journal Petroleum Technology, v. 189, p. 105-110.

50272-101

REPORT DOCUMENTATION PAGE	1. REPORT NO. MMS 88-0089	2.	3. Recipient's Accession No.
4. Title and Subtitle: Geological and Operational Summary, North Aleutian Shelf COST No. 1 Well, Bering Sea, Alaska			5. Report Date: Published Nov. 1988 6.
7. Author(s): Ronald F. Turner, and others			8. Performing Organization Rept. No.
9. Performing Organization Name and Address: U.S. Minerals Management Service, 949 East 36th Avenue, Room 110, Anchorage, Alaska 99508-4302			10. Project/Task/Work Unit No. 11. Contract(C) or Grant(G) No. (C) (G)
12. Sponsoring Organization Name and Address			13. Type of Report & Period Covered: Final 14.

15. Supplementary Notes

16. Abstract (Limit: 200 words)

Discusses the first continental offshore stratigraphic test (COST) well drilled in the North Aleutian Basin Planning Area, Bering Sea, Alaska. The well was drilled to determine the hydrocarbon potential of the area. The report covers drilling operations; lithology and core data; velocity analysis; geologic setting and tectonic framework; seismic stratigraphy; well log interpretation and lithostratigraphy; paleontology and biostratigraphy; geothermal gradient; organic geochemistry; abnormal formation pressure; geologic hazards and shallow geology; and environmental considerations.

17. Document Analysis a. Descriptors

b. Identifiers/Open-Ended Terms

Bering Sea; North Aleutian Shelf COST No. 1 Well; Continental Offshore Stratigraphic Test (COST) Wells; Deep Stratigraphic Test Wells; Alaska

c. COSATI Field/Group

18. Availability Statement	19. Security Class (This Report)	21. No. of Pages
Release unlimited; NTIS PB 89-128227	Unclassified	262p., 2 plates
	20. Security Class (This Page)	22. Price

(See ANSI-Z39.18) See Instructions on Reverse

OPTIONAL FORM 272 (4-77)
(Formerly NTIS-35)
Department of Commerce

☆ U.S. GOVERNMENT PRINTING OFFICE: 1988—691-088/80,002 REGION NO. 10

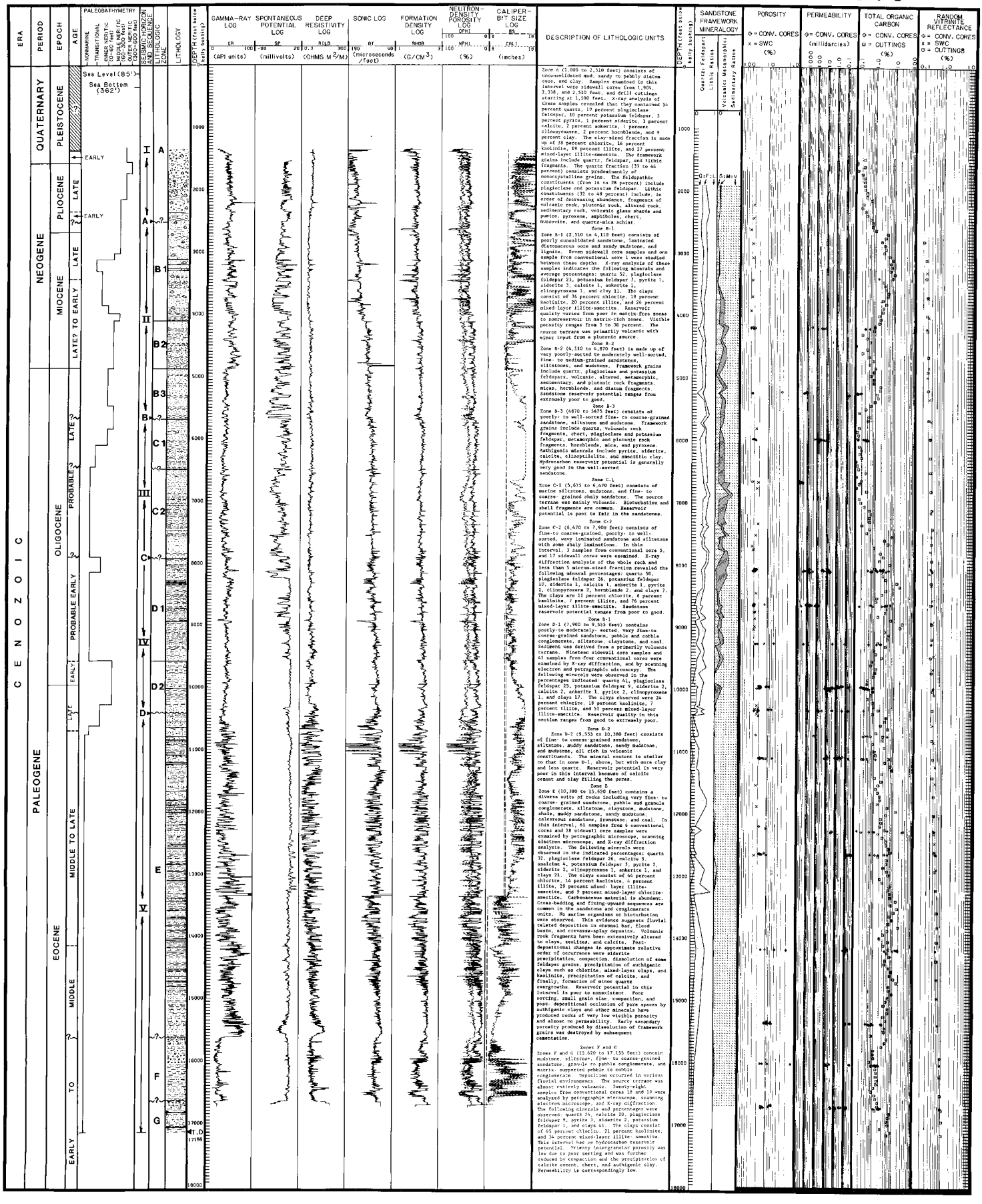

Zone A (1,000 to 2,510 feet) consists of unconsolidated mud, sandy to pebbly diatom ooze, and clay. Samples examined in this interval were sidewall cores from 1,905, 2,338, and 2,510 feet, and drill cuttings starting at 1,590 feet. X-ray analysis of these samples revealed that they contained 54 percent quartz, 19 percent plagioclase feldspar, 10 percent potassium feldspar, 3 percent pyrite, 1 percent siderite, 1 percent calcite, 2 percent ankerite, 1 percent clinopyroxene, 2 percent hornblende, and 9 percent clay. The clay-sized fraction is made up of 38 percent chlorite, 16 percent kaolinite, 19 percent illite, and 27 percent mixed-layer illite-smectite. The framework grains include quartz, feldspar, and lithic fragments. The quartz fraction (33 to 44 percent) consists predominantly of monocrystalline grains. The feldspathic constituents (from 16 to 28 percent) include plagioclase and potassium feldspar. Lithic constituents (32 to 48 percent) include, in order of decreasing abundance, fragments of volcanic rock, plutonic rock, altered rock, sedimentary rock, volcanic glass shards and pumice, pyroxene, amphiboles, chert, muscovite, and quartz-mica schist.

Zone B-1

Zone B-1 (2,510 to 4,110 feet) consists of poorly consolidated sandstone, laminated diatomaceous ooze and sandy mudstone, and lignite. Seven sidewall core samples and one sample from conventional core 1 were studied between these depths. X-ray analysis of these samples indicates the following minerals and average percentages: quartz 52, plagioclase feldspar 23, potassium feldspar 7, pyrite 1, siderite 3, calcite 1, ankerite 1, clinopyroxene 1, and clay 11. The clays consist of 36 percent chlorite, 18 percent kaolinite, 20 percent illite, and 26 percent mixed-layer illite-smectite. Reservoir quality varies from poor in matrix-free zones to nonreservoir in matrix-rich zones. Visible porosity ranges from 3 to 36 percent. The source terrane was primarily volcanic with minor input from a plutonic source.

Zone B-2

Zone B-2 (4,110 to 4,870 feet) is made up of very poorly-sorted to moderately well-sorted, fine- to medium-grained sandstones, siltstones, and mudstone. Framework grains include quartz, plagioclase and potassium feldspars, volcanic, altered, metamorphic, sedimentary, and plutonic rock fragments, micas, hornblende, and diatom fragments. Sandstone reservoir potential ranges from extremely poor to good.

Zone B-3

Zone B-3 (4870 to 5675 feet) consists of poorly- to well-sorted fine- to coarse-grained sandstone, siltstone and mudstone. Framework grains include quartz, volcanic rock fragments, chert, plagioclase and potassium feldspar, metamorphic and plutonic rock fragments, hornblende, mica, and pyroxene. Authigenic minerals include pyrite, siderite, calcite, clinoptilolite, and smectitic clay. Hydrocarbon reservoir potential is generally very good in the well-sorted sandstone.

Zone C-1

Zone C-1 (5,675 to 6,470 feet) consists of marine siltstone, mudstone, and fine- to coarse- grained shaly sandstone. The source terrane was mainly volcanic. Bioturbation and shell fragments are common. Reservoir potential is poor to fair in the sandstones.

Zone C-2

Zone C-2 (6,470 to 7,900 feet) consists of fine-to coarse-grained, poorly- to well-sorted, wavy laminated sandstone and siltstone with some shaly laminations. In this interval, 3 samples from conventional core 5, and 17 sidewall cores were examined. X-ray diffraction analysis of the whole rock and less than 5 micron-sized fraction revealed the following mineral percentages: quartz 56, plagioclase feldspar 26, potassium feldspar 10, siderite 1, calcite 1, ankerite 1, pyrite 2, clinopyroxene 2, hornblende 2, and clays 7. The clays are 11 percent chlorite, 6 percent kaolinite, 7 percent illite, and 76 percent mixed-layer illite-smectite. Sandstone reservoir potential ranges from poor to good.

Zone D-1

Zone D-1 (7,900 to 9,555 feet) contains poorly-to moderately- sorted, very fine-to coarse-grained sandstone, pebble and cobble conglomerate, siltstone, claystone, and coal. Sediment was derived from a primarily volcanic terrane. Nineteen sidewall core samples and 45 samples from four conventional cores were examined by X-ray diffraction, and by scanning electron and petrographic microscopy. The following minerals were observed in the percentages indicated: quartz 41, plagioclase feldspar 25, potassium feldspar 9, siderite 2, calcite 2, ankerite 1, pyrite 2, clinopyroxene 1, and clays 17. The clays observed were 24 percent chlorite, 18 percent kaolinite, 7 percent illite, and 51 percent mixed-layer illite-smectite. Reservoir quality in this section ranges from good to extremely poor.

Zone D-2

Zone D-2 (9,555 to 10,380 feet) consists of fine- to coarse-grained sandstone, siltstone, muddy sandstone, sandy mudstone, and mudstone, all rich in volcanic constituents. The mineral content is similar to that in zone B-1, above, but with more clay and less quartz. Reservoir potential is very poor in this interval because of calcite cement and clay filling the pores.

Zone E

Zone E (10,380 to 13,620 feet) contains a diverse suite of rocks including very fine- to coarse- grained sandstone, pebble and granule conglomerate, siltstone, claystone, mudstone, shale, muddy sandstone, sandy mudstone, calcareous sandstone, ironstone, and coal. In this interval, 61 samples from 6 conventional cores and 28 sidewall core samples were examined by petrographic microscope, scanning electron microscope, and X-ray diffraction analysis. The following minerals were observed in the indicated percentages: quartz 32, plagioclase feldspar 26, calcite 9, analcime 4, potassium feldspar 3, pyrite 2, siderite 2, clinopyroxene 1, ankerite 1, and clays 21. The clays consist of 44 percent chlorite, 14 percent kaolinite, 2 percent illite, 29 percent mixed- layer illite-smectite, and 9 percent mixed-layer chlorite-smectite. Carbonaceous material is abundant. Cross-bedding and fining-upward sequences are common in the sandstone and conglomerate units. No marine organisms or bioturbation were observed. This evidence suggests fluvial related deposition in channel bar, flood basin, and crevasse-splay deposits. Volcanic rock fragments have been extensively altered to clays, zeolites, and calcite. Post-depositional changes in approximate relative order of occurrence were siderite precipitation, compaction, dissolution of some feldspar grains, precipitation of authigenic clays such as chlorite, mixed-layer clays, and kaolinite, precipitation of calcite, and finally, formation of minor quartz overgrowths. Reservoir potential in this interval is poor to nonexistent. Poor sorting, small grain size, compaction, and post- depositional occlusion of pore spaces by authigenic clays and other minerals have produced rocks of very low visible porosity and almost no permeability. Early secondary porosity produced by dissolution of framework grains was destroyed by subsequent cementation.

Zones F and G

Zones F and G (15,620 to 17,155 feet) contain mudstone, siltstone, fine- to coarse-grained sandstone, granule to pebble conglomerate, and matrix- supported pebble to cobble conglomerate. Deposition occurred in various fluvial environments. The source terrane was almost entirely volcanic. Twenty-eight samples from conventional cores 18 and 19 were analyzed by petrographic microscope, scanning electron microscope, and X-ray diffraction. The following minerals and percentages were observed: quartz 24, calcite 20, plagioclase feldspar 9, pyrite 3, siderite 2, potassium feldspar 1, and clays 41. The clays consist of 45 percent chlorite, 21 percent kaolinite, and 34 percent mixed-layer illite- smectite. This interval has no hydrocarbon reservoir potential. Primary intergranular porosity was low due to poor sorting and was further reduced by compaction and the precipitation of calcite cement, chert, and authigenic clay. Permeability is correspondingly low.

Stratigraphic Column and Summary Chart of Geologic Data, North Aleutian Shelf COST No. 1 Well, Bering Sea, Alaska

UNITED STATES DEPARTMENT OF THE INTERIOR
MINERALS MANAGEMENT SERVICE

DEPTH (ft)	TEMP. (°F)	DESCRIPTION OF SELECTED SAMPLES[1] CUTTINGS △ SIDEWALL CORES □ CONVENTIONAL CORES ○ (DIGIT INDICATES CORE NO.)
0	36	
1,000	52	
		□ CLYST, LT GY-BRN, (80%), SS, LT BRN, (20%), PYR, TR (TR)
2,000	69	□ SLTST/SS, VF-M GR,SFT
		□ CLYST, LT GY-BRN, SDY
3,000	86	□ SLTST/SS, LT BRN/GY-BRN, F-M GR, SFT
		○ 1. CLYST, LT GY-BRN, TR COAL, TR MICA
4,000	103	□ CLYST, LT GY-BRN, (60%), COAL, (10%)
		○ 2. SS, LT BRN/GY-BRN, F-M GR, ARG, MICA
		□ SS, GY-BRN, VF-F GR, QTZ, TR MICA, CLY MTS
5,000	120	□ SLTST, LT GY-BRN, SL SDY, TR CARB, SFT
		○ 3. SS, GY-WH/BLK, VF-M GR, CLY MTS, FRI
		□ SLTST/SS, AS ABOVE
6,000	136	○ 4. SLTST/SS, LT GY-BRN, F-CRS GR, MIC, CLY,(65%), COAL/LIG, (5%)
		□ SLTST/SS, AS ABOVE
		○ 5. SS, GY-WH/BLK, F-CRS GR, CLY MTS, FRI, COAL, (TR)
7,000	153	:: SLTST, AS ABOVE, (70%), SS, INTBD, (30%)
		□ SLTST/CLYST, (70%), INTBD SS, (30%), COAL LAM, (TR)
8,000	170	○ 6. SS/SLTST, GY-BRN,F-M GR, CARB ○ 7. SS/SLTST, AS ABOVE, (95%), COAL, (5%)
		○ 8. SS, LT BRN, F-CRS GR, GLAU, SL CALC, CLY, COAL, (TR)
9,000	187	○ SS, DK VGY, F-M GR, QTZ, CLY MTS, (90%), CLYST, DK GY-BRN, (10%)
		○ 9. SS/SLTST, GY-BRN, F-M GR, CARB LAM
		□ SS, AS ABOVE, (70%), SLTST, GY-BRN, SFT, TR CARB, (30%)
10,000	204	○ 10. SLTST/SS, GY-BRN, VF-M GR, GLAU
		○ 11. SLTST/SS, LT GN, VF-M GR, CLY MTS, (75%), SHELL, (25%) CLYST, LT BRN, SFT, CARB
		○ 12. SH, DK GY-BRN, (90%), COAL LAM, (20%)
11,000	220	○ 13. SLTST, LT GY-BRN, (50%),SS, GY, F-CRS GR, CARB, (30%),CARB LAM, (20%)
		□ SLTST, LT BRN-BRN, SFT, CARB, (TR)
		□ VOLC. TUFF, GY-BRN, SFT
12,000	237	□ COAL
		○ 14. COAL, BIT, (80%), SH, GY, COAL LAM, (40%)
		○ 15. SH, GY-BRN, SLTY, COAL LAM, (85%),COAL, (15%)
13,000	254	□ CLYST, BRN-GN, SFT, V CARB
		□ VOLC. TUFF, (95%), COAL LAM, (5%)
		△ COAL, (50%), SLTST, (15%), VOLC. TUFF, (15%), SS, (10%), SH, (10%)
		△ COAL, (70%), SLTST,(15%), SS, (15%)
14,000	271	○ 16. SH, BRN-BLK, SDY LAM, COAL LAM
		△ SLTST, (40%), SS, (25%), COAL, (25%), CHT, (10%)
15,000	288	△ SS, (40%), SLTST, (30%), COAL, (15%), CHT, (10%)
		○ 17. SS,VGY, F-CRS GR, QTZ/VOLC., V HD, (80%), SLTST, GY, V HD, (20%), COAL LAM
		△ SLTST, DK BRN, SHY, SL CALC, SL CARB, (85%), SS, (15%), VOLC. TUFF, (TR)
16,000	304	○ 18. SH, DK GY-BRN
		△ SH, DK GY-BRN, M, (80%), SS, (10%), SLTST, (TR)
		○ 19. SH, DK GY-BRN, M, (80%), SLTST, GY-BRN, M, SHY, (20%) △ SH, DK GY-BRN, M, (45%), COAL, (30%), SS, (15%), VOLC. TUFF, (10%)
17,000	321	△ SH, DK GY-BRN, M, (40%), SLTST, DK GY-BRN, SHY, SL CARB, (25%), SS, (15%), COAL (10%), VOLC. TUFF, (10%)
17,156 TD	324	△ SH, AS ABOVE, (40%), TUFF SD, GY-GN, (20%), COAL, (20%), SLTST, AS ABOVE, (20%)

1. THE SAMPLES DESCRIBED WERE SUBMITTED TO ROBERTSON RESEARCH (US), INC. FOR ANALYSIS. ABBREVIATIONS ARE DEFINED IN APPENDIX 1. SIDEWALL CORES WERE COLLECTED TO 13,291 FEET. DESCRIPTIONS OF CUTTINGS SAMPLES ARE USED FOR GREATER DEPTHS.

TOTAL ORGANIC CARBON (%)

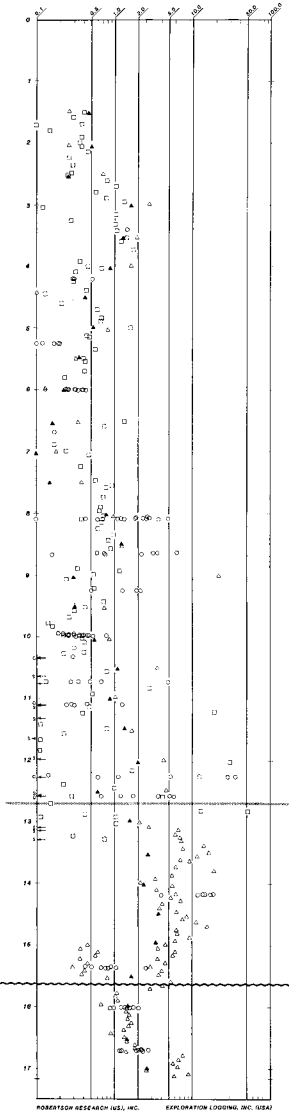

ROBERTSON RESEARCH (US), INC.
CONVENTIONAL CORE SAMPLES ○
SIDEWALL CORES □
CUTTINGS SAMPLES △
VERY LOW VALUE COPE DIAGRAM)
c CONVENTIONAL CORE
s SIDEWALL CORE

EXPLORATION LOGGING, INC. (USA)
CUTTINGS SAMPLES ▲

ROCK EVAL PYROLYSIS

GENETIC POTENTIAL, S_1+S_2 (ppm)

TRANSFORMATION RATIO, $\frac{S_1}{S_1+S_2}$

ROBERTSON RESEARCH (US), INC.
CONVENTIONAL CORE SAMPLES ○ ○
SIDEWALL CORES □ □
CUTTINGS SAMPLES △ △
DIGITS REPRESENT THE NUMBER OF CONSIDERED DATA POINTS.

ROBERTSON RESEARCH (US), INC.
CONVENTIONAL CORE SAMPLES ○
SIDEWALL CORES □
CUTTINGS SAMPLES △

C_{15+} ORGANIC EXTRACT

$\frac{C_{15+}\text{ BITUMEN}}{TOC}$ AND $\frac{C_{15+}\text{ HYDROCARBONS}}{TOC}$

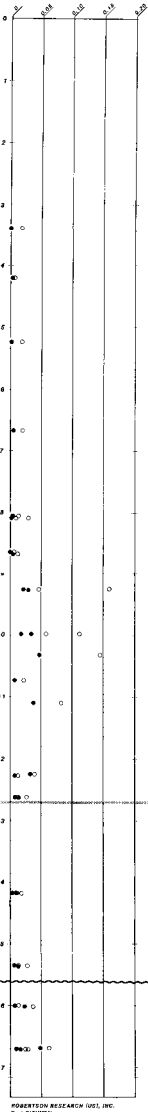

ROBERTSON RESEARCH (US), INC.
C_{15+} BITUMEN ○
TOC
C_{15+} HYDROCARBONS ●
TOC

HEADSPACE GAS

$\frac{C_1-C_5}{TOC}\left(\frac{ml}{gl}\right)$

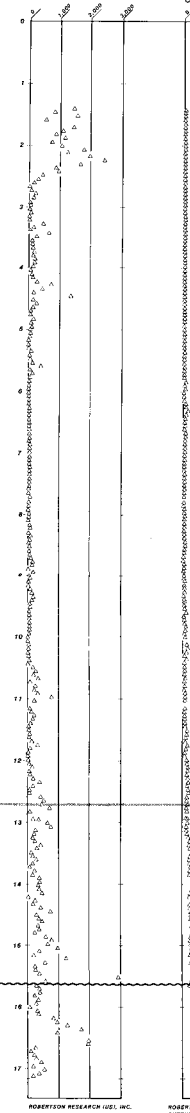

WETNESS $\frac{C_2+C_3+C_4}{C_1+C_2+C_3+C_4}(100)$

ROBERTSON RESEARCH (US), INC.
CUTTINGS SAMPLES △

ROBERTSON RESEARCH (US), INC.
CUTTINGS SAMPLES △

TEMP. (°F)	DEPTH (ft)
36	0
52	1,000
69	2,000
86	3,000
103	4,000
120	5,000
136	6,000
153	7,000
170	8,000
187	9,000
204	10,000
220	11,000
237	12,000
254	13,000
271	14,000
288	15,000
304	16,000
321	17,000
324	17,156 TD

ORGANIC RICHNESS AND HYDROCARBON POTENTIAL, NORTH ALEUTIAN COST NO. 1 WELL, BERING SEA, ALASKA.